

# **FIRE ENDURANCE OF MULTICELLULAR PANELS IN AN FRP BUILDING SYSTEM**

THÈSE N° 3235 (2005)

PRÉSENTÉE À LA FACULTÉ ENVIRONNEMENT NATUREL, ARCHITECTURAL ET CONSTRUIT

Institut de structures

SECTION D'ARCHITECTURE

ÉCOLE POLYTECHNIQUE FÉDÉRALE DE LAUSANNE

POUR L'OBTENTION DU GRADE DE DOCTEUR ÈS SCIENCES

PAR

**Craig D. TRACY**

M.Sc. in Civil Engineering, Lehigh University, Bethlehem, Etats-Unis  
et de nationalité américaine

acceptée sur proposition du jury:

Prof. T. Keller, directeur de thèse  
Prof. M.A. Hirt, rapporteur  
Dr E. Hugi, rapporteur  
Prof. J. Lesko, rapporteur  
Dr A. Zhou, rapporteur

Lausanne, EPFL  
2005



For my dad.



---

## Abstract

Fiber-reinforced synthetic polymers (FRP) are the building materials that may permit both the improvement of long-term building performance and the simplification of the construction process. Thanks to their high specific strength, low thermal conductivity, good environmental resistance, and their ability to be formed into complex shapes, FRP materials are well-suited to fulfilling many building functions. By integrating traditionally separate building systems and layers into single *function-integrated* components and industrially fabricating those components, the amount of on-site labor can be greatly reduced and overall quality can be improved. In order to profit from the advantageous qualities of FRP, however, it is essential to address the unique weaknesses and disadvantages of the material. Most notably, the problems of poor fire safety and high material costs must be overcome.

In response to these challenges, a new multiple-story building system employing FRP materials is proposed. Within this system, fire safety is ensured through the use of an internal liquid cooling system, which circulates a cooling medium through the load-bearing FRP elements to maintain their temperature within a safe operating range. This system is made cost-effective through the integration of the building's heating and cooling system. By controlling the temperature of the circulating liquid, the building's structural elements can serve as heating or cooling emitters (radiators). Further, the addition of the liquid within the cells of the FRP elements helps maintain a more constant interior climate through the "thermal flywheel" effect, which improves energy efficiency and comfort.

Experimental investigations were performed to explore the fire safety aspects of the proposed system. An existing FRP cellular bridge deck material was adapted to incorporate an internal liquid cooling system. After several preliminary investigations, large-scale experiments involving structural and fire loading were conducted on both liquid-cooled and non-liquid cooled specimens. The experiments demonstrated the efficacy of the system in protecting load-bearing FRP elements from the weakening effects of high temperatures, especially those that are stressed in compression. Structural fire endurance times were improved from less than one hour to more than two hours (EC1 Part 1.2) through the implementation of the liquid cooling system.

Alongside the experimental program, a series of mathematical models were developed. Numerical thermochemical and thermomechanical models simulate the response of loaded liquid-cooled FRP panels in fire, while analytical models predict the post-fire mechanical behavior of fire-damaged sections. All models provide predictions that are within 10% of experimentally measured values.

## Version Abrégée

Les matériaux composites en polymères renforcés par des fibres (FRP) permettent d'améliorer les performances à long terme des bâtiments et de simplifier le processus de fabrication. Grâce à leur haute résistance spécifique, faible conductivité thermique, bonne résistance aux actions environnementales et à leur capacité à être produits sous des formes complexes, les matériaux en FRP sont adaptés pour une utilisation multifonctionnelle dans le bâtiment. L'intégration de systèmes et de couches du bâtiment traditionnellement séparés en un composant unique à fonctions intégrées ainsi que la fabrication industriellement de ce composant, permet de réduire de manière considérable le temps de travail in-situ et d'améliorer la qualité de l'intégralité des travaux. Afin d'exploiter les nombreux avantages des matériaux en FRP, il est cependant essentiel d'adresser les faiblesses et les inconvénients propres au matériau. Notamment, les problèmes liés à la faible sécurité à l'incendie et le coût élevé du matériau doivent être surmontés.

En réponse à ces défis, un nouveau système en FRP de bâtiment à plusieurs étages est proposé. Dans ce système, la sécurité au feu est assurée par l'utilisation d'un système de liquide de refroidissement interne qui circule par les éléments porteurs en FRP afin de maintenir leur température dans une plage de fonctionnement sûre. Ce système devient rentable en intégrant le système de chauffage et de refroidissement du bâtiment. En commandant la température du liquide de circulation, les éléments structuraux du bâtiment peuvent fonctionner en tant que chauffage ou émetteurs de refroidissement (radiateurs). De plus, la présence du liquide dans les cellules des éléments en FRP permet d'entretenir un climat intérieur plus constant par l'effet de "volant thermique", ce qui améliore l'efficacité énergétique et le confort.

Des études expérimentales ont été conduites afin d'examiner le comportement au feu du système proposé. Un matériau cellulaire existant en FRP, utilisé pour les tabliers de pont, a été adapté afin d'y incorporer un système de liquide de refroidissement interne. Suite aux études préliminaires, des expériences structurales et d'incendie à grande échelle ont été conduites sur des éprouvettes sans et avec liquide de refroidissement. Les expériences ont démontré l'efficacité du système de protection des éléments porteurs en FRP sur leur dégradation sous hautes températures, particulièrement ceux sollicités en compression. Les durées caractérisant la résistance au feu exigée ont été améliorées en augmentant de moins d'une heure à plus de deux heures (EC1 partie 1.2) par l'introduction du système de liquide de refroidissement.

Simultanément au programme expérimental, plusieurs modèles mathématiques ont été développés. Les modèles numériques thermo-chimiques et thermomécaniques permettent de simuler la réponse des panneaux en FRP réfrigérés par un liquide et chargés pendant l'incendie, alors que les modèles analytiques permettent de prévoir le comportement mécanique des sections brûlées après l'incendie. Les différents modèles fournissent des prévisions entre 10% des résultats expérimentaux.

---

## Zusammenfassung

Glasfaserverstärkte Kunststoffe (GFK), als Baumaterialien eingesetzt, sind in der Lage sowohl die Bauwerksfunktionen dauerhaft zu verbessern als auch den Konstruktionsprozess zu vereinfachen. Dank ihrer hohen spezifischen Festigkeit, geringen Wärmeleitfähigkeit, guten Witterungsbeständigkeit und der Möglichkeit sie in zusammengesetzten Formen auszuführen, eignen sich GFK Materialien, vielfältige Bauwerksfunktionen zu übernehmen. Das Zusammenführen traditionell getrennter Bausysteme und Abschnitte zu funktionsintegrierten, industriell vorgefertigten Bauelementen verringerte die Arbeiten vor Ort erheblich und verbesserte die Qualität insgesamt. Um jedoch aus den vorteilhaften Eigenschaften des GFK Nutzen zu ziehen, ist es unerlässlich sich mit den einzelnen Schwächen und Nachteilen dieses Materials auseinanderzusetzen. Insbesondere die Probleme hinsichtlich des geringen Feuerwiderstands und der hohen Materialkosten müssen überwunden werden.

Als Antwort auf diese Herausforderungen schlagen wir ein neues mehrstöckiges Bausystem aus GFK Materialien vor. Als Bestandteil dieses Systems sorgt ein internes Kühlsystem, welches eine Kühlflüssigkeit durch die lasttragenden GFK Elemente strömen läßt um die Temperaturen innerhalb eines sicheren Betriebsbereiches zu halten, für den notwendigen Feuerwiderstand. Durch die Einbindung des Heiz- und Kühlsystems in die Konstruktion kann das System wirtschaftlich hergestellt werden. Durch Temperaturänderung der Kühlflüssigkeit können die tragenden Bauteile zum Heizen bzw. Kühlen eingesetzt werden.

Darüber hinaus hilft die Flüssigkeit in den Zellen der GFK Elemente, ein konstanteres inneres Raumklima durch den so genannten "thermal flywheel" Effekt aufrecht zu erhalten wodurch die Energie effizienter genutzt und die Behaglichkeit gesteigert wird. Um die einzelnen Aspekte des Feuerwiderstands zu erforschen wurden versuchsgestützte Untersuchungen durchgeführt. Zu diesem Zweck wurde ein bereits bestehendes zellenförmiges Brückendeckelement so umgebaut, dass ein internes Flüssigkeitskühlsystem installiert werden konnte. Nach mehreren Voruntersuchungen wurde ein Großversuch unter jeweils flüssigkeitsgekühlten und trockenen Bedingungen durchgeführt, der sowohl statische als auch Brandlasten einschloss. Die Versuche zeigten die Wirksamkeit des Systems, lasttragende GFK Elemente vor dem sie schwächenden Einfluss hoher Temperaturen, besonders im Druckbereich, zu schützen. Die Feuerwiderstandszeiten des Tragwerks konnten so durch den Einsatz des Flüssigkeitskühlsystems von weniger als einer auf bis zu zwei Stunden erhöht werden (EC1, Teil 1.2).

Neben dem Versuchsprogramm wurde eine Reihe mathematischer Modelle entwickelt. Numerische thermochemische und thermomechanische Modelle simulieren die Antwort belasteter flüssigkeitsgekühlter GFK Profile unter hohen Temperaturen während analytische Modelle das mechanische Verhalten abgebrannter Teilprofile abschätzen. Die Abweichungen der von den Modellen gelieferten Prognosen lagen innerhalb 10% der versuchstechnisch ermittelten Werte.



## Acknowledgements

Over the course of my research, I have been fortunate enough to be supported and inspired by a large group of colleagues and friends. I would like to offer my most sincere gratitude to a few of those exceptional individuals:

- Professor Dr. Thomas Keller for providing the opportunity, for having confidence in me to allow the topic of the thesis to stray so far from our safe roots in structural engineering, for his guidance and council, and for handling all of the peripheral issues related to Ph.D research so that I could focus on the interesting parts.
- Dr. Erich Hugi, Peter Schneulin, Dr. Karim Ghazi-Wakili, and Thomas Frank at the EMPA for the assistance, advice, and sponsorship of the experiments and parts of the numerical investigations, and for trusting me not to burn down their laboratory.
- The Swiss National Science Foundation for providing the funding for the research.
- Martin Marietta Composites and especially Grant Godwin for the generous donation of the experimental materials; Larry Dickinson and Greg Solomon for the technical support.
- The EMPA fire laboratory technicians: Rene Menet and Marco Manfredi, whose efforts were so often rewarded by burns on their hands and noxious smoke in their lungs, and whose inventiveness and dedication were directly responsible for success of the experimental program, and who let me drive the 25 ton overhead crane.
- Dr. Aixi Zhou for his careful review of the experimental and numerical portions of the thesis.
- Professor Dr. Jack Lesko for the discussions on the proposed system and for his valuable input on the numerical models.
- Professor Dr. Manfred Hirt for his participation in the thesis examination.
- Dr. Julia DeCastro and Florian Riebel for the abstract translations, for helping me to improve my level of French from awful by American standards to poor by European standards, and for the friendship.
- Marlène Sommer for the administrative support.
- My mother Charlene Tracy and my sister Jessica Mirzaian for watching my split infinitives and verb tense agreement and for a lifetime of steadfast support and encouragement that is largely responsible for who I am and what I have achieved.

Indeed I am grateful to many people for their contributions, but I must acknowledge the one person whose love and commitment has truly carried me through.

Always remember the distinction between contribution and commitment. Take the matter of bacon and eggs. The chicken makes a contribution. The pig makes a commitment.

- John Mack Carter

I am forever indebted to my wife Alice for her tireless support and understanding, and I promise to make her bacon and eggs until we grow old and fat, and never again to refer to her through a metaphor involving pigs.

# Document Overview

Abstract.....	<i>iii</i>
Version Abrégée.....	<i>iv</i>
Zusammenfassung.....	<i>v</i>
Acknowledgements.....	<i>vii</i>
Table of Contents.....	<i>xi</i>
<b>1. Introduction.....</b>	<b>1</b>
<b>2. FRP Buildings &amp; Building Systems.....</b>	<b>11</b>
<b>3. The State of the Art.....</b>	<b>39</b>
<b>4. The Proposed System.....</b>	<b>117</b>
<b>5. Experimental Investigations.....</b>	<b>149</b>
<b>6. Mathematical Modeling.....</b>	<b>205</b>
<b>7. Conclusion.....</b>	<b>265</b>
Bibliography.....	273
List of Symbols.....	287
List of Figures.....	279
List of Tables.....	295
Curriculum Vitæ.....	299

## Appendix

<b>A. Fire Reaction Experiments - Technical Report.....</b>	<b>301</b>
<b>B. Liquid Cooling Experiments - Technical Report.....</b>	<b>329</b>
<b>C. Structural Fire Endurance Experiments - Technical Report.....</b>	<b>355</b>
<b>D. Numerical Model Source Code.....</b>	<b>407</b>



# Table of Contents

Abstract.....	iii
Version Abrégée.....	iv
Zusammenfassung.....	v
Acknowledgements .....	vii
<b>Ch 1. Introduction .....</b>	<b>1</b>
1. Context and Motivation.....	3
2. Objectives .....	5
3. Methodology.....	5
4. Scope .....	6
5. Terminology.....	6
<b>Ch. 2. FRP Buildings &amp; Building Systems.....</b>	<b>11</b>
1. Background.....	13
2. Chronology.....	15
3. Case Studies .....	24
3.1. <i>Monsanto House of the Future, 1957</i> .....	24
3.1.1. Background.....	24
3.1.2. Description.....	24
3.1.3. Discussion.....	26
3.2. <i>Fiber-Shell System, 1968</i> .....	29
3.2.1. Background.....	29
3.2.2. Description.....	30
3.2.3. Discussion.....	33
4. Conclusions .....	36
<b>Ch. 3. The State of the Art .....</b>	<b>39</b>
1. Introduction.....	41
2. Modern FRP Buildings and Systems .....	42
2.1. <i>Constructed Buildings and Systems</i> .....	42
2.1.1. GE Living Environment Concept House - USA, 1989.....	42
2.1.2. Nestehaus - Finland, 1992.....	44
2.1.3. Advanced Composite Construction System® - UK, 1986-96.....	46
2.1.4. BEET® Building System - Norway, 1993.....	48
2.1.5. Royal Building System® - Canada, 1996 .....	51

2.1.6. American Structural Composites - USA, 1999 .....	53
2.1.7. Eyecatcher Building - Switzerland, 1999.....	54
2.1.8. PDG Domus - USA, 1999.....	56
2.1.9. Ambiente® Housing System - USA, 2000.....	58
2.1.10. Davis Station Living Quarters- Antarctica, 2003 (ongoing).....	60
2.1.11. Spacebox® - Netherlands, 2004.....	62
2.2. <i>Concepts and Design Exercises</i> .....	63
2.2.1. Dock Tower - Switzerland, 2002 .....	63
2.2.2. Woven Building - USA, 2002.....	65
2.2.3. ASSET Supaflor® - Denmark, 2002 .....	67
2.2.4. Sphere - UK, 2004.....	69
2.3. <i>Conclusions: Modern FRP Buildings and Building Systems</i> .....	71
3. Fire Safety for Fiber-Reinforced Polymeric Structures .....	74
3.1. <i>Definition of the Problem</i> .....	74
3.1.1. Objectives of Fire Safety Measures .....	74
3.1.2. Building Fire Codes .....	75
3.1.3. Combustibility of FRP Materials .....	78
3.1.4. Temperature Dependence of FRP Material Properties .....	80
3.1.5. Heat-Induced Damage Mechanisms .....	82
3.2. <i>Solution Methods</i> .....	83
3.2.1. Passive Fire Safety Measures.....	84
3.2.2. Active Fire Safety Measures.....	95
3.3. <i>Conclusions: Fire Safety for FRP Structures</i> .....	99
4. Numerical and Analytical Modeling of FRP in Fire .....	102
4.1. <i>Fire Exposure Models</i> .....	102
4.2. <i>Post-Fire Mechanical Models</i> .....	103
4.3. <i>Thermochemical Models</i> .....	106
4.4. <i>Thermomechanical Models</i> .....	112
4.5. <i>Conclusions: FRP in Fire Modeling</i> .....	115
<b>Ch. 4. The Proposed System</b> .....	<b>117</b>
1. Introduction.....	119
2. General Description .....	121
2.1. <i>Basic Wall Element</i> .....	121
2.2. <i>Basic Floor Element</i> .....	122
2.3. <i>Selected Geometrical Characteristics</i> .....	123
2.3.1. Wall Element.....	123
2.3.2. Floor Element:.....	123
3. Structural Concept .....	124
3.1. <i>Global Building Stability</i> .....	124
3.2. <i>Flooring System Structural Concept</i> .....	125
3.3. <i>Wall System Structural Concept</i> .....	128

---

4.	Production and Assembly.....	130
4.1.	Industrial Fabrication .....	130
4.2.	On-Site Assembly.....	131
5.	Architectural Functions.....	133
5.1.	Shelter.....	133
5.2.	Form.....	133
5.3.	Surface Treatments.....	133
5.4.	Natural Lighting.....	134
5.5.	Building Acoustics.....	135
6.	Mechanical Services.....	136
6.1.	Heating and Cooling System .....	136
6.1.1.	Emitters.....	137
6.1.2.	Distribution .....	140
6.1.3.	HCS Sources.....	141
6.1.4.	Control.....	141
6.2.	Ventilation, Plumbing, and Electrical.....	141
7.	Building Physics.....	143
7.1.	Steady-State Heat Transfer.....	143
7.2.	Transient Heat Transfer.....	143
7.3.	Thermal Mass.....	144
8.	Conclusions .....	147
<b>Ch. 5.</b>	<b>Experimental Investigations .....</b>	<b>149</b>
1.	Introduction.....	151
2.	Materials .....	152
2.1.	Physical Description .....	152
2.2.	Production Method .....	153
2.3.	Constituent Materials.....	154
2.4.	Adhesives .....	156
3.	Facilities.....	157
3.1.	Coupon-Level Experimental Facilities.....	157
3.2.	Small Horizontal Oven .....	157
3.3.	Large Horizontal Oven.....	158
4.	Fire Loading Regimes.....	160
5.	Thermal and Thermomechanical Property Experiments.....	161
5.1.	Dynamic Mechanical Analysis.....	161
5.1.1.	Basic Principles.....	161
5.1.2.	Description of Technique.....	161
5.1.3.	DMA Performed .....	162

5.1.4. Results .....	162
5.2. <i>Thermogravimetric Analysis</i> .....	163
5.2.1. Basic Principles .....	163
5.2.2. Description of Technique .....	164
5.2.3. Results .....	164
5.3. <i>Steady-State and Transient Heat Flow Analysis</i> .....	165
5.3.1. Basic Principles .....	166
5.3.2. Description of Technique .....	166
5.3.3. Summary of Results .....	168
6. Fire Reaction Experiments.....	169
6.1. <i>Objectives and Motivation</i> .....	169
6.2. <i>Materials</i> .....	169
6.3. <i>Procedure</i> .....	170
6.4. <i>Post-Experimental Inspection of Specimens</i> .....	171
6.5. <i>Discussion of Results</i> .....	172
6.6. <i>Conclusions from the Fire Reaction Experiments</i> .....	174
7. Liquid Cooling Experiments .....	175
7.1. <i>Objectives and Motivation</i> .....	175
7.2. <i>Experimental Set-up</i> .....	175
7.3. <i>Description of Specimens</i> .....	176
7.4. <i>Experimental Procedure</i> .....	177
7.5. <i>Results</i> .....	178
7.5.1. Lower Face Sheet Temperatures.....	178
7.5.2. Water Temperatures .....	179
7.5.3. Post-Experimental Inspection of Specimens.....	180
7.6. <i>Discussion of Results</i> .....	180
7.6.1. Comparison to the Fire Reaction Experiments.....	180
7.6.2. Heat Transfer to Water.....	181
7.6.3. Internal Pressure .....	184
7.7. <i>Conclusions from Liquid Cooling Experiments</i> .....	184
8. Structural Fire Endurance Experiments .....	185
8.1. <i>Objectives</i> .....	185
8.2. <i>Materials</i> .....	185
8.3. <i>Experimental Set-up</i> .....	186
8.3.1. Oven.....	186
8.3.2. Liquid Cooling System .....	186
8.3.3. Structural Loading.....	187
8.3.4. Instrumentation.....	188
8.4. <i>Procedure</i> .....	189
8.5. <i>Results</i> .....	190
8.5.1. Deflections.....	190
8.5.2. Strains.....	191
8.5.3. Specimen Temperatures.....	192

---

8.5.4. Water Temperatures.....	193
8.5.5. Structural Damage and Permanent Deformations .....	194
8.5.6. Post-Fire Strength and Stiffness.....	196
8.6. <i>Discussion of Results</i> .....	197
8.6.1. Strains .....	197
8.6.2. Stiffness Reduction.....	198
8.6.3. Heat Transfer to Water .....	198
8.6.4. Failure of SLC03.....	201
8.6.5. Liquid Cooling.....	201
8.7. <i>Conclusions from the Structural Fire Endurance Experiments</i> .....	202
9. Conclusions from Experimental Program.....	204
<b>Ch. 6. Mathematical Modeling.....</b>	<b>205</b>
1. Introduction.....	207
2. Analytical Mechanical Modeling .....	208
2.1. <i>Undamaged Section at Ambient Temperature</i> .....	208
2.1.1. Applied to Experimental Specimens .....	208
2.1.2. Applied to Proposed Flooring System.....	209
2.2. <i>Fire-Damaged Section at Ambient Temperature</i> .....	215
2.2.1. Two-Layer Model.....	216
2.2.2. Three-Layer Model.....	219
2.3. <i>Post-Fire Safety of the Proposed System</i> .....	223
2.3.1. Loads.....	224
2.3.2. Resistance.....	225
2.3.3. Resistance Factor of Safety.....	225
3. Numerical Modeling.....	227
3.1. <i>Numerical Thermochemical Model</i> .....	228
3.1.1. General Description .....	228
3.1.2. Geometrical Simplifications.....	229
3.1.3. Boundary Conditions .....	230
3.1.4. Special Considerations.....	235
3.1.5. Material Properties .....	239
3.1.6. Meshing .....	241
3.1.7. Governing Equations.....	241
3.1.8. Results.....	242
3.2. <i>Numerical Thermomechanical Model</i> .....	245
3.2.1. General Description .....	245
3.2.2. Justification for Thermal-Mechanical Coupling.....	247
3.2.3. Geometrical Simplifications.....	247
3.2.4. Mechanical Boundary Conditions .....	248
3.2.5. Thermal Boundary Conditions.....	249
3.2.6. Structural Load.....	251
3.2.7. Thermal load.....	251

3.2.8. Material Properties.....	251
3.2.9. Meshing.....	256
3.2.10. Governing Equations .....	256
3.2.11. Results .....	257
4. Conclusions.....	262
<b>Ch. 7. Conclusion .....</b>	<b>265</b>
1. Overview.....	267
2. From Existing FRP Buildings to the Proposed System .....	267
3. Experimental Investigations.....	268
4. Mathematical Modeling .....	269
5. Suggested Future Work.....	270
<b>Bibliography .....</b>	<b>273</b>
<b>List of Symbols .....</b>	<b>285</b>
<b>List of Figures .....</b>	<b>287</b>
<b>List of Tables.....</b>	<b>295</b>
<b>Curriculum Vitæ .....</b>	<b>299</b>

## Appendix

<b>Ch. A. Fire Reaction Experiments - Technical Report.....</b>	<b>301</b>
1. Motivation and Summary.....	303
2. Origin, Preparation, and Description of Specimens .....	303
3. Experiment Proceedings .....	304
4. Post-Experiment Inspection of Specimens .....	305
5. Discussion of Results.....	305
<b>Ch. B. Liquid Cooling Experiments - Technical Report.....</b>	<b>329</b>
1. Motivation and Summary.....	331

2.	Description of Specimens.....	332
2.1.	<i>Origin and Description of Basic Elements</i> .....	332
2.2.	<i>Instrumentation</i> .....	332
3.	Experimental Set-up.....	333
4.	Experimental Proceedings.....	334
4.1.	<i>Selection of Water Flow Rates</i> .....	334
4.2.	<i>Duration of Experiments</i> .....	334
4.3.	<i>Temperature Loading</i> .....	334
5.	Post-Experimental Inspection of Specimens.....	335
6.	Discussion of Results.....	335
6.1.	<i>Comparison to Charring Experiments</i> .....	335
6.1.1.	Damage to Hot Faces.....	335
6.1.2.	Temperature Profile.....	336
6.2.	<i>Heat Transfer to Water</i> .....	336
6.3.	<i>Internal Pressure</i> .....	337
7.	Conclusions.....	338
<b>Ch. C. Structural Fire Endurance Experiments - Technical Report</b> .....		<b>355</b>
1.	Motivation and Summary.....	357
2.	Origin and Description of Specimens.....	358
2.1.	<i>Description of Materials</i> .....	358
2.2.	<i>Origin of Specimens</i> .....	358
2.3.	<i>Preparation of Specimens</i> .....	358
2.4.	<i>Instrumentation</i> .....	359
3.	Experimental Set-up.....	361
3.1.	<i>Oven Preparation and Support Conditions</i> .....	361
3.2.	<i>Liquid Cooling System</i> .....	361
3.3.	<i>Loading system</i> .....	362
4.	Design of the Experiment.....	363
4.1.	<i>Selection of Flow Rates</i> .....	363
4.2.	<i>Selection of Load</i> .....	363
4.3.	<i>Duration of Fire Exposure</i> .....	364
4.4.	<i>Temperature Loading</i> .....	364
4.5.	<i>Experimental Procedure</i> .....	364
4.6.	<i>Experimental Notes</i> .....	365
4.6.1.	SLC01 Notes.....	365
4.6.2.	SLC02 Notes.....	366
4.6.3.	SLC03 Notes.....	367

5.	Post-Fire Inspection of Specimens.....	367
5.1.	SLC01.....	368
5.2.	SLC02.....	368
5.3.	SLC03.....	369
6.	Discussion of Results.....	369
6.1.	Measurement of Deflections.....	369
6.2.	Prediction of Initial Deflections.....	370
6.3.	Strains.....	372
6.4.	Stiffness Reduction.....	373
6.5.	Loss of Cross-Section.....	374
6.5.1.	Two-Layer Model.....	374
6.5.2.	Three-Layer Model.....	375
6.6.	Leakage of SLC01.....	376
6.7.	Failure of SLC03.....	377
6.8.	Liquid Cooling.....	377
6.9.	Experimental Set-up and Procedure.....	377
6.9.1.	Areas for Improvement.....	377
6.9.2.	Successful Innovations.....	378
7.	Conclusions.....	379
8.	Appendix.....	380
<b>Ch. D.</b>	<b>Numerical Model Source Code.....</b>	<b>407</b>
1.	Thermochemical Model Source Code for ANSYS 7.0.....	409
2.	Thermomechanical Model Source Code for ANSYS 7.0.....	413

# 1

## **Introduction**



## 1 Context and Motivation

Historians distinguish each stage of human civilization by the technology of its day. From stone to semiconductors, new materials have helped to take man from the Stone Age to the Information Age. Yet even today, the overwhelming majority of buildings are constructed from materials and in methods that have remained essentially the same over the past hundred years. Indeed iron has given way to steel and masonry has been largely replaced by reinforced concrete, but one can still imagine that an Ancient Roman laborer would not feel entirely lost on a modern construction site.

Though very few fundamental advances in the conception of buildings have been made in the past century, significant efforts have been made to improve traditional building methods. In most cases, these improvements have been made at the expense of more components, more skilled trades, more stages, and, in general, more complication. Thanks to the work of influential engineers and architects such as D.H. Burnham, J. Root, W.L. Jenny, and L. Mies van der Rohe, the single-layer masonry wall has given way to the 5-10 layer curtain wall system commonly found in modern buildings. New layers have been added over the years to improve the thermal performance, weathering resistance, durability, and safety of buildings. Each layer is added to perform a function for which the other layers are not well suited. As building performance standards and expectations continue to increase, the number of layers and components is likely to increase as well.

The fundamental disadvantage with this methodology is that as buildings become more complex and the amount of work performed on the construction site increases, so does the construction costs and the potential for the introduction of flaws. Modern building methods are an unfortunate compromise between what is easy to build (simple single-layer systems) and what provides the best performance over the life of the building (complex multiple layer systems). High performance, high-quality buildings cannot be built from simple single-layer components using traditional construction materials because the materials themselves are not suited to perform multiple functions. For example, the high strength and stiffness of steel make it ideal for load-bearing functions, but its high thermal conductivity make it a poor choice for thermal insulation. Using traditional materials such a steel and concrete, improvements in building performance will almost always come at the cost of more complexity during construction.

Since their discovery in the early 20th century, many have seen synthetic polymers and especially fiber-reinforced synthetic polymers (FRP) as the materials that could simultaneously permit the simplification of the construction process and the improvement of long-term

building performance. Thanks to their high specific strength, low thermal conductivity, good environmental resistance, and their ability to be formed into complex shapes, FRP materials are well-suited to fulfilling many building requirements. By integrating several layers into single function-integrated components and industrially fabricating those components, the amount of on-site labor can be greatly reduced. Further, by integrating the load-bearing system with the building envelope, greater efficiencies can be achieved in material usage and in-service energy costs. Overall, FRP materials have a strong potential for fueling the next great advance in the conception of buildings.

Unfortunately, the early attempts to implement this conviction in 1950's, 60's and 70's were mostly unsuccessful. In general, the projects were defeated by the insufficient treatment of the unique weaknesses of FRP materials. More specifically, efficient solutions were not found to ensure adequate fire safety and the higher material costs were not mitigated by savings in other respects. These problems were compounded by an array of social, legislative, and economic issues, including the general perception of plastics as low-quality substitute materials, the existence of exclusive material-specific "prescriptive" building codes, and the inflation of crude oil prices.

A new generation of experimentation with load-bearing FRP buildings began in the late 1980's and continues to gain momentum. Thanks to such efforts (and a host of other factors beyond control of building designers), the social and legislative issues that burdened the first generation of projects are slowly diminishing. With respect to the perception of plastics, the use of FRP materials in high-performance luxury items (sports cars, yachts, golf clubs, etc.) and high-technology applications (space vehicles, biological prosthetics, etc.) has helped to establish advanced composites as highly desirable materials instead of low-cost substitutes for "better" traditional materials. Good progress in overcoming the legislative barriers is also being made as performance-based building codes gradually replace prescriptive codes. Thus, the only remaining issues that significantly obstruct the realization of an advanced FRP building system are the problems of fire safety and high material cost.

The next fundamental advance in the conception of buildings will involve the simplification of on-site construction and the increased use of industrially fabricated components. The multifaceted strengths of FRP materials make them ideally suited to the production of such components. The exploitation of these many strengths is, however, only half of the winning equation. In order to successfully implement this concept where previous attempts have failed, efficient and reliable solutions will be needed to mitigate the unique weaknesses of FRP materials.

## 2 Objectives

The objective of the research program is to develop concepts for a multiple-story<sup>1</sup> building system using primarily FRP in a *material-adapted* manner, i.e. in a manner that best exploits the strengths of the material while mitigating its weaknesses. These concepts were to be advanced to a level that meets the following list of developmental landmarks:

- Detailed evaluation of structural fire safety
  - Definition of the fire safety requirements and objectives
  - Evaluation of the available methods of satisfying these requirements and objectives
  - Specification of existing methods where possible
  - Development of new methods where necessary
- General design
  - Basic design of major structural components, including shapes, materials, connection methods, and dimensions
  - Definition of the global structural system for building stability
  - Basic consideration of architectural concerns, including shelter, light, occupancy, and surface treatments
  - Description of production and assembly techniques
  - Basic consideration of building physics, including thermal insulation and weather resistance of the building envelope, interior climate control, and human thermal comfort
  - General layout of mechanical systems, including distribution of heat, electricity, light, and fresh air

## 3 Methodology

In order to make the most efficient use of energy and resources, a strong emphasis was placed on resolving the issues that most hinder the success of multiple-story FRP building systems. Thus, the first step was to define these issues through a study of the historical and current

---

1. The term “multiple-story” is used within this thesis to refer to buildings with multiple *elevated* stories and thus designates buildings with a minimum of two stories above the ground level.

projects related to the structural use of FRP in buildings. Next, the existing methods of resolving these issues were studied. Wherever possible, the most appropriate and effective existing solutions were adapted or directly prescribed for the proposed system. Wherever existing solutions were not available or not appropriate within the material-adapted approach, new solutions were conceived. For the new solutions that were without precedent, experimental and numerical methods were pursued to establish their feasibility. The final form of the proposed building system is the result of the integration of all of these existing and new solutions.

## **4 Scope**

From the social climate of the 1960's to the chemistry of polymerization, the subjects involved in this thesis are as diverse as they are numerous. This is the inescapable consequence of the many fundamental choices that are made in the conception of a totally new building system. As such, this thesis was not intended to be an exhaustive optimization of every aspect of the multiple-story FRP building system that is proposed herein, but a first step that substantially establishes the feasibility of such a system.

As described in the previous section, many aspects of the system were inspired by well-established principles and practices. For such aspects, a basic evaluation was sufficient to demonstrate their feasibility. The solution involving the integrated structural fire protection and the climate control systems, however, is largely unprecedented in conjunction with FRP materials and thus required a more thorough evaluation. Accordingly, a large portion of the research program was devoted to the study of the structural fire protection concept with the expectation that the climate control aspect would be studied by future researchers.

## **5 Terminology**

Unfortunately, many scientific and engineering terms are also used in common language with different or less specific meanings. Even within the scientific community, though, there are sometimes several conventions that are followed because a general consensus has not been reached. Therefore, in the effort of clarity, some of these somewhat ambiguous or often misunderstood terms that relate to the topics in this thesis are defined below.

### *Matrix / Resin:*

The *matrix* is the binder material that envelopes the reinforcement in a *composite* material (see definition below). *Resins* are one of the many ingredients in matrix materials (along with fillers, curing agents, mold release agents, stabilizers, etc.) and are composed of polymers.

### *Polymer / Plastic:*

*Polymers* are a broader category that contain a wide range of materials, all of which having a long chain structure consisting of thousands or millions of repeated molecules. Carbohydrates, rubbers, and DNA are all polymers. The precise definition of the term *plastic*, however, is less clear. Some chemistry dictionaries indicate that plastics are only the *thermoplastic* subcategory of polymers, while others indicate that they must be organic. The only consensus seems to be that plastics can only *synthetic* polymers, i.e. not naturally occurring. In general, the confusion of the scientific community is magnified tenfold in the general population, thus the term *plastic* has been avoided in this text wherever possible.

### *FRP / PMC*

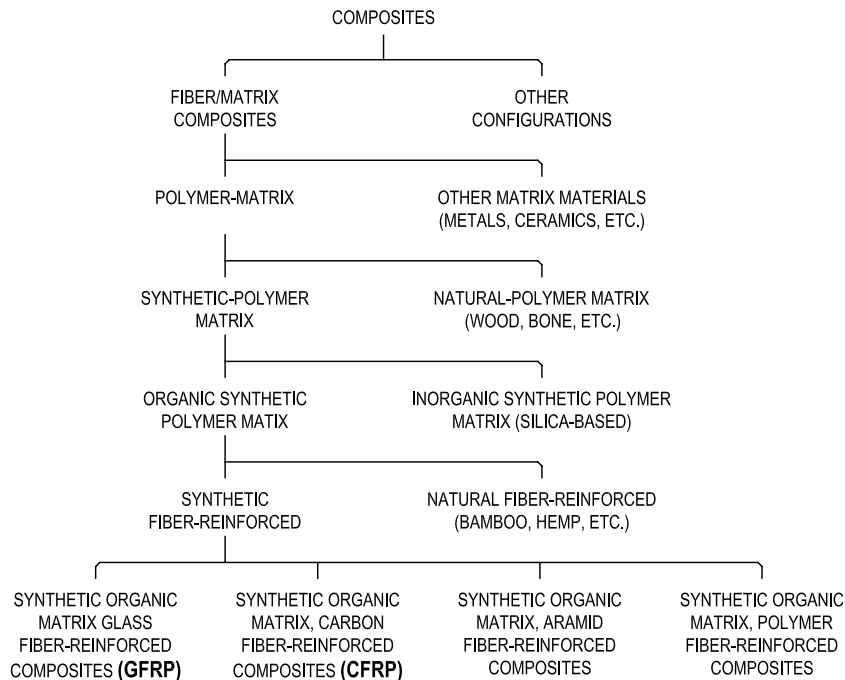
These abbreviations refer to the same material: composites consisting of fiber reinforcement and polymer matrices. *FRP* stands for *fiber-reinforced polymer* (also *fiber-reinforced plastic* - see the previous heading for an explanation of why this term is avoided), and *PMC* stands for *polymer-matrix composite*. Neither is more correct than the other, and usage appears to be a matter of tradition and preference. Additional variations of the terms may specify the exact reinforcement, such as *GFRP* or *CFRP* to specify glass or carbon fiber, or to indicate the production method, such as *PFRP* to indicate composites produced by pultrusion.

Beyond the series of abbreviated terms, there is a vast array of strings that mean essentially the same thing: *fiber-reinforced polymer*, *fiber-reinforced plastic*, *polymer-matrix composite*, *fiber-matrix composite*, *organic-matrix composite*, and *synthetic-resin composite*, etc. The term FRP or fiber-reinforced polymer will be used in place of all of these for the remainder of this text.

### *Composite / Advanced Composite*

*Composites* include an enormous range of materials, though the word is often used to specify the subcategory of FRP composites. Composites are substances composed of multiple materials of which large units (on a molecular scale) remain chemically separate, but act in many ways as a single material. FRP materials are only one of many materials that fit this description. The Figure 1-1 illustrates the situation of the FRP materials within the family of composites.

Figure 1-1. FRP vs. composite materials



As shown, the term *composites* can apply to carbon nano-tube reinforced epoxy resin, straw-reinforced mud bricks, or simply wood. For this reason, the term *advanced composites* is sometimes used to exclude these other materials.

### *Thermal Conductivity / Thermal Conductance / Heat Transfer Coefficient / Thermal Resistance / Thermal Transmittance / R-Value / U-Value*

These terms are easily confused because they all refer to the transfer of heat through materials and definitions vary slightly by country and industry. In general, the *thermal conductivity* is a material property that describes the rate of heat flow through a **unit** area over a **unit** time when subjected to a 1°C temperature gradient. It is represented by the greek symbol  $\lambda$  (or  $k$ ) and given in the units W/m·K. *Thermal conductance* is very similar to  $\lambda$  but is used for a **finite** area and **finite** thickness of a material, and is thus a system property rather than a material property (units W/K). The *heat transfer coefficient* refers to the radiation and convection conditions at the surface of a structure. It is represented by the letter  $h_r$  or  $h_c$  and is given in the units W/m<sup>2</sup>·K.

The previous terms are primarily used in science and engineering, while the following terms are more often used in the building industry. They are linked to specific arrangements of materials, including all layers, air gaps, and surface conditions, and are thus system properties. The *thermal transmittance* or *U-value* incorporates both the thermal conductance and heat transfer coefficients of a particular assembly, such as a wall structure or window frame. The terms

*thermal resistance* and *R-Value* are synonymous and are the reciprocal of the thermal transmittance.

As stated, these values are easily confused and their definition varies by location and industry. Thus, wherever possible, descriptions will be made in terms of the basic values of thermal conductivity,  $\lambda$ , and heat transfer coefficient,  $h$ .

### *Heat Flux / Heat Flow Rate / Total Heat / Heat Generation Rate*

This list of values is confusing because they all are represented by letter  $Q$  or  $q$  and refer to the transfer of energy as heat. The *heat flux* is the amount of energy being transmitted as heat per **unit area**. It is represented by the symbol  $q$  and given in the units  $\text{W}/\text{m}^2$ . The *heat flow rate* is the rate of energy being transmitted as heat through a **finite area**. It is represented by the symbol  $Q_{dot}$  and given in the units  $\text{W}$ . The *total heat* is the total amount of energy transferred to a system, which is represented by the symbol  $Q$  and given in the units  $\text{J}$ . Finally, the symbols  $q_d$ ,  $q_w$ , and  $q_{gen}$  represent the total amount of heat generated or consumed per unit mass (units  $\text{kJ}/\text{kg}$ ) through a reaction. The first two symbols refer to the decomposition of polymers and the vaporization of water, respectively, while the third symbol is a general term for any heat generation or consumption reaction.

### *Emissivity / Emittance / Absorptance / Reflectance*

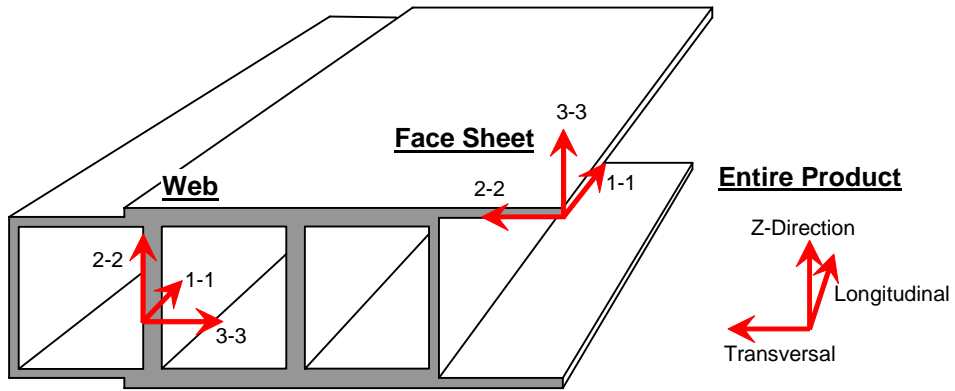
These terms all refer to radiation between surfaces or between a surface and the environment. *Emissivity* and *emittance* are synonymous and describe the ability of a surface to emit radiation relative to a perfectly emitting “black body.” They are represented by the symbol  $\epsilon_r$  and given as a unitless number between 0 and 1. Similarly, the *absorptance* is the ability of a surface to accept radiation relative to a perfectly absorbing “black body”, represented by the symbol  $\alpha_r$ . Finally, the *reflectance*,  $\rho_r$ , is the ability of a surface to reflect radiation. The three are related in that emissivity equals absorptance and the two are the inverse of the reflectance.

### *Longitudinal / Transversal / Z-direction / 1-1 / 2-2 / 3-3*

All of these terms refer to directions within different coordinate systems. Two scales are considered: the assembly/product, and the material. On the assembly/product scale, the longest dimension is termed the *longitudinal* direction. The second largest dimension is termed the *transversal*, and the shortest dimension is the *Z-direction* (see Figure 1-2).

On the material scale for FRP, the direction in which the most reinforcement is oriented is the  $1-1$  direction. The second direction in which reinforcement is oriented is termed the  $2-2$  direction. Finally, the  $3-3$  direction is the direction in which the least reinforcement is oriented.

Figure 1-2. Global and local coordinate systems



# 2

## **FRP Buildings & Building Systems**

*Historical Development*



## 1 Background

The development of synthetic polymers can be traced back to Leo Hendrik Baekeland's patent for the synthesis of Bakelite in 1907. This first phenol-formaldehyde (PF) resin was gradually joined by other key polymers such as polystyrene (PS), polyamide (PA, *Nylon*), polyvinyl chloride (PVC), and melamine formaldehyde (MF). In the decades that followed, these new materials found use in a myriad of old and new products, though their penetration in the construction market was limited to superficial components such as electrical insulation, floor coverings, counter tops, and vapor barriers [127 pg. 206].<sup>1</sup>

Later in the 1940's, military interest in stronger and lighter new materials lead to experimentation with the reinforcement of synthetic polymers by various high-strength fibers. Glass fiber, already produced as an insulation material, possessed the perfect characteristics for this application. By the end of the WWII, the aerospace community had successfully developed and tested FRP materials for use in filament-wound rocket engines and other structural members in airplanes. Some short years later, the boat industry adopted the technology to build stronger, lighter, and more corrosion resistant hulls [84 pg. 4]. It took another ten years, however, until the construction industry began any significant experimentation with the use of FRP's as the primary structural material in buildings.

“Demonstration houses were built of plastics materials in a number of countries... from as early as 1933, but these were all limited exercises in the obvious use of currently-available plastics materials, and were often merely publicity vehicles for a certain manufacturer's product range. This type of house still goes on, and still makes as little contribution to plastics in architecture as it ever did.”

Arthur Quarmby, 1974

The leap to structural service was finally made in the context of the cultural and demographic changes occurring in 1950's America. In Europe as well, a decade of war left many countries in urgent need of new housing [30 pg. 136]. In America, people were moving out of the cities and into the newly invented suburbs. Planned communities such as the famous Levittown comprised much of the over two million homes being built every year [50]. But despite these efforts, a vast housing shortage ensued along with a strain on the supply of building materials.

For the victors of World War II, the 1950's were also a time of great pride, optimism for the future, in technology, and in progress. Advertisers began to refer to the “Jet Age” as people

---

1. Special exception can be made for phenolic resin glues that allowed the production of tougher and more weather-resistant plywoods, which had a profound effect on the construction industry.

embraced Norman Bel Geddes' "Futurama" visions of the world [194]. Synthetic polymers not only fit into this vision, but also came to be its most enduring symbol.

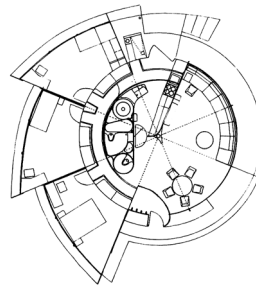
At the same time, powerful chemical companies such as Dow, Monsanto, and BASF were searching for new markets for their materials. The shortage of housing and of traditional building materials (most notably wood) combined with this emerging vision of the future seemed to provide the perfect conditions for the introduction of a fiber-reinforced polymer home. The 1950's and 60's saw the construction of approximately seventy prototype FRP homes, with a scarce few actually going into production. The most notable of these models will be discussed in the following chapter.

## 2 Chronology

This section lists some of the significant buildings from the 1950's to the 1970's that incorporated load-bearing FRP elements.

**Year**    *Project Title* – Architect/Engineer – Location

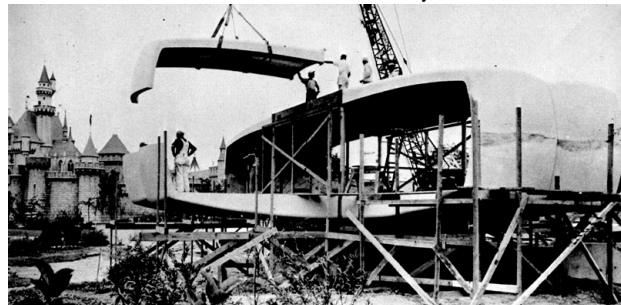
1956    *Maison en Plastique* – Ionel Schein, Yves Magnant, René Coulon – France



Regarded by many as the first building to use FRP in load-bearing elements, the prototype was designed for the Salon des Arts in Paris. Following a modular approach and gaining inspiration from the shell of a snail, the house consisted of a circular core that could be enlarged by the addition of modules around the perimeter [155 pg. 46]. All of the exterior walls, partitions, floors, and roofs were made from FRP sandwich panels. The continuous bonding of the acrylic windows allowed them to become part of the load-bearing system. Furniture and bathroom utilities were built-in from synthetic polymers as well. The structure was entirely demountable, being disassembled and reassembled fifteen times in its career [116 pg. 58].

---

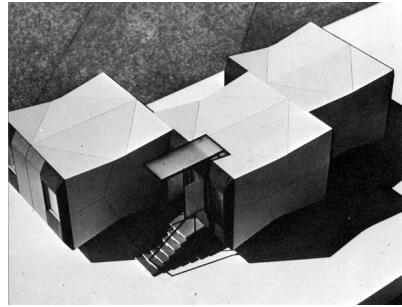
1956    *Monsanto House of the Future* – Richard Hamilton, Marvin Goody, A. Dietz – USA



Refer to Section 3.1 for details of this project.

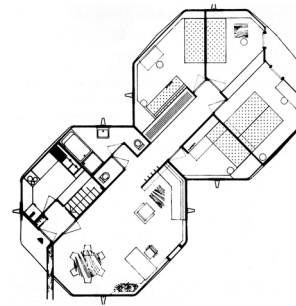
---

1957 Untitled – Cesare Pea – Italy



This prototype was built for the XI<sup>th</sup> Milan Exhibition (Triennale at Milan). 4.8 m square boxes 2.7 m tall were constructed from glass-reinforced polyester with a honeycomb paper core. The design allowed for different arrangements of the units, as well as the addition of units as required. One notable aspect was the integration of the heating, air-conditioning, and ventilation system. Some units included electrical heating elements in the face sheets of the walls and floors using a graphite-coated glass fiber cloth, while others passed air ducts through the cores of the walls and floors [116 pg. 58].

1958 *Schalenhaus Doernach* – Rudolph Doernach – Germany



Germany's first FRP system was displayed at the Stuttgart Plastics Exhibition. This design also followed the modular approach, using four identical panels to form a hexagonal space. An early model consisted of a foam core laminated to aluminum face sheets, while later models were produced from GFRP laminate face sheets and a coated paper honeycomb core [116 pg. 59], [155 pg. 62]. 9 m spans created a 50 m<sup>2</sup> floor plan, and larger structures were created by connecting other hexagonal units. Some models incorporated a system of tubes through the honeycomb core that, when filled with a liquid, increased the fire resistance, added thermal mass, and improved the sound insulation (though the system still did not achieve the F30 fire resistance required by code). Differential solar heating caused a disturbing cracking sound as

the bents realigned along their pop-riveted joints. In addition, the steel pop-rivets eventually rusted and stained the white exterior surfaces [45 pg. 24].

---

1960 *Polyvilla* – J. Ladyjenski, S. A. Sodibat – Belgium



Approximately 250 units of this type were built between the years of 1960 and 1973, which represented the largest production of FRP homes in the world. The skeleton of the structure consisted of PVC tubes filled with concrete in the factory. The 2.0 m tall by 2.6 m wide wall panels incorporated glass-reinforced polyester face sheets and a phenolic foam core to create a 50 mm thick sandwich structure [163 pg. 23].

---

1961 *Signal Relay Room System* – Arthur Quarmby, Mickleover Ltd. – England



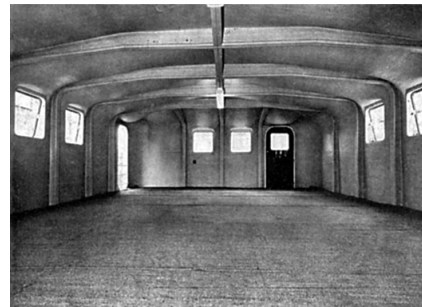
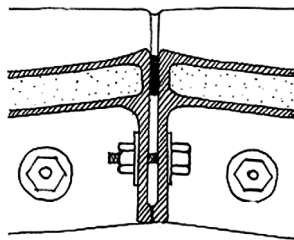
Built to house new electrical equipment for the Eastern Region of British Railways, the system was designed to allow the quick installation of weatherproof, expandable, low-maintenance shelters in a variety of shapes and sizes. The shell elements were fabricated from glass-reinforced FRP face sheets bonded to a phenolic foam core. Connections were made via bolts through the solid polyester flanges. In all, nearly 300 signal relay rooms were built using the system [155 pg. 60].

---

1962 Untitled – USSR

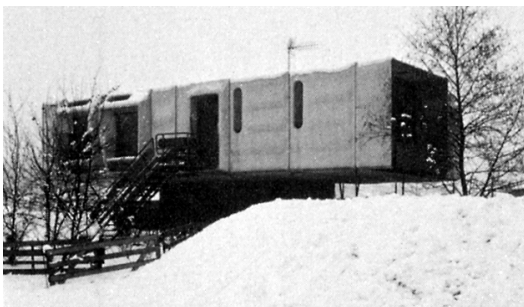
This first Russian prototype revealed the government's strong interest in prefabricated housing. The design attempted to recreate the standard family-sized apartment in a single stackable unit. Many western architects disapproved of the approach, as it did not allow any diversity of form or arrangement. The structure, however, seemed to be successful in its use of foam/GFRP laminate sandwich construction. Its presence in Leningrad had much influence on later FRP housing designs in Poland and Hungary [197 pg. 58].

1963 *Telephone Exchange Room* – Mickleover Ltd. – UK

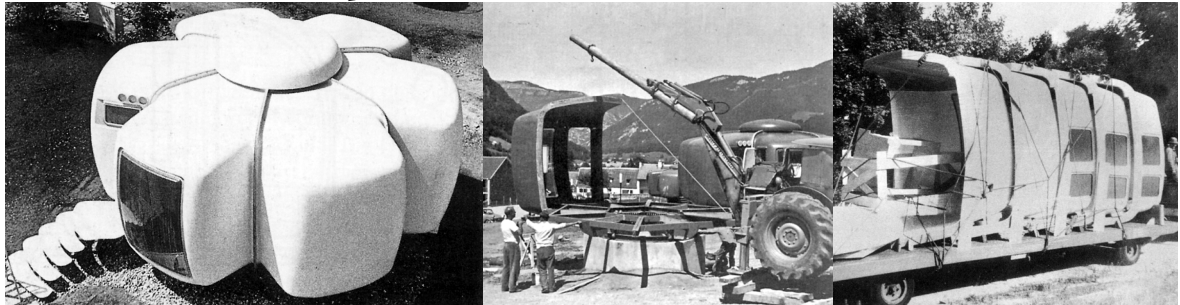


Further developing the design of the Signal Relay Room System, Quarmby and Mickleover designed a two-story system for the Bakelite corporation. In the same year, a thicker-walled version of the system was erected as a biological research laboratory for the British Antarctic Survey [155 pg. 59]. Through the use of phenolic foam and fire-retarded polyester resins, both the relay room system and the two-story system achieved a Class 1 surface flame spread rating according to British Standard 476 [197 pg. 62].

1965 *All Plastic House* – Dieter Schmid – Italy

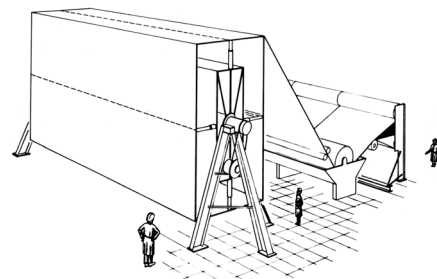


This prototype was built using FRP sandwich panels. The foundation consisted of steel columns and a concrete automobile garage [45 pg. 40], [59 pg. 141].

1967 *Orion / Bulle Six Coques* – Jean Maneval, Gérard Ifert, Rudolf Meyer – France

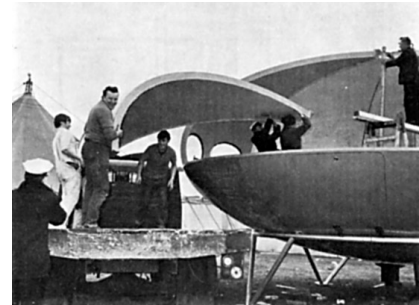
Taking notes from the Monsanto House, Orion's designers chose the modular approach to minimize on-site assembly. An entire house was transported on a single truck with the six bubble-shaped elements stacked horizontally. A concrete foundation and steel beams were built on-site to receive the elements, which were lowered into place by a small crane, bolted together, and then topped off with an FRP cupola. The FRP elements themselves were composed of fire-retarded glass-reinforced polyester face sheets bonded to a polyurethane foam core [45 pg. 48]. Movable and fixed windows were made of an acrylic resin. An electrical heating system was installed in the factory. Bathroom and kitchen units were also prefabricated, as well as all of the furniture inside. Different combinations of sleeping, kitchen, bathroom, and living room units were achieved by the choice of the elements [8 pgs. 52-9].

The first appearance of the houses was in a vacation village in the high Pyrenees town of Gripp, where 20 units were erected. One unit received particular notoriety for being mounted on an electrical motor-powered rotating base. Approximately ten other units were built up until production ceased in 1970 [200].

1968 *Fiber-Shell* – Ezra Ehrenkrantz, TRW Systems Corporation – USA

Refer to Section 3.2 for details of this project.

1968 *Futuro* – Matti Suuronen, Yrjö Ronkka – Finland



Perhaps one of the best-known examples of FRP structures, Futuro was a modular structure that was initially designed to satisfy a very specific niche. The goal was to create a ski lodge that had good thermal insulation, was easy to assemble on rough terrain, and could be quickly warmed-up. Suuronen's experience in FRP dome structures clearly influenced the final form, which many have likened to a flying saucer. The walls were composed of glass-reinforced polyester face sheets bonded to a polyurethane foam core. The structure was assembled by bolting the eight lower and eight upper panels together upon its tubular steel base. An electric heating system was reportedly capable of bringing the interior temperature to a comfortable level amidst Finnish winter conditions in under thirty minutes [87].

The prototype gained worldwide attention at various building expositions and manufacturing licenses were sold to companies in twenty countries. In the years that followed, the roughly sixty Futuro's that were built found service in the commercial, residential, hospitality, and military sectors. Despite its cult-like popularity, the project was a financial failure, suffering from high costs, poor business management, and a lack of consumers willing to accept its quirky appearances. Fire resistance of the system is unspecified, though it interesting to note that significant modifications were made in this respect for the units that were manufactured for the military [113].

1968 *Kunststoffhaus / fg 2000 System* – Wolfgang Feierbach – Germany

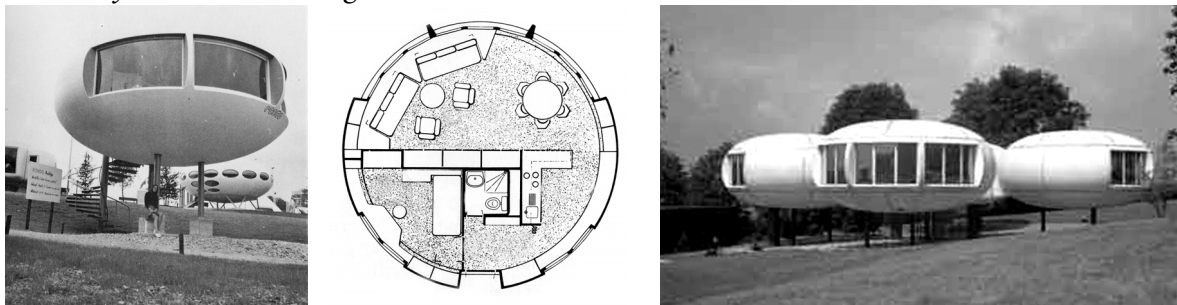


Among the speediest of assembly systems, workers assembled the 26 wall and 13 roof elements in one day, without heavy lifting equipment. Rejecting the modular approach of previous FRP projects, the segmental approach was adopted to allow greater design flexibility. The elements were produced from 5 mm thick glass-reinforced polyester face sheets bonded to a 70 mm polyurethane foam core [8 pg. 101]. The interior surfaces were covered with flame-retarded carpeting, which served to hide the bolted connections of the elements as well.

Over seventy residential, commercial, and industrial structures were built using the system over the ten years that followed [53]. The highly stylized interior of the original house shown in the figure above quickly fell out of fashion and was later renovated to become an office. Connection details and surface finishes remained points of discontent [113 pg. 80].

---

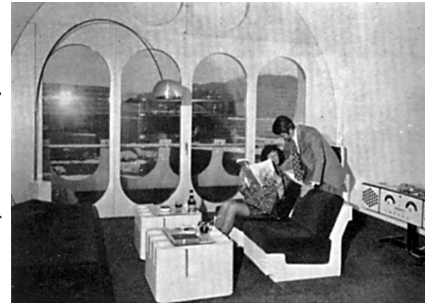
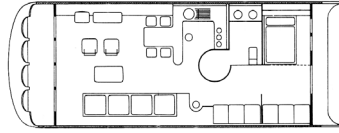
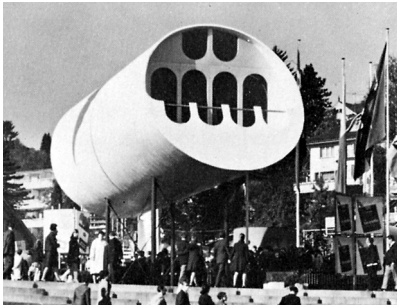
1969 *Système Rondo* – Angelo S. Casoni & Dante M. Casoni – Switzerland



Strongly resembling the rotational paraboloid form of the Finnish Futuro house, Swiss architects Casoni & Casoni also chose the modular approach for their FRP home concept. Once again, this approach was chosen because it allowed quick assembly times in difficult site conditions. Entire modules could be transported by truck, train, or helicopter. The shell panels of the system were composed of fire-retarded glass-reinforced polyester face sheets bonded to a polyurethane foam core to form a 60 mm thick sandwich. Space below the floor was used for storage and also contained the electrical heating system. The structure was supported by three steel columns, which allowed installation on a variety of site conditions, including in water. The designers imagined the modules could be used as vacation homes, apartments, or hotel rooms, and could be arranged as single installations or grouped systems many modules high (being supported by a structural steel frame). Mass production of the modules began in 1970, though it ended not long after. The image above shows the Rondo prototype in front of the Futuro at the Foire Suisse d'Echantillons in Basel [196].

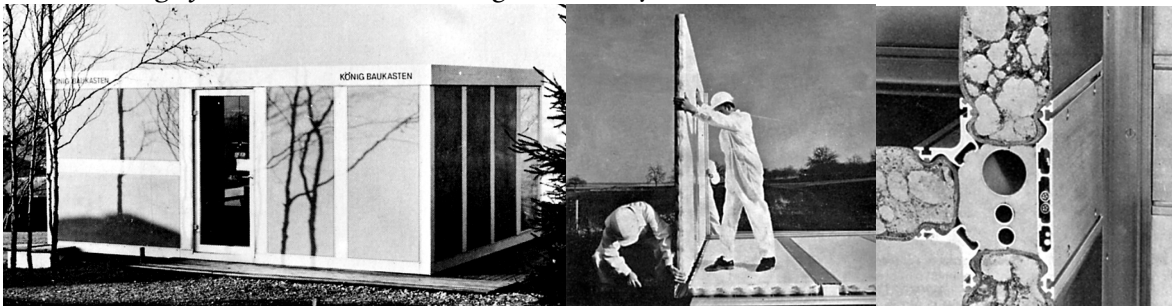
---

1970 *Tube House BASF* – Franz U. Dutler – Germany

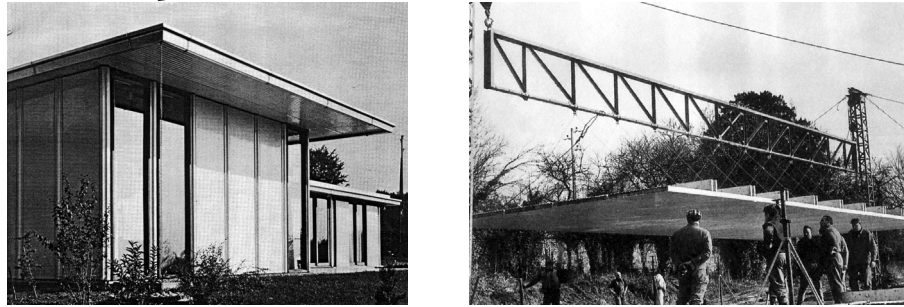


Much like the Rondo and Futuro systems, the BASF prototype consisted of a modular structure that sat on a steel supports. The shell was made from glass-reinforced polyester face sheets and a foam core produced through filament winding, a technique that was already in use for liquid storage tanks and airplane fuselages. Electricity, water, and wastewater were routed through the steel supports to connect with the local grid. The system never went into mass-production [163 pg. 36].

1970 *König System* – Baukasten, König – Germany

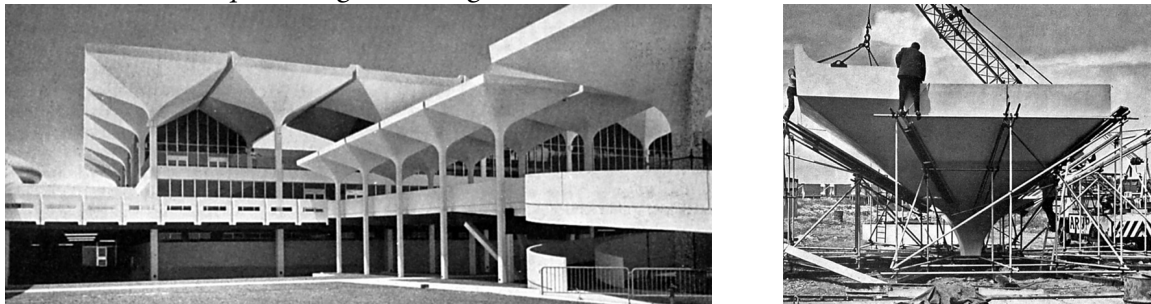


One of the few systems to adopt the segmental approach, the König system consisted of standard wall, floor, ceiling, window, door, and bathroom panels. The panels were produced from glass-reinforced polyester face sheets and polyurethane foam cores, which in turn were connected by slotted polyurethane foam-filled aluminum channels. Small tubes within the channels provided a conduit for electrical cables [163]. Single story buildings were built using the system as the load-bearing structure, while multiple story applications required a traditional skeleton [164 pg. 310].

1971 *Maison en Plastique* – Jean Prouvé – France

Among many of Jean Prouvé's prefabricated home systems was the FRP concept house built in St. Gobain, France. Much like the König System, the house was built from standardized roof and wall panels connected by universal connector pieces. The panels were fabricated in a continuous process from glass-reinforced polyester face sheets and polyurethane foam cores, which allowed production of nearly infinite lengths. The joints were sealed with neoprene gaskets. Conceived mainly around the production method of the elements, little innovation was achieved in the architectural or engineering sense [89].

---

1972 *Dubai Airport* - Page & Broughton, Mickleover Ltd. – United Arab Emirates

Constituting the largest FRP structure of its day, the Dubai Airport enclosed a surface area of more than 27,000 m<sup>2</sup>. The structure was composed of glass-reinforced polyester columns that arched out in the horizontal plane to form the roof. Transport of the 19.4 m square column/roof elements from the plant in England to the site in the United Arab Emirates was accomplished by dividing the elements into 13 pieces. The pieces were assembled on-site with bolted connections, which remained visible after completion. In all, 114 of the column/roof elements and one 10 m diameter FRP dome were needed to complete the airport [164 pgs. 261-5].

---

Note: Other FRP-based building systems such as inflatable, membrane, dome, sprayed-on foam, and folded systems have been omitted, as only the modular and segmented projects shown above have any significant relevance to the proposed system.

## 3 Case Studies

### 3.1 Monsanto House of the Future, 1957

#### 3.1.1 Background

At the forefront of the structural use of FRP in buildings in the 1950's was Albert Dietz of the Plastics Research Laboratory at Massachusetts Institute of Technology's Department of Building Engineering and Construction. Funded by the Monsanto Chemical Company and in cooperation with MIT architects Richard Hamilton and Marvin Goody, Dietz designed an innovative building using FRP elements as the primary structure. The project, called the "Monsanto House of the Future", was Monsanto's attempt to carve out a share of lucrative construction industry for their synthetic polymers. From the beginning, it was designed with the intention of mass production, though this was never realized. Construction of the prototype cost nearly one million dollars, however Monsanto estimated that the mass-produced models would come at a more reasonable \$20,000 [127 pg. 209]. Still, the model home stood proudly in Disneyland's "Tomorrowland" where it was visited by nearly 20 million people over its ten-year life [186].

#### 3.1.2 Description

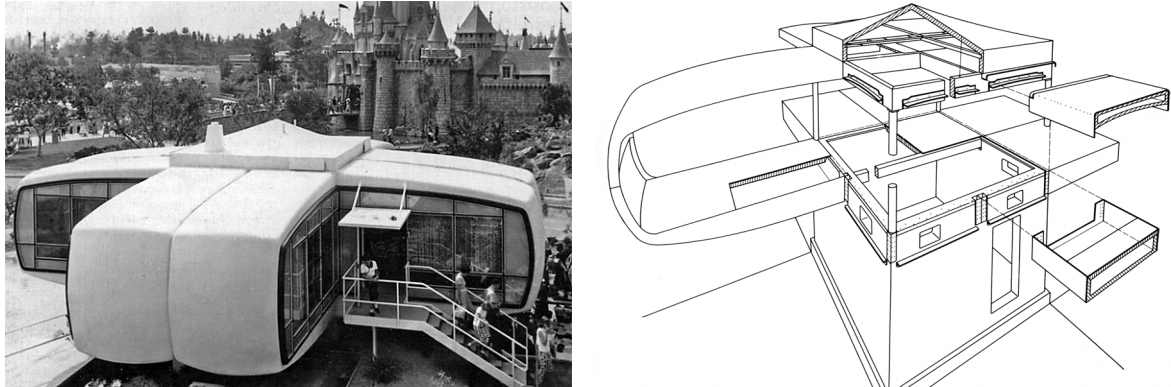
##### *Design*

From the beginning of the project, the MIT team was clear in their intention to choose a design concept that was appropriate to the material. They would not simply build the standard light-wood framed house using fiberglass studs and FRP shingles.<sup>2</sup> They insisted that the "ultimate form" be "peculiar to the plastics fabrication process." In this effort, the team selected a more material-adapted system using FRP shell elements. The popular "squirle" shape, as dubbed by the famous architect Bruce Goff, was chosen because it combined the structural stability of a spherical shell with a more livable rectangular interior space.

---

2. It is interesting to note that other model homes were built in previous decades using non-reinforced resins, including the Vinylite House of the 1933 Chicago World's Fair and an unnamed house displayed at the 1938 Frankfurt Building Exhibition. The projects were not terribly revolutionary, though, as their rather dubious innovation consisted of substituting traditional materials for synthetic polymers in an otherwise standard structure.

Figure 2-1. Monsanto House of the Future (left), Exploded diagram (right)



The Monsanto House was composed of four large C-shaped cantilevered FRP sections radiating from a concrete core. Each cantilevered section consisted of two continuously curving shells or *bents*, that began as the bottom chord, wrapped around to form the outside wall, and then returned to form the roof. The compressive forces generated by the cantilever at the bottom chord were resisted by the concrete foundation. The tensile forces at the top chord were resisted by a laminated wood beam system that tied together the opposite sides of the core. Live-load deflections of the floor were limited to  $1/360$  of the span, which, for a material with a relatively low stiffness, meant that the ultimate strength of the bents was many times greater than the required value. Dietz proudly claimed “The House of the Future was designed for a jam-packed cocktail party in a howling wind storm during an earthquake.”

The empty space between the curving outside shell and the flat interior floors was used as a plenum for the heating and ventilation system. At the center of the four bents was a 4.9 m square core containing the kitchen and bathrooms, which stood directly over the concrete foundation (see Figure 2-1).

### *Fabrication and Assembly*

Though the Monsanto House was meant to be the prototype of a mass-production model, its fabrication was ironically labor intensive. In similar fashion to the fabrication of boat hulls and bath tubs of the day, the bents were produced by hand lay-up. Three months and many skilled craftsmen were required for the process.

The process began with the lamination of ten glass fiber mats onto a doubly-curved wooden mold using a polyester resin. This resulted in laminates that were 8 mm thick, which included a pigmented gel coat. Rigid polyurethane foam was then sprayed onto the interior of the laminates to serve as the thermal and acoustical insulation. Sandwich panels serving as the floors or ceiling completed the box-profile of the bents (see Figure 2-1-right). These sandwich

panels consisted of thin glass-reinforced polyester face sheets bonded to a phenolic resin-impregnated paper honeycomb core [85 pg. 73].

The bents were fabricated in two halves such that the 2.4 m x 2.4 m x 4.9 m sections could be stacked and shipped to the site by truck. On-site, the halves were bolted and bonded together with an epoxy adhesive [127 pg. 209].

The intention was to develop a home that could arrive to the site in identical sections and be assembled by a small crew in mere hours. The construction of the demonstration unit, however, was far more complex. Due to inaccuracies of the molding process, the sections had to be first cut to rough dimensions by an awkwardly large handsaw and then ground to finished dimensions by disc sanders. Bonded joints also needed to be roughened by sanding to ensure adhesion [127 pg. 210]. When completed, the gel coat had been so scuffed and dented by the construction process that repair was necessary, which then required a coat of paint to hide the repairs [85 pg. 73].

### 3.1.3 Discussion

The Monsanto House was a landmark in the wave of FRP houses because it was designed using engineering principles. Previous projects were mostly expressions of the vision of architects and did not reflect a rational engineering design approach. Albert Dietz, with his considerable experience in the design of structural applications of FRP materials, demonstrated that stresses and deflections could be accurately predicted in such structures. The outstanding structural performance of the Monsanto House confirmed his calculations, giving the engineering world a more optimistic outlook for design in the material.

#### *Public Acceptance*

In the end, Monsanto Houses were never mass-produced and the prototype was demolished in 1968.<sup>3</sup> The public that once marveled at its futuristic flying saucer appearances in the 1950's and 1960's came to ridicule its naïve optimism in the 1970's.

There may have been several factors that resulted in the ultimate public rejection of the project. The first and perhaps most influential factor was the attitude of the consumer. The home is the single greatest financial investment one normally makes in life. Perhaps some people were willing to invest smaller sums into quirky new products such as the VW Beetle, but had great

---

3. The house reputedly resisted attack by wrecking ball, torch, jackhammer, shovel, and all manner of saw before it finally succumbed to a crane-driven clamshell, which chewed its way through the structure over the course of two weeks [85 pg. 75].

difficulty spending the big sums on something that didn't look like their parents' house. In addition, there were worrisome questions of resale value and insurance [169 pg. 419].

“...it is unlikely that curved roof shapes will find home buyer acceptance in the near future even if they are competitive in the cost with traditional construction. This is so because the home buyer is aware that a future return on the sale of his largest single investment depends on how well his house conforms to an accepted pattern of individual and community preferences.”

Irving Skeist [169]

Above all else, the projected \$20,000 cost of the mass-production homes would have proven quite impossibly low.

“On a cost basis such an all-plastics structure in 1956 could not compete with the traditional techniques, even taking into account all the advantages offered by plastics.”

Z.S. Makowski [116]

The issue of conformity and trade marking seemed to trouble consumers as well. The fact that the modules were so distinctive meant that people would not live in their own houses, but Monsanto Houses. The subtle difference would effectively strip the home of any personal identity, even if it was claimed that the system allowed for personalization.

“By the time Tomorrowland was redesigned in 1967, model homes had devolved from symbols of progress into icons of conformity, so the Monsanto House was replaced...”

Robert Haddow [75]

### *Technology*

As discussed, there were problems on the manufacturing side as well. Contrary to the image projected by marketing agencies, injection molding machines were not producing pristine and identical modules every few seconds [36 pg. 921-7]. In truth, 1957 molding and vacuum technology did not produce terribly consistent parts and quality control was far behind the standards of the steel and aluminum industries [147 pg. 3.59]. Many sectors of 1950's composites manufacturing remained a labor-intensive skilled craft rather than an automated science.

Further, the materials were, at best, unproven in long-term service. It would later become evident that many of the early FRP systems were quite susceptible to ultraviolet light degradation, water absorption, and fiber blooming.

### *Legislative Barriers*

It appears that synthetic polymers suffered from the same sort of code-driven discrimination that hindered the implementation of many new materials. Still years before the development of performance-based building codes, there was no clear way to define the certification or approval of FRP materials [127 pg. 213]. This again led to problems in obtaining building permits and eventually in insurance coverage.

### *Fire Resistance*

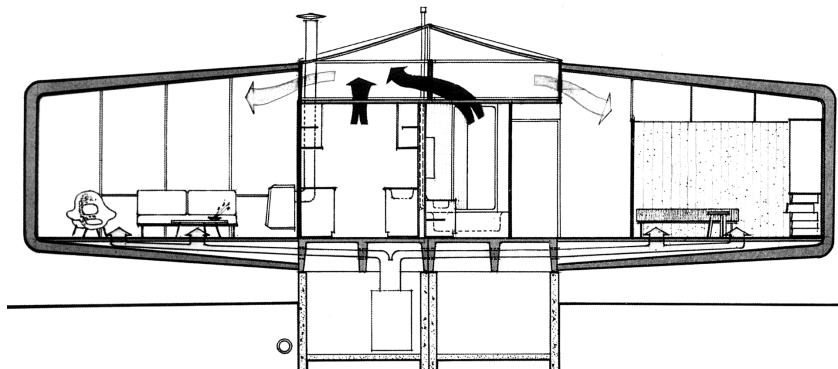
Fire threat, above all, seems to have received little attention. The laminates used in the Monsanto House were dubbed “self-extinguishing”, though it is unclear if this was based on any established standard. Large-scale production and sales to the general public would most likely have put this weakness under greater scrutiny.

### *Integration of Functions*

One area in which the project was quite successful was in the integration of architectural and structural functions into single components. As previously mentioned, the space between the flat floor panels and the curving exterior shell was used for the heating, ventilation and air-conditioning (HVAC) system (see Figure 2-2). The air travelled from the furnace through conduits to the sub-floor plenums, through the plenums, and finally entered the living space through circular grilles in the floor. A thermostat used sensors to control the temperature, humidity, and even odor [85 pg. 73].

The layout of the rooms also fulfilled several architectural requirements at the same time. By having the rooms radiate outwards, there were no common walls between bed rooms or living rooms. This increased the privacy of the rooms and reduced the transmission of sound. Further, enclosing the side walls of the bents with glazing meant that each room had substantially more windows than it could have in a rectangular configuration.

Figure 2-2. HVAC distribution diagram



The foundation was also a fine example of the integration of functions. Though it was designed to serve a structural support that would allow placement of the house on a variety of site conditions, it also enclosed the boiler, furnace, and other building services. In addition, the foundation raised the somewhat vulnerable FRP skin up out of reach from mischievous hands, burning cigarettes, abusive gardening equipment, and most other serviceability threats.

## 3.2 Fiber-Shell System, 1968

### 3.2.1 Background

In 1968, the United States Department of Housing and Urban Development (HUD) announced the launch of a new program aimed at solving the country's housing shortage. The program, dubbed *Operation Breakthrough*, was intended to promote innovation in building systems and industrial fabrication techniques by guaranteeing large markets for companies willing to invest in the research and development. In all, 22 companies were selected to submit proposals, from which a handful proceeded to mass-production and sale of their housing systems.

The launch of the program coincided with the interests of the Aerojet Corporation, who was looking for a way to adapt their missile production technology to the housing market. Licensing their technology to the TRW Systems Corporation, a proposal was made to the HUD for a filament-wound "Fiber-Shell" modular housing system. By the year 1973, over 1,800 Fiber-Shell homes were scattered across the United States (see Figure 2-3) [50 pg. 190].

Figure 2-3. Fiber-Shell housing complex



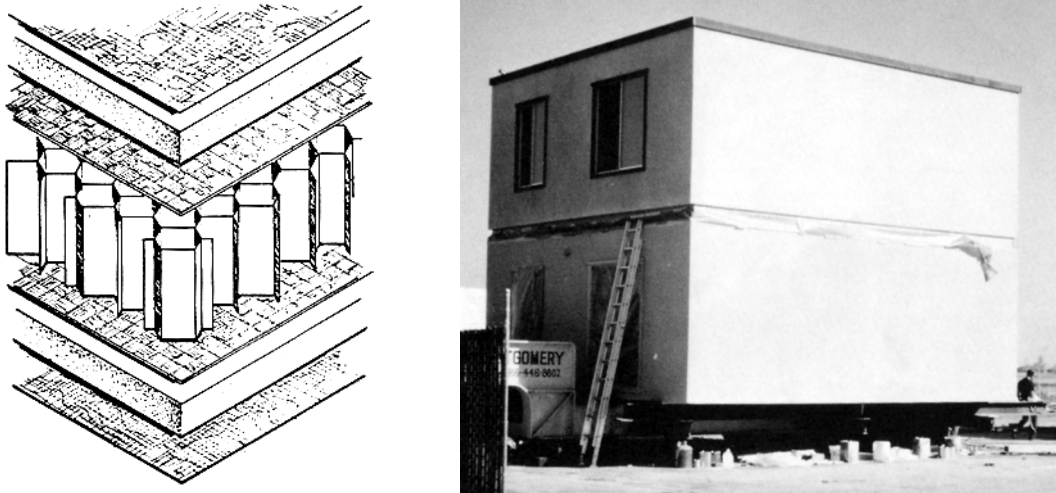
### 3.2.2 Description

#### *Design*

If the Monsanto and Futuro Houses represented the spirit of the “Plastic-as-Plastic” architectural movement of the 1950’s and early 60’s, Fiber-Shell was clearly the champion of the “Plastic Hidden Away so Nobody Knows it’s Plastic” movement of the late 1960’s and early 70’s. It was not possible, from any angle inside or out, to distinguish the FRP-structured Fiber-Shell houses from a conventional (albeit unattractive) townhouse. Both the traditional forms and common finishes of the system betrayed its ballistic missile lineage.

The fully-developed building system was produced in two varieties: one of house-sized tubes filament-wound on an enormous mandrel, and one as sections manufactured in flat panels and bonded to form tubes. The first approach resulted in extremely strong structures, though there was no flexibility in the dimensions of the structure and their size made them difficult to transport (see Figure 2-6). The second approach was developed because it allowed for a more economical use of materials, cheaper tooling, more flexibility in dimensions, and easier transport.<sup>4</sup>

Figure 2-4. Laminate (left), Arrangement of modules in Sacramento housing complex (right)

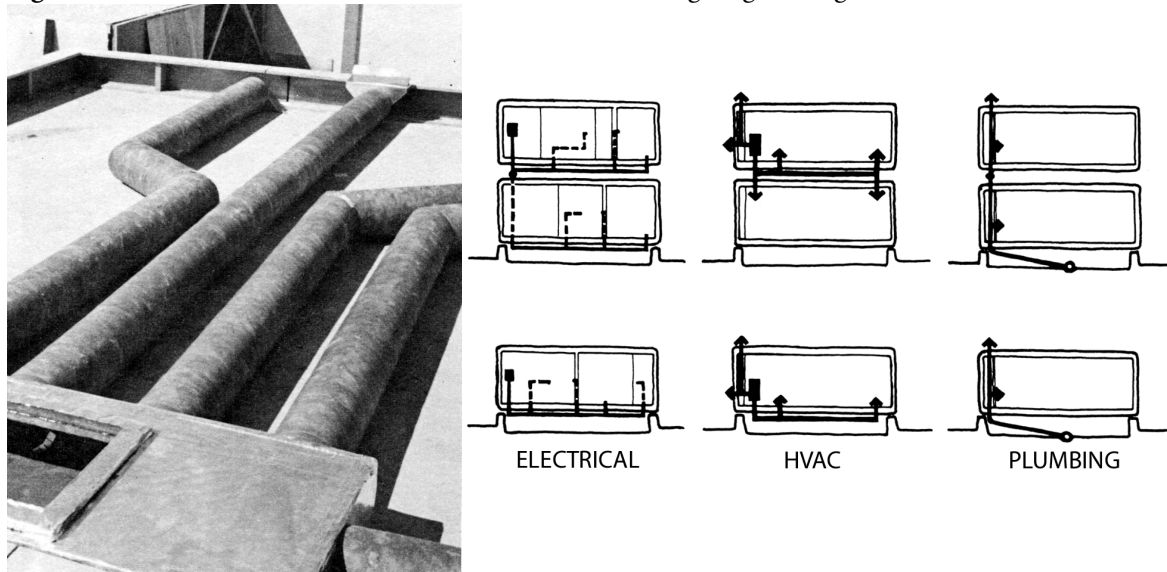


Both systems implemented a sandwich structure for the walls and floors. Strongly resembling the composition of the recently demolished Monsanto House, the sandwich was formed from a phenolic resin-impregnated honeycomb core bonded to a glass-fiber-reinforced polyester resin

4. Because the system had been described in the first proposal as being filament-wound, the major design deviation to a flat panel system was not allowed within the confines of the Operation Breakthrough contract. Thus, twenty units were produced by filament winding to satisfy the HUD contract, while the rest were produced by the flat panel approach [143 pgs. 220-221].

laminate. To pass fire codes, however, a layer of gypsum board (two layers on party walls and roof panels) was then bonded and stapled to both faces of the sandwich [143 pg. 215]. On the exterior face, a novel product that resembled stucco but was made from chopped glass/polyester resin with aggregates for texture and pigments for color was applied to provide weather protection. The inside also received a final layer for aesthetic reasons.

Figure 2-5. HVAC distribution between levels (left), Routing diagram (right)



The completed homes were typically composed of two large vertically-stacked tubes, which could then be stacked horizontally in townhouse-style (see Figure 2-4). Maximum dimensions of the floor panels were 6.60 m x 9.75 m, which amounted to the typical 130 m<sup>2</sup> home shown in Figure 2-6. Interior partitions, stairs, and the walls at the open ends of the tubes were prefabricated from standard wood studs, plywood, and gypsum board.

A 22 cm thick ring-shaped spacer was placed in between the tubes in both the horizontal and vertical orientation. This provided a convenient place to route the building services and improved the acoustic isolation of neighboring units. Figure 2-5 shows an example of the routing of the building services through the space in between the stacked tubes.

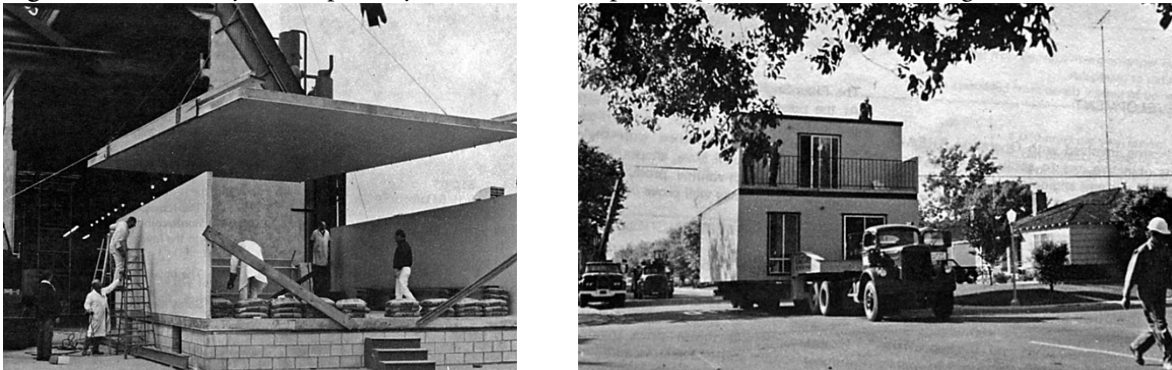
### *Fabrication and Assembly*

Due to the size of the finished tube sections, fabrication was intended to be conducted by temporary plants built within eight kilometers of the housing development. The expensive custom-built machinery could then be moved to new developments when the work was completed. In this manner, the maximum amount of prefabrication could be done in the plant while keeping transport costs to a minimum.

In the original scheme, the previously described sandwich system and additional layers were laminated on the enormous mandrel of a filament-winding machine. When the tube was completed, the mandrel was collapsed and one end-wall was attached to brace the tube against racking.

The second scheme employed a slightly more complicated assembly to eliminate the need for the expensive and dimensionally-limiting mandrels. In this process, flat panels were fabricated by simple lay-up and vacuum forming techniques. Wood strips were included along the perimeter to seal the honeycomb core and facilitate connection to other panels. Dowels and a polyester adhesive were used to connect the panels into room-sized tubes.

**Figure 2-6.** Assembly of flat panel system (left), Transport of pre-assembled house (right)



Both methods resulted in large tubes that were then joined to form the complete house structure. Prefabricated interior partition walls, end walls, plumbing walls, stairwells, kitchens, and bathrooms were also installed in the plant. The final stage of manufacture added the plumbing, electrical system, exterior trim, and roofing. The completed house was then transported by trailer to the construction site, where it was lowered onto a concrete foundation.

### *Testing*

Because the building system employed non-traditional materials, extensive physical testing was required to achieve code acceptance. The first round of tests was performed to verify the structural fitness and reliability of calculation methods for the system. Next, the fire performance, water absorption, acoustic isolation, and thermal insulation of the system were investigated. After more than a year of study, the system was accepted within the standard building codes as well as the stricter standards set by the HUD program.

### 3.2.3 Discussion

#### *Durability*

The Fiber-Shell system is of particular interest because of its relative success in the short term and its complete failure in the long term. Most of the homes at the Sacramento, California development are still in use today, though they have not aged well. Project designer Ezra Ehrenkrantz admitted in his 1989 case study:

“The favorable results obtained by the chemists in accelerated weathering and other tests working with the then existing resin technology were not confirmed in practice. A few years later, plywood was used to resurface the exterior.” [50]

Further, a more recent article from the Sacramento Bee (a local newspaper) provides an update on the Fiber-Shell development:

“Vincent Sotolongo works at home, and each day, pieces of the ceiling fall on his desk. A toxic mold has spread from the living room and bedrooms throughout the house, and a bucket in the hall catches leaks from the bathroom upstairs. The walls, stained brown and black, are separating from the floor. Outside, the paint cracks and peels off in sheets. Sotolongo’s two-story house at the Greenfair development in East Sacramento is falling apart. And it can’t be repaired.”

Silvia Martínez [120]

This is the state of many of the Fiber-Shell homes today. As of December 2000, the HUD offered to buy back fifty of the homes in the worst condition so that they could be demolished. It appears that although some synthetic polymers can be stubbornly long-lived, there is no guarantee that the structures that they compose will be so durable.

Future structures will take advantage of better materials with a larger knowledge base and more long-term behavioral data, though many of the design pitfalls remain. If nothing else, the Fiber-Shell project illustrates the problems associated with a system that does not allow for maintenance. Plumbing and electrical systems will inevitably require repair and update and must remain accessible. And even if interior and exterior surfaces do not require regular maintenance, the unforeseen will occasionally occur, and should not mean the replacement of the entire module.

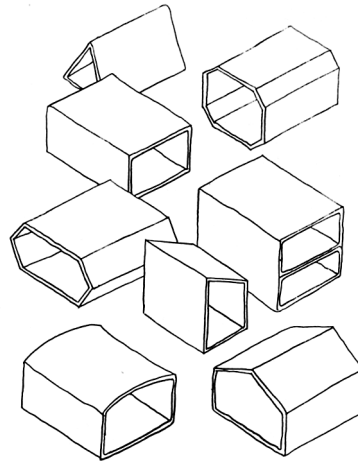
#### *Constructive System*

The Fiber-Shell System is also an interesting case because of the way its constructive system evolved. It was initially conceived to follow the modular approach, in which large room-sized modules are prefabricated and then joined together in the factory or on-site to form the completed structure. Thus, the final architectural form could be slightly modified by varying the arrangement of the modules in the structure. To improve the flexibility of system, the

designers hoped to develop other mandrels that could be used to manufacture modules of different shapes and dimensions (see Figure 2-7).

These hopes were dampened when the project moved to production, however, as the design and construction of the first mandrel proved difficult, time-consuming, and extremely expensive. In addition, the method of creating the modules by filament winding did not permit the most efficient use of the already expensive raw materials. The result was that extremely high-volumes of production would have been required to justify the costs of a single mandrel. The multiple mandrels required to permit any substantial diversity would have been far too costly.

**Figure 2-7.** Other mandrels that could be used to produce different modules



This problem is common to nearly all of the projects that followed the modular approach. As discussed in the analysis of the Monsanto House, modular construction limits the diversity of architectural form to a finite catalog of arrangements. Further diversity requires another large investment by the manufacturer to design other modules and their specific tooling. For very repetitive applications such as telephone booths or military barracks, this is certainly an efficient method of producing structures. When a greater level of flexibility is desired, however, the economies of design and production quickly diminish. A segmented approach becomes justified at a certain threshold.

Such was the case with the Fiber-Shell system. When the modular approach proved too inefficient, the production of the tubes was broken down into the production of individual flat panels. This technique allowed the manufacture of tubes in a nearly unlimited variety of dimensions and shapes by simple and generic equipment.

### *Social Considerations*

The Fiber-Shell project also illustrates the importance of tradition in the commercial success of a building system. The following excerpt from the TRW's 1973 HUD proposal [143] explains why the system was conceived to appear standard.

“Fiber-Shell does not present an unconventional appearance, despite the use of novel materials. This is important, because customer resistance to change in the appearance of the living environment is well known. The uniqueness of Fiber-Shell is hidden within its walls, floors, and ceilings.”

This is not to maintain the idea that all new building systems must conform to the traditional paradigm in order to succeed; it serves only to illustrate the point that structures are built for people, and their preconceptions about synthetic polymers must be considered in any new design. Fiber-Shell was, in fact, the worst kind of example to the general public because it presented FRP materials as cheap substitutes for the “real thing”, and then performed in the exact manner that one would expect from a cheap substitute. New systems will battle against the public's prejudices created by such failures as the Fiber-Shell System.

### *Fire Resistance*

As in many of the early FRP structures, the issue of fire resistance was ignored rather than truly solved. Considerable weight and expense was added and much durability was lost by the inclusion of the gypsum board layers. A more material-adapted solution would not have wasted the weather resistance and light weight of the polyester/honeycomb sandwich structures by enveloping them in traditional materials.

## 4 Conclusions

The first phase of FRP buildings and building systems was mainly targeted at the residential housing market. Very few of the load-bearing FRP structures could be built taller than a single story, and none taller than two stories. Throughout the phase, many of the projects seemed to be conceived according to a similar set of guidelines:

- Envelopes should be integrated with the load-bearing system as single elements.
- Structures should be modular with large room-sized sections produced industrially and assembled on-site.
- Structures should overcome the comparatively low material stiffness through the use of form-active structures such as curved or folded shells.
- Foundations should allow the placement of the structure on a wide variety of site conditions.
- Structures should not conform to traditional architectural standards, but express their technology and modernism.
- Structures should allow modification, upgrade, and disposal according to the modern family's changing needs.

Unfortunately, most of the production-oriented projects proved financially unfeasible and the demonstration projects were eventually rejected by the architectural community. These failures are attributed to several factors:

- Legislative barriers and the lack of performance-based codes
- Poor weathering characteristics
- Social issues (trademarking, departure from traditional designs, change in perception of synthetic polymers from “high-tech” to “cheap substitute”).
- Unresolved structural fire endurance or non-material adapted protection methods (e.g. gypsum board layers)
- Increased oil prices (from which synthetic polymers are produced) and improved supply of traditional building materials

Many of these factors are beyond the control of designers, though not all. Several important lessons can be learned from the projects of the first phase:

- The modular approach (room-sized or larger components) is only sensible for very repetitive buildings with little diversity of form. The segmented approach (smaller components) is better-suited to buildings where a degree of customization is desired.
- In the short term, it is easier to sell buildings that are designed to mimic traditional materials and methods. Unfortunately, this often results in a non-material adapted application of the materials. Use of the materials in such a manner is partially responsible for the public's perception of synthetic polymers as cheap substitutes.

As discussed, the success of future systems will hinge upon a better treatment of the fire threat. In a 1974 text, German designer Rudolph Doernach excused the lack of fire resistance of his FRP building system by writing:

“Das Problem der Brandstabilität von mind. F30 war 1957 nicht lösbar.” [45]

[The problem of fire resistance was not solved. An F30 (fire endurance rating) was not attainable in 1957.]

Whether this is true or not, future systems cannot be conceived without a basic fire safety strategy and will be required to comply with more stringent building codes.



# 3

## **The State of the Art**

*Modern FRP Buildings & Building Systems, Fire Safety for FRP Structures, and the  
Modeling of FRP Materials in Fire*



## 1 Introduction

As indicated by the subtitle, the subjects treated in this review of the state of the art are diverse and numerous. This is the inescapable consequence of the many fundamental choices that are made in the conception of a totally new building system. Given that the basic building material will be FRP, it was logical first to review the current technology in related building systems (only one load-bearing FRP building taller than three stories has even been built). Thus, the first section of this chapter provides a review of the notable FRP buildings and building systems that have been constructed or proposed since the concept was resurrected in the late 1980's.

Once these projects were reviewed, the problems and solutions they embodied were considered in the context of a multiple-story FRP building system. It was found that the issue of fire safety, while permissibly ignored in small single and two-story structures, would pose a formidable challenge to a multiple-story system. Therefore, the next step was to review the possible methods of developing a total fire safety strategy for multiple-story systems. The second section of this chapter provides a brief review of these methods.

Finally, as the conception of total fire safety strategies became the focus of this research project, physical investigations were performed to confirm the feasibility of the newly proposed system. To accompany these physical investigations, mathematical simulation techniques were employed both to study phenomena that are not easily measured and to allow the optimization of the proposed system. Thus, the final section of this chapter provides a review of the mathematical models that can be used to simulate the behavior of FRP materials in fire.

## **2 Modern FRP Buildings and Systems**

As described in the previous chapter, the first wave of structural FRP buildings began in the mid-1950's and continued for roughly 15 years. Many factors lead to the demise of the first wave, including the oil crisis in 1973 (synthetic polymers are created from oil) and the changing public perception of synthetic polymers. What was first regarded as a high-technology futuristic material later became a low-cost, low-quality substitute. In addition, the outrageous curved shapes that were explored in the earlier experimental buildings were mocked by the following generation of architects and designers. Prescriptive material-specific building codes created a legislative barrier by providing no means to certify new construction materials. Economically, the full potential of the material was not exploited in that the high unit cost was not mitigated by significant savings in labor, schedule, or maintenance. The culmination of these problems left researchers and developers with a distaste for FRP materials that lasted for nearly a decade and is occasionally still palpable.

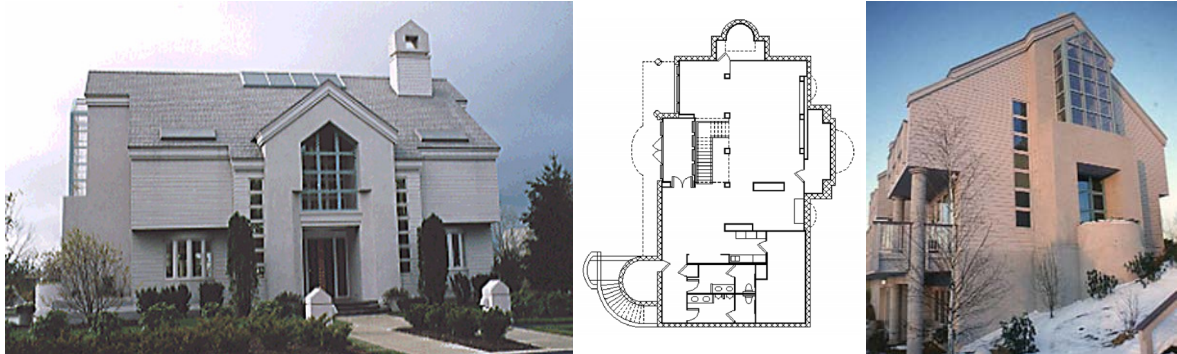
Towards the end of the 1980's, many of the issues that troubled the first wave of FRP projects had faded. Oil prices stabilized, performance-based building codes began to be adopted, and the appearance carbon-fiber composites in luxury and high-technology applications helped to improve the public perception of synthetic polymer materials. Thus, a new wave of structural FRP buildings began in 1989. Some of the key projects that were built within this wave are briefly described in the following section, while other proposals or design exercises that were not built are described in Section 2.2.

### **2.1 Constructed Buildings and Systems**

#### **2.1.1 GE Living Environment Concept House - USA, 1989**

Just as in the first wave of FRP buildings, the first big step in the second wave was taken by a plastics manufacturer attempting to expand its market. Instead of the Monsanto Corporation, however, General Electric (GE) was the plastics producer who took the initiative to redesign the family dwelling. The GE Living Environment concept house was built just nearby the company headquarters in Pittsfield, Massachusetts in 1989.

Figure 3-1. GE Living Environment House



Designed by architect David George of Richard-Nagy-Martin, the design and construction cost approximately five million dollars and involved the collaboration of 45 different manufacturers [190]. From the washing machines to wall cladding, the project was a showcase of modern systems and products that was described by GE as a “living laboratory”. Making use of many recycled products from the automotive and aircraft industries, 30% of the building consisted of polymeric materials, of which the greatest portion was unreinforced thermoplastics.

#### 2.1.1.1 Structural System

Standing on a concrete foundation, the structure is two stories tall. Polymer form work was used to pour the foundation and remained in place as insulation and the interior surface finish. Traditional timber members were encased in engineered-wood corrugated wall and floor panels for the load-bearing members. Connections between the members were made by bolting and adhesive bonding [28].

#### 2.1.1.2 Production and Assembly

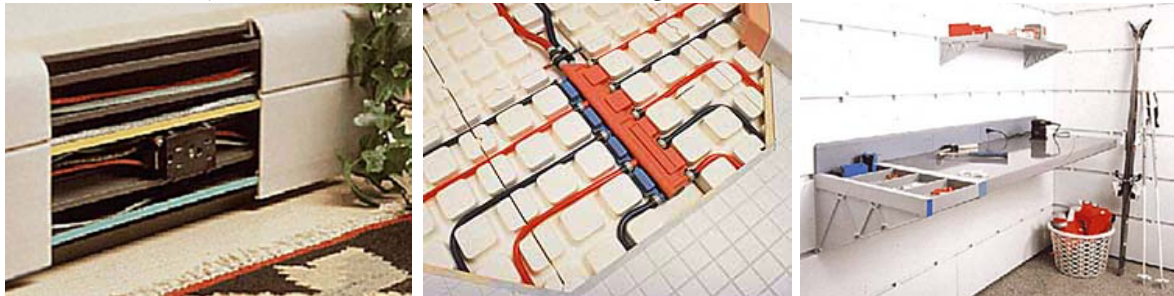
As a prototype, very little automation was used. For future projects, GE imagined a two-stage industrial manufacturing system. In the first stage, the basic panels would be fabricated in a large central plant. For the second stage, these panels would be shipped to smaller mobile plants, where final finishes and detailed components would be installed. In this manner, finished panels would only travel a short distance to the construction site [190].

#### 2.1.1.3 Integration of Functions

The completed wall panels served as both the vertical structural system and the building envelope. Thermoset cladding on the exterior provided weather protection, while gypsum on the interior provided fire resistance. Radiant heating and cooling was achieved through a network of pipes hidden behind the gypsum layer. Electrical wires were routed through hollow molded baseboards and inside door frames. Plumbing was routed through high-density foam

waffle slabs below the finished floor and in plumbing walls (see Figure 3-2). Numerous energy-efficient concepts were incorporated such as heat recovery and greywater utilization.

**Figure 3-2.** Molded baseboard raceway (left), Utilities embedded in waffle slab (middle), Integrated shelf connection system in foundation wall form work (right)



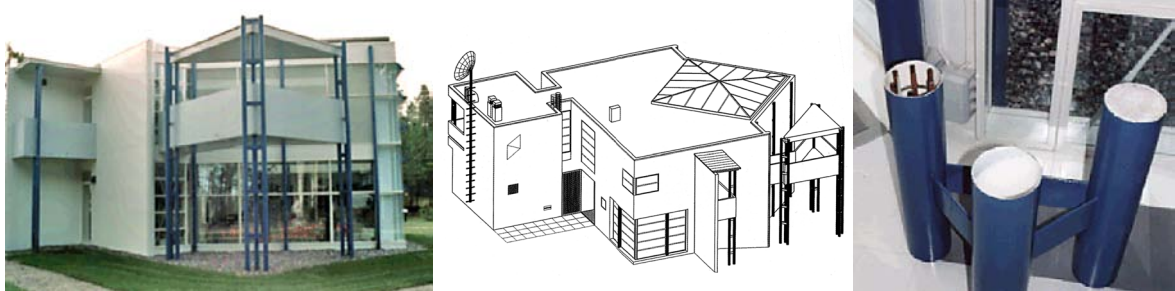
#### 2.1.1.4 Discussion

At the time of its construction, GE envisioned the construction of a second unit using 75% polymeric building materials by the year 2000 [29]. No such project was ever built, and interest in the Living Environment house has mostly diminished. Using mostly “off-the-shelf” products that were already available to consumers, it was the combination of products in a single building that brought attention rather than the invention of any new concepts. The manners in which building functions were integrated was fairly successful, though not much different than in the Monsanto House of 1956. Overall, the project reintroduced the concept of industrially-produced FRP building system to the public in a traditionally-styled and environmentally friendly package.

#### 2.1.2 Nestehaus - Finland, 1992

Imagining that GE was planning to produce an FRP building system (instead of what they actually produced: a standard wood-framed building with vinyl siding), Finland’s largest petrochemical company raced to produce their own version of the FRP home. Consisting of 75% polymeric materials, the Nestehaus was built in Porvoo, Finland in 1992 [198]. Extensive use was made of fiber-reinforced thermoplastic materials to allow easy recycling. A strong emphasis was placed on energy efficiency for the cold Finnish climate. The project was described as an attempt to draw attention to the possible applications of plastics in buildings rather than to build a production prototype.

Figure 3-3. Nestehaus (left), Floor plan (middle), Tri-column section (right)



#### 2.1.2.1 Structural System

All of the major load-bearing components consisted of pultruded glass-fiber reinforced thermoplastic tubes and pipes filled with steel reinforcement and high-strength fiber-reinforced concrete (see Figure 3-3). The resulting members were stiff, weather resistant, and created weaker thermal bridges than standard concrete members would. A space frame incorporating long-fiber reinforced polypropylene members supported the roof [173].

#### 2.1.2.2 Production and Assembly

As a demonstration unit, no attempts at automation were made. Construction was slow and labor intensive, with most of the work being completed on-site.

#### 2.1.2.3 Integration of Functions

An under-floor hydronic heating system was embedded in the concrete floor slab. Otherwise, very little integration was attempted. The traditional skeleton and curtain wall system used in nearly all modern concrete and steel structures was mimicked.

#### 2.1.2.4 Discussion

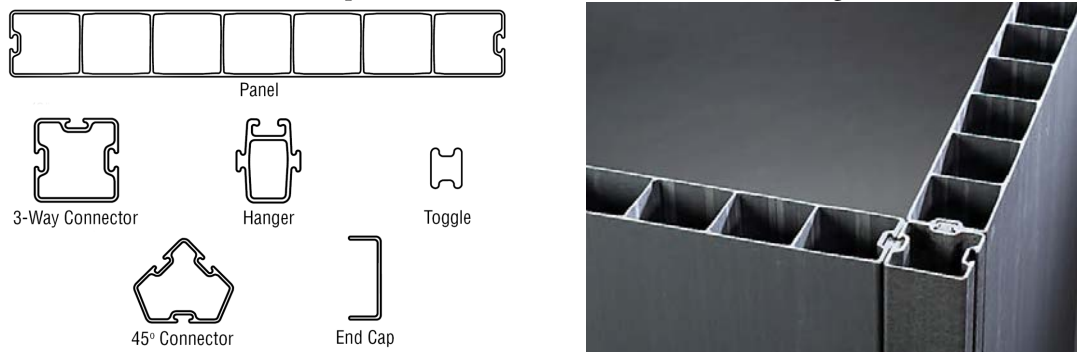
The project drew considerable attention, though much of it for its faults rather than its achievements. The extensive use of standard PVC (polyvinyl-chloride) on the interior surfaces indicates that no attention was given to fire resistance or interior air quality [161]. PVC materials are among the largest contributors to “sick building syndrome”<sup>1</sup> and produce copious amounts of toxic fumes (most notably hydrogen chloride, which turns to hydrochloric acid when it comes in contact with moisture in the lungs) and heavy black smoke during combustion. As an aside, it seems to have been a poor decision to present their FRP building in Scandinavia, where the building material that the FRP replaced (wood) is plentiful and so highly revered.

1. Sick Building Syndrome is a generic term for a long list of health issues related to the pollution of indoor environments. The off-gassing of toxic chemicals from construction materials such as formaldehyde glues and PVC surfacing materials are among the worst offenders [118].

### 2.1.3 Advanced Composite Construction System® - UK, 1986-96

The Advanced Composite Construction System, or ACCS,<sup>2</sup> is a simple interlocking FRP panel system that was developed by the Maunsell Structural Plastics between 1986 and 1996. The system consists of pultruded flat panels that are joined by slotted connectors. The panels are roughly 8 cm thick and 61 cm wide and have a box-shaped cellular cross section. The slotted connectors have a dog-bone shaped cross-section. Corners of 90° and 45° are made with single-celled elements, as shown in Figure 3-4. All of the components are made by the pultrusion process<sup>3</sup> with glass fiber and either polyester, fire-retarded polyester, or fire-retarded vinyl ester, depending on the application.

Figure 3-4. The main ACCS components (left), Assembled corner section (right)



#### 2.1.3.1 Noteworthy Projects

Evolving from an earlier bridge enclosure system by Maunsell, the ACCS has been used most successfully as a protection and inspection platform system for steel-framed bridges. The first primary structural applications of the system were in the Aberfeldy footbridge in Scotland and the Bond Mills draw bridge in England (see figure Figure 3-5).

Figure 3-5. Box-beam assembly (left), Aberfeldy footbridge (middle and right)



2. ACCS is only produced by the Strongwell corporation under the name Compositesolite®.

3. See Chapter 5 Section 2.2 for further details of the pultrusion process.

Later, the system was used extensively to enclose the eight bridges that comprise the Second Severn Crossing between England and Wales. For this large project, the on-site construction management offices were also erected using the ACCS as the wall, floor and ceiling panels (see Figure 3-6). Representing the first application of the system in buildings, the two-story offices were later converted to a visitor's center after the completion of the bridges.

**Figure 3-6.** Severn Visitor's Center (left), Automated car wash enclosure (right)



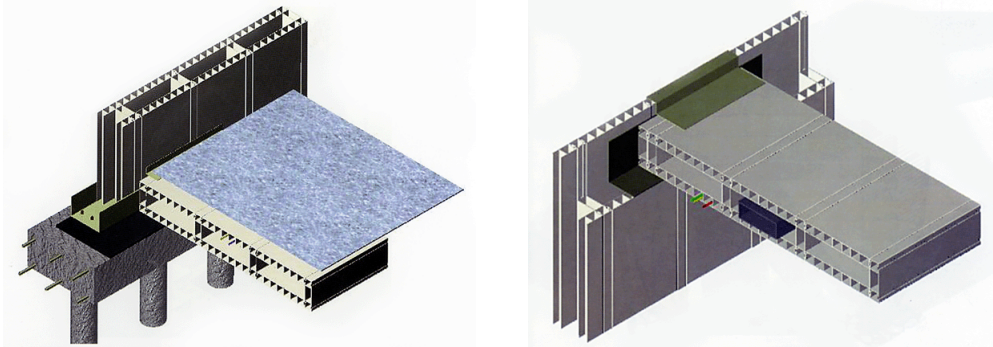
### 2.1.3.2 Structural System

For short spans and small loads, the thin panels are capable of working as a single layer. For larger spans or loads, however, dual-wall stiffened sections (c.f. Aberfly footbridge) are necessary. The interior cells can be filled with expanded foam to prevent local buckling, as it was done for the Bond Mills draw bridge. For large spans in buildings, a traditional beam and slab arrangement could also be used. Connections between elements are made using the slotted connectors and structural adhesives. A series of structural evaluations were performed by Lee *et al* in [104] and Duthinh *et al* in [48].

### 2.1.3.3 Integration of Functions

In the few examples of the system in buildings, the only integration of functions was in the use of the panels as the load-bearing elements and the building envelope. Minguzzi explored the application of the system to large multiple-story buildings in his 1998 book *Fiber Reinforced Plastics* [131]. His concept involves the use of the system to create hollow wall and floor sections using ACCS panels on each face (see Figure 3-7). The large space in between could be used for the routing of building utilities. Unfortunately, the proposed system only allows transmission of utilities in one direction, and makes no provisions for how the utilities enter and exit the cavities. Further, the vertical cavities are interrupted at each story by the floor panels. Finally, no consideration was made of structural fire endurance. While the materials are available in fire resistant formulations, this only ensures that the materials will not contribute to the fire; structural collapse would still occur at relatively low temperatures.

Figure 3-7. Building applications of the ACCS proposed by Minguzzi [131]



#### 2.1.3.4 Discussion

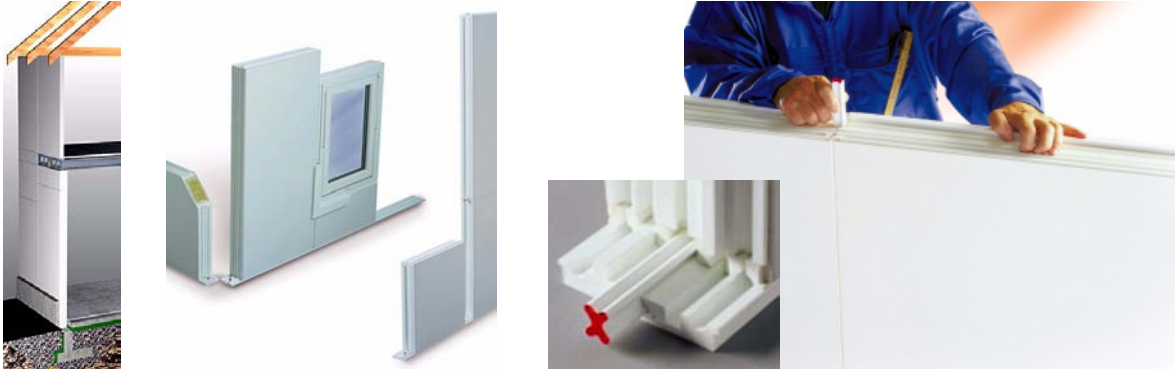
Over time, problems have been encountered in the small group of single and two-story buildings. The largest problem appears to be water leakage through the slotted joints. As the toggle connectors are slid into the grooves of the panels, they tend to push most of the adhesive out the other end, which leads to poor bond quality. Manufacturing tolerances of the pultruded components has also been a problem in that the elements do not always fit together well.

The future of the ACCS does not appear to be in the multiple-story buildings. While many new bridge enclosure projects are underway and have the full support of the British highway authority, the use of the system in buildings has been reduced to some small niche applications in industrial plants and chemical treatment centers. Due to the lack of any structural fire endurance strategy, future applications of the system in primary load-bearing structures is unlikely.

#### 2.1.4 BEET® Building System - Norway, 1993

Recognizing the potential that is wasted when FRP materials are produced in sections copied from steel, Norwegian engineer Jan Holm Hansen developed the Building Elements Easy Together (BEET) System. The system consists of standardized sandwich panels that are joined through a unique keyed connection (see Figure 3-8-right). The basic BEET Element is 120 cm wide and is available in four heights from 200 cm to 350 cm. The panels are also available in two thicknesses (11.2 and 21.2 cm) for different levels of thermal insulation and stiffness. Surfaces are finished with a layer of acrylic paint, though a pebble-dashed exterior finish is also available. Standard door and windows that are compatible with the system are used.

Figure 3-8. The BEET Building System: Two-story schematic (left), Keyed connections (right)



#### 2.1.4.1 Structural System

The standard sandwich panels are produced by bonding glass-reinforced polyester face sheets to an oriented-fiber mineral wool core. Pultruded glass-reinforced polyester sections are bonded around the perimeter of the panels to create a water-tight unit and to create the tongue-and-groove connection shown in Figure 3-8-right. Other core materials such as polyurethane or aluminum foam can be used for specialized applications. The panels can also be left hollow or filled with concrete, sand, or water. A basic panel with the mineral wool core of dimensions 1.2 m x 3.5 m weighs approximately 150 kg and can thus be maneuvered with very small lifting equipment. Elevated floors and roofs are built using wood trusses or precast concrete panels.

#### 2.1.4.2 Integration of Functions

As in all of the sandwich panel systems discussed, the structural system and building envelope are integrated into single components.

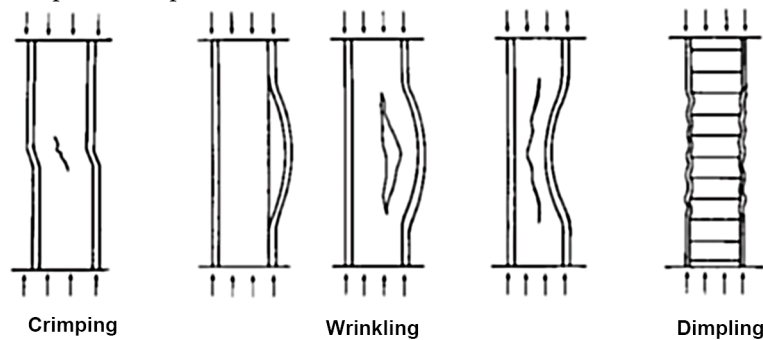
#### 2.1.4.3 Discussion

The manufacturer states in the product literature that the basic panels can achieve a fire resistance rating of up to REI 120 (see Section 3.1.2.1 for an explanation of fire ratings). While this seems impressive, it should be noted that the 20 cm thick mineral fiber core can easily achieve an EI 120 rating (no structural resistance criterion) without the application of the BEET system's face sheets. When the sandwich panel is exposed to fire, the hot side is most certainly destroyed within the first half-hour of exposure. The face sheet on the cold side, however, is well protected by the mineral fiber core and thus the component is able to maintain enough structural resistance to support the minor vertical loads imposed on the walls of single-story structures. Single-sided sandwich panels are structurally inefficient, though, and such a high fire rating would be difficult to achieve with the higher compressive loads imposed on the walls of multiple-story buildings. Thus, it appears that the system can provide a good standard

of fire resistance as long as the mineral-fiber core is used and the vertical loads are small (relative to the ultimate capacity of the component).

The product literature also states: “In most cases, the roof structure can be erected on top of the walls without any further support.” The company also asserts that buildings of up to three stories have been built using the system. The first statement suggests that the panels are only capable of supporting the roof in limited configurations. Given that roof loads are far lighter than those imposed by extra stories, it seems unlikely that three-story buildings can be supported by the standard panels. The mineral fiber used in the core of the standard panels is excellent for insulation and fire resistance, but very poor structurally. Weak core structures lead to several types of compressive failures such as those shown in Figure 3-9 [179]. It is likely, therefore, that the load-bearing capacity required for multiply story-applications is achieved by the replacement of the mineral-fiber core with a better structural material, such as concrete.

**Figure 3-9.** Sandwich panel compressive failure modes [179]



If this is the case, it would seem difficult to justify the complication of the system over insulated concrete form (ICF) systems such as the Royal Building System (see Section 2.1.5). Such systems are structurally superior because the concrete is poured monolithically and steel reinforcement may be inserted, as well as thermally superior because the concrete is not used in place of the insulation layer.

Regardless of its possible weaknesses in multiple-story applications, the system has been quite successful in single-story applications. As with the ACCS (see Section 2.1.3) and numerous other pultruded profiles, a large portion of the successful applications have been in wet or harsh chemical environments. In such applications, the higher material costs are offset by lower operating and maintenance costs. In addition, the smooth water-tight surface finishes are easily cleaned and thus facilitate the adherence to hygienic standards. As such, the BEET Building System has become very popular with the Norwegian health care, pharmaceutical, and food-related industries. To date, a combination of hospitals, fisheries, meat packing, pharmaceutical

plants, and water treatment facilities account for the more than 40 buildings that have been erected using the system.

### **2.1.5 Royal Building System® - Canada, 1996**

The Royal Building System was patented in 1996 by North America's largest PVC extruder, Royal Group Technologies, Ltd. In the system, the PVC elements form the finished wall surfaces, provide insulation, and serve as the form work for the reinforced concrete that is poured within (see Figure 3-10). Thus, it is not a load-bearing FRP building system, but an extrapolation of the insulated concrete forms (ICF) that are commonly used in foundation walls.

#### *2.1.5.1 Structural System*

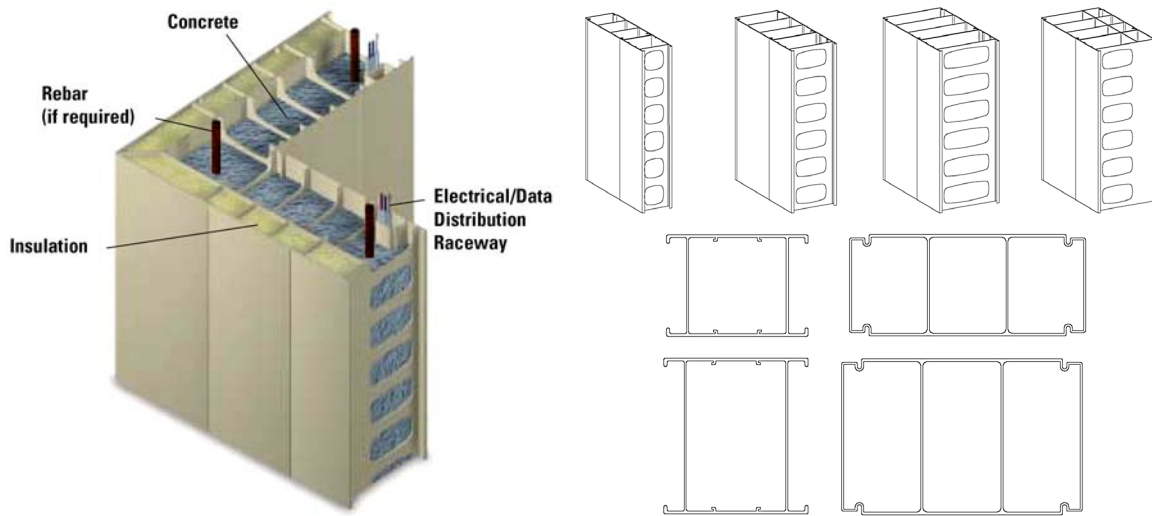
The main components of the system are cellular PVC panels produced by extrusion. Slots are used to connect adjacent panels with a flexible adhesive. Concrete is poured into the panels, and may flow in between panels through holes punched in the webs.<sup>4</sup> Steel tubes may be added inside the cells to keep the panels straight during the pouring of the concrete. Steel reinforcing bars may also be necessary depending on the loading conditions. Wall panels are available in 10 cm, 15 cm, and 20 cm depths, not including the optional insulation layer on the exterior.

Standard construction materials are used for the floor and roof decks. These materials differ depending on the location, loading conditions, spans, and building use. Steel shelf angles are bolted into the wall panels to support the various floor systems.

---

4. A similar system of concrete-filled PVC tubes was used in the Belgian "Polyvilla" system developed in the early 1960's (see Chapter 2 Section 2).

Figure 3-10. The Royal Building System: Insulated wall panel (left), Various wall elements (right)



#### 2.1.5.2 Integration of Functions

The wall elements serve as both the building envelope and load-bearing structure. As shown in Figure 3-10, cavities are provided in the wall panels for the transmission of utilities.

#### 2.1.5.3 Discussion

The Royal Building System is not a load-bearing FRP system. What makes the system relevant, however, is that it has been enormously successful, and in doing so has overcome many of the social and legislative barriers that have troubled previous FRP systems. In the years since its introduction, thousands of buildings, including schools, hospitals, factories, and private homes have been built in over 40 countries worldwide. There are many positive implications for FRP structures in general:

- A detailed design manual has been published, and the system has been accepted by nearly all major building codes and regulating bodies [90].
- Repair and maintenance methods for exposed polymeric surfaces have been developed and are well documented [157].
- Scientific studies on the off-gassing and “sick-building syndrome” by industrial hygienists has shown that the system contributes very little the pollution of indoor air [151].
- The construction of numerous luxury homes has helped remove the stigma of polymeric building materials as cheap substitutes.

The fire resistance of the system is very vaguely described by the company as “less likely to burn than wood.” Indeed PVC has some inherent fire resistance, but this statement makes no denial

that the combustion PVC produces more toxic gasses and black smoke than wood. Structural fire endurance of the polymeric elements is irrelevant because they are not load-bearing.

Nonetheless, the use of the system is increasing at a rate of roughly 20% each year. The opportunities of the system are perhaps the greatest in developing countries, where low-cost, easily assembled buildings with good resistance to extreme weather conditions are most needed.

### 2.1.6 American Structural Composites - USA, 1999

Replacing plywood in standard structural insulated panels (SIPs) with FRP sheets, American Structural Composites introduced an all-composite building system in 1999. The system is targeted at the low-cost single-story construction sector.

#### 2.1.6.1 Structural System

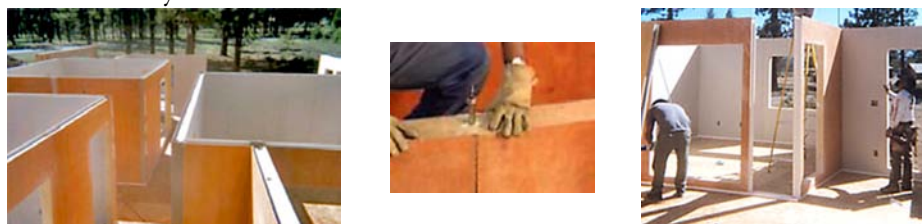
Pultruded glass fiber-reinforced phenolic face sheets are bonded to extruded PVC I-beams. A polyisocyanurate foam is expanded in between the PVC beams. Connections between panels are made through a slotted PVC connectors, which are bonded and locked by a vertical steel pin (see Figure 3-11). Connections to the concrete foundation are made through pultruded channel sections that accept the wall panels. Roof elements are riveted to walls and may span up to 8 m.

#### 2.1.6.2 Production and Assembly

All panels are manufactured in the company plant in Reno, Nevada, USA. Two grades of panels are produced: a residential grade with gypsum board on the interior face, and a sturdier industrial grade with FRP on both faces. Panel widths of 60 cm and 180 cm and lengths up to 5.5 m are available. The face sheets are produced from phenolic resins, meaning that they have excellent fire properties, but cannot be easily pigmented (hence the orange color), and thus require a conventional surface finish. Paint, tile, acrylic stucco, or simulated brick are applied on-site.

Openings for doors and windows are cut by a computer-guided router in the factory and standard doors and windows are installed on-site.

Figure 3-11. The ASC System



### 2.1.6.3 Integration of Functions

One again, the wall panels serve as the building envelope and the load-bearing system. PVC conduits are embedded in the foam core at 60 cm intervals to allow the transmission of utilities.

### 2.1.6.4 Discussion

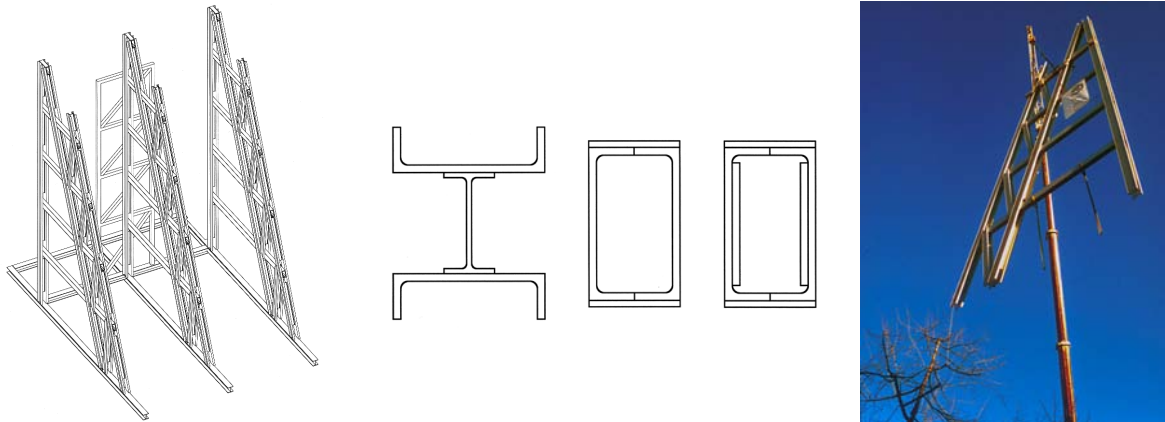
After winning the Composite Fabricators Association's award for Composites Excellence in 1999, the future of the system appeared strong. After the construction of only a handful projects, however, financial and managerial difficulties lead to the disappearance of the company (the company could not be contacted for a more precise description).

Overall, there seems to be very few significant advantages of the system over traditional plywood SIPs. Indeed the phenolic face sheets are more fire resistant than wood, but they must be covered by other materials for durability and aesthetic reasons (highly reminiscent of the Fiber-Shell system described in Chapter 2 Section 3.2). One of the most important justifications for the use of higher cost FRP materials is that they may serve as the structure and envelope at the same time. The need for additional painting or surface effects both inside and outside the building, and the fact that these surfaces will need regular maintenance removes this advantage altogether. Further, assembly of the system is quicker and simpler than traditional stick-building and masonry methods, but not quicker or simpler than with plywood SIPs.

### 2.1.7 Eyecatcher Building - Switzerland, 1999

The Eyecatcher was erected in 1999 to demonstrate many of the modern construction materials and techniques at the *Swissbau*, or Swiss Building Fair in Basel. With five inhabitable stories above ground, it is the tallest load-bearing FRP building in existence. Its FRP skeleton is exposed on both the outside and inside of the building, though there is little thermal bridging because of the low thermal conductivity of the members. The building envelope is composed of cellular FRP sandwich panels filled with aerogel beads, which allows a certain degree of translucency (Figure 3-13-right) and good thermal insulation. After receiving more than 20,000 visitors during the fair, the building was disassembled and rebuilt in its final location a few blocks away [97].

Figure 3-12. The Eyecatcher: Frame schematic (left), Built-up members (middle), Frame (right)



### 2.1.7.1 Structural System

Vertical and lateral loads are resisted by three trapezoidal trusses composed of FRP members (Figure 3-12-left). These members were created by adhesively bonding individual pultruded elements together. The vertical members are composed of two channel sections adhesively bonded to an I-beam, creating a lightweight column section that is resistant to buckling (Figure 3-12-middle). The horizontal members are composed of two channel sections bonded along their flanges to create a rigid box section. Additional plates above the flanges improve the bond and increase the bending stiffness of the members. Some members were also stiffened with web plates.

All permanent connections were made by a combination of adhesive bonding and bolting, while bolting alone was used for the temporary connections related to the disassembly and re-erection of the structure after the building fair.

Figure 3-13. The Eyecatcher: Under construction (left), Completed (middle), Translucency (right)



### 2.1.7.2 Integration of Functions

Subsequent projects have shown that the panels could provide significant shear resistance for the lateral stability of the building, which would have allowed a reduction in the dimensions of the vertical members. At the time of the building's design, however, insufficient testing had

been conducted with respect to the use of the translucent sandwich panels in structural applications, and thus the envelope of the building was not integrated with the load-bearing system [97].

### 2.1.7.3 Discussion

The issue of fire safety was partially resolved through the installation of an active suppression system. When a fire is detected, water sprinklers are engaged and the fire department (located very nearby) is automatically alerted. Because the pultruded FRP columns have very little passive fire resistance,<sup>5</sup> however, it was only possible to receive approval from the building authority by a special variance accorded to demonstration structures.

It is important to remember that the Eyecatcher was intended as a demonstration project and that the objective was never to build a prototype for mass production. As such, the costs and construction speed are less important than the fact that a five story FRP building now stands and is used like any other office building. The building has thus-far been a successful venture and has aided in the battle for public acceptance of FRP materials in buildings. In addition, the project proves that FRP materials can be used in a material-adapted manner without looking like the flying saucers and foam igloos of the 1950's and 60's.

### 2.1.8 PDG Domus - USA, 1999

Similar to the GE Living Environments House, the modular homes currently available from PDG Domus incorporate exterior cladding and roofing materials composed of FRP materials. The homes are industrially fabricated in large modules and then bolted together on-site (see Figure 3-14). Assembly of a typical home takes only two days and costs 10-15% less than similar homes made by the traditional stick-building technique.

**Figure 3-14.** First PDG Domus unit built (left), Assembly of modules (right)



5. Passive fire resistance refers to the ability of a building or building element to resist burning without any active physical intervention.

### 2.1.8.1 *Production and Assembly*

The basic component of the walls, floors, and ceilings is a panel composed of several layers. At the core of the panel are standard steel studs such as those used in commercial partition walls. Gypsum board is then bonded to both sides of the studs using a flexible polyurethane adhesive. Electrical and plumbing is then installed in the cavity before it is filled with expanded isocyanurate foam.

The exterior wall and roof panels receive an additional layer of FRP cladding, which is composed of a modified acrylic resin,<sup>6</sup> glass fiber mats, and a ceramic whisker filler. The laminate is produced by the VARTM technique, where resin is forced into a closed mold containing the reinforcement with the aid of a vacuum pump. As described in Section 3.2.1.1.c, modified acrylic resins have a very low viscosity due to the replacement of the styrene monomer with methacrylate, which allows for high filler loadings. The ceramic filler used by PDG Domus was developed to maximize the ability to create detailed textures, while improving fire and weather resistance. As a result, the FRP cladding can be given the appearance of traditional building materials without the associated weaknesses.

Welded steel frames are built around the perimeter of each panel as well as around all window or door penetrations. The panels are bolted and adhesively bonded into large modules, which then receive surface finishes such as carpeting or painting, lighting and plumbing fixtures, cabinets, and stairwells. The completed modules are then shipped to the construction site. Small cranes lift the modules into place and the steel frames are bolted and adhesively bonded together.

### 2.1.8.2 *Structural System*

As described, the structural system is a traditional welded steel skeleton with diaphragm action provided by the FRP and gypsum sheeting.

### 2.1.8.3 *Integration of Functions*

Though the homes are shipped to the site in a nearly completed state, there is very little fundamental integration of functions. The panels are complex multi-layer assemblies where each layer of material serves one single purpose.

### 2.1.8.4 *Discussion*

It is unfair to state that PDG Domus has missed the point with their prefabricated home system. The homes are quick and economical to build and have lower maintenance costs than

---

6. See the Modar<sup>®</sup> system described in Section 3.2.1.1.c-*Representative Products*

homes built by traditional methods. Yet it seems that the system is highly convoluted and is only competitive due to the high degree of industrial fabrication. The thermal performance of the homes is, at best, similar to that of traditionally built homes. This is no doubt a result of the use of steel studs and welded steel frames, which create thermal bridges through the envelope. The SIPs systems employed by ASC (Section 2.1.6) and Ambiente (Section 2.1.9) are not only simpler to produce, but are more energy efficient as well. The fact that these two systems only support one story structures, while all of the available building systems that are capable of supporting multiple stories have steel or concrete structural systems suggests that adequate structural fire endurance could not be economically achieved in a purely FRP system.

### 2.1.9 Ambiente® Housing System - USA, 2000

The Abersham Technology Group and Wardrop Engineering presented the Ambiente Housing System at the Composite Fabricators Association (CFA) Housing Competition in 2000. Their system is very similar to the ASC System (presented at the same competition the year before - see Section 2.1.6) in that FRP SIPs are connected through pultruded members to form single-story buildings. What is unique is the use of a syntactic glass foam<sup>7</sup> for the core of the sandwich panels and that FRP cables are used to post-tension the structure.

The construction costs are kept low compared to traditional building techniques thanks to the high level of industrial fabrication, which allows quick assembly by relatively unskilled workers. Material costs are also relatively low a result of the use of recycled glass in roughly 80% of the system. These low costs permit the marketing of the system in the low-income housing sector, especially in developing countries where there is a high demand for simple homes with good resistance to extreme weather conditions.

#### 2.1.9.1 Structural System

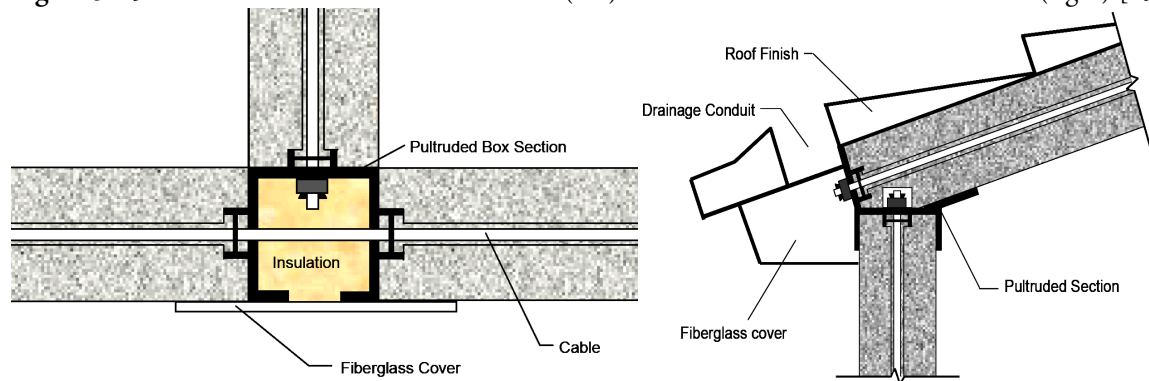
As mentioned, the basic components of the system are sandwich panels. The 1.2 m wide panels consist of 3.2 mm thick FRP face sheets (most likely glass-reinforced phenolic sheets, though this information is not available from the manufacturer) bonded to a 150 mm thick syntactic foam core. The connection between panels is made through pultruded FRP members. No adhesive is used in the joints but some caulking is necessary to create a water and air-tight seal. To create a monolithic wall or roof unit, FRP cables are fed through passages within the cores of the panels and post-tensioned. Cables also hold the roof down to the walls and walls down to

---

7. Syntactic foams consist of small air-entrained glass beads or *cenospheres* bonded together by a resin; usually phenolic for its high temperature resistance. These foams are known for very good insulation levels and high bearing capacity, and make excellent fire barriers.

the concrete foundation, making the structures highly resistant to earthquakes and strong winds.

**Figure 3-15.** Connection between wall elements (left) and between wall and roof elements (right) [153]



A variation of the system is under development at the University of Manitoba [153] for use in Northern Canada, where the extremely cold climate results in permafrost. All structures built on permafrost must be well insulated such that they do not melt the ground, which would lead to significant settlement. The Ambiente group is developing a floor joist that would elevate the habitable space away from the soil and further improve the thermal performance of the building, though specific details are as yet unavailable.

#### 2.1.9.2 Integration of Functions

As with all of the various SIPs systems, the building envelope is load-bearing, and thus there is some integration between the structural and architectural systems. In addition, plumbing and electrical utilities are embedded in the panels during manufacture. The passages that are used for the post-tensioning cables can also serve as conduits for electrical wires. The surfaces of the panels are the final interior and exterior wall finishes. For the exterior, a stucco-like effect is standard for the walls and Spanish tile effect is standard for the roof, though various other options are available.

#### 2.1.9.3 Discussion

The wall panels have a three-hour fire rating by the ASTM E-119 [7], a standard test for the fire endurance of building components that includes both structural and back-face temperature failure criteria. For a single story building, however, the structural loads are extremely small and thus the E-119 certification is more a tribute to the thermal performance of the syntactic foam core rather than the structural fire endurance of the panels.

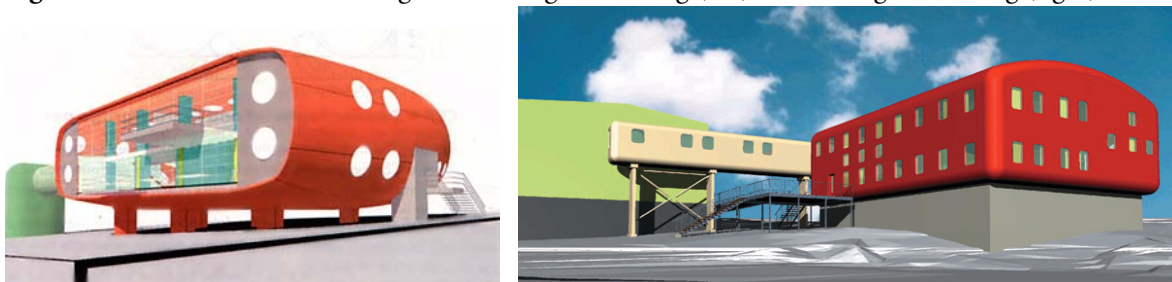
The system is currently produced in Puerto Rico and the UK with thousands of units built in both locations. The company plans to expand production to South America, Europe, Asia, and

North America. In light of the growth of the Ambiente and Royal Building Systems, it appears that many developing countries will soon be checkered with single-story FRP buildings.

### 2.1.10 Davis Station Living Quarters - Antarctica, 2003 (ongoing)

Through an intensive design competition for the replacement for the aging research facility at Davis Station, Antarctica, the Australian Antarctic Division awarded design of the facility to architects Michael Heenan and Nicola Middleton. Their submission involved an egg-shaped building with a load-bearing FRP envelope (see Figure 3-16-left). The neo-futuristic shape was conceived to minimize wind loads (wind speeds can reach 325 kilometers per hour in the region) and snow accumulation on the building. The curved shape was also chosen to maximize the interior space relative to the surface area of the envelope and thus improve the thermal efficiency of the building (temperatures can drop as low as  $-40^{\circ}\text{C}$  in the winter). As the initial design was further developed, however, concessions were made to constructability and ease of use of the interior space, resulting in the more conventional shape shown in Figure 3-16-right [19].

Figure 3-16. Davis Station building: Initial design rendering (left), Final design rendering (right)



Besides the harsh environmental conditions, the remote location of the construction site also posed significant difficulties for construction. Through the use of FRP materials, large lightweight sections will be prefabricated in Australia or South America and then transported to the site for assembly.

Figure 3-17. Davis Station building: Rendering of complex (left), Completed bridge structure (middle), Rendering of building interior (right)



### 2.1.10.1 Structural System

The exterior walls of the building will be 20 cm thick load-bearing sandwich panels. Glass fiber is the primary reinforcement of both the interior and exterior face sheets, though highly stressed regions may also include carbon or aramid reinforcement as well. The core structure will be made from expanded polystyrene or balsa, depending on the location and local stresses. An unspecified fire retarded resin will be used for the interior face sheet and the exterior face sheet will receive a pigmented gel coat. The flooring system is unspecified.

An Australian boat-builder has been engaged to produce the wall panels in 8 m x 2.4 m sections. The sections will be produced by hand-layup in large molds and then cured in a large oven. The panels will then be transported to the site in shipping containers and assembled using a combination of adhesive bonding and bolting. The finished structure will include two stories and stand 8 m tall. The 17 m x 23.5 m footprint amounts to a total floor area of 800 m<sup>2</sup>.

### 2.1.10.2 Integration of Functions

Once again, the building envelope is the load-bearing.

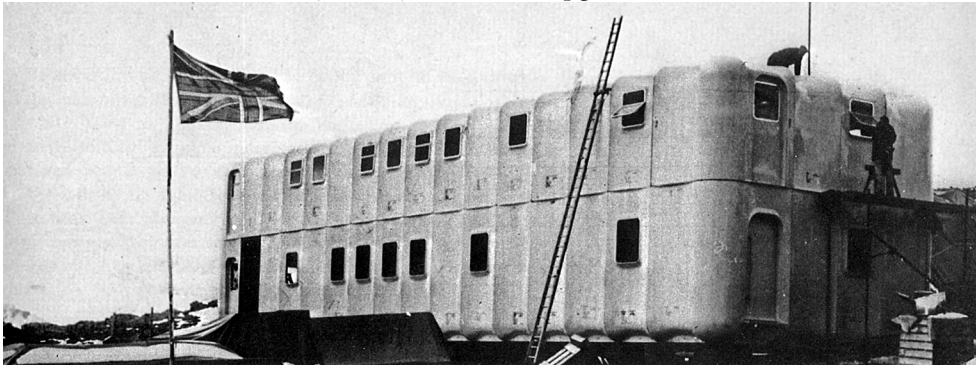
### 2.1.10.3 Discussion

To date, only the 23 m long bridge connecting the old facility (shown in green in Figure 3-17-left) to the new facility has been constructed (see Figure 3-17-middle). Studies will be performed on the bridge section to verify the safety and durability of the system before the construction of the main building. In the absence of major setbacks, the main building should be completed in the summer of 2005. If the entire Davis Station project proves successful, the Australian Antarctic Division will eventually replace all of its installations using the same system [195].

Many reports covering the project suggest that it will be the first load-bearing FRP building in existence. The architects themselves claim to have conceived of the building on a “clean sheet of paper,” reportedly being inspired by their experiences with sailboats. These claims are obviously exaggerated, if not because of the dozens of the other FRP building that have been built in previous decades, then certainly because of the one erected by the British Antarctic Survey in 1963. A similar bonded/bolted sandwich panel approach was used for the British installation, which was an adaptation of the industrialized UK Railway Signal Relay Room System (see Chapter 2-*Chronology*). If the designers of the new building were truly not influenced by the old building, the similarities between the two buildings are no coincidence. Harsh climates and remote locations are one of the most appropriate applications of modular FRP sandwich systems. In such applications, the high material costs are easily offset by the low shipping

weight, quick and easy on-site assembly, and excellent thermal performance of the finished buildings. For these reasons, it is highly likely that FRP sandwich systems will see increased use in remote locations and extreme environments in the future.

Figure 3-18. British Antarctic Survey facility - 1963 [155 pg 59]



### 2.1.11 Spacebox® - Netherlands, 2004

Designed by Holland Composites to serve as temporary housing, the Spacebox units are small self-contained studios that are shipped to the site as complete modules. The FRP sandwich envelope is not load-bearing, but the modules can be stacked up to three stories high thanks to a tubular steel frame. All plumbing and electrical utilities are built into the units during manufacture, including the water boiler, electrical convection heater, kitchen appliances, and all lighting and plumbing fixtures. Hundreds of the units have been installed at Universities in the Netherlands and many more are planned throughout Europe.

#### 2.1.11.1 Structural System

The basic sandwich panel consists of a glass fiber-reinforced polyester outer layer, a styrofoam core, a cementitious fire-proofing layer, and a non-FRP inner finish layer. Timber joists are embedded in the foam core of the floor panels to provide structural resistance. A tubular steel frame passes through the wall panels to support modules placed above (see Figure 3-20).

Figure 3-19. Cluster at Delft Technical University (left), Construction at Utrecht University (right)



### 2.1.11.2 Integration of Functions

As in the PDG Domus system, all of the building systems are integrated into the modules during manufacture, yet separate components or materials are needed for each system. For example, the wood and steel components serve only in the structural system, the cementitious inner layer serves only for fire resistance, the glass/polyester outer layer serves only as the envelope, etc. Thus, there is no significant integration of functions.

Figure 3-20. Mechanical connections and steel supports



### 2.1.11.3 Discussion

Like PDG Domus, Spacebox is a traditional building system that essentially incorporate FRP materials as cladding. The units are not altogether different from the mobile homes and construction site trailer offices that have been produced for decades. The system is significant, however, in the fact that the FRP materials are not disguised as they are in nearly all of the other commercially successful systems. Instead, the material is celebrated in the doubly curved shapes and brightly-colored gel-coat finishes.

## 2.2 Concepts and Design Exercises

The remaining systems and projects that will be discussed are only design exercises or preliminary proposals that have not yet been built or were never intended for construction.

### 2.2.1 Dock Tower - Switzerland, 2002

The Dock Tower is the first example of these projects. Presented at the 2002 *Swissbau* or Swiss Building Fair (three years after the Eyecatcher), the tower was part of design study where innovative tall buildings were designed in concrete, wood, and FRP. As part of the study, a two-story section of the building was constructed and was displayed at the building fair [97].

The Dock Tower was designed to be 36 stories tall with an overall height of 108 m. The floor plan of the tower is circular with five elevator shafts round the perimeter and stairwells in the

center. Large circular windows stretch floor-to-ceiling in normal spaces while enormous rectangular windows were planned for the double-story “sky gardens” (see Figure 3-21).

**Figure 3-21.** Dock Tower: Elevation renderings (left and middle), Selected floor plan (right)



### 2.2.1.1 Structural System

The circular plan of the building with its load-bearing members placed around the perimeter was inspired by the most structurally efficient forms found in nature, such as plant stems. The walls surrounding the five elevator shafts along perimeter as well as five smaller utility shaft walls towards the center were to provide the vertical load resistance and would be built from pultruded cellular FRP members. The façade was designed to brace the elevator walls and would have been built from thin translucent FRP panels filled with aerogel beads. The acrylic windows were to be continuous with the façade such that they could aid in the load-bearing system. The floor deck was to be built from cellular pultruded members as well, and would serve as diaphragms to distribute the lateral load and brace the vertical members. All connections were to be made using adhesive bonds.

### 2.2.1.2 Integration of Functions

As mentioned, the façade served as both the building envelope and the lateral bracing for the vertical load-bearing system. As such, the windows had to be made smaller than in the typical “glass box” curtain wall building. To permit more natural light to enter, therefore, the two-story “sky gardens” with large windows were placed in a spiral pattern up through the building. In addition, the use of only 30% glass reinforcement and the aerogel filling in the façade material itself would allow 70% translucency while still maintaining some load-bearing capacity.

The surfaces of the elevator walls facing the exterior of the building were to be used for solar electricity generation. Additional electricity would be generated by wind turbines on the roof such that the building's ventilation system could be powered off-grid.

### *2.2.1.3 Discussion*

The Dock Tower, while only a design study, successfully demonstrated the kind of energy-efficient and lightweight structures that can be built using FRP materials. To mitigate the relatively high cost of the materials, the circular shape and the integration of the structural system with the envelope maximizes of the usable interior floor space with respect to the area of the façade. The circular shape also minimizes wind loads, while the overall light weight permitted by the FRP materials would have resulted in smaller inertial earthquake loads. Structural fire endurance was addressed through the specification of an internal liquid cooling system (a precursor of the system proposed in Chapter 4), as well as the definition of separate fire zones with adequate egress modes.

## **2.2.2 Woven Building - USA, 2002**

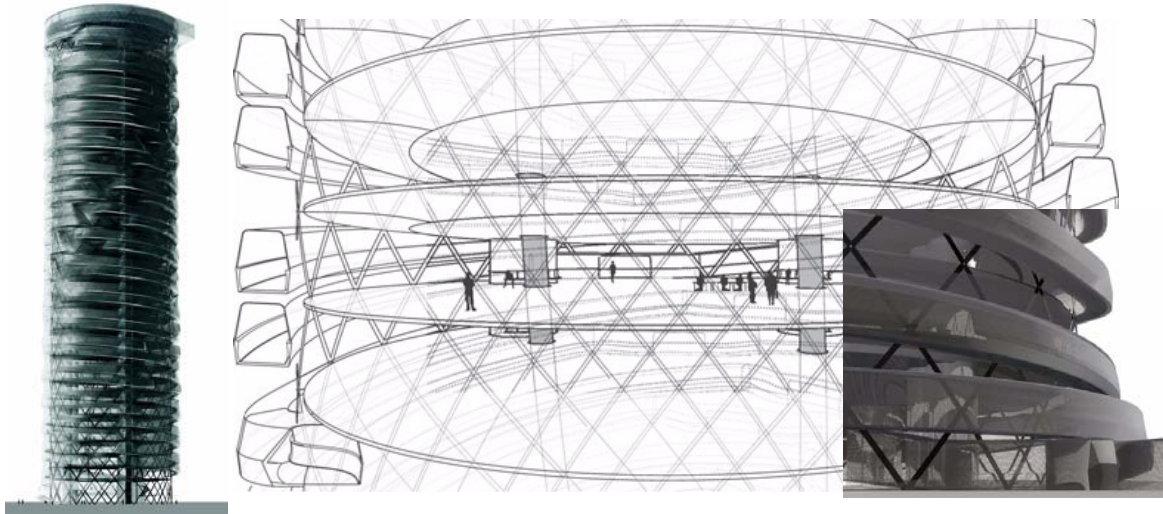
The concept for a 40 story all-FRP tower was unveiled at a 2002 conference sponsored by the Cap Gemini Earnst & Young Center for Business Innovation [80]. Dubbed the “woven building,” the tower was conceived by architect and Harvard/Columbia/MIT Professor Peter Testa in conjunction with the New York office of Arup Engineering.

The envelope of the proposed tower consists of a crossed-helical pattern of carbon tendons integrated into a translucent foil skin. The stairwells/ramps wrap around the building outside of the envelope, while the elevator shafts would be dispersed throughout the interior of the building (rather than the standard practice of grouping them in a central core). Two large shafts would travel the whole height of the building and create natural ventilation through a buoyancy-driven chimney effect.

### *2.2.2.1 Structural System*

Making one complete revolution over the height of the building, 30 carbon tendons form the vertical load-bearing elements. Half of the 30 mm thick and 300 mm wide tendons revolve in one direction and half in the other. Similar to a Chinese finger trap, vertical load on the structure would result in an outward radial force. This force would be resisted other carbon tendons that run across the building, and by stair tubes that wrap around the exterior of the envelope. The greater the vertical load, the higher the stress in the horizontal tendons, and thus the stiffer the floor structure would be [18].

Figure 3-22. Woven Building elevation (left), Section (middle), Detail (right) [18]



#### 2.2.2.2 Production and Assembly

The most interesting aspect of the constructive aspects is the manner in which the carbon tendons would be produced. In order to create continuous tendons over the height of the building, a system involving robotic pultruding machines is proposed. These robots would climb the building and produce the tendons in place, much in the same way that concrete caissons can be slip-formed.

#### 2.2.2.3 Integration of Functions

In a most dramatic fashion, the structural system is integrated with the building envelope. Though the foil façade is not directly load-bearing, it serves to brace the carbon tendons through the stability of its curved shape. The carbon tendons would not create strong thermal bridges because vast majority of the carbon fiber reinforcement (which has a high thermal conductivity) is oriented parallel to the envelope. In addition, the stair tubes that wrap around the building help to resist the outward radial stresses from the helical design.

#### 2.2.2.4 Discussion

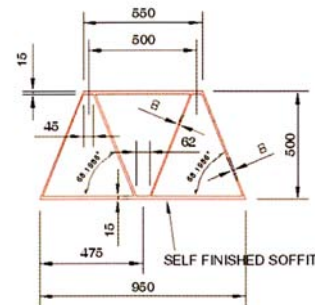
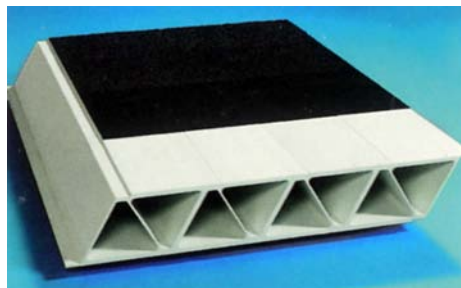
During the 2002 conference in which the concept was introduced, the issue of fire safety dominated the questions as the September 11<sup>th</sup> attacks were still fresh in the minds of the audience. Testa later admitted that the fire safety of the building would be a formidable challenge. Though the epoxy resin used to create the tendons could be retarded such that it would not contribute to a fire, it would still be highly vulnerable to temperature-induced buckling due to other burning objects. This is especially true given the very fine thickness of the tendons.

Nonetheless, the concept is continuously evolved by architect Testa and engineer Arup. Testa claims that all of the technology exists to build such a building, and that it is only a matter of cost [80]. Perhaps future versions will have an improved system for ensuring the structural fire endurance times required for very tall buildings.

### 2.2.3 ASSET Supaflor® - Denmark, 2002

The Danish pultruder Fiberline has produced a cellular FRP decking material called ASSET (Advanced Structural SystEms for Tomorrows Infrastructure) since 1998 (see Figure 3-23). The product was conceived as a lightweight and low-maintenance replacement for deteriorated concrete bridge decks or for new bridges. In exploring other markets for the deck, the Supaflor concept was developed in 2002. The main idea of the Supaflor is that the cellular profile of the deck can be used to route mechanical services and thus more stories can be fit into the same height of building.

Figure 3-23. Four adjacent ASSET bridge deck sections (left), The Supaflor section (right) [52]



#### 2.2.3.1 Structural System

The decking is a glass fiber-reinforced polyester composite produced by the pultrusion process. Due to the nearly unidirectional nature of the reinforcement, loads are mostly transferred in the long axis of the deck and not transversely [100].

The Supaflor profile would be a much larger version of the bridge deck profile to allow greater spans and more space for the mechanical systems. While the bridge deck is only 18 cm deep and two cells wide, the Supaflor is 50 cm deep and three cells wide.

The bonds between pultruded profiles would be made with structural adhesives. End supports are not specified, though Figure 3-24 shows some sort of connection to a box section running in the transverse direction. The system is only intended for flooring and thus requires a vertical structural system of traditional materials.

2.2.3.2 Integration of Functions

As shown in Figures 3-24 and 3-25, the flooring system would allow for the integration of the heating and cooling, fire sprinkler, ventilation, and lighting systems, as well as the electrical and data conduits and connections. As such, the system was targeted at buildings that are highly serviced such as offices, hospitals, data centers, and pharmaceutical buildings. In addition, the surface of the profiles can serve as the final ceiling surface, though some protective floor covering would be necessary.

Figure 3-24. Cross section of the flooring system with mechanical systems [52]

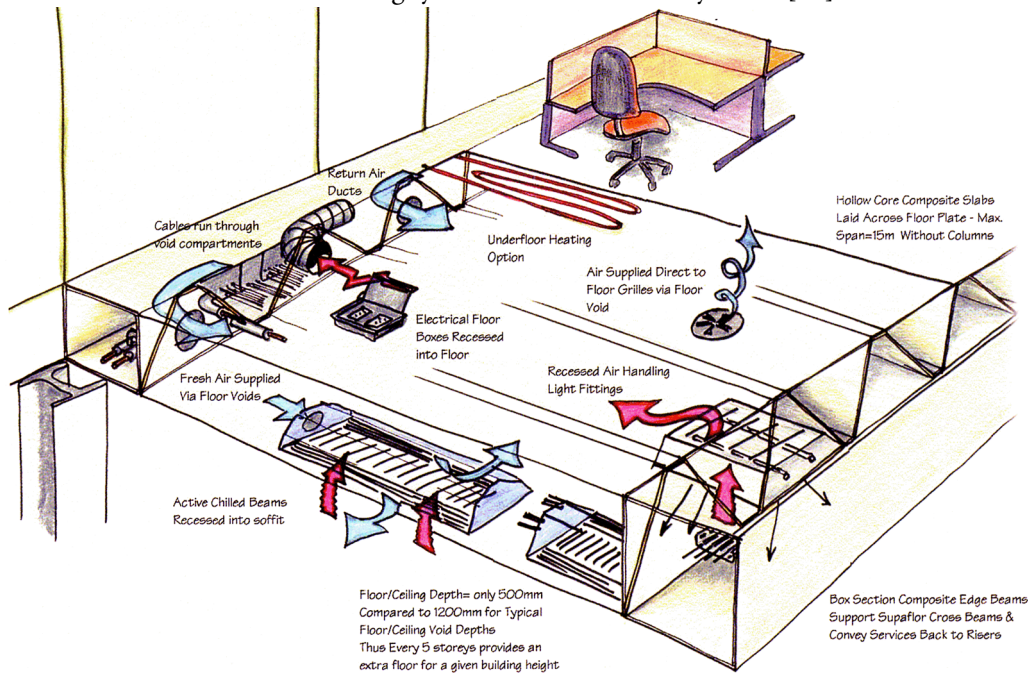
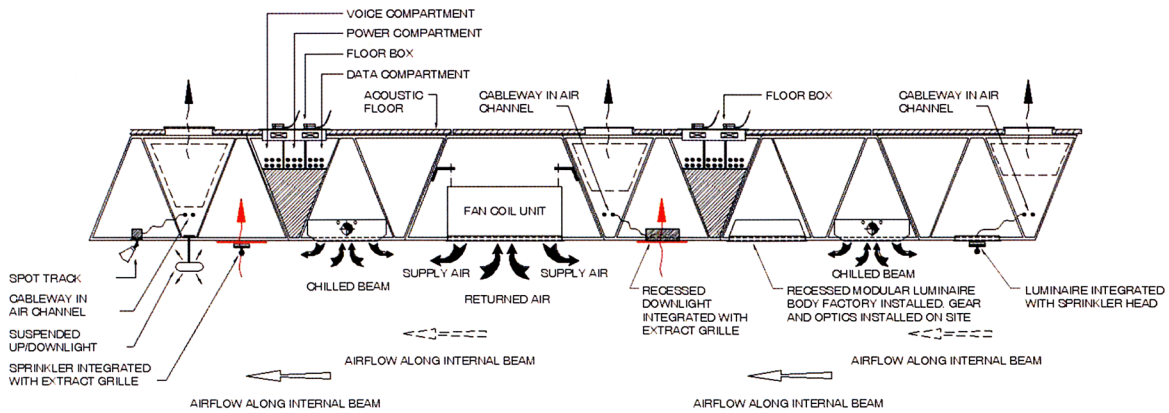


Figure 3-25. Cross section of the flooring system with mechanical systems [52]



### 2.2.3.3 Discussion

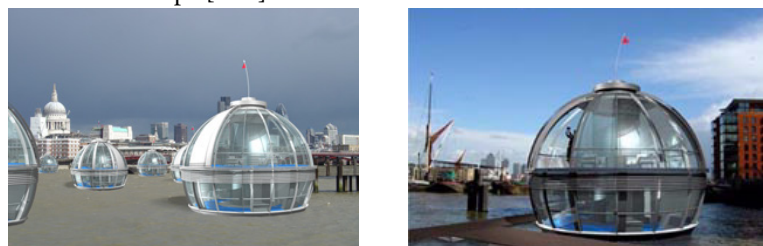
It is unclear whether Fiberline will pursue the Supaflor concept. Though the basic concept appears feasible, the development of all of the associated systems might be cost-prohibitive. As shown in Figure 3-25, nearly all of the mechanical components would need to be specially designed to fit inside the trapezoidal cells or to recess in the face sheets.

The end connections would also be a troublesome area in that in order to distribute the mechanical services in two dimensions, all of the services that pass through the various cells of the floor deck would have to pass through box sections at the ends as well. This would necessitate relatively large box sections, which are not optimal for the transfer of shear in their transverse direction. Further, Figure 3-24 shows that the vertical structural system (drawn as steel wide-flange sections) interrupts the box sections, which would mean that the mechanical services within the box sections could only travel one column bay.

### 2.2.4 Sphere - UK, 2004

Returning to the futuristic shapes of the late 1960's, architect Marcin Panpuch earned a commendation from the Royal Institute of British Architects for his design of a spherical FRP home in 2004. Proposed as a solution to the problem of overcrowding in London, the bubble floats on water and could be anchored along the Thames. The structure would be 12 m in diameter and three stories tall. The bottom floor is designated for mechanical equipment and especially the batteries, whose great weight would provide ballast. The second floor houses the sleeping areas and main entrance, while the third floor is a "flexible use" space. The kitchen, bathroom, and spiral staircase are located in the cylindrical core.

Figure 3-26. Sphere house concept [148]



#### 2.2.4.1 Structural System

Much of the structural system is unspecified. The basic theme appears to be a carbon fiber-reinforced spherical frame with translucent insulative panels for the above-water portion and insulated aluminum panels for the below-water portion.

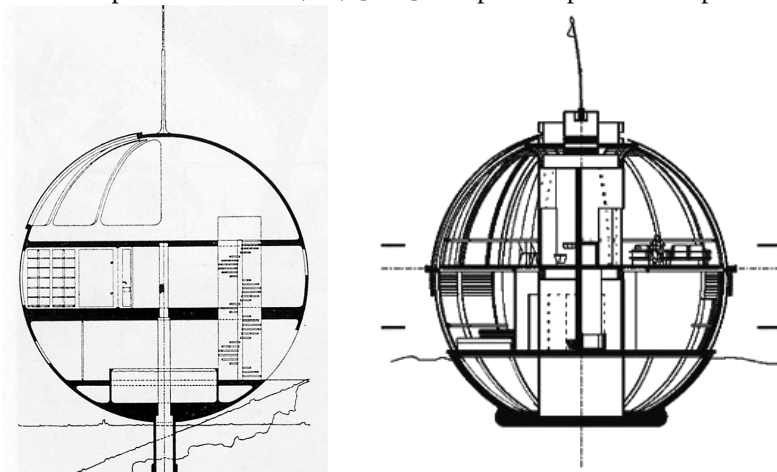
#### 2.2.4.2 Integration of Functions

As mentioned, the electrical batteries and mechanical equipment are also used as ballast. Locating these heavy items at the base of the structure would help to maintain the upright position of the sphere when floating in water. In addition, the photo-voltaic (PV) solar panels serve as privacy blinds for the completely glazed structure.

#### 2.2.4.3 Discussion

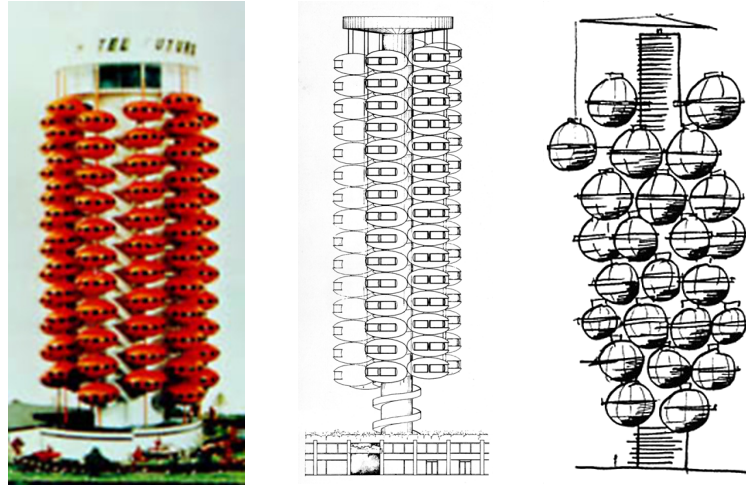
From the antenna on the roof down the spiral staircase to the mechanical space below, Panpuch's concept appears to be an update of Roland Hanselmann's "Sphere" house (Figure 3-27) built back in ca. 1970 (it even has the same name). High cost carbon fiber is most likely specified in place of glass fiber for marketing appeal and a high-tech look. A healthy dosage PV solar panels are supposedly added to make the homes more environmentally friendly. The fact that it requires more energy to produce a PV solar panel than the panels tend to generate during their life span is not emphasized, as the panels are actually needed because of the problems of connecting a nomadic floating home to the city's electrical grid.

Figure 3-27. Hanselmann's Sphere - ca.1970 (left) [163], Panpuch's Sphere concept- 2004 (right) [148]



The suggestion that the homes could be organized into tower clusters [148] is particularly unoriginal. As shown in Figure 3-28, nearly identical proposals were made for the elliptical FRP homes designed by Finnish architect Matti Suuronen and Swiss architects Casoni & Casoni in the late 1960's. Though limited numbers of the homes were built, the tower cluster concepts remained only concepts.

Figure 3-28. Futuro Hotel concept - 1968 (left), Rondo System concept - 1969 (middle) [155 pg. 120], Sphere concept - 2004 (right) [148]



Finally, the idea of constructing a living environment on water with a spherical shape below water is fundamentally flawed. Even with significant ballast, there is no shape more likely to rock, spin, and roll, than a sphere.

## 2.3 Conclusions: Modern FRP Buildings and Building Systems

### *Modern Building Systems*

Seven modern building systems involving FRP materials have been discussed: ACCS, BEET, Royal, ASC, PDG, Ambiente, and Spacebox. For the difficulties described in Section 2.1.3 related to connection quality, the ACCS is better suited to bridge enclosures than to buildings. The Spacebox system, though significant for its successful resurrection of the “plastic as plastic” philosophy of the 1960’s, does not involve the structural use of FRP materials and is therefore not entirely relevant to this project (likewise, the steel-framed PDG system).

This leaves the BEET, Royal, ASC and Ambiente Building Systems. The BEET system is an efficient system for single-story structures with elevated hygiene requirements or harsh environmental conditions. The advantages it presents quickly diminish, however, with increased building height or in less demanding environments. The latter three systems appear to be efficient solutions to the worldwide shortage of low-income housing. The ICF approach used by the Royal system is suited to a wide range of single and two story buildings (including those described for the BEET system), but involves the placement of concrete on-site. The SIPs approach employed by American Structural Composites and Ambiente Housing Systems, on the other hand, is more restrictive in that it can only be used to build single-story structures, but allows quicker and simpler assembly in remote locations. Despite these minor differences,

all of the systems are intended for buildings of less than three stories. As such, the FRP components do not have to support heavy loads and are not subject to very strict (if any) fire performance requirements. It is highly unlikely the solutions that appear to work well in these rather simple applications would be sufficient in the more demanding category of tall buildings.

### *Demonstration Buildings*

Three modern demonstration buildings involving FRP materials have been discussed: GE, Neste, and Eyecatcher. Of these three, only the Eyecatcher employs load-bearing FRP components. While the GE and Neste projects were mostly marketing tools for the materials manufacturers, Eyecatcher was more of an exploration of the ways in which FRP materials can change the way buildings are conceived. The pultruded skeleton that penetrates the non-load bearing envelope was a first step towards a more function-integrated approach (as seen in the Dock Tower and Woven Building).

### *Concepts and Design Exercises*

Four modern concepts and design exercises involving FRP materials have been discussed: Dock Tower, Woven Building, ASSET Supaflor, and Sphere. For the reasons discussed in Sections 2.2.3.3 and 2.2.4.3, the Supaflor and Sphere systems are rather poorly conceived. There are several practical and fundamental problems with both proposals such as end connections for Supaflor and stability for Sphere.

The Dock Tower and Woven Building are the only concepts for tall-buildings incorporating FRP structures that have undergone significant development. The Dock tower demonstrated the possibility of creating a new type of energy-efficient tall building with its highly insulative translucent façade and pultruded bearing elements. The envelope and structural systems were successfully integrated, though the structural fire endurance strategy was not fully developed. In the Woven Building as well, the envelope was integrated with unique load-bearing system, but no structural fire endurance strategy was proposed.

### *Significance to the Proposed System*

While several building systems are currently available for the construction of load-bearing FRP structures, very few can support more than one story and none can support more than three stories. The potential for constructing taller buildings with FRP materials was demonstrated by the five-story Eyecatcher Building. Structural fire endurance requirements in the Eyecatcher, however, were only satisfied by nature of the building's classification as a demonstration unit. Future multiple-story FRP buildings will be subjected to higher standards of structural fire endurance.

Though there are many single and two-story FRP systems in existence, there is no system in production, nor any system ever produced, nor even any well-developed proposal that would allow the construction of multiple-story FRP buildings. This is primarily because no material-adapted solution has been developed to provide sufficient structural fire endurance to FRP members stressed under the weight of a multiple-story building. Approaches that involve the protection of the FRP members through superficial layers negate the advantages presented by the material and are therefore neither material-adapted nor cost-effective. The potential of FRP materials to simplify the construction and improve the long-term performance of multiple-story buildings is dependent on the development of cost-effective methods to provide sufficient structural fire endurance.

## 3 Fire Safety for Fiber-Reinforced Polymeric Structures

### 3.1 Definition of the Problem

In the engine of an automobile or under a frying pan, fire is a useful tool that man has learned to implement to his great benefit. In the case of the built environment, however, it is a dangerous and costly menace that, if uncontrolled, can reduce a building to ruins and take the lives of all of those within. The menace of fire is as old as civilization itself and shows no sign relent:

- In AD64 during Nero's reign, 10 of Rome's 14 districts were totally destroyed by fire.
- In 1666, the Great Fire of London destroyed 13,200 homes and 94 churches.
- In 1871, The Chicago Fire killed 766 people and destroyed 17,500 buildings.
- In 1906, a fire in San Francisco killed over 1,000 people and destroyed 28,000 buildings.
- In 2001, fires in the World Trade Center in New York City resulted in the death of 2,800 people including 410 police and fire fighters.

These examples are dramatic, but in fact more lives are lost and more property is damaged each year through small fires than through large disasters [141 pg. 1]. In 2003, roughly 4,000 lives were lost and \$14 billion in assets were destroyed by unwanted fire in the USA alone [144].

Thanks to improved fire safety strategies, the rate of fatalities and property loss has begun to decline over the past decades. In order to continue this trend, fire safety must be considered at the initial conception of new buildings. The principles of fire-safe design are outlined in Sections 3.1.1 and 3.1.2. The unique risks related to the use of FRP materials in buildings are discussed in Sections 3.1.3 and 3.1.4, and the possible ways in which these risks can be reduced are described in Section 3.2.

#### 3.1.1 Objectives of Fire Safety Measures

Building fires threaten both life and property in numerous ways. Over the years, as insurance company requirements have given way to government-supported building codes, the focus of fire safety in buildings has shifted from the protection of property to the protection of life [33 pg. 1-42]. In order to design adequate protective measures, it is first necessary to define the possible threats that building fires present:

- **Heat and flames:** Contact with an object at 65°C causes burns within one second. Direct contact with flames (which are more than ten times hotter) causes immediate burns. Even without direct flame contact, however, air heated above 150°C causes edema (blockage of the respiratory tract), exhaustion, and dehydration [86 pg. 54].
- **Oxygen depletion:** Normal air contains roughly 21% oxygen. If the fire consumes enough oxygen that the level drops down to 17%, muscular dexterity degrades through anoxia. If it drops further to 14%, mental capacity and decision making are impaired. A further reduction to 8% causes death within 6 to 8 minutes [86 pg. 53].
- **Smoke:** By limiting visibility, smoke may prevent the escape of occupants or inhibit the efforts of rescuers.
- **Toxic combustion products:** There are hundreds of gasses produced during combustion that have been proven to be toxic at sufficient concentrations. Surprisingly, more fire-related deaths are caused by carbon monoxide (CO) poisoning than any other toxic product or even any other threat [86 pg. 55]. Other common poisons are carbon dioxide (CO<sub>2</sub>), nitrogen dioxide (NO<sub>2</sub>), sulfur dioxide (SO<sub>2</sub>), hydrogen chloride (HCl), and formaldehyde (CH<sub>2</sub>O) [193].
- **Structural collapse:** The failure of individual building components, such as a floor deck, or the global collapse of the building can lead to death by direct physical trauma or by the obstruction of escape routes.

The objective of fire safety measures is to reduce these threats to the levels that are deemed acceptable by the community.

### 3.1.2 Building Fire Codes

Building codes are laws or regulations that set minimum standards for the design and construction of the built environment. Fire codes are a special type of building code intended to ensure a minimum level of fire safety.<sup>8</sup>

In general, two types of codes exist: prescriptive and performance-based. Prescriptive codes are an older format that specify the exact details of how to achieve fire safety goals for the building category and usage. These details include the use of materials and products, assembly methods, and overall building design. Performance-based building codes are newer format in which the

---

8. It is interesting to note that more than 50% of all building codes in use were written to address fire-related issues [33 pg. 1-44].

exact fire safety goals are specified as well as the criteria to determine whether those goals are met [33 pg. 1-43]. The manner in which the goals are achieved is not specified.

Prescriptive codes are built on a long tradition and are generally favored by parties with an established economic interest in the construction industry. They are usually simpler to follow because very little evaluation or analysis is required and a finite number of options are acceptable. There are, however, two significant disadvantages to this format:

- The fire safety measures are only adapted to the general parameters of the project, such as building category and usage. Within these general parameters, variations in the specific conditions of the project result in differing levels of actual fire safety.
- Innovation is discouraged. It can be prohibitively difficult to obtain certification for products and assemblies that are not specifically described in the code.

Performance-based codes were conceived to overcome these two disadvantages. By defining the safety goals rather than the exact measures, the level of fire safety is assured. New products receive certification or a rating through validated models or standardized tests. Organizations such as the ISO, ASTM, UL, and DIN<sup>9</sup> develop and publish standard test procedures. The tests are performed for *fire reaction* properties such as:

- Heat release/oxygen consumption (ASTM E1354-04a / ISO 5660-1:2002)
- Ignitability (ASTM E2102-04a / ISO 5657:1997)
- Mass loss (ASTM E2102-04a / ISO 5660-1:2002)
- Smoke production (ASTM E662-03e1 / ISO 5659-1:1996)
- Flame spread (ASTM E1321-97a / ISO 5658-2:1996)

Other tests are performed to determine system-dependent *fire resistance* characteristics such as the ASTM E119-00a, ISO 834-1:1999, and EN 1365. Test procedures such as the Single Burning Item (EN 13238) and Room Corner Test (ISO 13784) can be used to measure several fire reaction and resistance characteristics simultaneously. These standard tests result in ratings that can be referenced by the building code. For example, a typical performance-based building code may require that all doors that form part of a fire compartment achieve an F-90, or 90 minute endurance rating under ASTM E-119.

---

9. ISO = International Standards Organization, ASTM = American Society for Testing and Materials, UL = Underwriter's Laboratories, DIN = Deutsches Institut für Normung

### 3.1.2.1 Fire Codes in the European Union

A unified building code for the European Union members has been under development by the European Committee for Standardization (CEN) since the 1970's. The current code that relates to fire safety in the design and construction of buildings is:

Eurocode 1: Actions on Structures: Part 1.2: Actions on Structures Exposed to Fire [32].

The code was first released in 1990 and most recently updated in 2002. Two forms of design fires are considered within the code: *normative* and *parametric*. The normative design fire is used in the prescriptive portion of the code and refers to the time-temperature curves provided by the ISO 834 standard [92]. The parametric portion of the code provides a performance-based design approach. Rather than using standard time-temperature curves, realistic fire scenarios can be considered using a choice of simple or advanced fire models.

The required performance of building components is denoted by the function that the component serves and the duration of fire exposure it must withstand. The designation "R" denotes retention of structural resistance, "E" denotes retention of the integrity of the component, and "I" denotes retention of thermal insulation. These letters are followed by a number (in multiples of 30) that denotes the minimum duration (in minutes) that these qualities are retained when subjected to fire conditions. For example, a rating of REI30 may be required for walls that are both load-bearing and form part of a fire compartment.

The code is intended to limit fire spread and preserve structural resistance primarily through the use of passive fire safety measures. Requirements for active measures and, in specific, fire sprinklers are deferred to national or local codes [74].

A more in-depth review of the status of fire codes addressing the use of FRP products within the European Union is provided by P. Briggs in [17].

### 3.1.2.2 Fire Codes in Switzerland

The design and construction of buildings in Switzerland is governed by the *Normes Suisses* (SN) published by the Swiss Society of Engineers and Architects (SIA). The current code that relates to fire safety in the design and construction of buildings is:

SIA 183: *La Protection Contre l'Incendie dans la Construction* [168].

This code is used in conjunction with the design methods outlined in the the European Standard (see Section 3.1.2.1), which was adopted into the code:

SIA 261:2003 *Actions sur les Structures Porteuses* [167].

Much of the specific fire safety requirements of SIA 183 are defined by the *Norme de Protection Incendie* published by the Association of Cantonal Fire Insurance Establishments<sup>10</sup> (VFK/AEAI) [183]. It is within this code that the fire endurance requirements are defined for load-bearing components. These requirements are summarized by building height:

- Single-story buildings: no requirements
- Two-story buildings: 30 or 60 minutes, depending on the building size, usage, etc.
- Three-story buildings: 60 minutes
- Taller than three stories: 90 minutes

Endurance times requirements are reduced to 30 minutes in all cases for buildings equipped with fire sprinklers because it is expected that the sprinklers will quickly suppress most fires.

### 3.1.3 Combustibility of FRP Materials

The physio-chemical process in which heat and light are produced through rapid oxidation of a fuel source is called combustion. With the exception of some unusual substances such as hydrogen gas, nearly all fuel sources are composed of organic compounds.<sup>11</sup> Conversely, all organic compounds are potential fuel sources. In order for combustion to begin, however, the fuel source must meet with an adequate supply of an oxidizing agent (normally oxygen in air) and an adequate energy source to heat the fuel to its ignition temperature. Further, the fuel and the oxidizing agent must be present in the proper form (only gasses combust), and in the proper concentrations. Adequate energy must also be available to break the covalent bonds within the compound and release the *free radicals*<sup>12</sup> that eventually react with the oxidizing agent. In one fire theory, these four essential ingredients to combustion are represented as sides in the “fire tetrahedron,” as shown in Figure 3-29. According to the theory, all sides of the tetrahedron must be present and in contact in order for combustion to proceed [54 pg. 28].

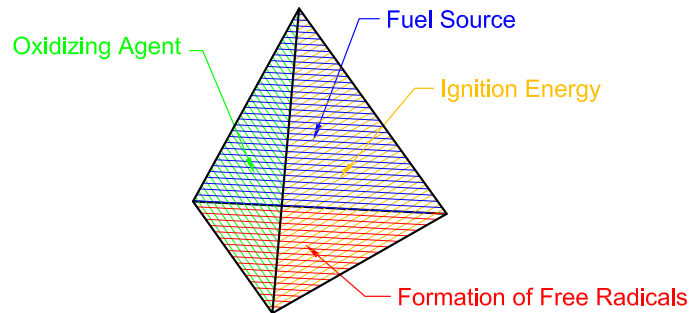
---

10. Literal translation by the author; VFK/AEAI = *Vereinigung Kantonaler Feuerversicherungen / Association des Etablissements Cantonaux d'Assurance Incendie*

11. *Organic* compounds are compounds that contain carbon-hydrogen bonds.

12. *Free radicals* are composed of atoms that have unpaired electrons and are thus highly reactive.

Figure 3-29. The fire tetrahedron



As the elimination of fuel sources from the built environment is almost as absurd as the elimination of oxidizing agents, fire prevention is usually focused upon the removal of dangerous energy sources. In the suppression of existing fires, however, it is often possible to arrest combustion through the removal of any one of the sides or combination of sides.

To better understand how FRP materials burn, it is convenient to imagine combustion as the final stage in a four-stage process [86 pg. 41]:

- I. **Heating:** Energy is transferred to the solid polymer to bring it from ambient temperature to the temperature at which it begins to chemically decompose,  $T_d$ .
- II. **Decomposition:** More energy is needed during this stage to break the covalent bonds of the organic compounds and thus reduce it to its decomposition products: solid residue (char, ash), partially decomposed polymer (various liquids), entrained particles (smoke), incombustible gasses, and combustible gasses (which are created from the aforementioned free radicals).<sup>13</sup>
- III. **Ignition:** This stage has no dimension of time; it is the instant at which all sides of the fire tetrahedron meet and combustion begins.
- IV. **Combustion:** In this final step, the exothermic reaction between the combustible gasses and the oxidizing agent provides the energy required for more of the solid polymer to decompose. As the fire produces more heat, more decomposition occurs, creating more fuel, which allows further combustion, and thus the cycle becomes self-propagating. The combustion may be flaming, as is customarily regarded as “fire”, or non-flaming (smoldering), as is illustrated by the burning of a cigarette. Burning rate and flame spread are strongly influenced by the ratio of the amount of energy produced by combustion to the amount of energy required for decomposition.

13. The decomposition stage is also known as *pyrolysis*, though this term is avoided because the definition is somewhat disputed. Some consider pyrolysis to be a unique form of decomposition that only occurs in the absence of an oxidizing agent [6], while others use the terms interchangeably [54].

A more in-depth discussion of the combustion of polymers is available in numerous texts, including those by Troitzch [181], Drysdale [47], Fire [54], Grand [70], Nelson [141], Cox [34], Landrock [102], and Hilado [86].

### 3.1.4 Temperature Dependence of FRP Material Properties

The physical properties of FRP materials (specific heat capacity, thermal conductivity, density, modulus of elasticity, etc.) do not change significantly in the range of operating temperatures. As such, they are often assumed to be constant in engineering design [64]. The small changes that do occur are reversible and thus do not permanently alter the material.

#### 3.1.4.1 Mechanical Properties

As shown by the *Elastic Modulus* curve in Figure 3-30, the mechanical properties of FRP materials change abruptly as they are heated beyond their operating temperatures [180]. Though there are several methods of defining the exact temperature, the glass transition temperature,  $T_g$ , is most often used to indicate the approximate range where these changes occur. As FRP materials are heated, the long polymeric chains in the resins stretch and slide by one another more easily and the composite changes from a glassy and brittle to rubbery and compliant. The strength and stiffness properties of FRP components are affected most severely in the directions where there is little or no reinforcement perpendicular to the stress.

Upon heating to still higher temperatures, the resin begins to decompose. Though there are several ways to define the exact temperature, the decomposition temperature,  $T_d$ , is used to indicate the approximate range where decomposition occurs. Once decomposition begins, all changes are irreversible and permanent [160]. When the resin has completely decomposed, the composite is no longer able to resist any forces.<sup>14</sup>

#### 3.1.4.2 Specific Heat Capacity, $C_p$

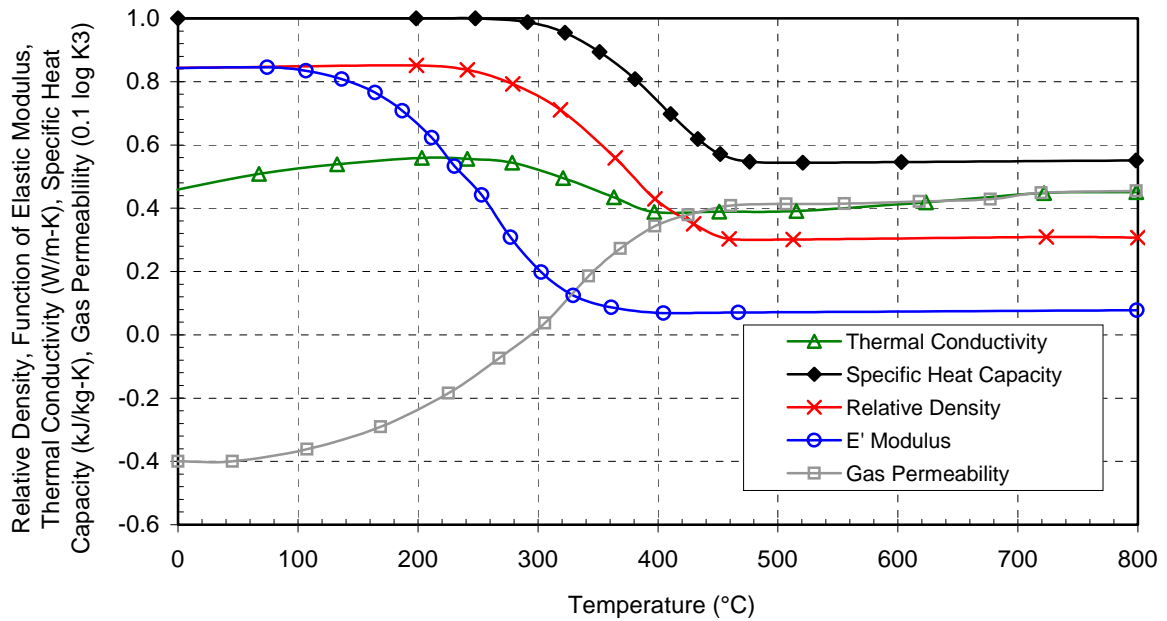
The specific heat capacity increases steadily from ambient temperatures until decomposition of the resin begins [103]. During decomposition, the specific heat capacity does not change significantly but the “apparent” or “effective” specific heat capacity abruptly increases [177 pg. 25]. This phenomenon was observed by several researchers, including Cerny [25], Chen [27], Henderson [81] (reproduced in Figure 3-31), McManus [126], and Fanucci [51]). The terms “apparent” or “effective” are used to describe the values that result from experimental measurement. In experiments, large amounts of energy are absorbed by decomposition of the resin, phase changes, and dehydration of absorbed water, which result in large humps in the  $C_p$

---

14. Excluding the special case of tension with the fiber ends anchored in sound matrix.

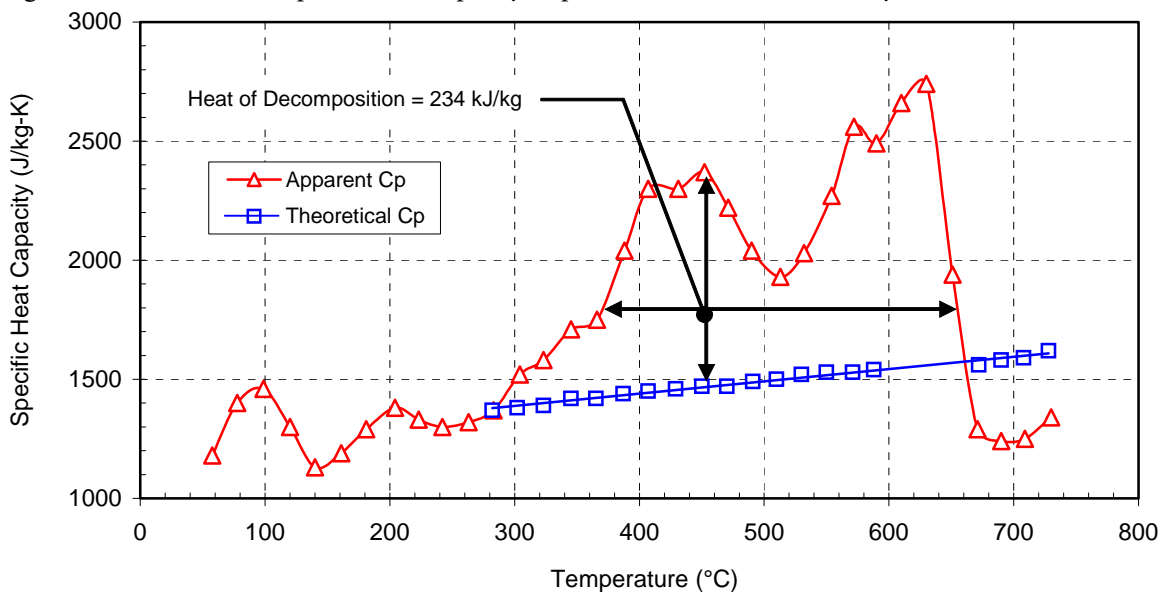
versus temperature curves (see Figure 3-31). If the energy absorbed through these effects is not separated from energy required to cause the temperature of the material to increase (sensible energy increase), the measurements are called “apparent” or “effective.”

Figure 3-30. Temperature dependence of selected properties of glass-reinforced epoxy composite [43]



Once all of the resin has decomposed, the heat capacity of the ash/reinforcement material begins to gradually increase once again [103]. This trend continues until the fibers decompose and only char and ash remains.

Figure 3-31. Effective or specific heat capacity of phenolic resin as measured by Henderson [81]



### 3.1.4.3 Thermal Conductivity, $\lambda$

Thermal conductivity also shows a gradual increase from ambient temperatures up to decomposition [103]. Once decomposition begins, the conductivity begins to decrease as a result of the formation of voids within the matrix (see Figure 3-30). This effect is less marked in the direction of the fiber reinforcement, as the heat is conducted more strongly by fibers and changes to the matrix are less influential [43]. After the resin has completely decomposed, the material properties fall fairly close to those of the fiber reinforcement alone. The conductivity of the ash/char/reinforcement materials begins to gradually increase once again [103]. This trend continues until the fibers decompose and only char and ash remains.

### 3.1.4.4 Density, $\rho$

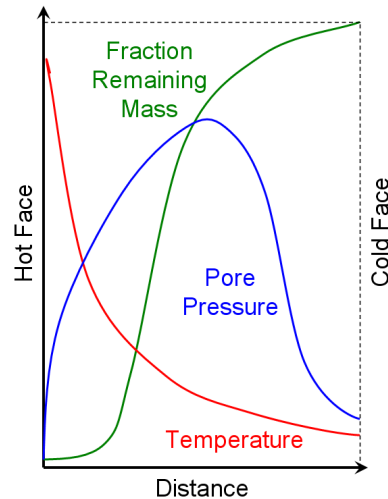
In the range of temperatures from ambient to decomposition, the density may slightly decrease as a result of thermal expansion (which increases the volume of a fixed mass) and evaporation of absorbed water (which reduces the mass of a fixed volume) [43]. Once decomposition begins, the density drops in parallel with the loss in mass of the resin (see Figure 3-30).

## 3.1.5 Heat-Induced Damage Mechanisms

In addition to the chemical degradation that occurs within the constituent materials at elevated temperatures, the manner in which the dissimilar materials are intermingled causes mechanical degradation of components as well. Because the coefficient of thermal expansion of the matrix is many times greater than that of the fibers, stresses are created by the uneven thermal expansion of the materials that result in micro-cracks in the resin [26].

Further mechanical damage occurs when the resin reaches  $T_d$  and decomposition gasses are released. Pressure increases inside microscopic pores (see Figure 3-32) and eventually builds high enough to burst the pores and escape the decomposition zone. This process causes the gas permeability of the decomposed regions to increase (see Figure 3-32). The uneven thermal expansion and pore pressure mechanisms eventually lead to delamination of the outermost reinforcement layers.

Figure 3-32. Schematic of pore pressure, temperature, and remaining mass through the thickness of a fire-exposed FRP plate [160]

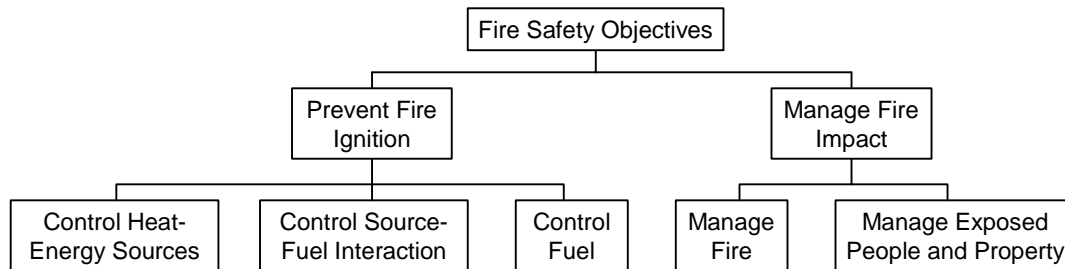


Beyond the self-destructive effects of uneven thermal expansion and pore gas pressure, FRP composites are also damaged by the erosive action of fire gasses in the process known as ablation [160].

### 3.2 Solution Methods

Adequate fire safety normally involves a combination of passive and active safety measures. Passive measures are intended to discourage the ignition of fires and manage the impact of fires through mechanisms that require no human intervention or automated response. Active measures involve a managed physical response by humans or automated systems. Both sorts of measures are implemented through the strategies shown in Figure 3-33. For example, the use of circuit breakers or fuses in an electrical system are an active measure that automatically detect a short circuit and stop the flow of electricity, and thus fall within the strategy “Control Heat-Energy Sources.” The use of inflammable wire insulation materials and metallic conduit are passive measures intended to “Control Fuel.” Working together, the risk of a short circuit causing ignition of a building fire is greatly reduced. The active and passive measures that are appropriate to FRP building components are described in the following sections.

Figure 3-33. Methods of achieving fire safety objectives [33 pg. 1-37]



### 3.2.1 Passive Fire Safety Measures

To understand the purpose of passive fire safety measures, it must be first considered that building fires rarely begin with the ignition of the building itself. The vast majority of fires begin with small burning items such as electrical fixtures, stoves, heating units, and most common of all, cigarettes [144]. The way in which these small fires become catastrophes is through the spread of fire to the building elements, which may then spread throughout the structure. The primary goal of passive safety measures is to prevent the conversion from small burning items to full inferno.

Passive measures can be introduced into buildings at all levels, from the molecular level of building materials to the global scale of building design. They are implemented to achieve four objectives [187]:

- Reduce the ability for construction materials and components to act as readily available fuel sources
- Reduce the impact of burning construction materials and components by reducing the amount of heat, smoke, and toxic gases they produce
- Create fire-hardened compartments that prevent the spread of fire throughout the building
- Protect load-bearing building components such that they remain structurally functional in fire conditions

These objectives are usually achieved through the use of non-combustible or weakly combustible coatings and layers such as gypsum board, masonry, lightweight concrete, etc. The use of such layers in an FRP building system, however, would largely defeat the advantages presented by FRP materials, and therefore are not a material-adapted solution.

The more suitable solution is to make the FRP components themselves less likely to serve as fuel sources and more capable of preventing the transmission of flames and heat. Three principle measures have been identified for the conception of fire-safe FRP components:

- Fire retardant additives or fillers in the matrix formulation
- Inherently fire resistant resins
- Intumescent materials as protective surface layers

In the following sections, the basic mechanisms of each of these methods are briefly described and their potential for imparting total fire safety (i.e. reduction of heat, smoke, and toxic gas production, and the prevention of heat-induced mechanical weakening of load-bearing members) is considered.

### 3.2.1.1 Fire Retardants

The first and most common passive fire protection method for FRP elements is the addition of special retardant agents to the matrix material. Decades of research have gone into the development of such agents such that there are countless different varieties now available. Some of the key characteristics that differentiate each of these agents are:

- **Active Mechanism:** Fire retardant agents can act through either **chemical** or **physical** mechanisms. Some common chemical means are the interruption of the gas phase reaction and the prevention of the formation of CO or CO<sub>2</sub> through the redirection of carbon to a char layer. Some common physical means are the cooling of the solid polymer through latent heat absorption, dilution of combustible volatile gasses, and the insulation of heat through the formation of a char layer [181 pg. 45].
- **Stage of Action:** Retardant agents can be classified by the stage or stages of combustion in which they are active (see Section 3.1.3). Mineral fillers, for example, can slow the heating process (Stage I) by increasing the specific heat capacity of the material. Some additive retardants impede the decomposition process (Stage II) by endothermically decomposing and evaporating at a temperature just below the decomposition temperature,  $T_d$ , of the resin [102 pg. 28]. Ignition (Stage III) can be retarded by reactive agents that decompose into heavy gasses, which in turn block oxygen and slow heat transfer to the reaction front [86 pg. 174]. There are also agents that impede combustion (Stage IV) by decomposing and combining with the decomposition products of the polymer to form incombustible end products [54 pg. 162].
- **Composition:** Fire retardants are often broken down into two major groups: organics and inorganics. The most important organic agents are based on phosphorus and halogens (iodine, chlorine, bromine and fluorine) [102 pg. 29]. The most important inorganic agents are aluminum trihydroxide (ATH), antimony oxide (ATO), and magnesium hydroxide [54 pg. 164].

- **Mode of Processing:** Once again, fire retardants can be categorized into two groups: **reactive** and **additive**. Reactive agents are introduced in such a way that they react with the polymeric resin to form a new compound, and are most commonly used for thermosets. Additive agents are simply mixed into the resin but remain chemically separate, and are most commonly used for thermoplastics [181 pg. 46]. One notable exception is the inorganic oxides, which are additive retardants frequently used for thermosetting resins.

References to these categories are made in the following descriptions of the most commonly used fire retardants. The strengths and weaknesses, of each family are discussed and some examples are provided of their commercially available forms.

#### 3.2.1.1.a Halogen and Antimony Trioxide (ATO) Fire Retardants

Historically the most commonly employed of all fire retardants, halogen agents are among the most effective of all the products available in reducing flammability. In recent years, concerns of the toxicity of the combustion gasses and thick smoke produced during burning, as well as environmental pollution issues have reduced the popularity of halogenated resins.<sup>15</sup> Varieties are based on iodine, bromine, chlorine, and fluorine, in order of descending effectiveness. Iodine agents are rarely used because their high reactivity tends to lead to activation during the manufacturing process, leaving the finished product unretarded. On the contrary, fluorine agents are rarely used because they have a low reactivity and do not activate when needed. Of the two remaining, bromine agents are roughly twice as effective as chlorine agents per weight, though they are also more expensive and are susceptible to ultraviolet light degradation [181 pg. 46]. Despite these drawbacks, bromine agents are favored by the industry over chlorine agents by a ratio of roughly 4:1 [181 pg. 16].

#### *Active Mechanisms*

Halogen agents are believed to act in both the ignition and the combustion stages of the combustion cycle (Stages III&IV - see Section 3.1.3), though the details are still subject to debate. The chemical reactions that take place are highly complex and are therefore beyond the scope of this review. The basic principles can be summarized as follows. The first mechanism of the retardant impedes the ignition stage by blocking oxygen from reaching the reaction front. The second mechanism of the retardant interferes with or replaces the oxygen in the gaseous phase reaction to form incombustible decomposition products, which in turn reduces the heat of combustion, reducing the fuel available for reaction [54 pg. 162].

---

15. There is strong movement in many European nations to ban their use altogether [115].

Halogen-based fire retardants are often used in conjunction with ATO, which creates a *synergistic* effect.<sup>16</sup> As little as a 2% loading of ATO allows the loadings of the bromine or chlorine retardants to be reduced from 17% to 9% while maintaining the same effectiveness [86 pg. 178]. Its primary use then is to improve mechanical, durability, and processing qualities by reducing fire retardant loadings rather than to increase fire resistance itself.

### *Strengths and Weaknesses*

Bromine and chlorine-based fire retardants are a highly cost-effective means of reducing the propensity of polymers to support combustion. For this reason, they are extensively employed in the thermosetting polyester and epoxy resins most commonly used in building materials. With the use of synergists such as ATO, their loading levels are low and do not radically alter the processability of the resin systems nor the durability or strength of the finished products.

Heated debate continues over the environmental and health-related issues of halogenated and ATO products. Concerns are not only for the toxicity and smoke production of the chemicals in fire conditions, but also their long-term accumulative effects to environment, as the halogenated products become waste and are incinerated. Industry defenders do not argue that the products are harmless, but that dangers are well documented and are therefore more acceptable than the unknown effects of newer fire retardant groups.

In Section 3.1.1 it was stated that the four threats to occupants in building fires are heat, smoke, toxic gasses, and structural collapse. While halogenated resins show greatly improved performance in the first category over unretarded resins, they perform actually worse in the following two, and show no improvement in the fourth. Thus, halogenated fire retardants are not a suitable solution to providing total fire safety for FRP structures.

### *Representative Products*

Nearly every resin manufacturer produces a halogenated fire retardant variant of their resins. Ashland Chemical's Derakane® 510-a is a good example of a brominated vinyl ester resin.

### *Further Reading*

Texts by Horrocks & Price [88] and Grand & Wilkie [70] provide current and exhaustive information regarding halogen-based retardants, their chemistry, processing, market usage, toxicity, and many other aspects. In regard to the ongoing discussion of the health and environmental issue, The Bromine Science and Environmental Forum ([www.bsef.com](http://www.bsef.com))

---

16. *Synergism* is defined as an effectiveness produced by two products that is greater than the sum of the two products working separately.

provides the voice of the bromine industry. The critical perspective is provided by (among many) [2] and [94]. Unbiased studies are also available in [41], [177] and [185].

#### *3.2.1.1.b Phosphorus-Based Fire Retardants*

Currently possessing the second largest market share and comprising one of the most diverse groups of agents, phosphorus-based retardants are quite frequently used [119]. They can be found in a myriad of forms that act through a number of different mechanisms. Some important varieties include elemental red phosphorus, phosphine oxide, ammonium phosphate, trialkyl phosphate, and aryl phosphate. There exist stand-alone retardant additives, synergistic products to be used with halogens or inorganic retardants such as aluminum trihydroxide (ATH), and intumescent gelcoat products for use on non-retarded composites [70 pgs.147-170].

#### *Active Mechanisms*

Due to the great variety of mechanisms through which phosphorus-based retardants act, the basic principles will be generalized as follows. The chemical decomposition of the retardant produces chemicals that react with the decomposing polymer to form carbonaceous char. This char layer insulates the solid polymer below, slowing heating and decomposition (Stages I & II). In addition, char formation indicates the impediment of the oxidation reaction, as carbon is directed to the solid phase rather than reacting to form one of the main combustion products: CO and CO<sub>2</sub>. The decomposition of the retardant also leads to the formation of water (which provides cooling through latent heat absorption) and incombustible gasses (which dilute the concentration of the combustible gasses).

#### *Strengths and Weaknesses*

As described above, the promotion of char formation is a highly desirable attribute in fire retardance. The fact that phosphorus-based retardants are already active in the decomposition stage is important, as it provides better protection to the layers of FRP that have not yet been degraded. Smoke and toxicity are also reduced in the best varieties though the fourth threat (structural collapse) is only indirectly addressed. Structural endurance can be improved by the reduced thermal conductivity of the char layer, which allows the material underneath to remain below  $T_g$  for a longer period of time.

Weaknesses include high loading levels for the stand-alone retardants, discoloring, inability to produce translucent resins, and the evolution of potentially corrosive gasses from the phosphoric acid produced during burning.

### *Representative Products*

Reichhold Corporation's produces a line of unsaturated polyester resins called NORPOL® 880 and 885, which incorporate phosphorus-based fire retardants. Clariant's Exolit® products include phosphorus-based additives for unsaturated polyester resins and fire retardant gel coats.

### *Further Reading*

Once again, the texts by A. Horrocks & D. Price [88] and A. Grand & C. Wilkie [70] provide current and extensive information regarding the many forms, chemistries, and applications of phosphorus-based fire retardants.

#### *3.2.1.1.c Inorganic Hydroxides*

Following the halogens and phosphorus-based agents, aluminum trihydroxide (ATH) holds the third largest portion of the fire retardants market [181 pg. 15]. Though they have existed for over 15 years, their popularity has grown considerably in recent years due to the legislative pressure mounting against halogen agents. Of the several other inorganic hydroxides in existence, magnesium hydroxide and magnesium carbonate are the only ones that are used in any significant quantity.

### *Active Mechanisms*

ATH interrupts the combustion cycle through three mechanisms. In the first, the agent slows heating by decomposing at temperature just below  $T_d$  of the polymer ( $\sim 220^\circ\text{C}$ ). This decomposition is highly endothermic, as large amounts of energy are required to convert ATH to water and aluminum oxide. A second cooling mechanism is triggered by this formation of water, which absorbs latent heat energy in its phase change from liquid to gas. Finally, the escape of water vapor interrupts Step 3 by diluting the combustible gasses [54 pg. 163].

Magnesium hydroxide works in a similar manner, though it is activated at a temperature roughly  $100^\circ\text{C}$  higher than ATH and its decomposition is even more endothermic.

### *Strengths and Weaknesses*

The main strengths of ATH additives are their low toxicity and smoke production, low cost, and their ability to interrupt the combustion cycle in the first stage.

As has been described, ATH is capable of reducing the first three threats to humans in a building fire (heat, smoke, toxicity). The ability of this retardant to delay Stage I in the combustion cycle is unique and an important means of delaying the fourth human threat: structural collapse.

Unlike other retardants, however, the effectiveness of ATH is directly proportional to its loading rate. In practice, high loadings (typically 35% to 65%) are required to meet fire performance criteria, which leads to high viscosity during processing and degraded mechanical properties [70 pg. 290]. Some manufacturers (Ashland, DSM) have developed acrylic-based resins with lower viscosities to allow for the high loadings of ATH.

### *Representative Products*

Reichhold Corporation produces an ATH retarded unsaturated polyester resin in their DION® FR 850 series. BYK-Chemie and Alusuisse Martins-werk jointly produce ATH fire retardant fillers.

Methacrylate-modified acrylics such as Ashland Chemical's MODAR® range and DSM Composite Resin's Synolite® range are similar to polyester resins except that they are cured with a methyl methacrylate monomer rather than a styrene monomer. This formulation results in a lower viscosity resin that allows for higher loadings of ATH while still retaining its processability and improving UV light resistance [192]. The high loadings of ATH allow these resin systems to perform extremely well in terms of reduced smoke production, heat release, and toxicity, and present the only significant competitor to phenolic resins (see Section 3.2.1.4) in these respects.

### *3.2.1.2 Nanocomposites*

The term *nanocomposites* describes the rapidly developing new field of polymers that incorporate nano-sized ( $10^{-9}$  m diameter) particulate fillers [154].<sup>17</sup> There are many varieties of the fillers, though the most popular ones used as fire retardants are layered silicates. These “organoclay” silicate particles are roughly 1 nm in thickness and several microns in diameter. Loadings of 10% or less (by weight) of such fillers have been linked to significantly reduced peak heat release rates and greater char production. In addition to improved fire reaction properties, nanocomposites often demonstrate better mechanical properties, lower permeability, greater solvent resistance, and increased electrical conductivity [13].

### *Active Mechanisms*

Like the intumescent materials and the phosphorous-based retardants, nanocomposites are active in promoting the creation of a char layer. This char layer insulates the composite below and slows the progress of Stages I & II (Heating & Decomposition). Researchers have noted not only an increase in char production, but also lower char permeability, which helps to

---

17. The word *composites* denotes the combination of the nano-sized fillers with the polymer, not the combination of the filled polymer with fiber reinforcement.

prevent the escape of decomposition gases to the reaction front [153]. In addition, the creation of char reduces the toxicity of the combustion products, as less carbon is available to form the CO and CO<sub>2</sub>.

The mechanics of how the fillers actually produce these qualities are only starting to be understood. It is interesting to note that nearly all of the beneficial qualities that nano-sized organic clay fillers can impart, rapidly diminish with increasing particle size, such that almost no benefit is observed for micro-sized (10<sup>-6</sup> m) particles [13].

### *Strengths and Weaknesses*

Nanocomposites have a strong advantage over other fire-retardant fillers in that they are effective at very low loadings. Only 2-10% (by weight) loadings of organoclays can produce improvements in fire behavior similar to 60% loadings of ATH/phosphorous fillers. Further, although the ambient-temperature mechanical properties of resins are degraded by nearly all other fire-retardant fillers and additives, nano-sized fillers may actually improve these properties. Lastly, the materials used to create the fillers are generally considered benign and environmentally friendly.

Like all of the previously described fire-resistance solutions, composites protected by nano-sized fillers are most useful in preventing the component from contributing to the heat, smoke, and toxicity of the fire. These are indeed critical issues, but for large multiple-story buildings, the issue of structural fire endurance is equally important. The formation of a char layer can slow heating of the in-tact composite and thus extend structural endurance time. Though the field is still in its infancy, it seems unlikely that it will be possible to achieve the 90-240 minute endurance times required of load-bearing members through the use of nanocomposites alone.

#### *3.2.1.3 Other Fire Retardants*

A number of other additives are available or in development that make use of melamine, zinc stannate, zinc borate, boron, and tin. Due to their relatively minor contribution to the fire retardants market and the redundancy of their mechanisms to agents already described, they will not be considered in this text.

#### *3.2.1.4 Inherently Fire Retardant Resins (Phenolic Resins)*

Since their invention in 1909, phenol-formaldehyde (PF) resins have been the standard of excellence for the fire performance of FRP materials. The thermosetting resole-PF resins have been the material of choice for many fire-sensitive applications such as rocket nozzles, blast protection, space vehicle re-entry shields, electrical insulation, tunnel linings, offshore oil platform decks and pipes, engine components, and many others. Without the use of any fire-

retardant fillers, they have extremely low flame spread indexes and produce very little smoke or toxic fumes.<sup>18</sup> Even today, among the numerous fire retardant formulations available, between 80% and 90% of the composites used in aircraft interiors are made using PF resins [134]. Surprisingly, with all of their superior qualities they are still relatively inexpensive.

### *Active Mechanisms*

The secret to the superior fire performance of PF resins is their tendency to form a thick, durable char layer. The more material that is retained in the char, the less fuel, smoke, and soot can be produced [70 pg. 220]. The highly aromatic network of the polymer results in the formation of a thick residue that retains much of the original carbon content upon decomposition. This residue is the basis of the carbonaceous char that forms and is stable at temperatures up to several thousand degrees. The char layer has a lower thermal conductivity than the basic composite such that it helps to insulate the in-tact composite from the heat of the fire (interruption of Stage I - Heating). In addition, this layer slows the escape of volatile decomposition gases from the composite below, which reduces the fuel available at the reaction front (interruption of Stage IV - Combustion).

For applications with the most stringent fire performance standards, further improvements can be achieved through the addition of halogens and antimony-oxide. Section 3.2.1.1.a provides a brief description of these fire retardant fillers.

### *Strengths and Weaknesses*

The most compelling strength of PF resins, once again, is its excellent fire reaction characteristics (low heat, smoke, and toxic gas production). Yet there is a reason why PF resins have not replaced all other resins systems in all applications. Until recent advances, the PF resins were only available in an orange reddish-color that slowly turned brown upon exposure to UV light.<sup>19</sup> Quality control can also be troublesome for some production techniques because of the tendency for water droplets to condense within the resin during curing. Finally, several hours of post-curing at elevated temperatures is necessary, which adds time and complication to the production process.

Manufacturing and durability issues aside, there is still one fundamental weakness that PF resins share with nearly all other organic resins: mechanical weakening at relatively low

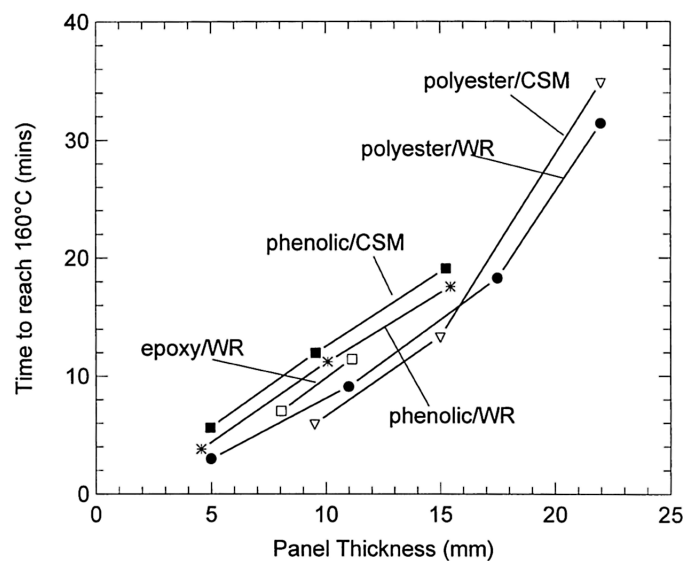
---

18. The Warrington Fire Research Centre has recently released a report in which the fire characteristics of several common resin systems were thoroughly tested and compared side-by-side [16]. PF resins are the clear winner in nearly every category. Further support is provided by Sorathia *et al* in [171].

19. Some manufacturers, such as Borden Chemical, are now offering pigmented gelcoat systems to improved the appearance and weather resistance of their PF resins, though these coatings do not have the same high standards of fire performance.

temperatures. Though PF resins are less likely to support combustion and less likely to threaten life through the production of heat, smoke and toxic gasses when they do combust, their mechanical properties degrade at temperatures only slightly higher than that of other standard resins [65]. Indeed, the char layer formed by PF resins helps to insulate the deeper in-tact portions of fire-exposed components, but the improvements are almost negligible. Dodds *et al* [43] report that the time for the cold face temperature of PF composites to reach 160°C when exposed to a hydrocarbon fire was fairly similar to that of epoxy and polyester composites (see Figure 3-34). Therefore, while PF resins are an excellent option for reducing flame spread, smoke generation, and heat release rate, their tendency to lose mechanical properties at temperatures (308-335°C) [84 pg. 122] much lower than those encountered in building fires (>700°C in the first 10 minutes) [92] means that the choice of resin alone cannot significantly reduce the threat of heat-induced structural collapse.

**Figure 3-34.** Time for cold face to reach 160°C versus thickness (CSM=chopped strand mat glass reinforcement, WR=woven roving glass reinforcement) [43]



For inhabited spaces, one further concern is off-gassing of the formaldehyde curing agent. The PF resins that are used as adhesives in engineered wood products (plywood, particle board, oriented strand board, etc.) have been linked to higher levels of formaldehyde gas, which is toxic and may cause long-term health problems [118].

### *Representative Products*

Borden Chemical produces a line of PF resins under the name Cellobond®.

### 3.2.1.5 *Intumescent Coatings and Fabrics*

Intumescent materials offer the possibility of imparting some fire resistance to FRP components without altering the basic composite. The materials work by expanding under fire exposure and decomposing into a thick carbonaceous char. This char layer protects the composite below by forming an insulative layer (interrupting Stages I & II - Heating & Decomposition). It is also functional in slowing the escape of volatile decomposition gasses from the composite to the reaction zone (interrupting Stage IV - Combustion).

Intumescent materials are available in several different forms. Thin (<2 mm) thermoplastic “paints” have weak abrasion and weather resistance, but may expand up to 50 times their original thickness when exposed to fire. Thicker (5-15 mm) thermosetting gelcoats are more weather and abrasion-resistant, but expand roughly 5 times their original thickness. Intumescent fabrics also exist and may be bonded to the finished surface or included during the manufacture of the composite. The performance of the paints, gelcoats, and fabrics varies enormously by many factors, including the manufacturer, application method, thickness, and type of fire exposure.

#### *Active Mechanisms*

There are four essential components in all intumescent materials: an organic acid or material that creates an acid upon heating, a material rich in carbon, an amine or amide, and a halogenated organic compound [70 pg. 219]. When intumescent materials are exposed to fire, they decompose endothermically into a viscous liquid. During this decomposition, the inert blowing agent is released to form small bubbles, while at the same time the acid is released to liberate the carbon. Further heating results in the cross-linking of the viscous liquid, which eventually is decomposed into a hard carbonaceous char [3]. Each step must occur at the correct temperature and in proper sequence. The process is only partially understood by researchers, as evidenced by the fact that most intumescent materials were developed through empirical methods.

#### *Strengths and Weaknesses*

Intumescent materials have several advantages over other fire retardance methods. Unlike fire retardant fillers and additives, intumescent materials are applied to the surface and thus do not affect the mechanical properties of the basic composite. In addition, they may be selectively applied to discrete regions of the component at any time after production. Finally, their active mechanism is mostly in Stage I (Heating), which is the most desirable from a thermomechanical point of view.

The fact that intumescent materials are only applied the surface can also be considered weakness. Over time, surface coatings can be worn away by weather or abrasion, leaving the component unprotected. During fire as well, the char layer created by intumescent coatings may fall away from the compound due to ablation or pore pressure [145]. Fiber reinforcement is sometimes added to prevent this, though too much reinforcement restricts the expansion of the layer. Lastly, many researcher have reported that even the thickest coatings are only effective against relatively short fire exposures. Mouritz *et al* [138] reported that the post-fire mechanical properties of plates with various intumescent coatings were roughly the same as those without the coatings after 30 minutes of exposure.

The greatest disadvantage of using intumescent materials, however, is best described by NIST<sup>20</sup> researcher Thomas Ohlemiller as “the evident paradox of using flammable materials as a fire barrier” [145]. Intumescent coatings provide no protection until they have been thoroughly burned. This initial stage where they are burning may result in higher initial heat release rates and smoke and toxicity production than if no coating was applied at all. For this reason, intumescent materials are not recommended for the protection of large surface areas inside habitable spaces.

### *Representative Products*

From roll-on “paints” to ceramic fabrics, there are literally hundreds of varieties of intumescent materials available. The first versions were developed for the protection of structural steel in the 1930’s, and the market has been evolving ever since. Some examples of coatings are Clariant Additive’s Exolit®, Scott Bader Company’s Crystic Fireguard®, while Technical Fibre Products’ Technofire® is an example of an intumescent fabric.

### **3.2.2 Active Fire Safety Measures**

Section 3.2.1 described the various methods in which FRP building components can be made less likely to burn, less sensitive to other burning objects, and less dangerous when they do finally burn. In addition to these methods, a category of measures involving an active, managed response are also available [22 pg. 11]. These measures are primarily dependent on the automated detection of fires in their early stages. Through smoke, heat, and signature gas detecting devices, active measures can be engaged to:

- ***Suppress the fire:*** Sprinkler systems can be particularly effective at extinguishing the fire at its source, reducing the demands placed on all of the other fire safety measures. Occupants and fire-fighters can also suppress fires in their early stages.

---

20. National Institute of Standards and Technology (Gaithersburgh, MD, USA)

- ***Dissipate the heat and smoke:*** Automated ventilation systems can improve visibility and air quality. Internal liquid cooling can draw heat away from load-bearing members and the walls of fire compartments such that they retain their structural integrity.
- ***Aid the escape or rescue of occupants:*** Aural and visual warning systems can alert the occupants of the fire. Emergency lighting and signage can help occupants to escape when visibility is reduced and the risk of disorientation is high.

As mentioned, nearly all active measures rely on automated detection systems. Thus, no further discussion of such systems is necessary: all new multiple story buildings should be built with automated detection systems. Aural/visual warning systems and emergency lighting/signage are also essential measures and cost very little for the large improvements in fire safety they impart.

Beyond these most fundamental measures, two further measures have been identified for the conception of fire-safe FRP buildings: sprinkler systems and internal liquid-cooling systems. In the following sections, each of these methods are described and their potential for imparting fire safety are discussed.

### 3.2.2.1 Sprinkler Systems

As separate plumbing and detection networks installed in buildings with no function other than fire protection, sprinkler systems are expensive. Yet when the threat of fire is considerable or there is the potential for great loss, fire sprinklers are the only method that can provide nearly 100% protection.<sup>21</sup> In fact, many building codes require the installation of fire sprinklers in certain conditions, often in public buildings where large groups of people congregate, or tall buildings where egress times are long [91].

The concept is fairly simple and widely understood, thus it not necessary to provide a lengthy description of the workings of fire sprinkler systems. In brief, a dedicated network of pipes is installed such that sprinkler heads can be positioned throughout the building. The functioning of these sprinklers can be initiated by an electronic detection system, or by heat-sensitive valves at each sprinkler head. When a fire is detected, a spray (or more recently, a mist) of water is emitted. The water absorbs the heat of the fire through a phase change to steam and thus arrests the combustion cycle. In certain applications where oil fires are expected, such as in restaurant kitchens, a special foam or gel replaces the water in the system.

---

21. Exception can be made for offshore, petrochemical, and military applications where there is a reasonable possibility of explosions damaging active systems, and thus passive systems are preferred.

### *Strengths and Weaknesses*

As previously mentioned, sprinkler systems can react at the very early stages of fire. They are capable of actively extinguishing the source, which is better in all respects than simply protecting certain components. This level of protection comes at a cost, however. Beyond monetary costs related to the installation and maintenance of the system, the network of pipes and sprinkler heads have a visual and spacial impact on the interior of the building. For these reasons, sprinkler systems are usually only installed where required by building codes or insurance policies.

#### *3.2.2.2 Internal Liquid Cooling*

The concept of internal liquid cooling is to circulate a liquid through critical components to remove heat in the case of fire. Though implemented in car engines, rocket nozzles, and steel building structures for decades, internal liquid cooling has never been investigated for the fire protection of load-bearing FRP components. Research in the related areas of the fire performance of water-filled FRP pipes and tubular steel columns provides an insight as to the efficacy of such a system.

##### *3.2.2.2.a Liquid-Filled Steel Members*

Roughly 30 buildings in the world that have been built incorporating internal liquid cooling in their structural steel skeletons [156]. In standard steel skeleton buildings, the members are protected by a layer of concrete or spray-on fire proofing, which must then be covered with another layer for durability and appearances. The attraction of internal liquid cooling as a structural fire protection method is that the steel members may be left exposed, which may be desirable visually or economically, or may be advantageous in terms of space, durability, or complexity (such as in a steel space frame with hundreds of small members).

Though the concept was patented in 1884, the first building to incorporate this system was the USX Tower built for the US Steel Corporation in 1969. The 64-story building is supported by tubular weathering steel columns that are exposed to the environment. Approximately \$1 million was saved through the omission of fireproofing [37]. Several years later, the Kansas City Bank Tower was constructed using cruciform-shaped columns and a tubular transfer truss featuring internal liquid cooling. Roughly \$300,000 was saved once again by the omission of fire proofing, while a dramatic visual effect was achieved [37].

A 5-story demonstration building using liquid-cooled tubular steel members was constructed by the University of Stuttgart in 1985 [12]. Upon the completion of the building, fires were set using four tons of dried wood. The fire was allowed to burn for eight hours before it was

extinguished. Measurements taken during and after the fire showed almost no deflection of the liquid-cooled steel members. The building was later renovated and is currently in use as offices.

Since then, several codes have been published for the design of liquid-cooled structural steel members, such as [21] by British Steel. Most of such codes refer to the original design guide by Bond in [14].

#### 3.2.2.2.b FRP Pipes

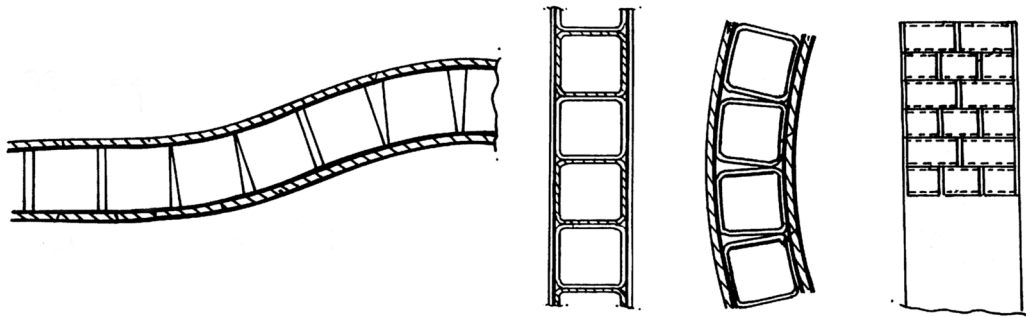
Starting in 1986, Marks *et al* [117] investigated the fire performance of glass fiber-reinforced epoxy pipes filled with stagnant water. The pipes were exposed to severe hydrocarbon-type fires and endurance times were set by the first occurrence of leakage. They found that the addition of stagnant water doubled the fire endurance of the pipes, though the double of 3 minutes is still not very much. They also found that the application of various protective coatings such as intumescent, cementitious products, phenolic foams, and additional “sacrificial” layers of the same FRP material could extend the endurance times into the range of 40-55 minutes.

Davies *et al* performed a similar investigation on a glass-epoxy pipe system in 1999 [39]. The focus in these tests was the comparison of different protective coatings with empty, stagnant, and flowing water inside. Once again, the pipes were exposed to hydrocarbon-type fires and endurance times were judged by the first leakage. The team found that the 3 minute endurance of the empty pipe was improved to roughly 10 minutes, after which violent boiling began and the cooling effect of the water diminished. In the flowing condition, however, no endurance limit could be found after more than two hours of exposure.

#### 3.2.2.2.c Hollow FRP Sandwich Panels

Research by the Shell Corporation into the use of FRP sandwich panels for ship components led to the design of a new core product. This core consisted of short rectangular tubes placed in a staggered pattern such that a high degree of drapeability could be achieved (see Figure 3-35). A patent was filed for this sandwich system in which the possibility of using this hollow space for the circulation of “cryogenic” or “heating and cooling fluids” is mentioned [73]. No use of the sandwich structure could be found in the literature, neither with or without the fluid circulation aspect.

Figure 3-35. Sketches from Guiton's patent of a unique sandwich system



### 3.3 Conclusions: Fire Safety for FRP Structures

In the preceding sections, various passive and active fire protection methods have been discussed. For each method, the potential for imparting total fire safety was considered. In general, it can be concluded that some passive protection methods are effective in reducing heat release, smoke, and toxic gas production, and can limit the participation of the contribution of the component to the fire.

These are indeed critical issues, but for multiple-story buildings, the issue of structural fire endurance is equally important. Except for the non-material adapted method of adding thick protective layers (e.g. gypsum board), none of the passive methods can significantly prolong the structural endurance times of FRP components in resin-sensitive stress states. Methods that promote the creation of an insulative char layer provide some temporary benefit in reducing the heat transferred into the in-tact region of the component, and thus the postponement mechanical degradation. The best methods for promoting char production involve the use phosphorus-based fire-retardants, intumescent surface layers, phenolic resins, or nanocomposites. Research has shown that while these methods are effective for short durations (<30min), they make little difference in the range of exposure times that load-bearing building components are expected to withstand [138].

Several active fire resistance methods have also been discussed. Fire sprinklers are a proven solution to arrest all four fire safety concerns (heat release, smoke and toxicity production, structural collapse). Economically, the installation and maintenance of such systems is considerably higher than most passive methods, and may have a negative visual or spacial impact. Internal liquid cooling has been investigated for steel structures and FRP pipes with outstanding success in both applications. No research has been reported on the use of internal liquid cooling for load-bearing FRP building components.

Overall, no passive or active method is without weaknesses or compromises. For this reason, a combination of methods is usually employed. For example, a component may be fire retarded using a combination of ATH and red phosphorous, and then covered with an intumescent layer, which was formulated using a nano-sized filler. The proper combination depends strongly on the application.

In reference to multiple-story load-bearing FRP structures, passive protection methods are appropriate for mitigating the first three fire safety risks. Of the many options available, methacrylate-modified acrylics and the new species of nanocomposites appear to offer the best balance between cost, efficacy, and unwanted side-effects. To delay structural collapse for the code-specified 90 minutes [167], however, either a thick protective layer of passive protection or an active protection method is required as well. As previously described, the addition of non-FRP exterior layers (e.g. gypsum board) defeats many of the advantages that make the material attractive in the first place. Thus, an active safety measure is more desirable. And while sprinkler systems are highly effective, internal liquid cooling may provide equal structural protection with the added value of replacing the building climate control system as well.

Table 3-1. Summary of fire safety measures

			Prevent Ignition	Reduce Heat Production	Reduce Smoke Production	Reduce Toxicity	Delay Structural Collapse	Comments
Passive Measures	Fillers & Additives	Halogen/ATO	excellent	good	poor	poor	minor indirect improvement	increasing environmental concerns
		Inorganic Hydroxides	good	good	good to excellent	good to excellent	minor indirect improvement	very high loadings necessary
		Phosphorus	good	good	good to excellent	varies widely	minor indirect improvement	high loadings for stand-alone retardants
		Nano-sized	good	good	good	good	minor indirect improvement	not yet widely available
	Intumescent Materials	good	good	varies widely	varies widely	minor indirect improvement	only effective for short exposures, can be worn off	
	Phenolic Resins	good	good	excellent	excellent	minor indirect improvement	difficult to process, lower mechanical properties	
	Protective Layers (Gypsum, Concrete, etc.)	varies	good	varies	varies	good	defeats advantages presented by use of FRP materials	
Active Measures	Sprinklers	excellent	excellent	excellent	excellent	good	costly, can be architecturally intrusive	
	Internal Liquid Cooling	no effect	no effect	no effect	no effect	excellent	Only useful in conjunction with other measures	

## 4 Numerical and Analytical Modeling of FRP in Fire

The task of modeling the behavior of FRP materials in fire is so complex that currently no single model even attempts to address all of the thermal, mechanical, chemical, and physical phenomenon as they truly interact in nature. The simple step of amassing all of the required material and system properties that would involve many three and four-dimensional interactions would be prohibitively complex in itself. By treating only one or two of these phenomenon in each model, the task becomes somewhat more reasonable. To further simplify matters, models often treat only selected phases of the total fire exposure process, i.e. before pyrolysis, post fire, etc. Still, all models are made possible through additional approximations, simplifications, and assumptions.

Of the wide range of models that could be considered to relate to the subjects of FRP in fire, four categories can be distinguished:

- Fire exposure models
- Post-fire mechanical models
- Thermochemical models
- Thermomechanical models

### 4.1 Fire Exposure Models

The first category of models consider only the fire itself. The simpler “zone” models separate the environment within an enclosure into discrete hot and cold regions, while the more complex “field” models employ computational fluid dynamics (CFD) to allow a more detailed two-dimensional or three-dimensional view. All models use the conservation of mass and energy to solve for temperatures and pressures, while the CFD models also use the conservation of momentum to solve for flow velocities and gas/smoke concentrations. These values can then be used by fire protection engineers for the design components or to satisfy code compliance. What is most relevant to this thesis, however, is that this output may also be used as the boundary conditions in thermomechanical models that simulate the behavior of structurally loaded building components.

Some examples of current zone models include *HAZARD I* from the National Fire Protection Agency (NFPA) and *CFAST* from the Building and Fire Research Institute (BFRI) at the National Institute of Standards and Technology (NIST) [23 pg. 28]. Some common field models include *BRANZFIRE* from the Building Research Association of New Zealand,

*DSLAYV* from the National Defense Research Institute of Sweden, *SOFIE* from the University of Cranfield, *FDS* from the BFRL, and *SMARTFIRE* from the University of Greenwich. A more complete listing of the currently available models is maintained by Combustion Science & Engineering, Inc. through their internet survey ([www.firemodelsurvey.com](http://www.firemodelsurvey.com)).

## 4.2 Post-Fire Mechanical Models

In the event that load-bearing polymer composite structures are subjected to high temperatures, it is often useful to be able to estimate the residual strength and stiffness of the damaged component. A significant percentage of the component's original strength may remain for several reasons:

- source extinguished before degradation of the entire section
- source did not provide enough energy to degrade entire section
- entire section was not exposed
- component is loaded in stress-state that does not rely on contribution from matrix

For large composite structures such as naval ships, offshore installations, and multiple-story FRP building systems, small fires may cause some local damage before they are extinguished (or self-extinguish) and before they lead to global failure. A reliable post-fire mechanical model would allow engineers and inspectors to evaluate the damage and to estimate the remaining capacity of the components. Informed decisions could then be made concerning repair and replacement.

Progress in the field of post-fire mechanical modeling has been fairly consistent since the early 1980's. Researchers seem to have focused on this particular type of model primarily because it can be very useful, but also because it is easy to validate (not necessary to place mechanical loading and measurement equipment nearby or inside ovens) and does not require the troublesome acquisition of accurate temperature-dependent material properties.

One of the first formal investigations into the post-fire mechanical properties of FRP materials was performed by Pering and Farrell in 1980 [149]. Carbon fiber-reinforced epoxy laminates were exposed to fire on both sides by gas-fueled burners for up to 15 minutes. Afterwards, the tensile and shear properties of the burnt laminates were determined through mechanical testing. The loss of mass over time was approximated as a single-step Arrhenius reaction using the law of the conservation of energy. An empirical correlation was then made between the rate of char formation and the shear strength/stiffness (assuming the same cross-sectional area), while the tensile strength/modulus was correlated to the loss of mass. No differentiation was

made between loss of strength due to loss of cross-section and loss of strength due to reduction in material properties. As the one material that was tested provided the empirical coefficients for the model, the experimental program was more of a calibration than a validation. No true validation was performed on other materials or thermal loading conditions.

Four years later, Springer presented a more generalized analytical model that built on Pering's work [172]. The approximation of loss of mass by energy balance and the Arrhenius reaction model was retained. The mass loss was validated on carbon/epoxy composites, but the mechanical portion of the model was only validated on cellulose materials.

The next group to address the issue of post-fire mechanical property modeling was Sorathia *et al* in 1993 [170]. Small coupons of many thermoplastic and thermosetting matrix composites were exposed to low heat fluxes in a cone calorimeter for up to 20 minutes. The coupons were then cut into strips and tested in flexure to obtain the "residual strength retained". A temperature-limit criterion was proposed for the determination of post-fire mechanical properties. Thereby, the portion of the material that does not exceed this critical temperature during the fire exposure is considered to retain all virgin mechanical properties, while the strength of the damaged portions is determined through reference to  $E$  vs.  $t$  curves acquired from dynamic mechanical analysis. No formal analytical models were presented, though the large data set could be useful for the validation of other researcher's works.

After the contributions by Sorathia *et al* and up until roughly 2003, the overwhelming majority of reports on the post-fire mechanical properties and models has been made by Gardiner, Mouritz, and Mathys [56-58], [66], [121], [132-138]. Through a large series of papers, the group has expounded upon an approach for determining the residual mechanical properties of fire damaged glass-reinforced polyester, vinyl ester, and phenolic composites. Validation has been performed on mostly small-scale specimens using a cone calorimeter, though Gardiner has also used kerosene pool fires for larger specimens.

The approach involves the discretization of the material into two layers: a fully-degraded region that is simplified as having little or no residual mechanical properties, and an unaffected region that is simplified as having the same properties as before the fire exposure. The thickness of the layers is idealized as being uniform across the plate. To determine the residual properties of the specimen, a "rule of mixtures" equation is used to calculate the proportional contribution of the two layers. In truth, the second half of the model involving the "rule of mixtures" method is not a unique approach and the equations presented are simply restatements of Euler-Bernoulli beam theory using transformed sections to simplify the composite cross-section (the same approach is used to calculate the stiffness of steel beams compositely acting with a concrete deck, for example).

The unique contribution of the model is in how the depth of the fully degraded “char” layer is determined. An empirical correlation was made between the depth of char, the duration of exposure, and the time that charring first occurred. Initially, calibration was made by physically measuring this depth, but this technique was later replaced by the use of a pulse-echo instrument and a percentage remaining resin content (RRC) criterion. Empirical data-fitting resulted in the RRC criterion that stipulates that regions in which less than 80% of the resin remains are considered part of the degraded region. This method has merit in that it is simple and does not require the knowledge of temperatures or heat fluxes during the fire exposure for the evaluation fire-damaged components, though it does require the estimation of the duration of the exposure and the time of the first appearance of char for prediction.<sup>22</sup>

Because the model is only used post-fire, the complications related to thermal expansion are completely avoided. The stresses across the cross-section, therefore, can be simply calculated by traditional beam theory. With the knowledge of the stress, the appropriate material properties may be applied the char layer. Empirical data fitting has resulted in the assumption that the stiffness of the char region is 8% of the pre-fire level in tension and 0% in compression. Thus, the ability to differentiate between the properties of the char in different stress states makes the method superior to all previous models. Accordingly, the agreement between the predicted and measured post-fire mechanical properties is quite good (typically within 10%).

Further verification of the model is still required before it can be considered to be the final word, however. The model has not been validated by any outside researcher, has never been applied to large-scale specimens with true flaming heat sources, and has never been applied to any fiber architecture besides woven laminates. Further, the small size of the specimens tested meant that exposure times were never longer than 20 to 30 minutes, with the majority of exposures lasting less than 10 minutes. With such short durations, no gross geometrical changes are encountered, such as the shedding of reinforcement layers. Finally, the specimens were never loaded *during* the fire exposure. Recent research at the Military Scientific Institute for Materials, Explosives and Lubricants in Germany indicates that the post-fire residual strength of specimens that are loaded during the fire exposure is much lower than that of specimens that are not loaded during the exposure [165-166].

Therefore, important variables that lead to gross geometrical changes such as fiber architecture, specimen size, and exposure duration, have not been greatly varied in the series of tests that constitute the current validation data set. The application of the model to large-scale specimens

---

22. Mouritz and Mathys have recently proposed a correlation between the heat release rate (a material property that can be accurately measured) and the time to the first appearance of char [140].

with mostly unidirectional fiber architectures exposed to realistic fire conditions for up to 120 minutes, such as those in the experimental portion of this thesis, will present a new perspective on the applicability of a two-layer approach to post-fire mechanical modeling.

Nonetheless, the Gardiner-Mouritz-Mathys team shifted their efforts in 2003 towards merging their model with an existing thermomechanical model [61-65], [139]. As almost all other current efforts focus on thermomechanical modeling as well, little innovation in the field of plainly post-fire mechanical modeling can be expected in the future.

### 4.3 Thermochemical Models

The simulation of the thermal behavior of polymeric materials at high temperatures (i.e. above the range in which they are chemically stable) is a complex problem involving many phenomena that are only partially understood. What would already be a difficult problem due to the high temperature-dependence of the thermal properties is further complicated by endothermic chemical decomposition, exothermic oxidation, char formation, phase changes, mass transfer, and the interaction between the formation of micro-cracks due to pore pressure and mechanical cracking due to uneven thermal expansion. For this reason, the effort that began roughly 50 years ago is still in progress.

Often the eventual goal of such modeling efforts is to describe a high-temperature mechanical behavior of FRP materials. Therefore many researchers have attempted to create coupled or sequential models in which the mechanical and thermal phenomena are solved simultaneously or iteratively. To maintain a sense of chronology in this review, only the thermochemical portions of these models will be discussed in the current section. The discussion of the mechanical aspects will be saved for Section 4.4, which is dedicated entirely to models of that type.

The origin of most current thermochemical models is found in the early studies on natural polymers, most notably cellulose (wood). In many ways, the thermal behavior of cellulose and synthetic-matrix organic composites is very similar. Of most importance is the fact that as organic materials, both tend to decompose into combustible gasses and a carbonaceous char. Therefore, one of the first thermochemical models that can be cited is actually one that relates to the pyrolysis of cellulose, presented by Bamford *et al* in 1946 [9]. Building on this one-dimensional model, Kung [101], and later Kansa [95], contributed to the development of charring models for wood. Di Blasi provides a thorough review of the dozens of charring models for wood introduced up through 1993 [42]. The most recent model, implemented through the software *CROW*, is reported by Janssens in 2004 [93]. The details of these models

will not be discussed as their relevant components have already been adopted by models that specifically address FRP materials.

With respect to the thermochemical modeling of polymers, the first studies focused only the decomposition of polymers without fiber reinforcement, such as the one presented by Woolley and Fardell in 1977 [193], Wichman in 1989 [188], and Fredlund in 1993 [55]. Probably the first model to be developed for fiber-reinforced synthetic polymers was by Griffis *et al* in 1981 [71]. The one-dimensional model used a finite difference method to solve the energy equation subjected to uniform and constant heat flux boundary conditions. Both radiation and convection were considered, as well as ablation and endothermic decomposition of the resin. The resulting temperatures profiles agreed well with the experimentally measured values for carbon fiber-reinforced epoxy plates, though the laser heating method employed does not translate well to real fire conditions. The model was later used in thermomechanical models by Chen *et al* in 1981 [27] and by Griffis *et al* in 1985 [72], which will be discussed in Section 4.4.

At roughly the same time, McManus and Coyne [126] also developed a thermochemical model for FRP materials, though it was not made available to the public because of its relation to military applications and its commercially-based financing. Similar to that of Griffis, the model solved the basic conservation equations though a finite difference method. The concept of an “effective”<sup>23</sup> or “apparent” specific heat capacity was introduced to capture the endothermic dehydration and decomposition of the resin. The thermochemical model was coupled with a mechanical model in a numerical computer code dubbed *TRAP*. The thermomechanical aspects of the code will be discussed in Section 4.4.

Validation of the thermochemical portion of the *TRAP* code was performed by Fanucci in 1987 [51]. In the analysis, the predictions of the code were compared to experimental results. With an interest in military applications such as nuclear and electronic pulse-hardened mobile tactical shelters, carbon fiber and Kevlar® reinforced epoxy composites were exposed to intense laser<sup>24</sup> and radiant electrical heating for extremely short durations (less than 5 seconds). Agreement between the results was reasonably good, though little correlation can be drawn between the processes that occur over a few seconds with heating rates of up to 50°C per second and actual building fire scenarios lasting minutes to hours.

What is more relevant from Fanucci’s work are the idealized material property curves he presented (which were originally proposed by McManus and Coyne in [126] but were not

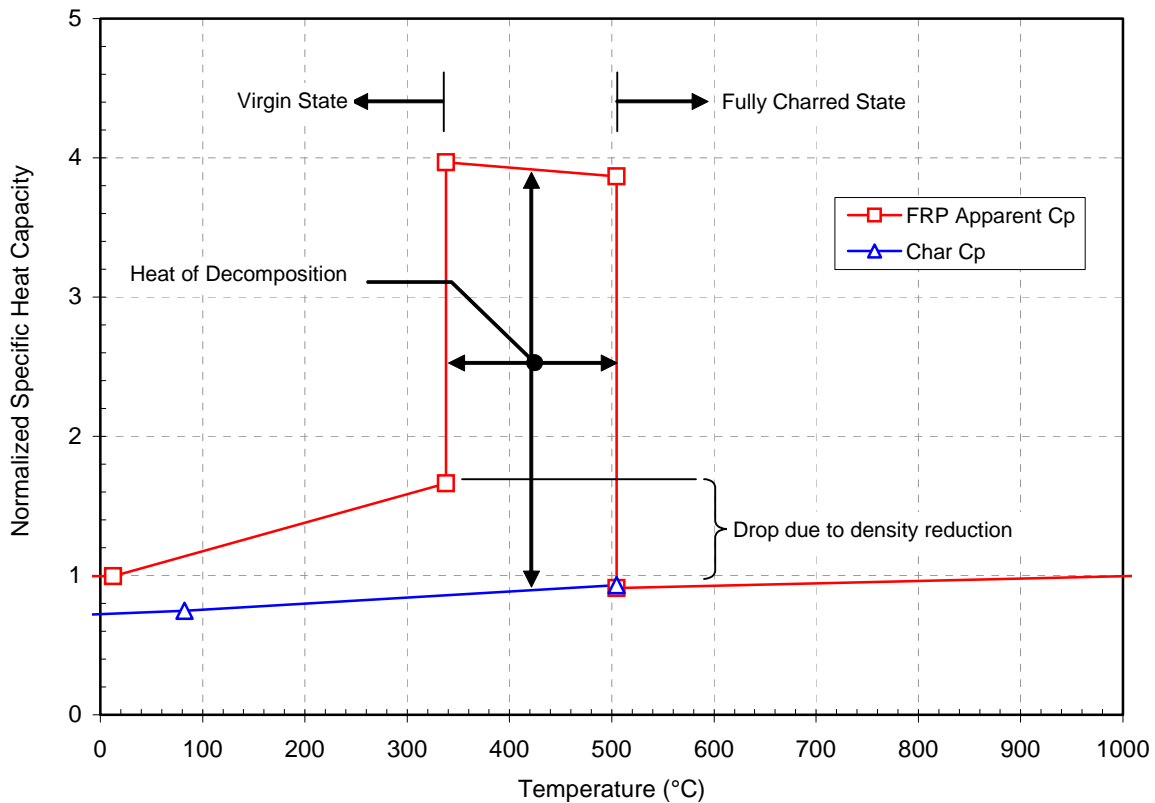
---

23. See Section 3.1.4.2 for an explanation of “effective” specific heat capacity curves

24. To simulate the fireball from a nuclear blast, a specially designed 6 m diameter parabolic mirror and an equally large heliostat were used in a desert testing location to create a high-energy laser beam from available solar energy.

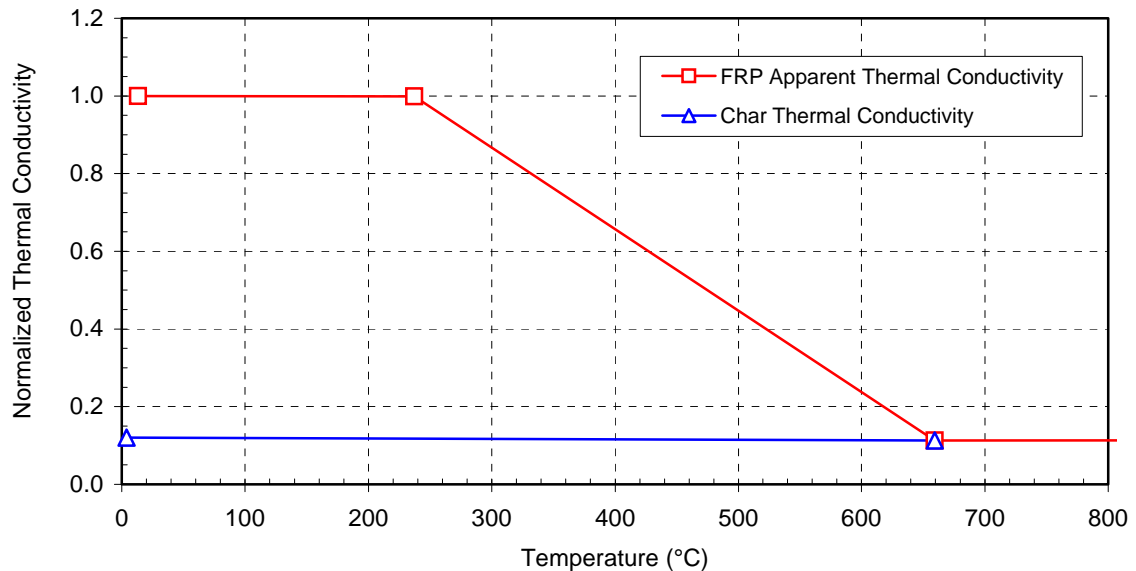
made available to the public). The effective specific heat capacity versus temperature curve that was presented by Fanucci in [51] is reproduced in Figure 3-36. The curve shows a large hump over the range of temperatures where resin decomposition occurs. The area between this hump and the curve of the fully decomposed composite equals the heat of decomposition of the composite.

Figure 3-36. Fanucci's idealized effective specific heat capacity curve for epoxy resins [51]



To represent the reduction in thermal conductivity that occurs as the composite cracks and delaminates, Fanucci also proposed an effective thermal conductivity versus temperature curve (see Figure 3-37). This curve reflects the true thermal conductivity of the composite until decomposition begins. The curve then gradually declines to meet thermal conductivity of the fully decomposed composite after decomposition is completed.

Figure 3-37. Idealized effective thermal conductivity curve for generic charring materials proposed by Fanucci in [51]



Shortly after the contributions by Griffis, McManus, and Fanucci, Henderson *et al* [81] presented a different thermochemical model in 1985 that now constitutes the foundation of many current efforts. In this model, the finite difference method was applied to the one-dimensional energy equation, the conservation of mass, and the continuity equation. Endothermic decomposition, convection of the decomposition gasses, and temperature-dependent materials properties were all considered.<sup>25</sup> Convection and radiation boundary conditions were modeled at the hot face while the cold face was considered to be *adiabatic*.<sup>26</sup> The concept of an “effective” or “apparent” specific heat capacity was discussed but not employed.

Comparison of the predicted temperatures and experimental values obtained by heating a glass fiber-reinforced phenolic composite by radiant electrical heaters revealed small discrepancies. These discrepancies were linked to the improper assumption of no thermochemical expansion, and to inaccurate material properties. Overall, the agreement was very good and improved with the consideration of thermochemical expansion in a later update [82].

The success of Henderson’s model is evident in the fact that most current thermomechanical models, such as those by Looyeh *et al* [110-111], Dodds *et al* [43], and Gibson *et al* [61-67], all

25. In a separate effort of nearly equal importance, Henderson *et al* developed methods for determining some of these temperature dependent material properties [83].

26. The term *adiabatic* means that no energy is transferred through the boundary.

use Henderson's basic formulation with small improvements. Once again, these models will be discussed in Section 4.4.

As described in Section 4.2, Springer presented a thermochemical model in conjunction with a thermomechanical model in 1984 [172]. The basic conservation equations were solved through a numerical "user friendly" computer code. The loss of mass was approximated as a single step Arrhenius reaction model, as in the original version of the model by Pering. Validation was performed by comparing predictions to the experimental data set from Pering [149] on carbon fiber-reinforced epoxy composites. Agreement was good, though no other materials or heating methods were tested.

After a lull of roughly three years, a flurry of thermochemical models were presented in the early 1990's. The new partnership of McManus and Springer resulted in an updated model presented in 1992 [124-125]. This model treated both thermochemical and thermomechanical phenomena, solving them simultaneously by interactive coupling. The approach was very similar to that of Henderson's latest work, though it was specifically developed for carbon fiber-reinforced phenolic composites. The thermochemical portion solved for temperature and pressure distributions, as well as vapor and char formation rates. Validation of the model was made by exposing disc-shaped specimens to a propane-fueled flame source. Agreement between the experimentally measured temperatures profiles and the predicted values was excellent. Predictions regarding heat-induced delamination were also fairly good. The only limitation of the model appears to be that it only allows for one-dimensional heat transfer.

At roughly the same time as McManus and Springer, Milke and Vizzini presented a purely thermochemical model for FRP materials in 1990 [128] and 1991 [129]. The major improvements from the previous models was the consideration of three-dimensional heat transfer, non-uniform boundary conditions, and ply-wise material properties. As in all of the previously described models, an implicit finite difference method was used to solve the basic conservation and continuity equations. Validation was performed by exposing carbon fiber-reinforced epoxy laminates to a radiant heat source for up to ten minutes. Because thermal imaging was the only method used to record temperatures, only the cold face temperatures could be recorded. The comparison of the cold face temperatures to the predictions was quite good up until the occurrence of delaminations, after which the temperatures were over-predicted. Further, the set-up of the experiments effectively created one-dimensional heat flow, which did not test one of the essential improvements of the model over previous attempts.

Sullivan and Salamon developed the third model to be introduced in the early 1990's [175-176]. Although the approach and solution method varied slightly from that of McManus' latest contribution, the simulated phenomena were much the same. Like McManus, Sullivan claimed

an improvement over previous models through the consideration of the effects of pore pressure on the mechanical stress state of the material. Although this would indicate a degree of thermochemical and thermomechanical coupling, the model could only consider thermally-induced stresses. As such, McManus' model was a more useful total package.

Validation was conducted through restrained thermal growth and free thermal expansion tests on carbon fiber-reinforced phenolic laminates. Agreement between the predicted and measured stress states was reasonably good, though there is little frame of reference since the other models that included thermal expansion (McManus 1992 [124-125], Henderson 1987 [82]) did not report on isolated validation experiments for this specific aspect.

First published in 1995, Gibson *et al* introduced a thermochemical model coupled with a thermomechanical model [68]. Though the referenced sources are Kansa [95] and Sullivan [175], the formulation of the governing equations is very similar to Henderson [82]. The one-dimensional model was implemented through another finite difference software code titled *COM\_FIRE*. Further development of this model can be followed in publications up through 2004 by collaborative efforts by Gibson *et al* [61-68], Davies *et al* [40], and Dodds *et al* [43]. Over that period, validation has been performed on glass reinforced polyester, vinyl ester, and phenolic laminates using the cone calorimeter, propane-fueled jet heaters, and radiant electrical heating sources. As one would expect given the success of the models upon which it was built, agreement between the predicted and measured temperature profiles was quite good.

Looyeh *et al* [106-111] introduced a thermochemical model in 1996 based primarily on the works of Henderson and Sullivan. Innovations to the one-dimensional model included the incorporation of complex boundary conditions at the cold face and the assumption of a non-zero final mass. The influence of surface contact between the layers of a multi-layer panel was explored in [111]. Collaboration between Looyeh, Gibson, Davies, and Dodds is evident in the similarity of the models. A thorough review of the various models developed is provided in [160].

Lua and O'Brien improved on Gibson's model in 2003 by the consideration of heating-rate dependent and mass dependent thermal properties in the heat diffusion equation [112]. A software code titled *TMAT* was developed for thermal analysis of woven composites. Using first the Matlab-based Woven Fabric Visualizer, *TMAT* can then be used to determine the thermomechanical material properties of that composite. These properties can then be input into the improved version of Gibson's *COM\_FIRE* code. Validation was made by comparison to other prediction methods rather than to experimental results.

Also in 2003, Miller and Weaver introduced a closed-form analytical model for idealized thermal conditions [130]. Though not intended as an engineering tool, the model provides a means to partially validate the more powerful finite difference and finite element models that is cheaper and faster than standard experimental techniques. Comparison of the analytically and numerically predicted temperature profiles was good, though the simplicity of the conditions (no chemical phenomena such as endothermic decomposition) does not validate the more difficult and less reliable portions of finite element models.

The most recent thermochemical model was introduced by Strakhov *et al* in 2004 [174], and appears to have been developed entirely independently from all of the models described above. The thermochemical model is coupled with a thermomechanical model that approximates three-dimensional structural behavior by extruding two-dimensional thermal cross-sections along segmented “superelement” portions of load-bearing components. The thermochemical phenomena considered are similar to the previously described models (endothermic decomposition, volatile and char formation rates, pore pressures, etc.). Once again, a unique software code was written to solve the basic equations of energy and motion. Some reference is made to validation of the model, though the Russian language sources are not easily obtained.

#### 4.4 Thermomechanical Models

The development of thermomechanical models goes hand-in-hand with the development of thermochemical models, as the former is not very useful without the latter. Further, the development of post-fire mechanical models has mostly diminished because thermomechanical models that work well at high temperatures should also work well for the simpler post-fire conditions. A great deal of overlap therefore exists in the personalities, publications, and models discussed in the previous sections and present section. Nonetheless the development of the three types of models has been described in separate sections for better organization.

One of the first thermomechanical models for FRP materials was introduced by Springer in 1984 [172]. As in the thermochemical models, this first model was an adaptation of an existing model developed for structural timber. The change in mechanical properties was correlated to the loss of mass through empirical coefficients with the tensile, compressive, and shear properties being affected equally. Failure was predicted through a Tsai-Wu criterion [182]. No experimental validation on FRP materials was performed.

In 1985, Chen *et al* [27] added a mechanical model to the thermochemical model presented by Griffis [71] in 1981. A maximum stress criterion was incorporated to predict failure due to

different loading and heating conditions. Comparison of the failure predictions with experiments on carbon fiber-reinforced epoxy laminates showed marginal agreement.

Griffis *et al* introduced an updated version of Chen's model<sup>27</sup> in 1986 [72]. Improvements over Chen's version included the replacement of the maximum stress failure criterion with the Tsai-Wu criterion previously employed by Springer. Agreement between the failure predictions and experiments on carbon fiber-reinforced epoxy laminates was again marginal, with the maximum stress criterion working slightly better than the Tsai-Wu.

In 1992, McManus and Springer presented the first thermomechanical model that considered the interaction between mechanically-induced stresses and the pressures created by the creation of decomposition gasses within the pyrolysis front [124-125]. Both the Tsai-Wu and maximum stress criterion were considered. While extensive numerical results are provided regarding the stress state within the experimental specimens, the comparison of those values to actual experimental results is not shown.

Dao and Asaro introduced the first thermomechanical model that did not rely on empirical coefficients in 1999 [38]. The model included a thermochemical model to determine the temperature distribution, though very simple boundary conditions were considered (temperature on hot face, temperature or adiabatic cold face). Thus, although no empirical coefficients were required for the mechanical portion, experiments were still necessary to determine these temperatures. Further, for the calculations in the mechanical portion, an unrealistic linear temperature distribution was assumed through the thickness of the laminate. A failure criterion correlating cold face and mid-thickness temperatures to collapse loads was devised. Agreement between predicted and observed failure times of thin glass fiber-reinforced vinyl-ester panels loaded in compression was fair.

Dutta and Hui devised a simple empirical model in 2000 that included the consideration of creep as a function of temperature and time [49]. Isothermal creep tests were performed at various temperatures on glass fiber-reinforced polyester laminates. Curves were fitted from these tests to map elastic modulus versus time. Superposition was then used to create a time and temperature dependent modulus. A failure criterion is mentioned but not explained and no comparison is made between the predicted and experimentally failure times. Nonetheless, a good data set is provided for the consideration of creep in long-duration ( $t > 30$  min.) fire endurance predictions.

---

27. The presence of the author C.I. Chang on all of the publications from Chen and Griffis shows the strong continuity of the model development.

Gibson *et al* [65] attempted to combine their thermochemical model with Mouritz's "two-layer" post-fire mechanical model [56-58], [66], [121], [132-138] to create a thermomechanical model in 2003. The remaining resin content (RRC) criterion successfully used in the post-fire models for determining the division between the two layers<sup>28</sup> was found to over predict the failure loads by up to 300%. In place of the RRC, then, a simple temperature criterion was chosen by correlation of the temperature profiles and the theoretical stress levels. A critical temperature of 170°C was found to fit best for glass fiber-reinforced polyester laminates in compression. Though the predictions were much improved over the RRC criterion, large discrepancies still existed.

In 2004 [63], the team revived the RRC criterion to define the boundary within the model for components stressed in tension. In comparison to the post-fire criterion of 80% resin remaining, a value of 10% resulted in the closest match to the experimental results for tensile loading during fire exposure. Previous experiences with other laminates lead to the conclusion that the values used in the RRC and temperature criteria (derived from experiments on polyester laminates) could be applied to vinyl ester and phenolic composites as well. Overall, the method is quite approximate and currently does not produce highly reliable results. With further development, however, the simplicity of the method could make it attractive as quick estimation tool.

In parallel with the previous effort, Gibson *et al* presented a second attempt at adding a mechanical model to their thermochemical model in 2004 [62]. A more advanced approach was taken in employing laminate theory in place of the "two-layer" model. Mechanical properties were assumed to degrade about the glass transition temperature following a normal distribution function. The different rates of decline between tension and compression properties are accounted for through a coefficient relating to the reaction rate of the resin. Agreement between the predicted and measured compressive failure loads was fair, but tensile loads were quite conservative.

Through purely experimental methods, Seggewiß studied the degradation of the mechanical properties of carbon fiber-reinforced epoxy, as reported in 2003 [165-166]. No model was suggested, but the data set could prove useful in the validation of other models. Some limitations are that only the cold face temperatures were measured and exposure times were shorter than 20 minutes.

Anilturk and Chan introduced another thermomechanical model in 2003 [4]. A simple one-dimensional thermal model was developed using energy balance and temperature boundary

---

28. The two layers are the heat-affected layer and unaffected region - see full description in Section 4.2.

conditions. Temperature profiles from the thermal model were used to assign stiffness moduli to individual ply layers. Failure was predicted through a modification of the Euler critical buckling equation to account for the fiber architecture of the laminate. Predicted critical buckling loads supposedly compared well with published data, though no graphical evidence was provided. Simulated fire exposure times were a short 20 seconds or less.

Bausano *et al* [10-11] focused on the prediction of kinking failures and compression strength of panels subjected to low heat fluxes. Because of the low heat fluxes and short exposures, only reversible heating processes were considered (i.e. no endothermic decomposition, convection of volatile gasses, etc.). Mechanical properties were correlated to temperatures through dynamic mechanical analyses. A unique failure prediction method was introduced that applied the Budiansky/Fleck microbuckling failure criterion [23] to the outermost 0° fiber. The method proved effective in predicting the failures in glass reinforced vinyl ester laminates exposed to higher heat fluxes, but suffered difficulties at the lower heat fluxes. Issues with the acquisition of data, both in the experimental set-up and for the basic model inputs were the likely source of error. Another possibility includes the increasing effect of creep as the heat flux reduces and the duration of the exposure to fire increases.

Halverson *et al* [77-78] simulated the thermomechanical response of a large-scale sandwich structure exposed to fire conditions. Both classical laminate theory and finite element methods were pursued. Building on the work of Burdette [24], the ambitious finite element effort considered the entire fire scenario, including computational fluid dynamic field modeling to determine the surface heat fluxes, thermal modeling of the heat transfer through the multi-layer panel, and thermomechanical modeling of the structural response of the panels to high temperatures. In comparison to the experimental results, temperatures were accurately predicted at the interfaces between the outer insulation layers and the FRP face sheets, while that of the face sheets and the core material was less successful. Agreement between predicted and measured out-of-plane displacements was fair.

#### **4.5 Conclusions: FRP in Fire Modeling**

The field of modeling the response of FRP in fire grew from initial efforts by the defense and aerospace industry. As such, early research focused on high heat flux, short duration exposures of thin carbon fiber-reinforced epoxy laminates. Since then, the focus has shifted to more economical glass fiber-reinforced polyester, vinyl ester, and phenolic composites for naval and offshore applications. The required endurance times are longer than in the initial military applications, though they are still low in comparison to civil infrastructure. Most multiple-story

buildings in Switzerland, for example, are required to resist 90 minutes of fire exposure [167]. Thus, if composites are to be used in load-bearing applications in buildings, it must be possible to simulate their fire endurance for such long durations.

At present, very few researchers have considered the thermomechanical response of composites for fire exposures lasting longer than 30 minutes, and none for more than 1 hour. This is partly because of the current applications of the materials, but also because nobody could make an experimental validation specimen last that long.

Thus, no thermochemical or thermomechanical models have been developed that consider the gross geometrical changes that occur over long fire exposures of FRP specimens. The delamination and loss of reinforcement layers results in thermal phenomena (such as the radiative shielding effect observed in the experimental investigations within this thesis) that are not sufficiently represented by the current group of models.

# 4

## **The Proposed System**

*A Function-Integrated Multiple-Story FRP Building System*



## 1 Introduction

The first step in the conception of the building system was to analyze the contemporary and historical construction projects that involved the use of load-bearing FRP elements. Chapter 2 presented a historical review of the relevant projects from the early phase of FRP in construction that took place between the 1950's and the mid-1970's. Chapter 3 Section 1 presented the relevant projects from the second phase that began in the late 1980's and has been gaining momentum ever since.

Through this review, it was determined that the lack of success of such systems was directly linked to the use of FRP in manners that are not appropriate to the material, or *material-adapted*. This is not surprising, as the introduction of new building materials is usually followed by an initial *material substitution* phase, i.e. a phase in which the methods and details developed for traditional materials are applied to the new material [46]. For example, the cross-sections of FRP members currently in production are simple copies of what is currently produced in steel. These shapes are the result of a century of refinement with respect to the unique characteristics of steel; they are not universally appropriate. Thus, a strong emphasis was placed on employing FRP materials in manners that demonstrate the full recognition of their unique characteristics.

In this effort, it was important to define the term *material-adapted* with respect to FRP materials. This was achieved by compiling lists of the strengths and weaknesses of FRP materials in comparison to traditional building materials. The key advantages of the materials were found to be:

- excellent strength-to-weight ratio
- good environmental resistance
- low thermal conductivity
- low permeability to air and water
- facilitate part-count reduction by integration of components during fabrication
- easy to produce in complex shapes, textures, and through-thickness colors
- can allow transmission of light

There are some characteristics, however, that place FRP materials at a disadvantage to traditional building materials:

- resins are combustible and have low maximum operating temperatures
- high unit cost

- low stiffness (glass fiber compared to structural steel)
- low hardness and thus low resistance to cosmetic damage
- low capacity to store thermal energy
- must be treated differently than the materials that have been in the hands of builders for hundreds of years, i.e. no inherited tradition

These lists were used through a *TRIZ* theory-inspired<sup>1</sup> logical framework to devise the new building system. Wherever possible, conventional design concepts were adapted to overcome the weaknesses listed above. Most notably, the issue of low operating temperatures was resolved through the adaptation of a solution that has been in use in other fields of engineering for decades but is unprecedented in the field of load-bearing FRP structures: internal liquid cooling. A well-established design principle was also adopted to minimize the issue of high unit cost: parts/systems integration. Within the proposed system, the fire protection, climate control, and thermal storage systems were combined into a single system. Further, the structural system and building envelope were merged to reduce components and achieve greater overall efficiency. As such, the proposed system reflects the innovative application of well-established design elements to new applications that are both effective and appropriate to the material.

---

1. According to G.S. Altshuller, father of *TRIZ* theory, 90% of engineering problems have already been solved for some other application or within another field. The theory involves the application a systematic method to differentiate the aspects of an engineering problem that are truly unique from the aspects that have already been resolved in some other form. For the aspects of the latter type, a simple list of 40 generic solutions was distilled from over 200,000 patents. Through the application of these solutions, an accumulated base of knowledge that extends far beyond the experiences of any single engineer can be exploited to solve the more mundane problems and the maximum amount of energy can be focused on the resolution of the truly unique problems. As such, it comes as no surprise that companies such as Ford, Xerox, and Boeing are strong advocates of the theory.

## 2 General Description

The proposed building system is composed of two basic elements: a floor deck and a wall panel. E-glass fiber was selected as the primary reinforcement because it is by far the most cost-effective option for applications where a low self-weight isn't critically important. The pultrusion process was chosen as the method of production because it is the most economical mass-production method for FRP products and the level of quality is generally very good thanks to 50 years of continuous refinement and the current high levels of automation. With this choice, however, comes one significant design limitation in that only shapes of continuous cross-section can be produced. Thus, both the floor and wall panels have continuous cross sections along their length.

Though both panel systems incorporate many new features, the most unique aspect of each is the integration of a liquid circulation system within their cellular structure. This system serves two purposes: to heat and cool the building climate through the regulation of the liquid temperature, and to cool the panels in the case of a building fire so that they may retain their load-bearing capacities for acceptably long durations.

A general description of each component and the related connection materials is provided in the following sections.

### 2.1 Basic Wall Element

A cellular panel shape was chosen to minimize material use and to permit the integration of the building envelope with the structural system. Tongue-and-groove style overlapping connections are made to adjacent panels by adhesive bonds. As shown in Figure 4-1, the width of the panel is a relatively narrow 50 cm to allow the assembly of walls of nearly unlimited widths.

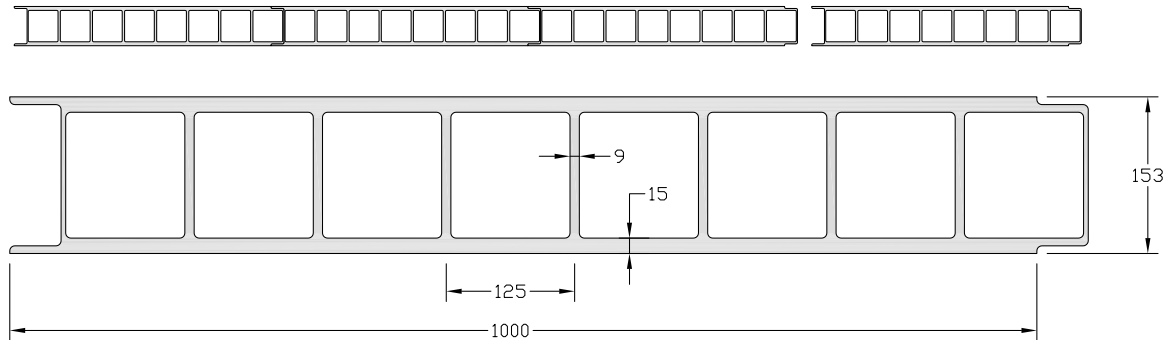
The depth of the pultruded portion (shaded grey) is 18 cm and was chosen as a compromise between the increase in structural and thermal efficiency with deeper sections and the associated loss of usable interior floor space.

The cells within the panel provide vertical chases for the mechanical services, form work for concrete columns, and conduit for the climate control/structural fire protection system (see Figure 4-2). A layer of rigid insulation is added to the exterior face of the exterior wall panels to reduce the heat transfer through the building envelope. Finally, a thin facing material is used to protect the insulation layer and to allow the customization of the exterior appearances. These layers are omitted for interior walls. Inter-story connections are made by "connector" elements that key into the wall panels for adhesive bonding (see Figures 4-8 and 4-9). The connector



the climate control/structural fire resistance system. The 100 cm width of the element is exactly twice that of the wall element and therefore requires half as many bonded joints per unit width.

**Figure 4-3.** Basic floor element (dimensions in mm)



As a fixed-geometry single unit, the stiffness of the element cannot be altered to adapt the panel to the span and loading conditions. In addition, its stiffness is too low to span the distances commonly desired in residential and commercial structures (6-9 meters). Therefore, a carbon tendon-truss frame can be added to the underside of each panel to increase stiffness of the floor panel and allow customization. Further details about the structural, architectural, mechanical, and constructive aspects of the wall system are provided in later sections.

## 2.3 Selected Geometrical Characteristics

### 2.3.1 Wall Element

Cross-sectional area:  $2.23 \times 10^{-2} \text{ m}^2$

Cross-sectional area of liquid-filled cells: (2x)  $1.65 \times 10^{-2} \text{ m}^2$

Cross-sectional area of concrete-filled cell: (1x)  $1.65 \times 10^{-2} \text{ m}^2$

Centroid (weak axis): 87.4 mm from building interior face

Moment of inertia (weak axis):  $6.82 \times 10^{-5} \text{ m}^4$

### 2.3.2 Floor Element:

Cross-sectional area:  $3.90 \times 10^{-2} \text{ m}^2$

Cross-sectional area of cells: (8x)  $1.42 \times 10^{-2} \text{ m}^2$

Centroid (weak axis): 76.3 mm from bottom face

Moment of inertia (weak axis):  $1.54 \times 10^{-4} \text{ m}^4$

## 3 Structural Concept

### 3.1 Global Building Stability

In order for a building to be stable, it must be able to resist gravity loads, bending and overturning moments, and inter-story shear loads due to wind and earthquakes (see Figure 4-4). The method in which each of these loads is transferred to the ground is described in the following sections.

#### *Gravity Loads*

Vertical loads on the floors and roof of the building are first supported by the floor decking/carbon tendon system. These panels work as stiffened beams to transmit the vertical load to their end supports at the wall panels. The wall panels then transmit these forces down the height of the building to the foundations (see Figure 4-5). Euler buckling is avoided by the bracing effect of the floor deck at each story.

#### *Bending Moments*

The building envelope is conceived to act as a tubular structure. When a bending or overturning moment is applied, a couple is created between the opposing faces of the building. Shear is transferred in this couple by the perpendicular walls (see Figure 4-5). In the case of buildings of exceedingly large footprints, additional load-bearing walls may be added at interior locations such as around elevator shafts and stairwells to increase the overall bending stiffness.

#### *Inter-story Shear*

Once again, the building envelope resists inter-story shear loads as a tubular structure. Horizontal loads on one building face are transferred to the perpendicular walls through diaphragm action of the floor decks. The perpendicular walls act as wide horizontal braces or shear walls, and thus resist the lateral loads (see Figure 4-5). Additional load-bearing walls may be added at interior locations as they would also be activated by diaphragm action of the floor decks.

Figure 4-4. Global building stability issues

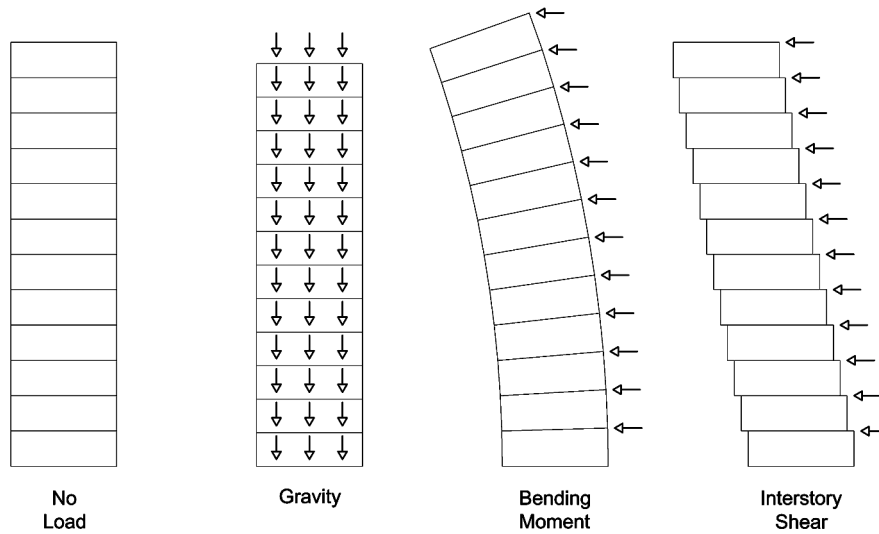
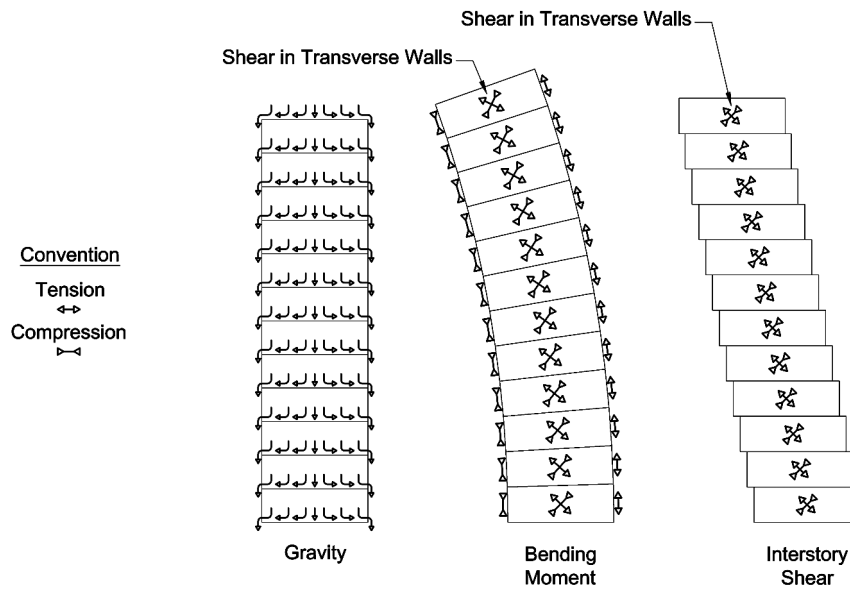


Figure 4-5. Global resistance mechanisms



### 3.2 Flooring System Structural Concept

Experiments have shown that very little bending moment may be transmitted in the direction transverse to the pultrusion axis [100]. Further, the low stiffness of the bonded connections between adjacent panels permits the distribution of point loads to a maximum of one other panel on each side; panels further away are fairly unaffected. Thus, the flooring system is conceived as a series of horizontally stacked one-way beams.

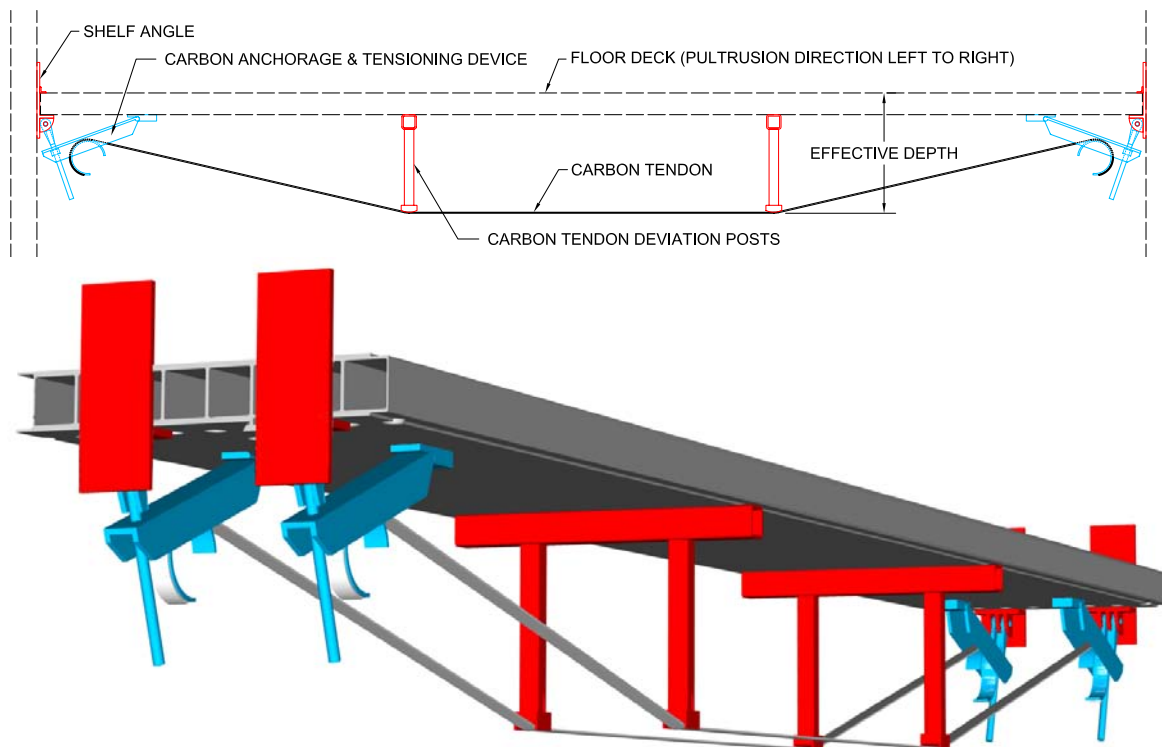
In many civil engineering applications of glass fiber-reinforced polymer shapes, dimensioning is strongly governed by serviceability limits rather than strength. The size of sections needed to

satisfy stiffness requirements may be many times the size required for strength [96], which leads to very safe but also very inefficient and uneconomical structures. To overcome this problem, a truss system employing carbon tendons has been added to the pultruded floor panels. This system greatly increases the rigidity of the floor panels by increasing the effective depth and by incorporating highly rigid materials.

The bending stiffness of a beam may be improved by increasing the dimensions of the beam (increase moment of inertia), or by using stiffer materials (increase Young's modulus). While stiffness increases linearly with increasing beam width or Young's modulus, it increases at the cube of increasing depth. Thus, increasing the depth of beams is by far the most efficient and economical method of improving bending stiffness (where space permits).

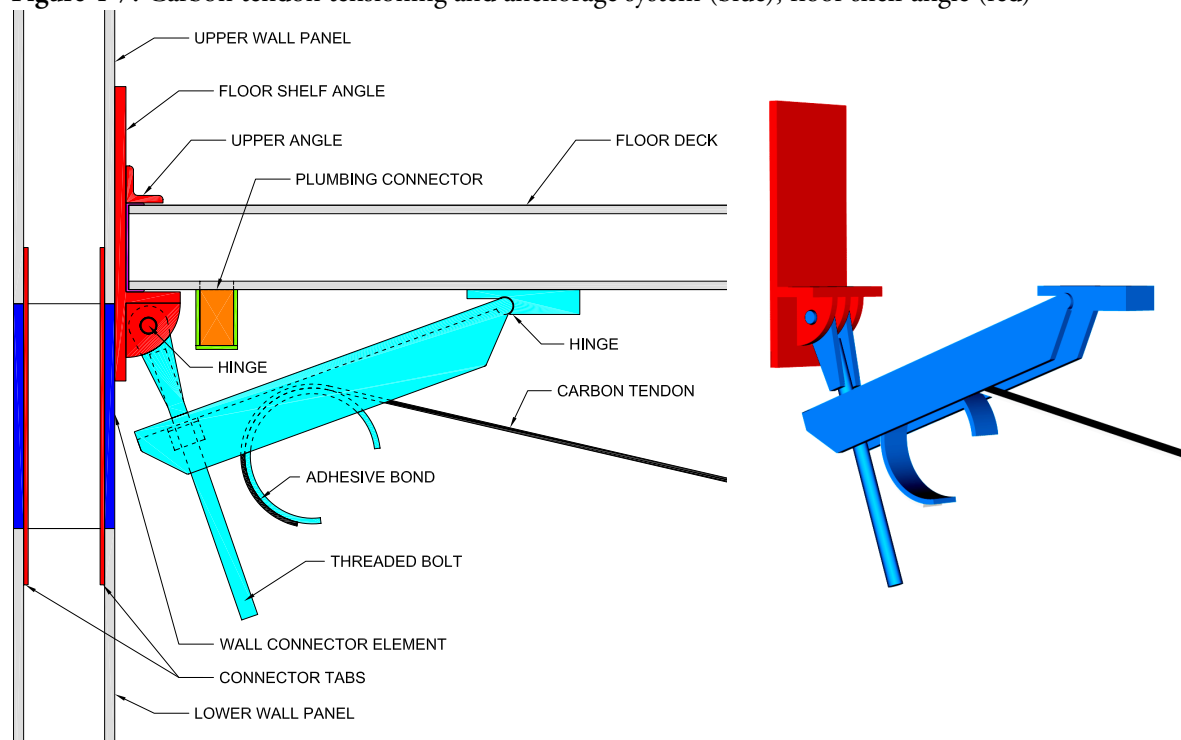
The carbon tendon system makes the greatest improvement to the bending stiffness of the floor panels by increasing the effective depth. By positioning the tendons far below the lower face sheet, the neutral axis shifts downward and a longer moment arm is created. For the proportions drawn in the figures (55 mm x 7 mm tendon 675 mm from bottom face of deck,  $E=250$  GPa), the tendon provides a 16x increase in the moment of inertia over the deck alone (from  $1.54 \times 10^{-4} \text{ m}^4$  to  $24.5 \times 10^{-4} \text{ m}^4$ ). This enormous improvement comes at minimal increases in dead load and employs readily available materials.

**Figure 4-6.** Schematic of carbon tendon system (dimensions vary by application)



A further advantage of the carbon tendon system is that it provides the possibility of adapting the stiffness of the floor based on the local loading, span, and headroom requirements. Greater spans or heavier live loads may be compensated by placing the tendons at a greater depth. Where headroom is restricted, the distance between adjacent tendons can be decreased for the same effect. For shorter spans such as in stairwells, the tendon system may not be necessary at all. In this manner, a single standardized section profile (made from a single pultrusion die) can be customized to a variety of conditions. For even more flexibility, however, a deeper profile of 20-25 mm and similar cross-sectional shape could also be produced.

**Figure 4-7.** Carbon tendon tensioning and anchorage system (blue), floor shelf angle (red)



The floor panels are supported by steel shelf angles at all four corners (see Figure 4-7), which are adhesively bonded to the wall elements and expansion bolted into the concrete filled cells. Three stiffeners below the lip of the shelf angle accept a hinged connection to the carbon tendon connectors. To prevent the outward buckling of the walls and to keep the floor panels firmly situated on the shelf angles, small angles are bonded on top of the floor panels and to the shelf angles.

To provide anchorage and allow post-tensioning of the carbon tendons, steel connector devices that form part of the shelf angle supports are bonded at the ends of the deck (see Figure 4-7). The tendons are adhesively bonded to curved steel plates to allow a gradual load transfer. The curved plates are held within a lever arm, whose rotation is controlled by a threaded rod. By

advancing the nut on the threaded rod, the lever is pulled towards the supports and thus the tendon is tensioned. As such, most of the tensile force in the tendon is resisted by compression in the floor panel and the peeling forces on the wall-to-shelf angle adhesive bond are small.

### 3.3 Wall System Structural Concept

To permit access into the wall cavity for mechanical services, the wall panels were not conceived as continuous sections with uniform load transfer. Instead, the wall system was designed to work as a series of somewhat independent columns. As such, penetrations may be made for mechanical services in between these “columns” without fear of compromising the structural integrity of the wall or piercing the water-filled load-bearing cells. Thus, the wall panel cross section consists of two trapezoidal tubes separated by a third inverted trapezoidal tube with thinner wall thicknesses.

The two portions of the section that create the vertical load resistance are reinforced primarily by unidirectional rovings. This maximizes vertical stiffness and reduces the coefficient of thermal expansion in the vertical direction. The portions in between vertical load-bearing tubes are reinforced primarily by  $+45^\circ/90^\circ/-45^\circ$  fiber mats and thus do not contribute to the vertical load resistance. Their function is to brace the vertical load-bearing tubes against buckling and to transfer shear between adjacent tubes for global stability.

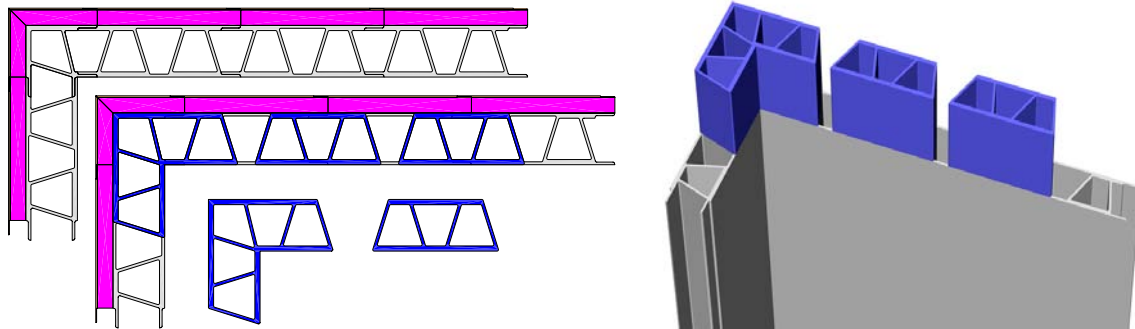
#### *Joints Between Adjacent Panels*

Tongue-and-groove keys allow easy alignment of adjacent panels for adhesive bonding. Depending on the specific conditions of the construction project (labor, transportation, lifting equipment, etc.), groups of panels may be bonded into super-panels at the factory to reduce the number of on-site bonds.

#### *Inter-story Connections*

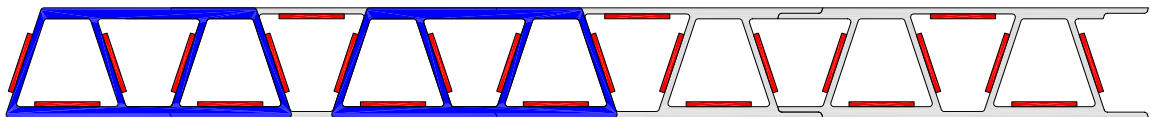
Inter-story connections are made by connector elements (see Figure 4-8). These elements incorporate the same vertical load-bearing tubes as the wall panels, but the connections between the tubes are staggered so that the connector elements straddle two wall panels. As in a brick wall, no bond directly traverses the height of the building. Thus, individual panels are interlocked both chemically by the bonds between adjacent panels and mechanically by the connectors above and below.

Figure 4-8. Inter-story wall connector elements (blue)



Alignment and continuity of the connector elements to the wall panels is made by adhesive bonding of flat FRP tabs on the interior surfaces of the cells. These tabs extend from lower wall panels, through the connector elements, and into the upper wall panels (see Figure 4-9).

Figure 4-9. Inter-story wall connector tabs (red)



### *Concrete Filling*

In multiple-story buildings, the load supported by vertical members changes in relation to the number of stories it supports. Thus, it is most efficient to place the strongest members at the base of the structure and reduce the capacity of the sections with increasing height. The wall system also provides this possibility. When two sections are bonded together, another inverted trapezoidal cell is formed. This cell is not required for the climate-control/fire resistance system and is inaccessible as a mechanical chase. Thus, it is a fairly wasted space that could be used for additional vertical load resistance. In effect, these unused tubes make perfect formwork for concrete columns, which may be reinforced with steel rebar according to the required load resistance. The incorporation of such concrete columns is also beneficial in that the columns help maintain structural continuity between stories and provide a solid anchorage point for wall-to-floor connections.

## 4 Production and Assembly

### 4.1 Industrial Fabrication

The basic floor element and the majority of the basic wall element is manufactured by the pultrusion process (see Figure 5-3 on page 153). As previously described, this process permits the production of high-quality sections of unlimited lengths in a highly automated and controlled environment. Initial tooling costs are higher than other more labor-intensive techniques, but these costs are steadily amortized by the high volume of production demanded by civil engineering projects.

For the wall panels intended for the building exterior, pultrusion of the basic element is only the first step. A layer of rigid foam insulation must then be bonded or expanded onto the outer face of the element. The thickness and composition of this insulation layer may be optimized for specific requirements of the project. In extremely cold environments, for example, the layer may be made thicker or with more effective (and more expensive) inert-gas entrained closed-cell foams with lower thermal conductivities. If the choice of the façade material suggests that fire may penetrate to this layer, fire resistant foams that will not contribute to the fire (fire retarded resins, phenolic foams, syntactic glass foams, etc.) would be preferable, though not necessary with respect to structural fire endurance.

The final layer that creates the façade is bonded on top of the foam (or the foam is expanded between the pultruded element and façade so that no bonding is required). This material may also be adapted to the particular project, as described in Section 5.3.

The wall connector elements (see Figure 4-8) are also produced by the pultrusion process. To facilitate alignment and create some tensile capacity in the wall-to connector joints, pultruded flat plates are bonded to some of the interior faces of the cells across the joints. These plates may be bonded to the connector elements in the factory such that only the bonds to the wall elements are necessary on-site.

The steel components, including the shelf angles, T-shaped wall ties, and carbon connector devices may be manufactured from common flat plates and/or rolled sections bent and welded into the desired arrangements. High strength steel threaded rods should be used for the carbon tensioning component.

## 4.2 On-Site Assembly

As in traditional building techniques, a standard concrete or masonry foundation is required to provide a flat working surface and to properly distribute the building's loads to the ground. Pultruded channels are bonded and bolted onto the top of the foundation walls to form a track. The channels accept the first story of the wall panels, creating a water-tight seal for both the water circuits within the wall panels and preventing ingress of water from outside of the building. Further, these channels create a structural connection that permits tensile load transfer, which can be important for global resistance to overturning moments (see Figure 4-4 and Section 3.1).<sup>2</sup>

The first story of wall panels is bonded into the track channel as they are tilted and slid into place. For a 3.4 m story height, each panel weighs approximately 130 kg, such that even the smallest lifting equipment would be able to maneuver several connected panels with their booms fully extended. Temporary diagonal braces ensure that the adhesive bonds cure with the walls in plumb. The pot life of commonly used epoxy adhesives is approximately 45 minutes, which provides sufficient time for the installation and alignment of large sections. The bonds become durable within 24 hours, meaning a cycle time of one story per day can be achieved.

Once the first course of wall panels is completed, the tabbed connector elements are bonded into place. When a large enough section of walls and connectors is assembled, steel rebar may be placed in the proper cells and the concrete can be poured.

The steel shelf angles are bonded to the inside face of the connector elements. These angles may be bonded in the factory for efficiency, or later onto the assembled wall for the best accuracy and adaptability to as-built conditions.

Next, the floor panels are lowered into position on the cured shelf angles. The carbon tendon deviation legs and tensioning devices may be bonded to the underside at any time before or after the installation of the panels in the building. As demonstrated in Section 4, the carbon tendon system is only required to meet stiffness requirements; the floor panels alone have the capacity to support normal live loads with a large margin of safety (even larger before the cells are filled with water). Therefore, the carbon tendons may be added to the floor panels whenever it is most convenient, such as after the installation of all of the plumbing, ventilation, and electrical services.

---

2. Though the system is not intended for tall buildings with high slenderness ratios (which experience tensile forces on their windward faces), tensile loads may also be caused earthquakes, or more commonly by the unusual demands made on the building during construction.

Installation of the tendons begins with the bonding of the ends of the carbon tendons to the curved plates on the anchorage devices. When fully cured, the nuts on the threaded rods are advanced to tension the tendon and to correct the curvature of the floor deck. As is customary in cantilevered concrete slabs, some degree of upward camber may be desired to offset the weight of the water and long-term creep in the deck, though adjustments may also be made throughout the life of the building.

All stories are constructed in the same manner as described above. Each story should be laterally braced by the installation of the floor panels before the next story of wall panels is installed. Special attention must be paid during construction to avoid high point loads on the floor deck. Practices that are common in traditional building construction, such as the operation of fork lifts or the use of scaffolding with small feet would damage the floor panels.

## 5 Architectural Functions

### 5.1 Shelter

The fundamental architectural requirement of shelter is automatically provided because the structure is, in fact, the envelope. Composed of thick synthetic polymers panels joined by continuous adhesive bonds, the envelope has an extremely low permeability to air and water. Thus, the interior environment is well protected from the weather outside.

### 5.2 Form

Thanks to the narrow width of the wall elements, buildings may be designed in a nearly infinite variety of arrangements. There is no restriction to a standard bay width or story height. Unlike the modular systems of the 1950's and 60's, there is no trademark shape or look that overshadows the expression of the architect. Though only straight and right angle wall elements are shown in the figures, other angles or curved elements could just as easily be produced.

The only true limitation in form is that no provisions have been made for transfer levels where the footprint of the building changes. These changes ordinarily require the transfer of enormous loads as the location of columns and load-bearing walls is shifted from one story to the next. Though not impossible, special solutions would be required in order to support such heavy loads.

### 5.3 Surface Treatments

#### *Building Façade*

The building façade was designed to fulfil two requirements: the protection of the insulation layer from weather and physical damage, and to provide total aesthetic freedom to the designer. A vast range of materials and products satisfy this first requirement; stamped metal panels, FRP cladding systems, stone, tile, stucco, and shingles are just a few of the examples. Thus the building façade may be customized to the specific requirements of the project. These requirements are dependent not only on the vision of the architect, but also the climate, neighborhood, code requirements, likelihood of wear/damage/vandalism, and of course, cost. The wall system was designed in recognition of the fact that no single material or product is the best solution for all situations, and thus provides great latitude in the selection of the façade.

### *Wall Finishes*

The interior face of the wall panels is also adaptable. Wallpaper provides the choice of color and texture while hiding the unsightly appearance of the bonded joints and the monotonous color of the pultruded elements. In addition, the paper conceals any repairs and may be easily replaced by the end-user when it is worn or outdated.

At the base of the walls, a hollow baseboard is installed to tidy the appearance of the floor-to-wall connection, including the shelf angles that protrude above the floor and the channels that are bonded to the ends of the floor panels. This baseboard also serves as a replaceable kick-plate to protect the wall panels from the inevitable wear and tear caused by furniture and foot traffic.

### *Flooring*

The choice of surface treatment for the floors is influenced by only one engineering concern. As the climate control originates from within the floor panels, materials with very low thermal diffusivities<sup>3</sup> will tend to slow the responsiveness of the system to changing thermal loads. Thus, heavy marble tiles or thick carpet padding, for example, may prevent the most efficient operation of the climate control system. Bearing this in mind, the flooring may be selected according to the visual, aural, economical, hygienic, and durability-related requirements of each space.

### *Ceilings*

According to the preferences of the designer, false ceilings may be suspended below the floor panels, or the structural and mechanical components may be left exposed. The typical treatment in such situations is to paint all of these components black and to suspend the lighting fixtures below. In any situation, the only reason to install a suspended ceiling is for visual impact, though there are also some benefits with regard to sound attenuation.

## **5.4 Natural Lighting**

Without the limitations of a column grid, window penetrations may be made at any location. As in any building, each unit area of window space reduces the thermal efficiency of the envelope, so the visual and natural lighting needs of the occupants must be weighed against the energy efficiency of the building as a whole. A minimum number of wall panels must be maintained for structural stability. The system is not adapted to some of the architectural forms

---

3. Materials that have a high density, high specific heat capacity, or low thermal conductivity have low thermal diffusivities, meaning their temperature changes relatively slowly as a result of a given heat flux.

that have evolved since the separation of the structural frame and the curtain wall, such as the famous “glass box” style that was dominant in commercial buildings from the 1960’s through the 1980’s. Instead, the far more energy-efficient and classically-styled building types with intelligently positioned and reasonably sized windows are favored.

## 5.5 Building Acoustics

### *Isolation*

Sound is transmitted through partitions by either small leakages of air or by vibration of the partition itself [79]. Thus, the more massive and air-tight the partition, the better it will isolate the acoustic environments on each side. As previously mentioned, the adhesively bonded wall and floor panels are essentially air tight, provided the penetrations made for the electrical and plumbing services are properly sealed. The addition of water and/or concrete to the cells more than doubles the mass of the panels, ensuring low sound transmission through the building envelope or from floor to floor.

Structure-borne sound should be reduced at the source by the use of resilient materials. Pumps, generators, and elevator equipment should be mounted on isolation slabs. Padding below floor finishes can greatly reduce the shock created by high-heeled traffic [114].

### *Resonance and Attenuation*

Acoustic quality within rooms is a separate matter from isolation and is best improved by the selection of surface finishes. Once again, resilient floor finishes also help to reduce resonance within the room. Some suspended ceilings tiles are specifically designed to attenuate sound and may further improve acoustic quality.

## 6 Mechanical Services

### 6.1 Heating and Cooling System

The fundamental concept behind the heating and cooling system (HCS) is to use the cellular structure of the wall and floor panels as a network of thermal emitters (what would otherwise be the radiators in traditional buildings). Water at a controlled temperature is circulated through the panels, which quickly assume the temperature of the water. The temperature of the panels then effects the temperature of the air in the room, absorbing heat if the water is cooler than the air temperature or emitting heat if it is warmer. Though this water circulation system is essential to the structural fire safety concept, it is through this integration with the HCS that the system may prove cost-effective.

#### *Design Logic of the HCS*

The ultimate goal of the design of any HCS is to provide the highest degree of thermal comfort to the widest group of occupants as possible.<sup>4</sup> Thermal comfort is affected by many parameters such as temperature, air currents, surface materials, as well as those related to the occupants (clothing, activity level, age, etc.). One key parameter is the vertical thermal gradient from the floor to the ceiling. It is nearly universally agreed that a greater level of comfort is achieved when the air at the occupant's head is several degrees cooler than at the feet. HCS systems that produce the exact opposite conditions, such as forced hot air systems, result in a sense of stuffiness that is aggravated by cold feet. Radiant under-floor heating systems, on the other hand, provide heat through the floor, and thus result in the ideal thermal gradient. The HCS of the proposed system takes inspiration from such under-floor systems, though the standard method of embedding a network of flexible pipes in a non-structural floor slab is simplified by the integration of the structural and mechanical systems.

The discussion of the HCS of the proposed system is divided into four sub-systems:

- emission system, where heat is transferred to the interior environment,
- distribution system, which brings the heat to or from the emitters,
- source, which creates or absorbs the heat, and
- control system, which regulates the functioning of the source.

---

4. The age-old maxim "you can't please all of the people all of the time" is quantified by HCS engineers, who calculate the "probable percentage dissatisfied" for a set of indoor climate conditions. A value of 10% is seen as excellent, while anything below 5% is considered impossible to achieve [156].

Each sub-system will be described in the following sections.

### 6.1.1 Emitters

#### *Emitting Surfaces*

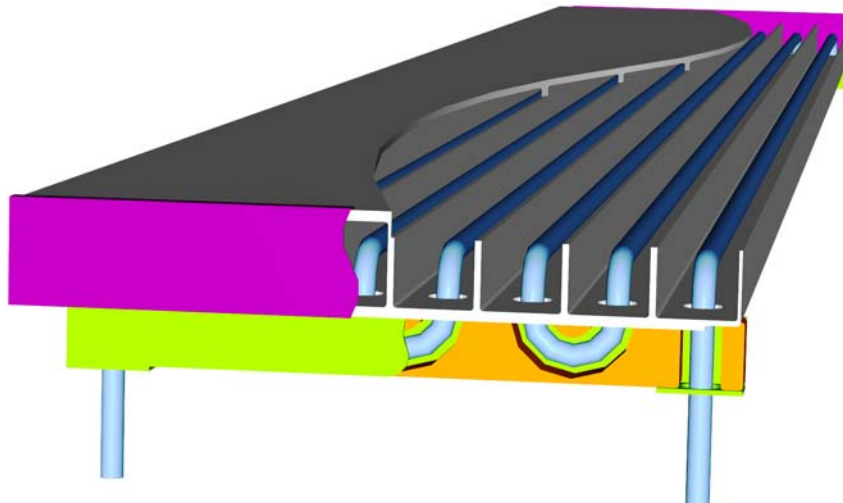
The proposed system is almost entirely composed of emitters. Every load-bearing component is potentially an emitter, as the liquid circulation system is required for structural fire protection regardless of whether it is needed for climate control. Thus, an enormous surface area is provided for the emission or absorption of heat. As such, the temperature differential between the emitters and the room environment may be very small indeed. This is highly advantageous for several reasons:

- allows the use of alternative heating sources (see Section 6.1.3 - *Sources*)
- safer in that no scalding hot surfaces exist to cause burns
- avoids condensation problems encountered with other liquid cooling systems

#### *Floor Circulation Pattern*

Water is circulated through the internal cells in a sinuous pattern. Entering at one end, the water travels the length of the panel, is transferred to the adjacent panel, and returns (see Figure 4-10). Depending on the length of the panel and the thermal loads in the room, one liquid circuit may be composed of one single outbound and return cell, or may travel several cells before returning to the source. The pattern may be varied so that circuits in front of windows, for example, can be made shorter and thus more effective than circuits towards the middle of the building.

**Figure 4-10.** Cutaway view of circulation path through a typical floor panel (n.b. liquid fills the entire interior of the cells - the tubes shown are only to demonstrate the path).

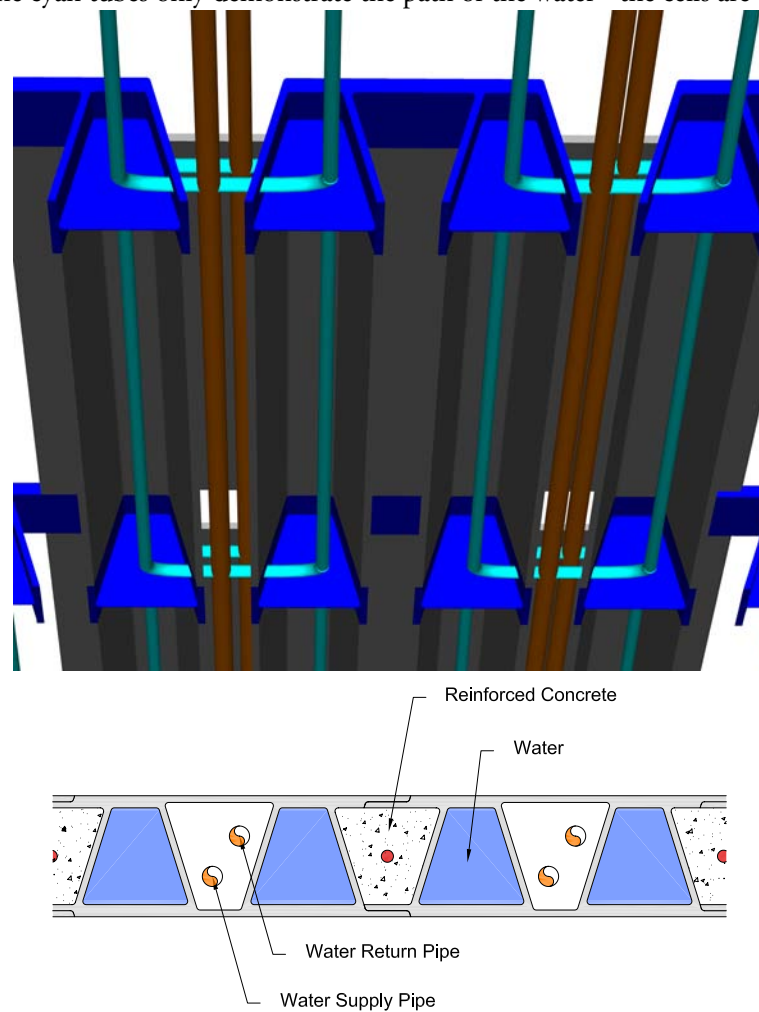


### *Wall Circulation Pattern*

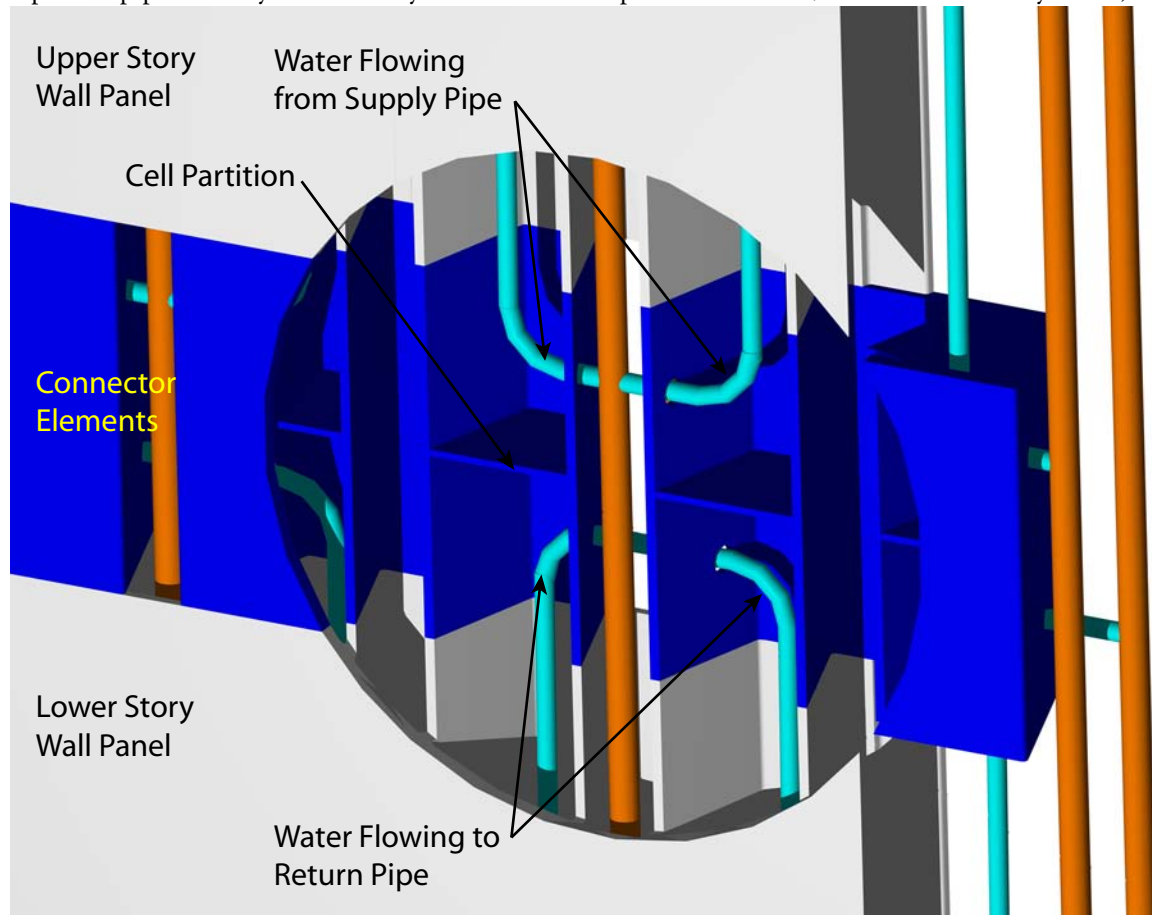
Water is only allowed to flow the height of one story so that hydrostatic pressure remains low within the cells. A pressurized supply line feeds the cells at the bottom, which then empty into a return line at the top. These supply and return lines are installed in the empty cells in between the water-filled cells. The connections from the supply and return lines are made through the connector elements. The supply connections are made in the upper half and the return connections are made in the lower half. A partition bonded mid-height in the cells of the connectors prevents the flow of water between stories.

Figure 4-11 shows cutaway views of the this pattern. While the orange tubes represent the supply and return lines, the cyan tubes are only drawn to demonstrate the path of the water - in reality the cells are entirely filled.

**Figure 4-11.** Cutaway view of the wall circulation path (n.b. only the vertical orange tubes actually represent pipes. The cyan tubes only demonstrate the path of the water - the cells are entirely filled.)



**Figure 4-12.** Cutaway detail of the wall circulation path (n.b. only the vertical orange tubes actually represent pipes. The cyan tubes only demonstrate the path of the water; the cells are entirely filled.)

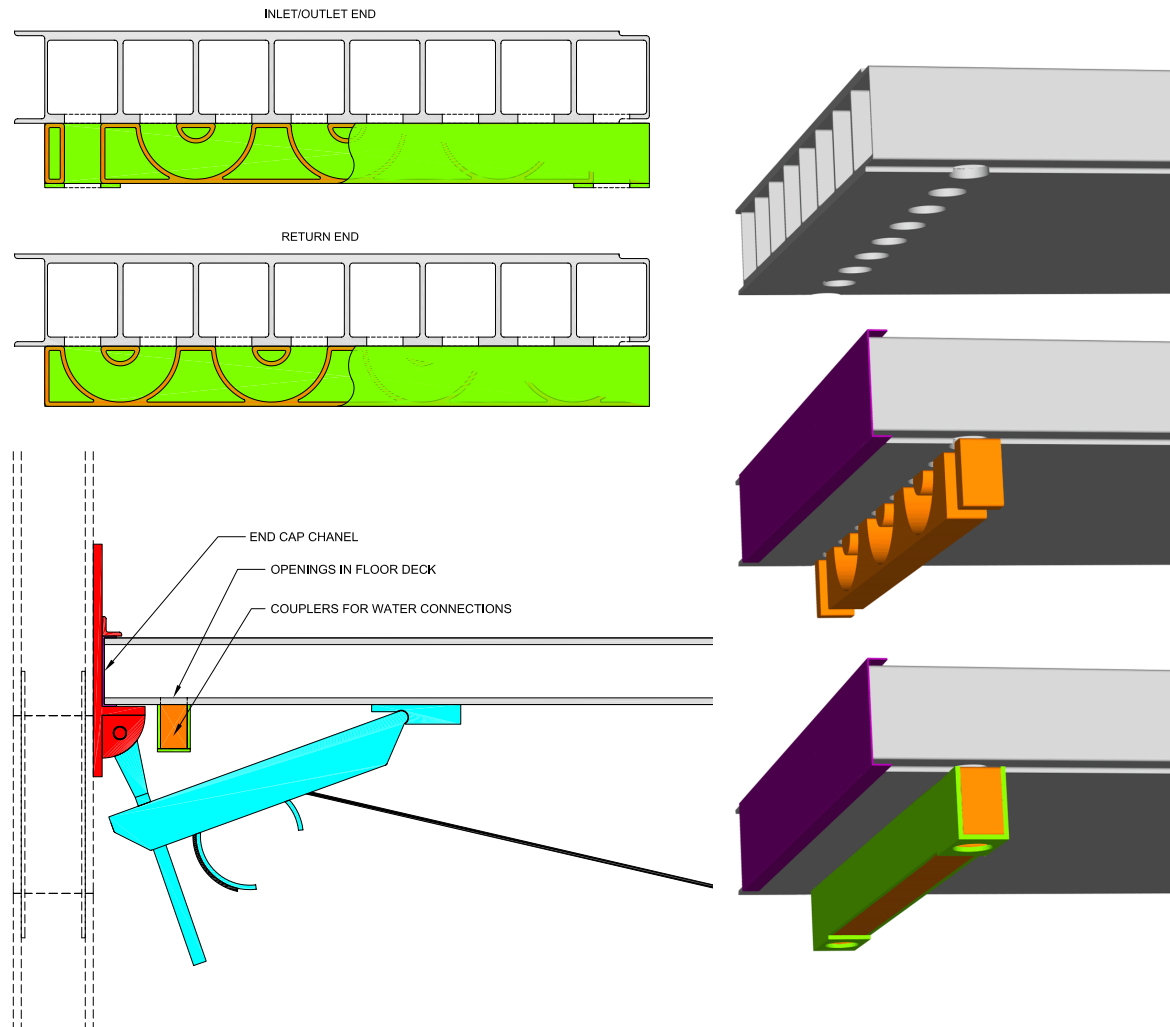


### *Floor Plumbing Connections*

Panels are made water-tight by bonding pultruded FRP channel sections to each end. The simplest way to create the sinuous flow pattern is to cut away a section of the web separating the two cells at the ends of the panels. Unfortunately, from the structural standpoint, the ends of the panels are where the webs are the most critical. Thus, an exterior plumbing connection is made through the lower face sheet.

Just beyond the flanges of the end channels, 60 mm diameter holes are bored through the face sheets in the center of each cell. At one end, these holes allow the water to exit one cell and enter the adjacent. At the other end, these holes are used for the same purpose, or to connect to the distribution system. Synthetic couplers as shown in Figure 4-13 simplify the task of completing the hundreds of connections that would be required for each room, and may be bonded on-site or in the factory.

Figure 4-13. Plumbing connections at the inlet/outlet end of a floor panel



### 6.1.2 Distribution

#### *Vertical Distribution*

The heated or chilled water that supplies the emitters is brought up through the building using the empty cells of the wall panels as vertical chases (see Figure 2.3). Though the cross section of the cells is relatively large and initially requires a lot of water to be completely filled, the required flow rate is quite low and can be supplied by small-diameter pipes at low pressure. Even if the flow rate must be augmented during a building fire, flow rates as low as 3 liters per minute have been shown to provide adequate structural protection by experimental investigations (see Chapter 5 - Section 7). Thus, insulated pipes with diameters small enough to fit inside the empty wall panel cells may be used to supply each tree of circuits at higher levels.

The rough-in work for this vertical distribution network should be completed during the assembly of the wall panels. Once the floors are in place, it is not possible to feed long pipes

into the empty cells of the wall panels. If the rough-in is not completed during assembly, either flexible pipes can be used or traditional plumbing walls will be needed. When installation is completed, the empty cells should be filled with loose insulation to reduce air-borne sound transmission between stories and to prevent drafts due to the chimney effect.

### *Horizontal Distribution*

Once the heated or chilled water has reached the intended story, it must be laterally distributed to the proper inlet/outlet location at the underside of the floor deck. The space below the floor deck is uninhibited by beams or stringers and thus provides free passage of the supply pipes in all directions.

### **6.1.3 HCS Sources**

In traditional hot water/steam/hot oil systems, the high temperatures needed to feed the small radiators excludes the use of alternative energy sources such as solar hot water heating and heat pumps. As described in Section 6.1.1, however, the surface area of the proposed system's emitters is enormous. With such a large area, only a very small temperature differential is needed to maintain the desired climate in the room. Thus, the temperature of the emitters does not need to be very high to heat the room or very low to cool the room, which opens up the possibility of using many alternative energy sources. Of course, the standard electrical, gas-fired and oil-fired furnaces are also perfectly suited to drive the system.

### **6.1.4 Control**

A predictive system is needed to control the functioning of the HCS. Since the introduction of radiant under-floor heating systems decades ago, predictive control systems have been under development and their accuracy continues to improve. Like under-floor heating systems, the HCS of the proposed system cannot react quickly to changing thermal loads. The thermal mass of the system is very large relative to the heat fluxes by which it is supplied, meaning that several hours may be needed to react to changing conditions. Predictive control systems employ thermostats not only inside the building, but also outside to monitor the weather conditions. This data is fed into a model that predicts the loads on the HCS several hours in advance and allows the controller to make the required adjustments.

## **6.2 Ventilation, Plumbing, and Electrical**

The empty cells of the wall panels may be used for the vertical distribution of:

- fresh air (duct work is not needed)
- plumbing services (cold water supply, hot water supply, hot water return, drain, and drain vent)
- electrical services (220V supply, telephone, network, cable, fire alarm, thermostat, etc.)

These cells may be penetrated at any location (for the installation of light switches, for example), and full access is provided at the inter-story connections. The gap between the connectors was dimensioned specifically so that the hands of workers can reach into the cell cavities.

As stated in Section 6.1.2, the empty cells should be filled with loose insulation when installation is completed to reduce air-borne sound transmission between stories and to prevent drafts due to the chimney effect.

Horizontal distribution is possible below the floor deck and above the carbon tendons, as it will be hidden by the suspended ceiling (or gloriously displayed in typical “dot com” decor). Further options are available for the distribution of the electrical services, which may be routed through the hollow baseboard.

## 7 Building Physics

### 7.1 Steady-State Heat Transfer

Building physics is the study of the heat, air, and moisture transfer processes that occur through the building envelope. In steady-state thermal problems, the rate of heat transfer (heat flux),  $q$ , is dependent on the overall thermal transmittance,  $U$ , of the envelope, and the temperatures of the interior surface,  $T_{SI}$  and exterior surface,  $T_{SE}$ .

$$q = U(T_{SI} - T_{SE}) \quad (4-1)$$

Similar to an electrical circuit, this overall thermal transmittance is calculated as the inverse sum of the individual resistances of each layer in the envelope,  $R_i$ , as well as the resistances at the interior surface,  $R_{SI}$ , and exterior surface,  $R_{SE}$ .

$$U = \frac{1}{R_{SE} + \sum_{i=1}^N R_i + R_{SI}} \quad (4-2)$$

The resistances of the exterior surfaces are functions of the radiative reflectivity and convective heat transfer coefficients of the faces, though values are fairly constant between building materials. The resistances of the layers is equal the thickness of each layer,  $d_i$ , divided by thermal conductivity,  $\lambda_i$ , and area perpendicular to heat flow,  $A$ .

$$R_i = \frac{d_i}{A\lambda_i} \quad (4-3)$$

Therefore, the steady-state rate of heat transfer through the building envelope is effectively only dependent on the thickness and thermal conductivity of the constituent materials.

### 7.2 Transient Heat Transfer

In real conditions, steady-state heat transfer does not exist. The reaction of materials to a thermal flux is not instantaneous, but a time-dependent decay problem that approaches steady-state conditions only after an infinite period of time. Thus, the temperature of the envelope is not only affected by the instantaneous heat flux that is applied, but also by all of the heat fluxes that have been applied in the past. The affect is called *thermal lag*, and the severity of this lag is

directly related to the thermal diffusivity,  $\alpha_d$ , of the material. The diffusivity of a material with density,  $\rho$ , and specific heat capacity,  $C_p$ , is defined by Equation 4-4.

$$\alpha_d = \frac{\lambda}{\rho C_p} \quad (4-4)$$

The higher the diffusivity, the quicker the material will change temperature as a result of a given heat flux. The diffusivities of some common materials are provided in Table 4-1.

The heat fluxes applied to the building envelope are constantly changing. The heat flux applied to the exterior of the envelope changes with the time of day, weather, and season, while interior heat fluxes vary in function of the lighting, appliances, office equipment, occupants (people emit roughly 100 W each), and other heat sources. In general, the exterior of buildings is exposed to higher heat fluxes during the day and in the summer months than at night and in the winter. On the inside as well, the general trend is for less heat to be produced at night than during the day. Thus, a daily and seasonal fluctuation of heat fluxes is observed in building climates.

### 7.3 Thermal Mass

It is the job of the HCS to smooth the peaks of these fluctuations to an acceptable level of thermal comfort. The size of the system, therefore, is determined by the height of the peaks. The higher the fluctuations, the more energy the HCS must be able to supply or remove per unit time. The smaller the fluctuations, the smaller and more efficient the HCS can be designed.

There is therefore a large interest in reducing the height of the flux peaks. Some techniques have been developed for this purpose, such as sunshading, but the most effective technique is also the oldest and simplest, and simply requires the use of thermally massive building materials. An envelope constructed of such materials serves as a sort of thermal flywheel or buffer. By absorbing large amounts of energy during times of high heat fluxes and releasing that energy at the times of low heat fluxes, a more stable thermal climate is created.

The term “thermally massive” is qualitative. To quantitatively compare the efficiency of materials for use for the storage of thermal energy, the thermal effusivity,  $b$ , is used<sup>5</sup> (see Equation 4-5) [76 pg. 25], [158]. Materials with high effusivities also have high densities and

---

5. A redundant term used by some engineers is the *thermal inertia*, which is simply the product of the specific heat capacity, thermal conductivity, and density, or the square of the *effusivity* [22 p. 48].

high specific heat capacities so that energy can be densely stored, and high thermal conductivities so that energy stored deep within the material is readily available at the surface.

$$b = \sqrt{\rho\lambda C_p} = \frac{\lambda}{\sqrt{\alpha_d}} \quad (4-5)$$

**Table 4-1.** Approximate thermal properties of common materials [47]

Material	$\lambda$ W/m·K	$\rho$ kg/m <sup>3</sup>	$C_p$ J/kg·K	$\alpha_d$ m <sup>2</sup> /s	$b$ J/m <sup>2</sup> ·K·s <sup>0.5</sup>
Steel (mild)	45.8	7,850	460	130x10 <sup>-7</sup>	12,900
Water	0.60	1,000	4,200	1.4x10 <sup>-7</sup>	1,590
Glass	1.10	2,540	840	5.2x10 <sup>-7</sup>	1,530
Concrete	1.00	2,100	880	5.4x10 <sup>-7</sup>	1,360
FRP	0.35	1,870	1,170	1.6x10 <sup>-7</sup>	875
Wood (yellow pine)	0.14	640	2,850	0.77x10 <sup>-7</sup>	505
Expanded Polyurethane	0.03	20	1400	11x10 <sup>-7</sup>	30

Table 4-1 shows the effusivities of some common materials. It is important to note that while this value is relatively high for traditional building materials such as steel and concrete, it is quite low for FRP. Thus, while an FRP building structure may have a very low coefficient of thermal conductivity, which is energy-efficient in steady-state conditions, it also has a very low thermal mass, which leads to high peak loads on the HCS system.

The solution to this problem is evident from the list of materials shown in the table. Per unit mass, there is no more cost-efficient form of thermal mass than water. With a specific heat capacity four times higher than FRP or concrete, it has the ability to store enormous amounts of energy per unit volume. The effusivity shown in the table is deceptively low, as the thermal conductivity used in the calculation of this value is rather irrelevant for a low-viscosity flowing liquid (heat is mostly distributed through liquids by mass transfer rather than conduction). In reality, there are very few materials that can out-perform water as a medium for thermal mass.

In relation to the proposed system, water filling greatly increases the thermal mass of the building without increasing the weight of the manufactured components. No additional building materials are required, meaning the components remain easy to transport, maneuver, and assemble.

Considering only the pultruded portion of the wall panels, a one-meter square area weighs approximately 83 kg, and stores heat at the rate of 97.5 kJ for each 1°C change in temperature.

With filling the appropriate cells, the same panel stores 374 kJ/°C, or roughly four times more energy. The greater volume of water in the floor panels means that heat is stored even more effectively therein. A one-meter square area weighs approximately 50 kg and stores 59 kJ/°C. With water filling, the same panel stores 536 kJ/°C, or roughly eleven times more energy. This is roughly equivalent to the storage capacity of a 24 mm thick concrete slab, though it is only 15 cm thick and, even with water filling, still weighs one third as much.

## 8 Conclusions

A unique multiple-story building system employing primarily FRP elements in material-adapted manners has been introduced. The advantageous characteristics of FRP materials are exploited through the integration of building functions into single elements:

- Vertical elements serve as the building envelope, vertical and lateral load-bearing structure, climate control system, and provide chases for various mechanical services.
- Horizontal elements serve as the floor deck, climate control system, and allow horizontal distribution of various mechanical services.

The main disadvantages of FRP materials have been overcome through various design features:

- The low thermal mass has been overcome through the incorporation of a liquid circulation system. This system increases the thermal mass of the walls panels by a factor of 4 and the floor panels by a factor of 11.
- The low structural fire endurance has also been resolved through a liquid circulation system. Because such a solution is unprecedented in the field of load-bearing FRP building elements, the effectiveness of this system has been investigated both experimentally (described in Chapter 5) and through mathematical modeling (described in Chapter 6).
- The low stiffness has been overcome through the introduction of a carbon tendon system, which provides a 16x increase in the effective moment of inertia of the floor panels with only a very slight increase in dead load.
- The susceptibility to cosmetic damage and durability problems has been addressed by the allowance for customizable surface finishes that may make use of the most appropriate materials and products.
- The high unit cost has been mitigated by part-count reduction, extensive industrial fabrication, low transportation costs, quick on-site assembly, and low long-term maintenance.



# 5

## **Experimental Investigations**

*Investigations Relating to the Thermal and Thermomechanical Efficacy of Internal Liquid Cooling for the Structural Fire Protection of FRP Components*



## 1 Introduction

Experimental investigations were conducted in conjunction with the numerical and analytical analyses. There were three basic objectives of the experimental program:

- explore the efficacy of internal liquid cooling for the fire protection of load-bearing FRP components
- provide thermal, thermomechanical, and fire reaction characteristics for numerical modeling input
- validate numerical model against system-scale experimental results

To accomplish these objectives, a methodology implementing three stages of experimental investigations was devised:

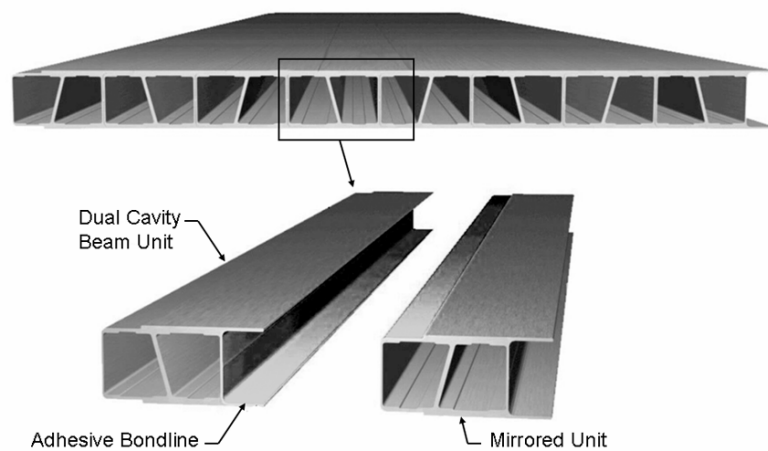
- coupon-level experiments for thermal and thermomechanical properties
- medium-scale experiments for fire reaction and liquid cooling without structural load
- full-scale system-level experiments for structural fire endurance with liquid cooling

A general description and the important results of each of these experiments is provided in the following sections. Further information relating to detailed procedures, instrumentation, and results are included in the experimental reports (Appendix A to Appendix C).

## 2 Materials

To facilitate the comparison of results between different experiments, all investigations were performed on the same material. All specimens originated from sections of an FRP decking material that is currently under commercial production. This deck, known as DuraSpan 766<sup>®</sup>, was developed by Martin Marietta Composites of Raleigh, North Carolina, USA, and is produced by Creative Pultrusions of Alum Bank, Pennsylvania, USA (see Figure 5-1).

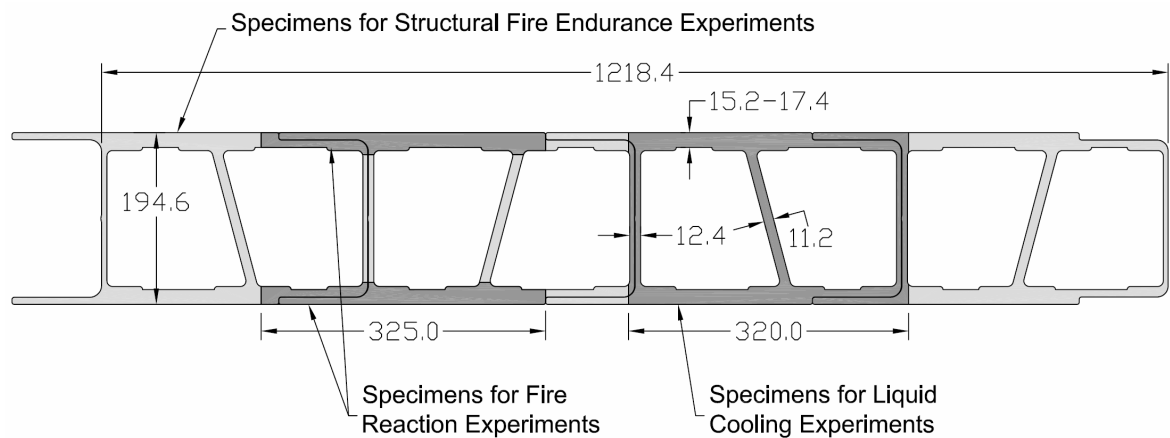
Figure 5-1. DuraSpan 766 Bridge Deck System



### 2.1 Physical Description

The form of the deck profile may be compared to a series of side-by-side I-beams united by upper and lower plates. The I-beams of this analogy are referred to as the *webs* and the upper and lower plates will be referred to as the *face sheets*. Each deck section consists of three webs and two face sheets. Tongue-and-groove connections are provided within the face sheets to permit adhesive bonding of adjacent sections. Figure 5-2 shows how the experimental specimens were derived from the decking material.

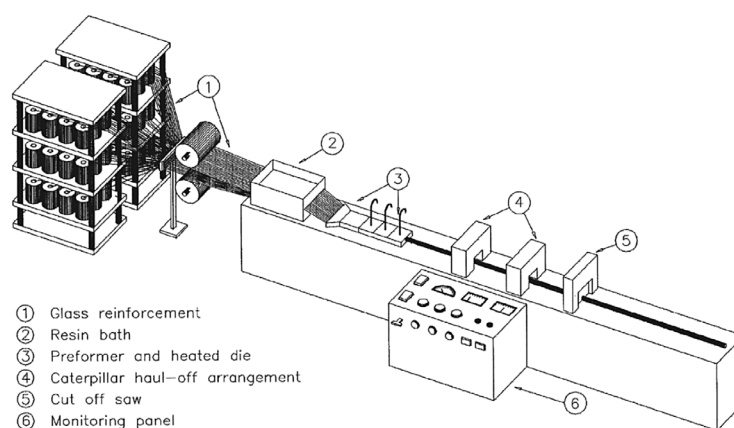
Figure 5-2. Derivation of experimental specimens (dimensions in mm)



## 2.2 Production Method

The deck sections are produced by the pultrusion process,<sup>1</sup> a process somewhat similar to the familiar extrusion process used for metals and thermoplastics. In this process, the glass fiber reinforcement is passes through a bath of liquid resin and is then pulled through a heated die, which both shapes and cures the composite at the same time (see Figure 5-3). Sections can then be cut to any length required, though storage and transportation may impose practical limits. Though new solutions are being introduced, current techniques do not permit changes in the shape of the cross-section within a single pultrusion run.

Figure 5-3. Diagram of the pultrusion process [35]

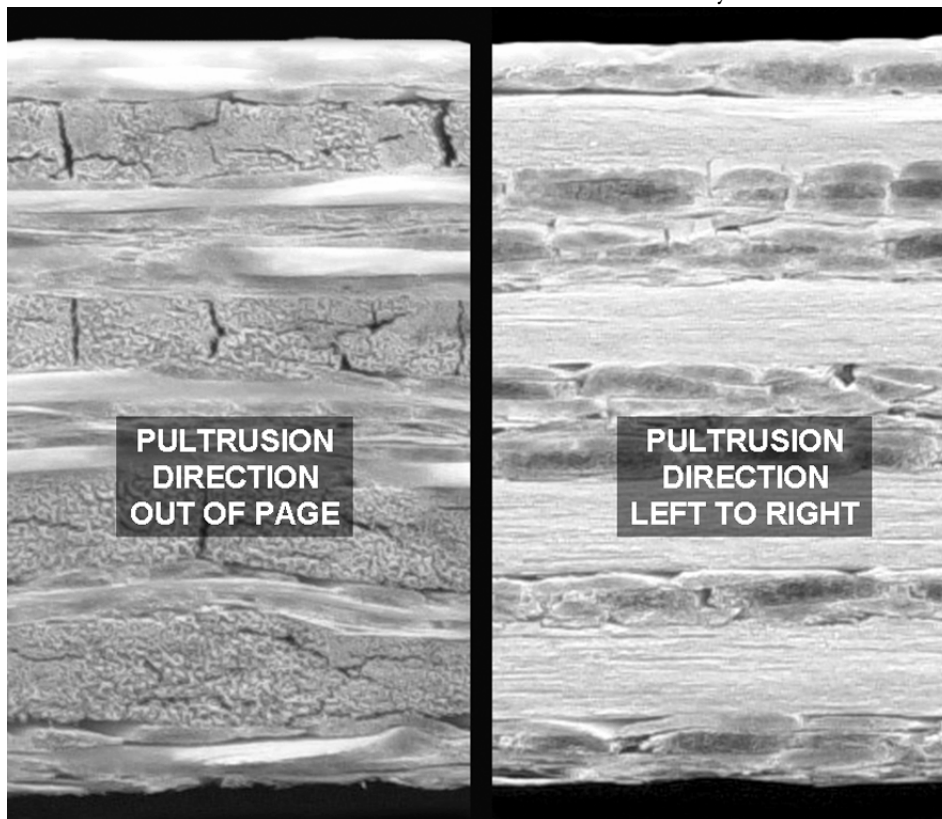


1. As the oldest automated production technique for FRP materials, (development began in the 1950's) current pultrusion techniques profit from a half century of refinement. Quality is generally good and uniform, and the high level of automation has made it the most cost-effective (by weight) method of producing composite parts.

## 2.3 Constituent Materials

The reinforcement of the section is arranged in a carefully engineered pattern of E-glass fiber fabrics and unidirectional rovings. The fabrics are composed of several reinforcement layers placed at  $90^\circ$ ,  $+45^\circ$ ,  $-45^\circ$  to the pultrusion direction, as well as random<sup>2</sup> layers. These individual layers are stitched together to create a single fabric. The unidirectional rovings are the bundles or fibers that run in the direction of the pultrusion run, and thus, the long axis of the sections. In Figure 5-4, the rovings appear as darker layers in Figure 5-4 *right* and smooth layers in Figure 5-4 *left*, while the mats and random layers appear as lighter layers in Figure 5-4 *right* and cracked layers in Figure 5-4 *left*. The borosilicate E-glass fibers used to create these layers is produced by Johnston Industries of Columbus, Georgia, USA.

Figure 5-4. Face sheet fiber architecture as seen after a resin burn-off analysis



The matrix is primarily composed of a *thermosetting* polymer, meaning that irreversible cross-linking occurs during curing (as opposed to thermoplastic polymers, which may be returned to liquid form by the addition of heat). Unsaturated isophthalic polyester (UP) provides the strength and durability of the matrix, while kaolin clay filler is used to reduce its volumetric

---

2. Random layers are layers where fibers are dispersed in all directions, creating a spaghetti-like mesh that has roughly equivalent strength and stiffness in all (in-plane) directions.

cost. The styrene monomer is added to induce curing. Small quantities of catalysts and mold release agents are also added. Proportions by volume of these components are approximately as follows: 74% unsaturated polyester, 22% kaolin clay, 3% styrene, <1% other. The unsaturated polyester is sold under the name Aropol® 7334 and is produced by the Reichhold Corporation of Durham, North Carolina, USA.

Properties of the constituent materials are provided in Table 5-1 and of coupons of the composite in Table 5-2.

**Table 5-1.** Properties of DuraSpan deck constituent materials ( $t$  = tension,  $c$  = compression) [199]

<b>Property</b>	<b>Resin</b>	<b>Fiber</b>
$V_f$	48%	52%
$M_f$	39%	61%
$E_t$	3.38 GPa	72.4 GPa
$f_t$	75.8 MPa	3.45 MPa
$f_c$	117.2 MPa	-
$T_g$	117°C	-
$T_d$	300°C	-
$T_s$	-	830°C

Table 5-2. DuraSpan coupon properties ( $x$  = longitudinal,  $y$  = transversal,  $z$  = through-thickness) [199]

Property	Face Sheets	Webs
$E_x$	21,240 MPa	17,380 MPa
$E_y$	11,790 MPa	9,650 MPa
$E_z$	4,140 MPa	4,140 MPa
$G_{xy}$	5,580 MPa	7,170 MPa
$G_{xz}$	4,140 MPa	4,140 MPa
$G_{yz}$	4,140 MPa	4,140 MPa
$f_{c-x}$	-261 GPa	-215 GPa
$f_{t-x}$	261 GPa	220 GPa
$\nu_{xy}$	0.32	0.30
$\nu_{xz}$	0.30	0.30
$\nu_{yz}$	0.30	0.30
$\rho$	1,870 kg/m <sup>3</sup>	-
$C_p$	1,170 J/kg·K	-
$\lambda_z$	0.35 W/m·K	-

## 2.4 Adhesives

Bonding of the pultruded sections that is performed by the manufacturer in the factory is completed using Pliogrip® 8000/6660 flexible polyurethane adhesive from Ashland Chemical of Covington, Kentucky, USA. All on-site and other miscellaneous bonding tasks were performed using Sikadur® 330 rigid two-part epoxy from Sika AG of Zurich.

### **3 Facilities**

All medium and large-scale investigations were performed at the Swiss Federal Laboratories for Materials Testing and Research (EMPA) in Dübendorf. With the support of the fire testing division staff of the Building Physics Group, all specimens were prepared and tested within the fire laboratory.

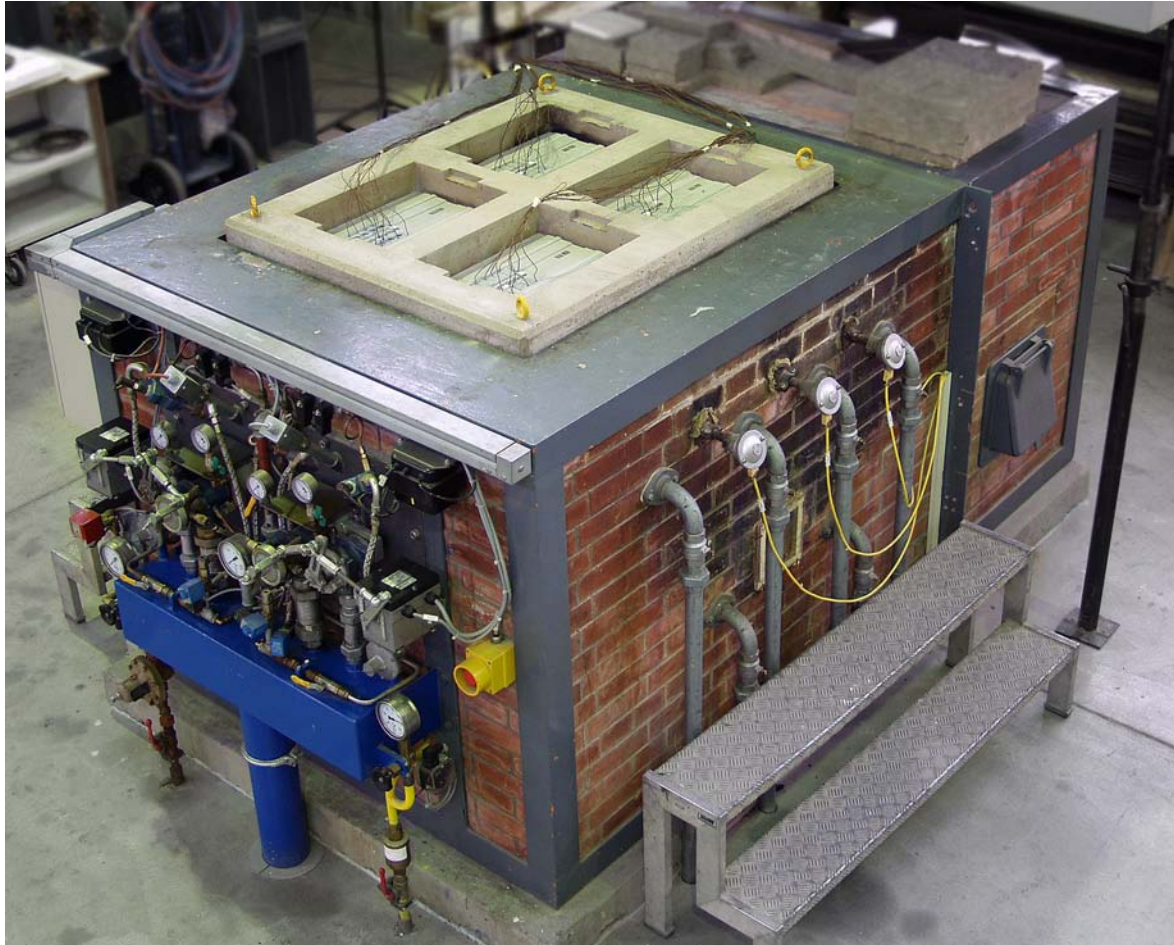
#### **3.1 Coupon-Level Experimental Facilities**

Thermogravimetric and dynamic mechanical analyses were performed at the laboratories of the resin producer and adiabatic calorimetry was performed at the Building Physics laboratory of the EMPA.

#### **3.2 Small Horizontal Oven**

All medium scale experiments were performed on the laboratory's small horizontal oven (see Figure 5-5). The oven is fired by two oil burners and has an internal volume of 0.5 cubic meters. Specimens of up to 105 cm wide and 125 cm long may be placed over the open top of the oven, or concrete frames may be used for smaller specimens. Six oven-piloting thermocouples are situated just below the exposed face of the specimen to measure the gas temperature. A computerized system uses the readings from these thermocouples to adjust the intensity of the burners. Windows on two sides of the oven allow a partial view of the hot face of the specimen. Interior surfaces of the oven are an unlined high-temperature brick. Measurements from up to 40 thermocouples may be recorded by the central data acquisition system, though more may be added externally. Structural loading is not possible.

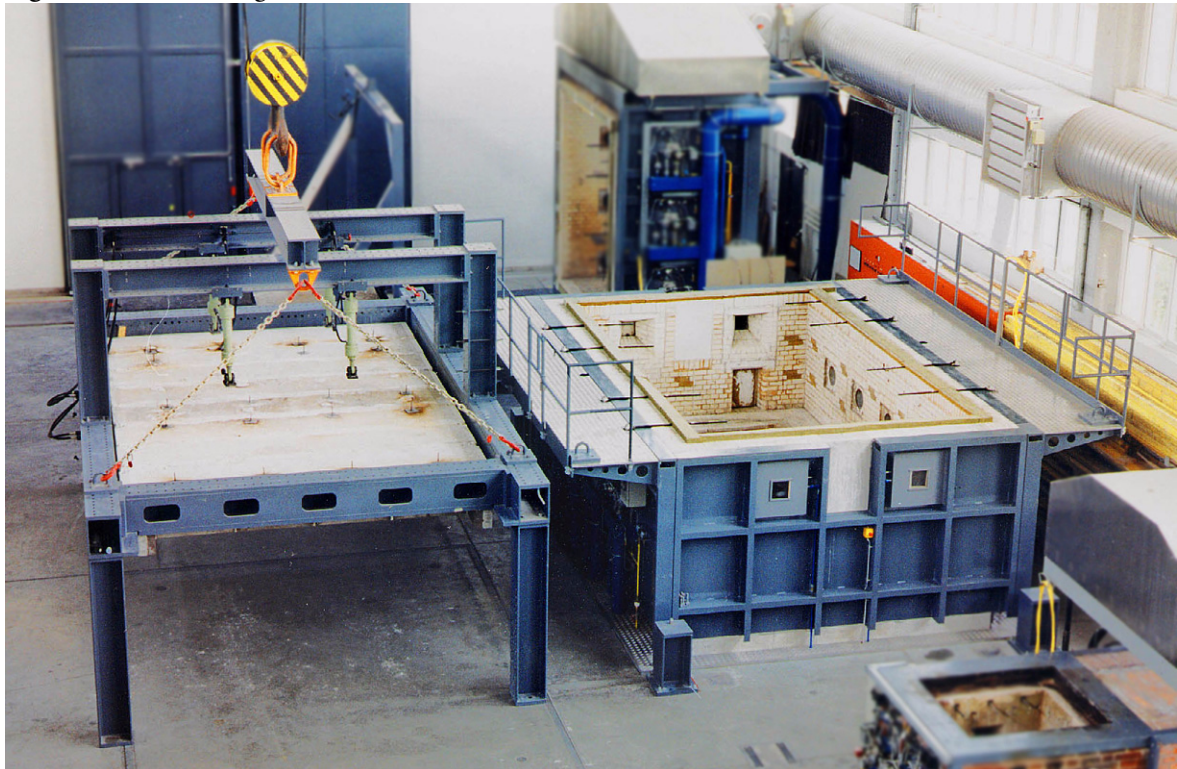
Figure 5-5. EMPA small horizontal oven with purpose-built concrete exposure frame



### 3.3 Large Horizontal Oven

All large-scale experiments were conducted on the laboratory's large horizontal oven (see Figure 5-6). The oven is fired by 10 oil burners and has an internal volume of 25.5 cubic meters. Specimens of up to 350 cm wide and 520 cm long may be placed over the open top of the oven, or concrete masks may be used for smaller specimens. Eight oven-piloting thermocouples are situated just below the exposed face of the specimen to measure the gas temperature. Once again, a computerized system uses the readings from these thermocouples to adjust the intensity of the burners. Four windows on two sides provide a partial view of the hot face of the specimen. Interior surfaces of the oven are also an unlined high-temperature brick. Measurements from up to 80 thermocouples may be recorded by the central data acquisition system, though more may be added externally.

Figure 5-6. EMPA large horizontal oven and structural reaction frame



To impose structural loads, a rigid steel frame surrounds the oven. Specimens are placed on the support frame, which positions the specimens just above the oven. Above the reaction frame, two loading frames may be positioned anywhere along the length of the specimen. Two hydraulic loading cells per loading frame may provide a total of four discrete loads. To provide access to the inside of the oven and to facilitate quick removal of specimens from the oven, the entire reaction frame/loading frame/specimen assembly may be lifted off of the oven using the overhead crane.

Load-controlled actuators are fed by a single hydraulic source so that all four loads are equal. The maximum load is 150 kN per actuator. Hydraulic pressure is supplied by mechanical pump, which uses a pendulum manometer to relate oil pressure to jack force. In addition, a digital manometer provides accurate oil pressure measurements. To determine the applied load from the digital manometer, two conversions must be made: manometer voltage (volts) to oil pressure (bars), and then oil pressure (bars) to jack force (kN). Though slightly convoluted, the arrangement is calibrated regularly and provides reliable results accurate to within 1 kN.

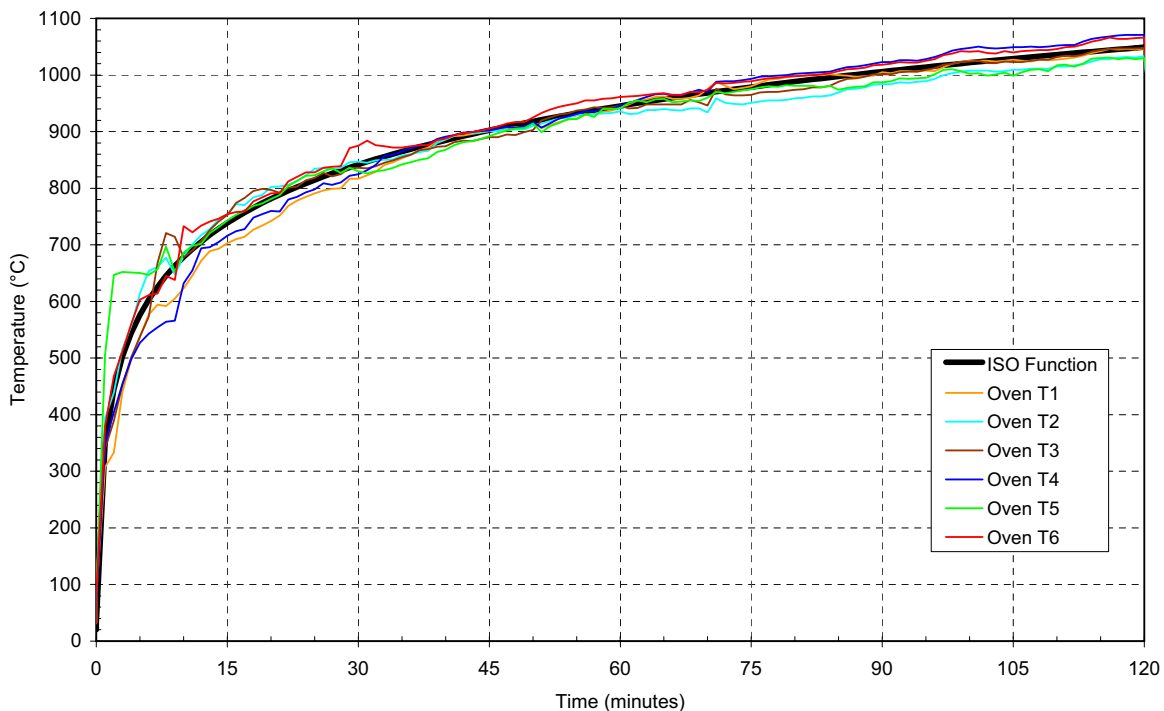
## 4 Fire Loading Regimes

All of the medium and large-scale experiments were performed with the fire exposure according to the ISO 834 cellulosic time-temperature curve [92]. Though from the standpoint of numerical simulation it would have often been more convenient to use fixed heat-fluxes rather than a time-temperature curve, such loadings were not possible on the oil-fired ovens. The ISO 834 curve recreates the most severe temperatures experienced in typical building fire over time and closely resembles other curves used throughout the world such as the American ASTM E-119, the British BS 476, and the German DIN 4102. Logarithmically increasing, the curve prescribes 500°C after roughly 4 minutes. The temperature,  $T$  (in °C), is given as a function of time,  $t$  (in minutes), and initial oven temperature,  $T_0$ , in the following equation.

$$T - T_0 = 345 \log_{10} (8t + 1) \quad (5-1)$$

Figure 5-7 shows the ideal ISO 834 curve along with an example of the actual temperatures recorded by thermocouples within the small horizontal oven. Though there is some instability in the first 10 minutes of the program, the oven quickly assumes an average temperature close to the ideal curve.

**Figure 5-7.** ISO 834 cellulosic time-temperature curve and typical oven gas temperatures measured by oven piloting thermocouples



## 5 Thermal and Thermomechanical Property Experiments

### 5.1 Dynamic Mechanical Analysis

To ascertain the relationship between the stiffness of the experimental material and temperature, dynamic mechanical analyses (DMA) were performed. The series was performed by the resin producer using a material that was specially fabricated to have the same properties as the experimental material.

#### 5.1.1 Basic Principles

In principal, dynamic mechanical analysis provides an approximation of the *relative* stiffness reduction of a specimen with respect to temperature. The approximation is relative in that stiffness measurements do not have any physical significance; the trend rather than the absolute magnitude of the stiffness versus temperature curve is important.

The reaction of synthetic polymers to load is somewhat delayed and therefore falls somewhere in between a purely elastic (Hookean) solid and a viscous fluid. This type of behavior is termed *viscoelastic*, as the materials deform in both a viscous and elastic manner. The key to DMA is the measurement of this time-dependent deformation, or *flow* of the specimen.

#### 5.1.2 Description of Technique

Though many variations of DMA exist, the basic procedure is the same. Specimens are loaded in a cyclic (usually sinusoidal) pattern within the elastic region of their stress-strain curve and the temperature is slowly varied. Sensors measure the temperature, load, and strain. The delayed deformation of the specimen is measured as a temporal offset of the strain versus time curve ( $\epsilon-t$ ) from the stress versus time curve ( $\sigma-t$ ). The overlap of the two curves represents the elastic contribution of the stiffness, or the *storage modulus*,  $E'$ . The areas outside of overlap of the two curves represents the viscous contribution of the stiffness, or the *loss modulus*,  $E''$ . The ratio of these two moduli,  $E''/E'$ , is denoted  $\tan-\delta$  and is called the *damping factor* or *loss tangent* [84 pg. 761].

Each of these three values ( $E'$ ,  $E''$ ,  $\tan-\delta$ ) may be used to determine the glass transition temperature,  $T_g$ , of the specimen. Plotted against temperature, each displays a peak or a noticeable change in slope at  $T_g$ . The unfortunate consequence is, however, that the  $T_g$  found by each of these methods may vary by as much as 30°C for the same run [84 pg. 761]. In general, the storage modulus curve provides the lower boundary value, or *onset*; the  $\tan-\delta$

provides the upper boundary, and the loss modulus provides a midpoint estimation of  $T_g$  [180]. It is up to the discretion of the engineer to determine which method is the most appropriate.

DMA may be conducted in tension, compression, bending, torsion, or shear loading. There is always some effect at the  $T_g$ , though its magnitude may vary enormously as the stiffness of the specimen is more dependent on the resin in some stress states (e.g. shear) than others (e.g. tension).

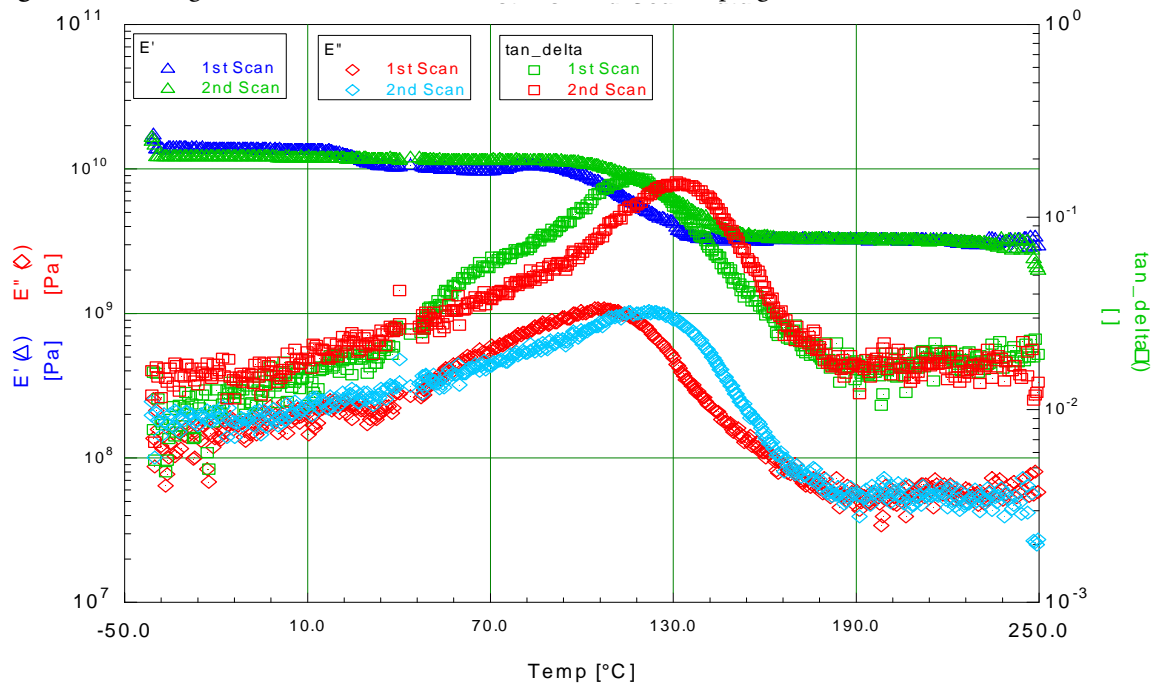
### 5.1.3 DMA Performed

Cyclic loads were imposed on a three-point-bending set-up of a Rheometrics Solids Analyzer from Rheometrics, Inc. The maximum thickness of specimen that can be tested on the instrument is 1/8" or 3.175 mm. Because no portion of the experimental profile was thin enough and it was feared that the heat produced by any machining operation to reduce the thickness would alter the material properties, unique specimens had to be custom fabricated. Mimicking the matrix formulation and approximating the fiber architecture of the experimental profile, a special pultrusion run was conducted to create the DMA specimens. The final sample size was 54 mm long x 12 mm wide x 3 mm thick.

The specimen was scanned in "dynamic temperature ramp mode" from -40°C to 250°C at a heating rate of 5°C/min and using a dynamic oscillation frequency of 1 hz. The same test specimen was scanned a second time under the same test conditions as noted above. The oven was purged with nitrogen during the scans.

### 5.1.4 Results

From the peak of the  $\tan-\delta$  curve, the glass transition temperature was found to be 117°C (see Figure 5-8), while the  $E'$  curve placed  $T_{g,onset}$  at 85°C on the first run. Because the same specimen was tested twice, a post-curing effect from the first run pushed these values roughly 15°C higher on the second run.

Figure 5-8. Storage modulus ( $E'$ ), Loss modulus ( $E''$ ), and damping factor ( $\tan\delta$ ) vs. time

## 5.2 Thermogravimetric Analysis

Thermogravimetric analysis (TGA) was performed to ascertain the rate of mass loss with respect to temperature and time and the decomposition temperature,  $T_d$ .

### 5.2.1 Basic Principles

Powder specimens from the composite are placed on a scale within an oven. The temperature of the oven is increased at a linear rate. As the temperature approaches  $T_d$ , the mass of the sample begins to decrease. The loss of mass of the specimen is graphed as function of the temperature and heating rate. The derivative mass loss curve shows a shoulder where the decomposition of the resin occurs at the highest rate (though peaks may occur at higher temperatures due to the decomposition of fillers or curing agents). This shoulder is often used to define  $T_d$ , while the temperature at which 5% of the mass is lost is considered the onset of decomposition,  $T_{d,onset}$ .

Different heating rates are used to verify the influence of heating rate on the rate of decomposition. Faster heating rates allow less time for decomposition reactions to proceed at given temperatures. As a result, the curve of remaining mass versus temperature appears shifted to higher temperatures. The difference in the magnitude of the curves shows the influence of reaction rates.

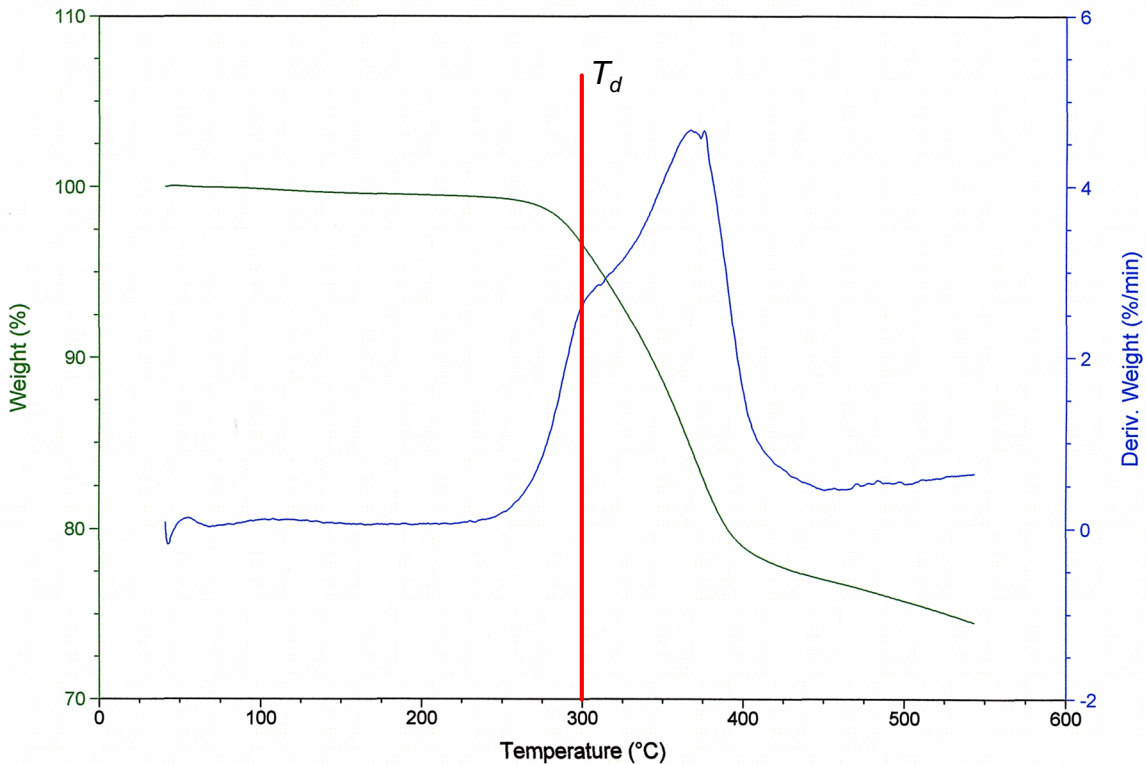
### 5.2.2 Description of Technique

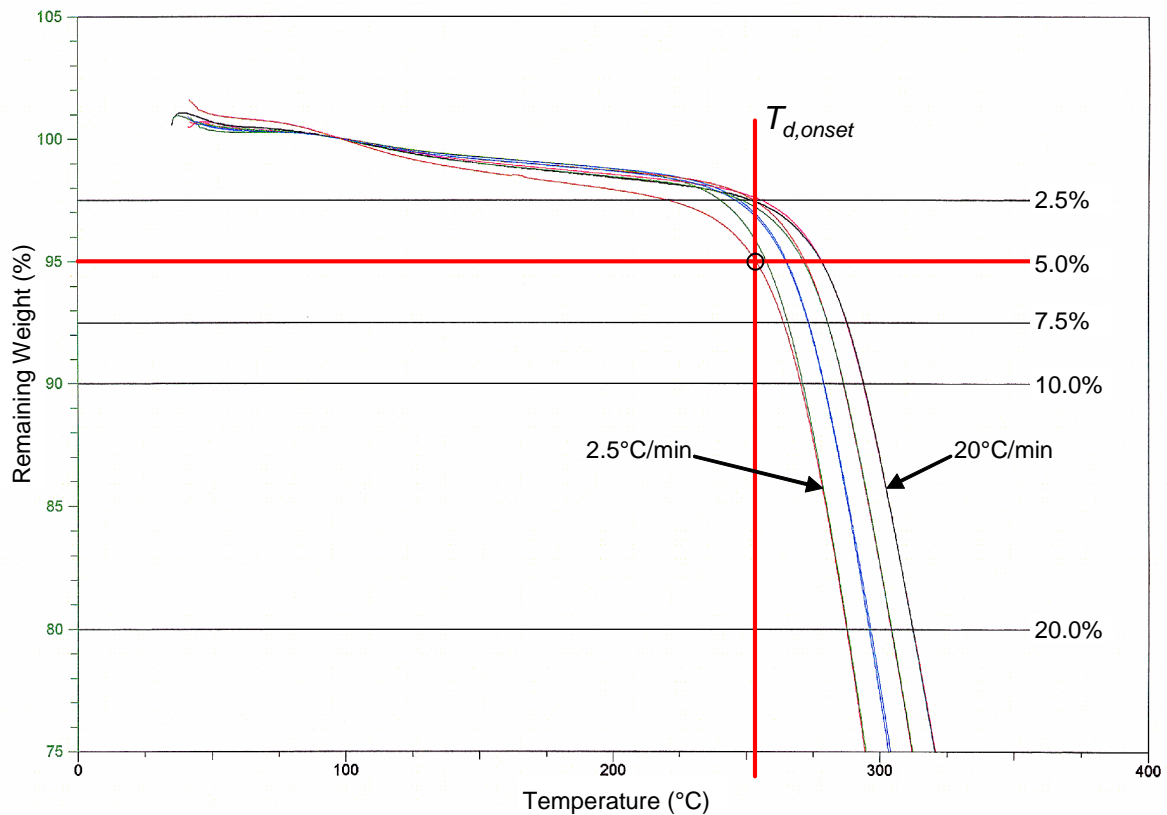
Specimens were created by grinding the composite into a powder using a rasp. The powder was analyzed by a TA2950 TGA from TA Instruments, Inc. The tests were run from ambient temperature to 550°C in an air atmosphere (one specimen was brought to 700°C). Four heating rates (2.5°C/min., 5°C/min., 10°C/min., and 20°C/min.) were used. Specimens were run in duplicate at each of the heating rates. The mass of the specimens was 5.3 mg ± 0.4 mg for all runs.

### 5.2.3 Results

The derivative weight curve (which represents the rate of weight loss) shows a shoulder at 300°C at all heating rates, which was taken to be  $T_d$  (see Figure 5-9). For the onset of decomposition, the most conservative temperature is provided by the slowest heating rate. At 2.5°C/min., 5% of the mass is lost at 255°C, which was taken to be  $T_{d,onset}$  (see Figure 5-10).

Figure 5-9. TGA remaining and derivative weight versus temperature (20°C/min. heating rate)



**Figure 5-10.** TGA remaining mass versus temperature (multiple curves for 2 samples at 4 heating rates)

### 5.3 Steady-State and Transient Heat Flow Analysis

The steady-state and transient heat transfer analyses are grouped together because they were performed on the same experimental apparatus on the same specimen, though their objectives differed. The steady-state analysis was performed to measure the thermal conductivity,  $\lambda$ , while the transient heat flow analysis was performed to obtain the specific heat capacity,  $C_p$ .

The thermal conductivity can be directly measured through numerous methods. Some of the most popular methods include the guarded hot plate method (ASTM C 177), guarded longitudinal hot plate (ASTM E 1225), and the heat flow meter method (ASTM C 518). A method similar to the guarded hot plate method was used to analyze the experimental material because it could be performed with the same apparatus as was used for the transient heat flow analysis.

The specific heat capacity cannot be directly measured, though it can be derived from the measurement of the thermal diffusivity,  $\alpha_d$ , through numerous methods. The calorific method (ASTM C351-82), differential thermal analysis (DTA) (ASTM E1356-03), and differential scanning calorimetry (DSC) [ASTM E 1269] are the most common, though they require the

use of very small specimens that do not properly represent the non-homogeneous and non-isotropic nature of composite materials. Other methods such as the transient plane source (TPS) [15], line source (ASTM D5930-97) [159], photothermal, laser flash (ASTM E1461-01), and non-adiabatic calorimeter [25] techniques may provide more representative values.

The method used to analyze the experimental material was developed by the Building Physics group of the EMPA and is a variation of the adiabatic calorimetry method. It was conceived to permit the evaluation of non-homogenous building materials such as concrete and layered or air-entrained insulation products. The apparatus employs an unusually large specimen so the materials may be analyzed in their proper structure rather than as a small non-representative coupon [60]. An additional convenience is that the apparatus may also be used without modification for the steady-state analysis for the measurement of thermal conductivity.

### 5.3.1 Basic Principles

For a system of cross-sectional area  $A$  (perpendicular to direction of heat flow) and thickness  $L$  in thermal equilibrium (steady-state conditions), the thermal conductivity can be calculated from the thermal gradient,  $\Delta T$ , and the heat flow rate,  $Q_{dot}$ , through the Fourier equation (expressed for one-dimensional heat flow):

$$Q_{dot} = -\lambda A \frac{\partial T}{\partial x} \Rightarrow \lambda = \frac{Q_{dot} L}{A \Delta T} \quad (5-2)$$

The transient thermal response of materials is a function of their density,  $\rho$ , thermal conductivity,  $\lambda$ , and specific heat capacity,  $C_p$ . These three properties are related through the equation for thermal diffusivity,  $\alpha_d$ :

$$\alpha_d = \frac{\lambda}{\rho C_p} \quad (5-3)$$

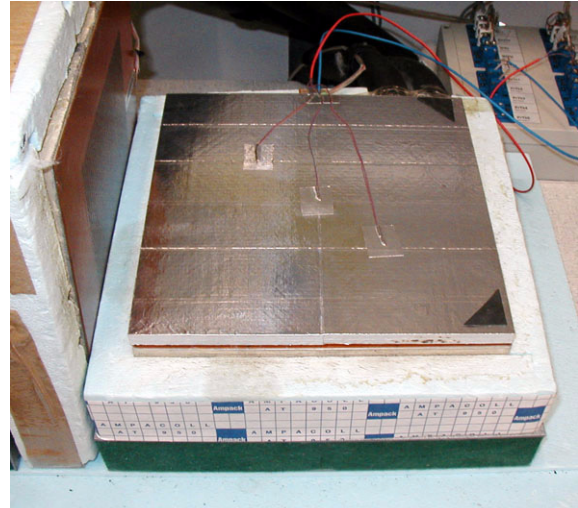
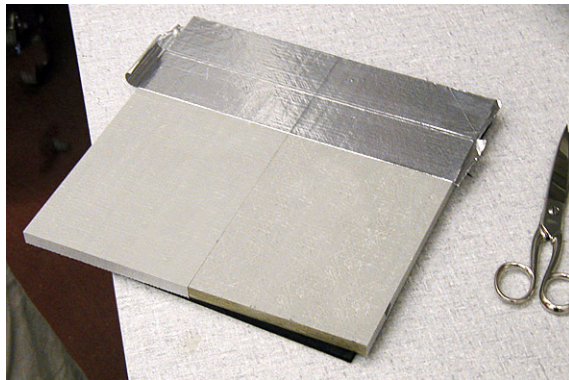
By imposing a thermal shock within the specimen (i.e. a rapid non-uniform change in temperature), the time-dependent response measured by thermocouples and heat-flux meters describes the diffusivity of the specimen. With the knowledge of the  $\rho$  from simple mass and volume measurements and  $\lambda$  from the steady-state analysis, the measurement of  $\alpha_d$  allows the derivation of  $C_p$ .

### 5.3.2 Description of Technique

Two 250 mm square samples of the material are covered with a foil tape to ensure comparable heat transfer characteristics at the interfaces and then instrumented with thermocouples on

both sides (see Figure 5-11). A thin electrical heating element is placed in between the two samples, which are sandwiched in between other electrical heaters or liquid-cooled aluminum plates, depending on the temperature range investigated (see Figure 5-12). The entire assembly is isolated from the ambient atmosphere by rigid foam insulation.

Figure 5-11. Application of foil tape (left), Completed assembly (right)



For the steady-state analysis, a thermal gradient is created by heating the inner faces of the samples and cooling the outer faces. After sufficient time has elapsed, the system reaches thermal equilibrium such that the temperatures and heat fluxes are constant with time at the boundaries of the sample. By the assumption that the system boundaries are adiabatic (heat only flows through the sample), the thermal conductivity is calculated by Equation 5-2, which represents the average value over the ranges of temperatures,  $\Delta T$ .

Figure 5-12. Electrical heating element (left), Liquid cooling element (right)



For the transient heat flow analysis, the assembly is allowed to reach thermal equilibrium over roughly two hours. Then, according to the loading program, step changes in temperature are made to the boundary conditions (thermal shocks). By the assumption once again that the

system boundaries are adiabatic, the amount of energy supplied by the heating element (measured by the electrical draw) can be compared to the change in temperature through the thickness of the samples. Steps changes are repeated after the assembly reaches thermal equilibrium to provide a series of measurements that span the desired range of temperatures.

Numerical evaluation of the measured values is then required to derive the specific heat capacity. The software *LORD 2000* applies the System Identification Technique [106], using the Downhill Simplex method for the first iteration and the Monte Carlo method for the rest of the iterations. The result of the calculation is an estimation of the specific heat capacity for each step change in temperature.

### **5.3.3 Summary of Results**

Testing of the material used in the experimental investigations was performed to provide measurements at 0°C, 20°C, 40°C, and 60°C. The average specific heat capacity of these values was found to be 1,170 J/kg·K and the average thermal conductivity (in the through-thickness direction) was found to be 0.35 W/m·K.

## 6 Fire Reaction Experiments

The unabridged report from these experiments can be found in Appendix A.

### 6.1 Objectives and Motivation

The objective of the Fire Reaction Experiments<sup>3</sup> was to examine, both qualitatively and quantitatively, the high-temperature behavior of the material that would be used throughout the entire experimental program. The material had never been examined under fire loading and its fire reaction properties were largely unknown. It was unclear, for example, whether it would exhibit significant charring behavior or how quickly the thermal degradation would march through the specimens. In addition, there were concerns that the smoke produced would be too copious for the ventilation system or too pungent for neighboring residents.

### 6.2 Materials

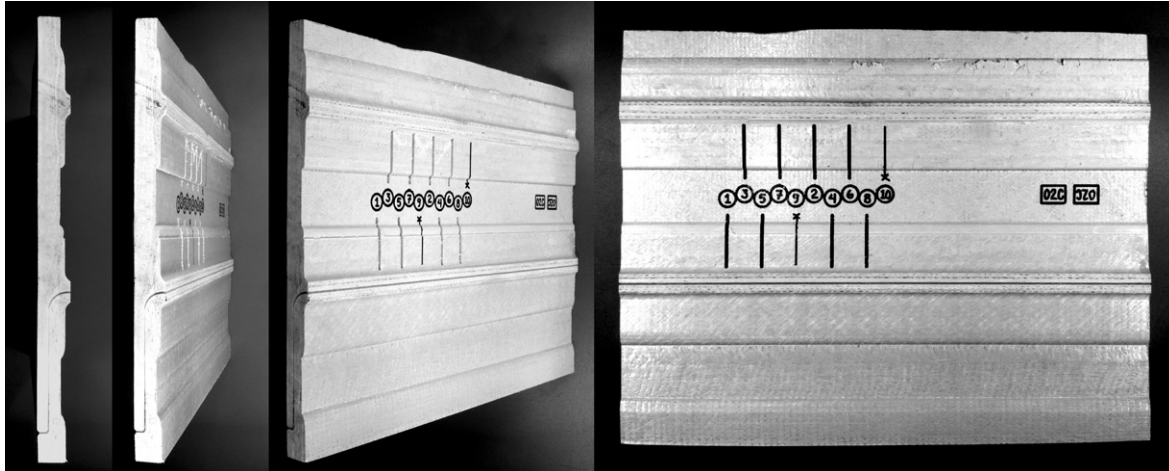
The eight specimens investigated were small samples of the DuraSpan 766<sup>®</sup> bridge deck (see Section 2). The specimens were cut from other specimens used in previous structural investigations by other researchers, though they showed no obvious signs of damage. Before testing, the materials were stored in an outdoor stockyard for approximately one year. The dimensions of the specimens were 32.5 cm x 41 cm (see Figures 5-2 and 5-13).

To facilitate the placement of thermocouples on the cold face, the face sheets were cut free from the webs. Ten 50 mm long x 2.5 mm wide slots were cut into the cold face of each specimen using a computer-piloted router (CNC machine); two slots were cut at depths of 3.80 mm, 7.6 mm, 11.4 mm, and 15.2 mm from the cold face. Thermocouples were then placed at the bottom of the slots and on the cold faces of the specimens. In the effort of maintaining thermal continuity in the vicinity of the thermocouples, the slots were refilled using a mixture of epoxy adhesive (see Section 2.4) and a powder made by grinding down other samples of the deck material. Further details concerning instrumentation can be found in Appendix A - Section 2.

---

3. The prefix “CE”, or *Charring Experiment*, plus a two digit number identifies the Fire Reaction Experiments.

Figure 5-13. Typical specimen for Fire Reaction Experiments



### 6.3 Procedure

In each of the two experiments performed, four specimens were placed in a custom-built concrete exposure frame on the EMPA's small horizontal oven (see Section 3.2) and exposed to fire conditions from below. Temperatures were measured by 10 thermocouples within each specimen, as well as by 6 thermocouples in the oven. The status of the hot and cold faces was recorded by still photos throughout the duration of the experiments.

The chronograph began with the firing of the oven's two oil burners. The intensity of the burners was automatically adjusted according to the mean internal oven temperature (as measured by the six thermocouples positioned just below the specimens) to follow the ISO 834 cellulosic time-temperature curve [92]. The first of the four specimens was removed from the oven after 15 minutes, the second at 30 minutes, the third at 45 minutes, and the fourth at 60 minutes.

The flames that engulfed the specimens upon their removal from the exposure windows were suppressed with wet rags. After cooling, the fire-degraded portions of the specimens were dissected layer-by-layer, and the status of the reinforcement and resin at each layer was recorded.

Figure 5-14. Hot face of specimen after 50 minutes of fire exposure



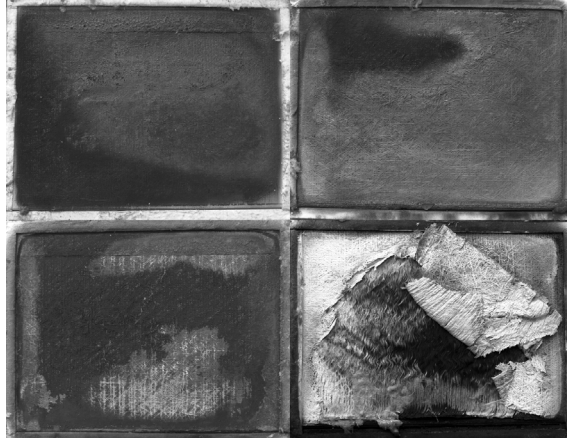
#### 6.4 Post-Experimental Inspection of Specimens

The damage to the specimens was congruent with the duration of the exposure. Those removed from the oven after 15 minutes showed decomposition of the resin at the surface but the all of glass fiber reinforcement remained pliable (see Figure 5-15 top left). The specimens removed after 60 minutes of exposure showed decomposition of the resin throughout the entire thickness and decomposition of the fibers in the 2-3 reinforcement layers closest to the hot face (see Figure 5-15 bottom right). In general, fire damage on the hot faces was most severe towards the center of the specimens. This is the result of several factors:

- As the specimens were recessed in the concrete exposure frame, the radiative view factor reduced towards the edges of the specimens.
- The specimens were continuously supported around their perimeter by the concrete exposure frame. While the reinforcement towards the center of the specimens could droop down and fall off into the oven, the areas towards the supports could not.
- The ablative effect was most likely stronger towards the center of the specimens where the gas velocities should be higher.

Damage to the cold faces was fairly uniform. The sporadic spreading of fire from the hot face, around the sides to the cold face lead to the placement of a strip of ceramic wool insulation around the perimeter of the cold face. Without the benefit of free convective cooling by the laboratory air, the areas below this insulation was more severely degraded than the rest of the cold faces.

Figure 5-15. Hot faces of specimens (clockwise from top left: 15, 30, 60, and 45 minutes)



The factory-bonded polyurethane joint (see Section 2.4) in one specimen appeared to have opened during the experiment. It was possible to pry the joint open further during the minutes after its removal from the oven. The joint regained enough strength to resist prying after it cooled.

## 6.5 Discussion of Results

The progression of damage to the hot face seemed to have proceeded in four stages. In the first stage occurring in the first five minutes, the resin-rich region near the surface (with polyester surface veil rather than glass reinforcement) quickly darkened to a brownish color as it decomposed. The second stage began with the appearance of flaming combustion roughly six minutes after the start of the exposure and continued for roughly two minutes. Flames then died down as the surface was blackened and the initial fuel source was depleted. Thus began the third stage in which no flames were seen and decomposition proceeded into the deeper layers. Also during the two minutes of this stage, the scoured glass fibers near the surface began to turn to a whitish char. The fourth and final stage began with the flaming combustion of gases from the decomposition occurring deeper within the laminate. This phase continued for the remainder of the experiment, as the reinforcement layers closer to the surface turned to the whitish char and the resin at deeper levels was decomposed.

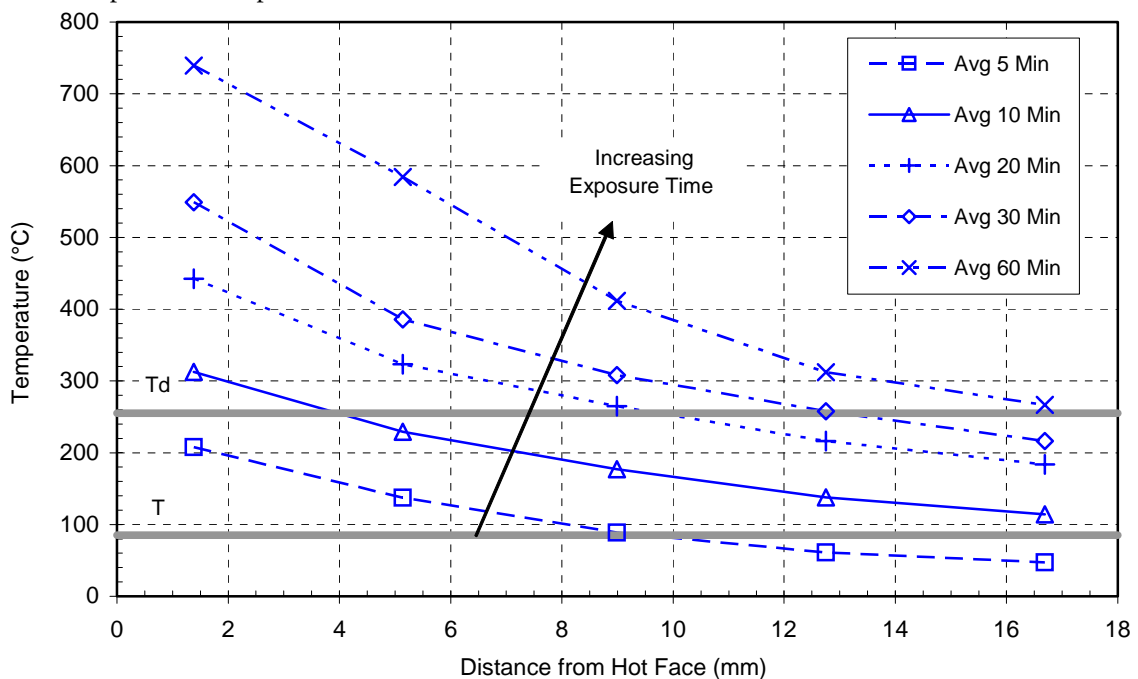
The persistence of flaming combustion suggests that no steady-state condition was reached and that the entire thicknesses would have eventually been consumed. The whitish char that remained was only the char from the burnt fibers. The black char from the resin did not remain on the outermost reinforcement layers and appeared only as a kind of powdery fiber coating on the deeper layers. It did not seal the surface or close the gaps between the fibers to prevent the escape of decomposition gasses from the deeper level. Thus, there was no significant fire-

resisting effect from the charring of the resin. The burnt-out reinforcement layers, however, probably provided some level of protection by blocking the radiation of the oven and reducing the ablative effects of the exhaust system.

The groups of thermocouples placed at similar depths measured similar temperature progressions. Some variation can be expected due to the uneven heating of the oven, as was visually noted during the experiments by the staggered progression of damages to the hot faces. In fact, the time at which landmarks such as the first appearance of brown, black and white patches, as well as flames varied from specimen to specimen by as much as ten minutes. Additionally, errors in the exact placement of the thermocouples and the accuracy of the thermocouples themselves could be responsible for some variation. Despite these sources of error, the average values showed a direct correlation between thickness of material below and temperature. The differences between curves of similar depth ranges show the extreme sensitivity of depth of measurement to temperature. This stands to reason, as the temperature gradient is extremely steep through the thickness of the specimens.

As discussed in the previous section, peeling of the polyurethane joint was evident in one of the eight specimens. It appears that the adhesive has a very low maximum operating temperature, above which it is quite ineffective. Perhaps uneven heating of the materials above and below the joint caused peeling stresses. It would be prudent to expect no strength from bonded joint of this type at elevated temperatures.

Figure 5-16. Temperature through thickness vs. time (data points represent average from four thermocouples on two specimens)



## 6.6 Conclusions from the Fire Reaction Experiments

- The cold faces reached the glass transition temperature (117°C - see Section 5.1) in roughly ten minutes. This suggests that such elements would quickly lose structural load-bearing capacity in true fire conditions (excluding elements loaded in pure tension, which do not greatly rely on the mechanical contribution of the matrix).
- The cold faces reached the onset of decomposition temperature (255°C - see Section 5.1) in just under 1 hour. This indicates that the material would even fail as a non-load bearing fire partition material by both of the code-imposed criteria [167] in under 1 hour:
  - cold face temperature criterion:  $\Delta T_{avg} \leq 140^\circ\text{C}$
  - flame spread criterion: with the cold face decomposing into flammable volatiles, the smallest ignition source would start flaming combustion on the the cold face

Overall, the experiments provided useful insight into the fire-reaction characteristics of the material that was needed for the design of the experiments that followed and for the validation of the thermochemical numerical model.

## 7 Liquid Cooling Experiments

The unabridged report from these experiments can be found in Appendix B.

### 7.1 Objectives and Motivation

The primary objective of the Liquid Cooling Experiments<sup>4</sup> was to study fire behavior and thermal efficacy of the liquid cooling system on the experimental material. Following the Fire Reaction Experiments (see Section 6,) where the cold face was cooled only by the natural convection of ambient air, the LC Experiments were conducted to observe the thermal behavior of the same material when cooled by flowing water.

An additional objective of the experiments was to explore the range of water flow rates that should be used for the large-scale Structural Fire Endurance Experiments (see Section 8). Keeping all variables constant in the three LC Experiments, the flow rate was varied from an extremely low 0.16 m<sup>3</sup>/hr to a moderately high 4.00 m<sup>3</sup>/hr.

Finally, the experiments were performed to discover and resolve the practical issues that would be encountered in the large-scale experiments. These issues include the design of reliable water delivery and data acquisition systems and the verification of techniques for achieving water-tightness in the specimens. With the threat of hundreds of liters of water suddenly pouring into the 1000°C large oven facility during the large-scale Structural Fire Endurance Experiments, the LC Experiments provided a low risk method to verify the safety of the method for both the people and the equipment.

### 7.2 Experimental Set-up

Three experiments were conducted using one specimen per experiment. Water was circulated through a single circuit in the interior cells of the specimens at fixed flow rates. Thermocouples recorded temperatures through the thickness of the hot face and of the water at the inlet and outlet. An analog manometer was used to measure the water pressure at the outlet connection. The EMPA's small horizontal oven (see Section 3.2) created realistic fire conditions below the specimens according to the ISO 834 cellulosic time-temperature curve (see Section 4) [92]. The first specimen was exposed for a cautious 90 minutes, while the remaining specimens were

---

4. The prefix LC plus a two-digit number is used to identify the three Liquid Cooling Experiments.

exposed for 120 minutes. The specimens were dissected after cooling to document the state of degradation of the hot face.

### 7.3 Description of Specimens

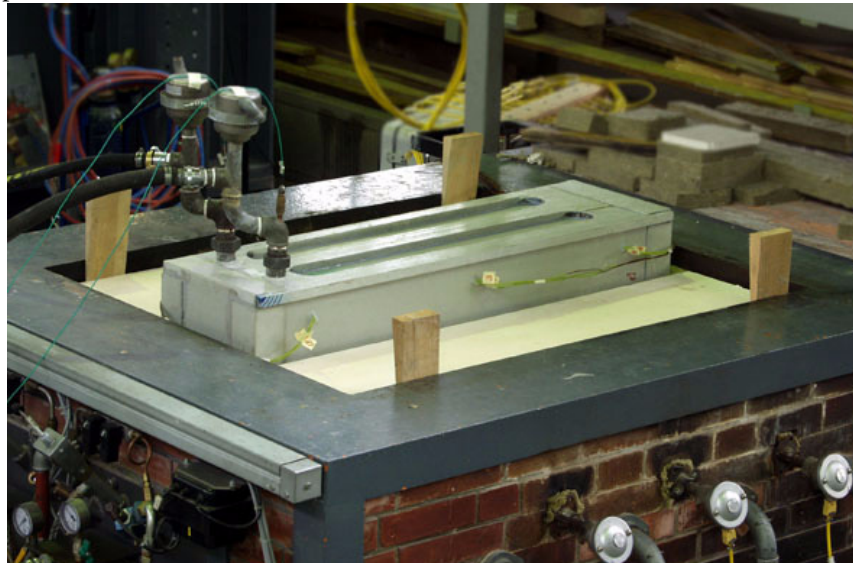
The specimens under investigation were, once again, sections of the DuraSpan® 766 bridge deck (see Figure 5-2). The particular samples used in this investigation were cut from specimens used previously in structural experiments at the CCLab in Lausanne and then stored in an outside stockyard for approximately one year. Taking from unaffected portions of the structural specimens, the thermal specimens showed no signs of damage.

The width of the specimens (32 cm) was chosen so that two full deck cells would be included and a complete water circuit could be created. The maximum length that would fit on the oven (113 cm) was chosen to reduce the influence of turbulence at the inlet/outlet and to encourage laminar flow. Due to the tongue-and-groove connection method of the deck elements, the tongues of a second deck element were bonded to the specimen to create a uniform face sheet thickness.

To create a watertight vessel, pultruded GRFP channel sections were bonded over the ends of the specimens (see Figure 5-17). Holes of 2.5 cm in diameter were bored through the upper face sheets at one end of each cell to make the plumbing connections. A rectangular section of 100 cm<sup>2</sup> was cut away from the web separating the two cells at the opposite end. This permitted the water to enter through an orifice at one end, pass through the length of one cell (Cell A), cross over to the other cell (Cell B), and return the length of the specimen to the outlet orifice.

In order to measure the temperature gradient between the oven interior and the flowing water, thermocouples were placed at the bottom of slots routed into the lower face sheet. In the effort of maintaining thermal continuity in the vicinity of the thermocouples, the slots were refilled using a mixture of epoxy adhesive (see Section 2.4) and a powder made by grinding down other samples of the deck material.

Figure 5-17. Specimen situated on small horizontal oven



## 7.4 Experimental Procedure

The first experiment, LC01, was conducted at a moderate flow rate of  $0.80 \text{ m}^3/\text{hr}$  ( $1.0 \text{ cm/s}$  flow velocity). The second experiment, LC02, was conducted at a moderately high flow rate of  $4.00 \text{ m}^3/\text{hr}$  ( $5.0 \text{ cm/s}$  flow velocity), which is five times the flow rate of LC01. The third experiment, LC03, was conducted at an extremely low flow rate of  $0.16 \text{ m}^3/\text{hr}$  ( $0.2 \text{ cm/s}$ ), which is one-fifth of the flow rate of LC01.

Two criteria were set to decide when to end each experiment: that water cannot leak into the oven and that the water cannot approach boiling. Taking caution in the first experiment, LC01 was stopped after 90 minutes, though neither of the limits had been exceeded. Gaining confidence from the post-experimental evaluation of the LC01 specimen, LC02 and LC03 were both run for a full 120 minutes, exceeding the code-required endurance time for load-bearing components in Swiss multiple-story buildings [167].

The experiments began with the circulation of water at the desired flow rate for approximately 10 minutes. This time permitted the water and the specimen temperatures to stabilize before the fire loading. The chronograph began with the firing of the oven's two oil burners. The intensity of the burners was automatically adjusted according to the mean internal oven temperature (as measured by the six thermocouples positioned just below the specimens) to follow the ISO 834 [92] cellulosic time-temperature curve.

## 7.5 Results

### 7.5.1 Lower Face Sheet Temperatures

The temperatures recorded through the lower face sheet of the specimens at various exposure times are provided in Figure 5-18. As shown, the thermal performance of all three specimens was quite similar. Regardless of the flow rate, the material towards the inner surface of the lower face sheet remained significantly cooler than in the Fire Reaction specimens (see Figure 5-19).

Figure 5-18. Temperature through thickness of LC specimens over time (Note: the first 5 mm of the x-axis is omitted because no thermocouples were positioned in that region)

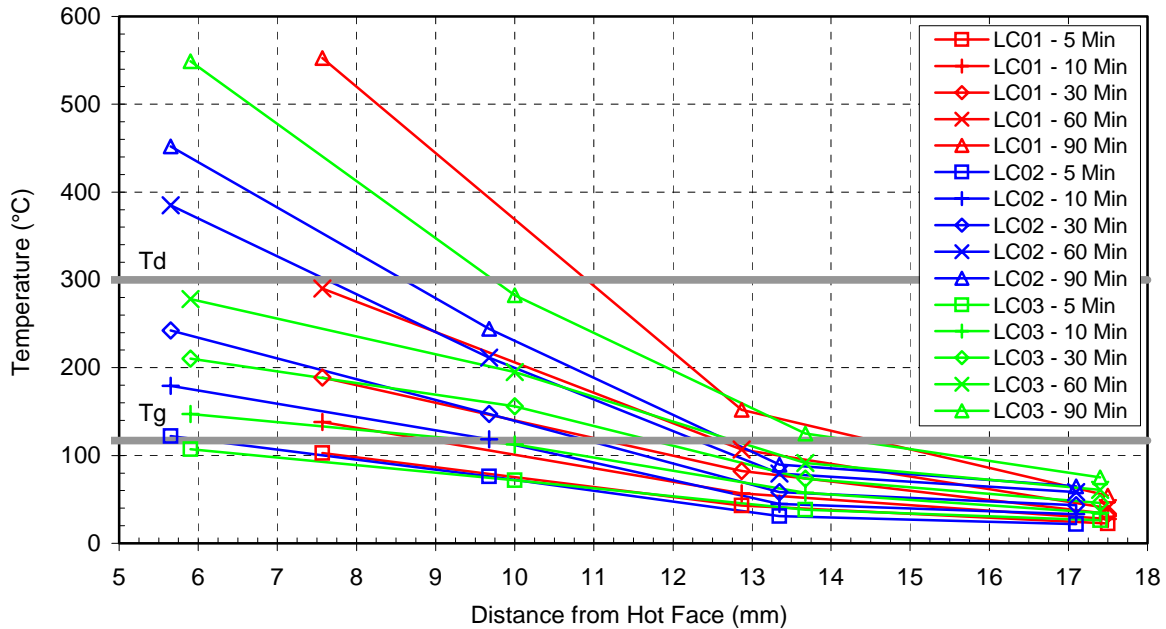
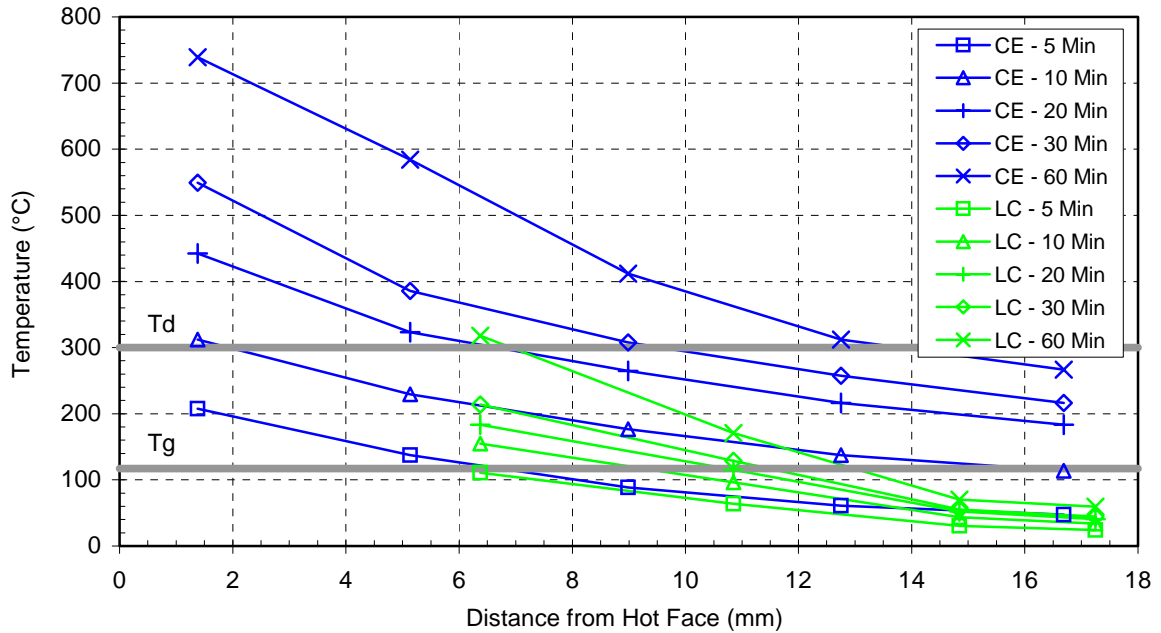


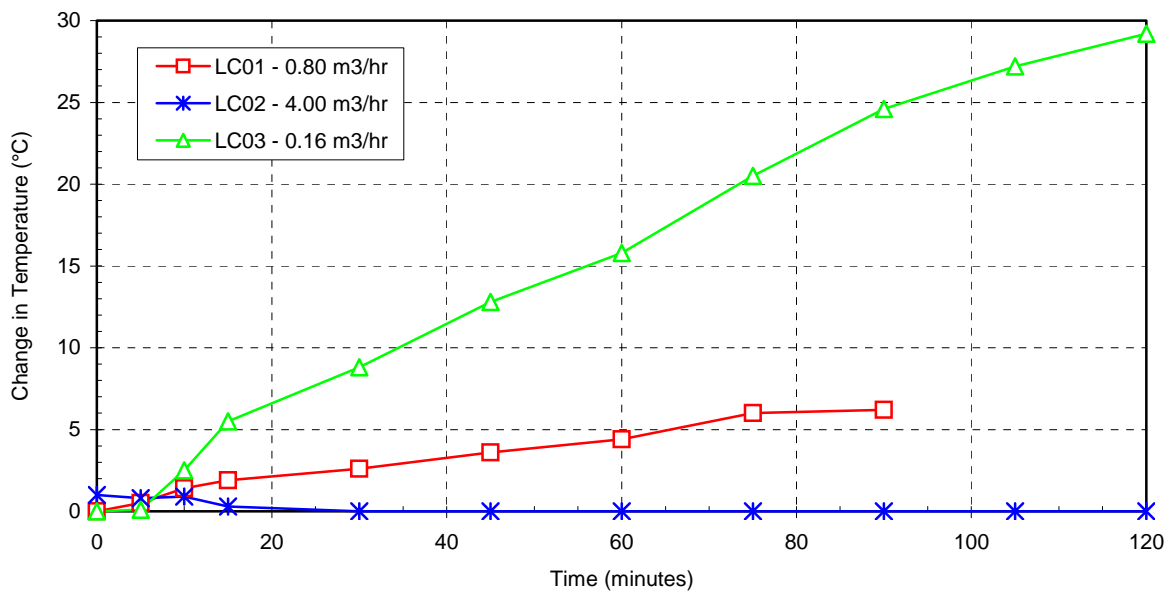
Figure 5-19. Comparison of average temperature profiles of LC and CE specimens



### 7.5.2 Water Temperatures

As shown in Figure 5-20, the change in water temperature depended directly on the flow rate. The outlet temperature of the water was approximately 30°C higher than at the inlet after 120 minutes of fire exposure at the slowest flow rate. The change in temperature of the water flowing at the highest flow rate was too small to be measured with the equipment used.

Figure 5-20. Change in water temperature (inlet minus outlet) vs. time



### 7.5.3 Post-Experimental Inspection of Specimens

The hot faces of the three specimens differed significantly from those of the Fire Reaction (CE) Experiments. While the hot faces of the CE specimens consisted of white glass char and black resin char powder, the LC specimens appeared far more damaged. The glass reinforcement appeared to have first melted and then drooped down directly into the burner flames. From there, it was completely oxidized into a sort of lightweight, brittle, foam-like char (see Figure 5-21) and eventually fell away. All three experiments incurred severe damage or loss of the first two of the four total roving layers. The condition of the third roving layer was commensurate with the flow rate, with nearly complete degradation in specimen with the lowest flow rate and minimal degradation in the specimen with the highest flow rate. The specimen with the medium flow rate appeared to fair nearly as well as the specimen with the highest flow rate, suggesting a threshold of diminishing benefits for increases in flow rate.

Figure 5-21. Hot face of the LC02 specimen after 120 minutes of fire exposure



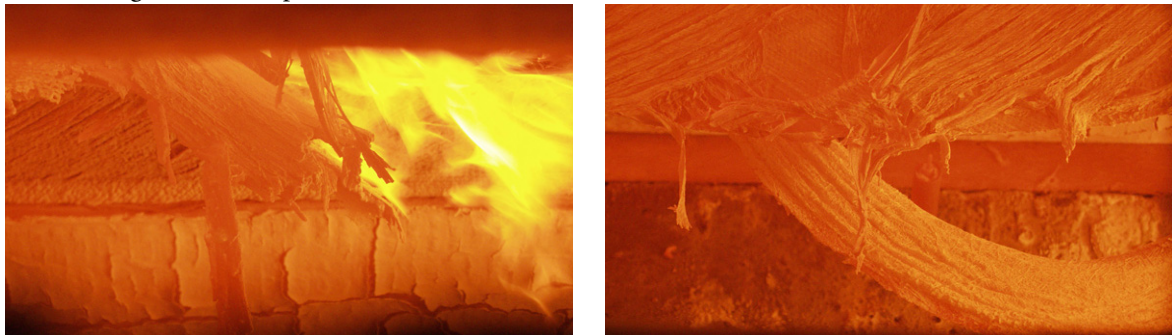
## 7.6 Discussion of Results

### 7.6.1 Comparison to the Fire Reaction Experiments

As was stated in the previous section, the hot faces of the LC specimens appeared to be more severely damaged than the Fire Reaction (CE) specimens. This is due to two important factors: the exposure time and geometrical shape of the specimens. The most harshly tested CE specimens were exposed to one hour of the ISO temperature curve, while LC specimens continued for another 30 to 60 minutes. Because this temperature curve follows a logarithmic function, doubling the exposure time has the effect of more than doubling the heat flux applied. The geometric differences were also an important factor because of the drooping effect in the reinforcement layers. In the Fire Reaction Experiments, the specimens were small rectangles that were supported on all edges. This meant that the layers of reinforcement were

less likely to droop down after the resin was decomposed and the glass was melted. The LC specimens, in contrast, were only supported on the short ends and were approximately triple in length. This configuration made the reinforcement layers more susceptible to the drooping behavior. As each layer sagged and fell down (as shown in Figure 5-22), the radiation shielding that it provided was lost and the damage was allowed to penetrate further. Thus, the differences in geometry and exposure duration make it difficult to render fair comparisons of the post-fire condition of the CE and LC specimens.

**Figure 5-22.** Drooping reinforcement on hot face of specimen LC01 after 45 minutes (left) and 90 minutes (right) of fire exposure



As shown in Figure 5-19, the LC specimens remained substantially cooler than the CE specimens. This effect is most prominent towards the cold faces with the greatest differences registering at the cold faces themselves. The effect was also more pronounced as the exposure time increased. While the curves all appeared similar during the first 10 minutes, the cold faces differed by approximately 200°C at 60 minutes. Comparing the steep slope of the CE cold face temperature curves to the relatively flat LC cold face temperature curves, it is likely that this disparity would have further increased with additional exposure time.

The thermocouples placed roughly 4 mm below cold face of the LC02 and LC03 were still below the glass transition temperature after 60 minutes, while those of the CE exceeded this limit in less than ten minutes. This suggests that liquid cooling could allow approximately 20% of the thickness of the face sheet to provide structural resistance for at least one hour of fire exposure in even resin-dominated loading conditions.

### 7.6.2 Heat Transfer to Water

Using the recorded input and output temperatures of the flowing water (see Figure 5-20), the amount of energy removed from the specimens by liquid cooling can be roughly calculated. The change in enthalpy,  $H$ , of a system is equal to the change in internal energy,  $U$ , plus the product of the pressure and the change in volume. For liquids and solids, where the volume is roughly constant, this simplifies to  $\Delta H = \Delta U$ . Furthermore,  $\Delta U$  is equal to the energy added,

$Q$ , minus the mechanical work done,  $W$ . As no mechanical work is done within the system under consideration,  $\Delta H = \Delta U = Q$ . Therefore, by the first law of thermodynamics, heat added to a system changes the enthalpy according to the following equation:

$$Q = mC_p\Delta T \quad (5-4)$$

where  $m$  is the mass of system,  $C_p$  is the specific heat capacity, and  $\Delta T$  is the change temperature (in this particular case, the change in water temperature from inlet to outlet). Because the system is not closed, however,  $m$  is not a mass but a mass flow rate,  $\dot{m}$  (units mass/time). The introduction of the units of time changes the value of the solution from energy to power. Thus, the symbol  $P$  is substituted for  $Q$ . Further, the power absorbed by the system is directly related to the surface area of the system that is exposed to fire. To remove the geometrical component, the value is divided by the fire-exposed area of the water circuit,  $A_{xp}$ . Thus, these three modifications of Equation 5-4 result in the following variation.

$$P = \frac{\dot{m}C_p}{A_{xp}}\Delta T \quad (5-5)$$

The symbol  $P$  represents the power drawn by the water from the heated specimen at any instant. Because  $P$  varies greatly with time and does not follow a linear growth in all experiments, it is insufficient to compare only the power drawn at any single moment in time. A more representative method is calculate the total power drawn over the duration of the experiment by integrating the change in water temperature with respect to time. Power multiplied by time is once again energy. Thus, the total energy absorbed,  $Q_{total}$ , over the duration from  $t_i$  to  $t_f$  is shown in the following equation:

$$Q_{total} = \frac{\dot{m}C_p}{A_{xp}} \int_{t_i}^{t_f} (\Delta T) dt \quad (5-6)$$

In order to evaluate the integral of the change in temperature with respect to time, a function must be fit to the measured  $\Delta T$  versus  $t$  curve. Though a logarithmic curve might be most suitable because the temperature loading also follows a logarithmic curve, a simple bilinear curve fits nearly as well and is easier to perform manually (see Figure 5-23).

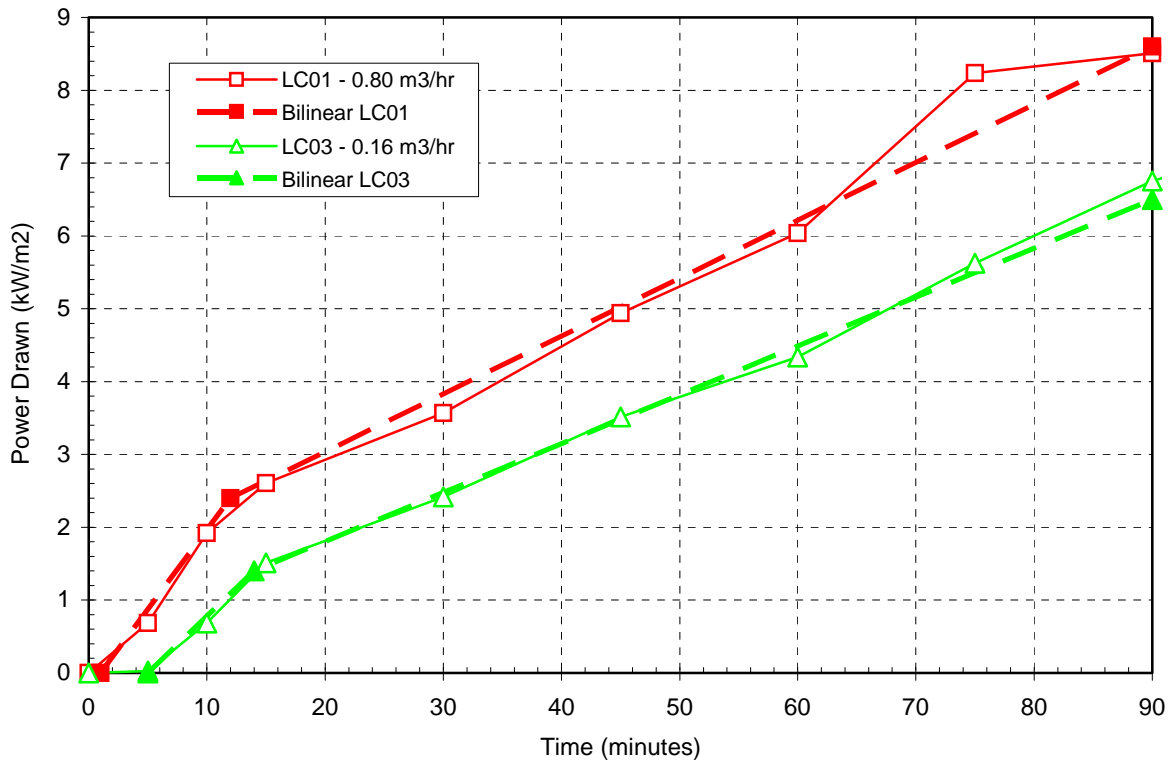
The results from Equation 5-6 evaluated from  $t_i=0$  to  $t_f=90$  minutes using the previously mentioned bilinear regression method and  $A_{xp}=0.34 \text{ m}^2$  are listed in Table 5-3.

Table 5-3. Total energy absorbed by water over 90 minutes of fire exposure

Experiment	Flow Rate (m <sup>3</sup> /hr)	Coordinates of Bilinear Regression						Q <sub>total</sub> (MJ/m <sup>2</sup> )
		(s)	(kW)	(s)	(kW)	(s)	(kW)	
LC01	0.80	60	0	720	2.4	5400	8.6	25.8
LC02	4.00	-	-	-	-	-	-	- <sup>a</sup>
LC03	0.16	300	0	840	1.4	5400	6.5	18.2

a. the high flow rate resulted in a very small change in water temperature that was beyond the precision of the instruments

Figure 5-23. Power drawn by flowing water per fire-exposed square meter vs. time



As expected, the amount of heat transferred to the water increased as the flow rate increased. This is explained by two factors. The first is that the convective heat transfer rate increases with increasing fluid velocity. The second is that the water remained cooler as the flow rate increased, which maintained a larger temperature gradient between the materials and thus a higher rate of heat transfer. This verifies that, within the range of water flow rates used, increasing the flow rate increases the cooling effect.

### 7.6.3 Internal Pressure

The act of forcing water to flow through a tortuous path within the specimen and then through the exit pipes and hoses caused friction. Increasing the velocity of the flowing water by increasing the flow rate increases the friction. The energy loss due to friction manifests itself as increased water pressure. Therefore, the higher the flow rate, the higher the internal pressure will be. This was observed in LC03 and LC02, where the internal pressure increased by roughly 0.6 bars as the flow rate increased from 0.16 m<sup>3</sup>/hr to 4.00 m<sup>3</sup>/hr. The pressure increase would have been even higher if a second exit hose were not added to the high flow experiment.

## 7.7 Conclusions from Liquid Cooling Experiments

The following conclusions can be drawn from the three LC experiments:

- Temperatures within the lower face sheets of the specimens remained significantly lower in the Liquid Cooling Experiments than in the Fire Reaction Experiments.
- The liquid cooling effect improved with increased flow rates.
- Approximately 20% of the thickness of the lower face sheet should be expected to be structurally sound after one hour of fire exposure in stress states that require a mechanical contribution from the matrix. Fibers outside of this region can provide additional structural resistance if they are anchored outside of the fire-damaged area and are stressed in tension.

## 8 Structural Fire Endurance Experiments

The unabridged report from these experiments can be found in Appendix C.

### 8.1 Objectives

The primary objective of the Structural Fire Endurance Experiments<sup>5</sup> was to demonstrate the feasibility of internal liquid cooling for the fire protection of load-bearing FRP elements. In addition, the experiments were performed to validate the thermomechanical numerical model. Finally, post-fire structural testing was performed to study the effect that high-temperature exposure has on the ambient-temperature strength and stiffness characteristics.

### 8.2 Materials

As in all of the experimental investigations, the specimens were samples of Martin Marietta Composites' DuraSpan® 766 bridge deck (see Section 2). In contrast to the CE and LC specimens, the SLC specimens were new sections of the material received directly from the manufacturer.

Each specimen consisted of three pultruded shapes that were bonded together by the manufacturer using a flexible polyurethane adhesive (Section 2.4). The finished panels measured 350 cm in length, 91.4 cm in width, and 19.5 cm in depth.

To maintain a constant face sheet thickness, the tongues from the unused exterior female connection were removed and bonded over the thin face-sheet portions of the exterior male connection on the opposite side (see Figure 5-2). To allow the water to flow the length of one interior cell and then return in the adjacent cell, notches of roughly 100 cm<sup>2</sup> were cut into the webs separating the cells at the far of the panels. Finally, a watertight vessel was created by bonding thin FRP channels to the ends of the panels using FRP angles for reinforcement.

---

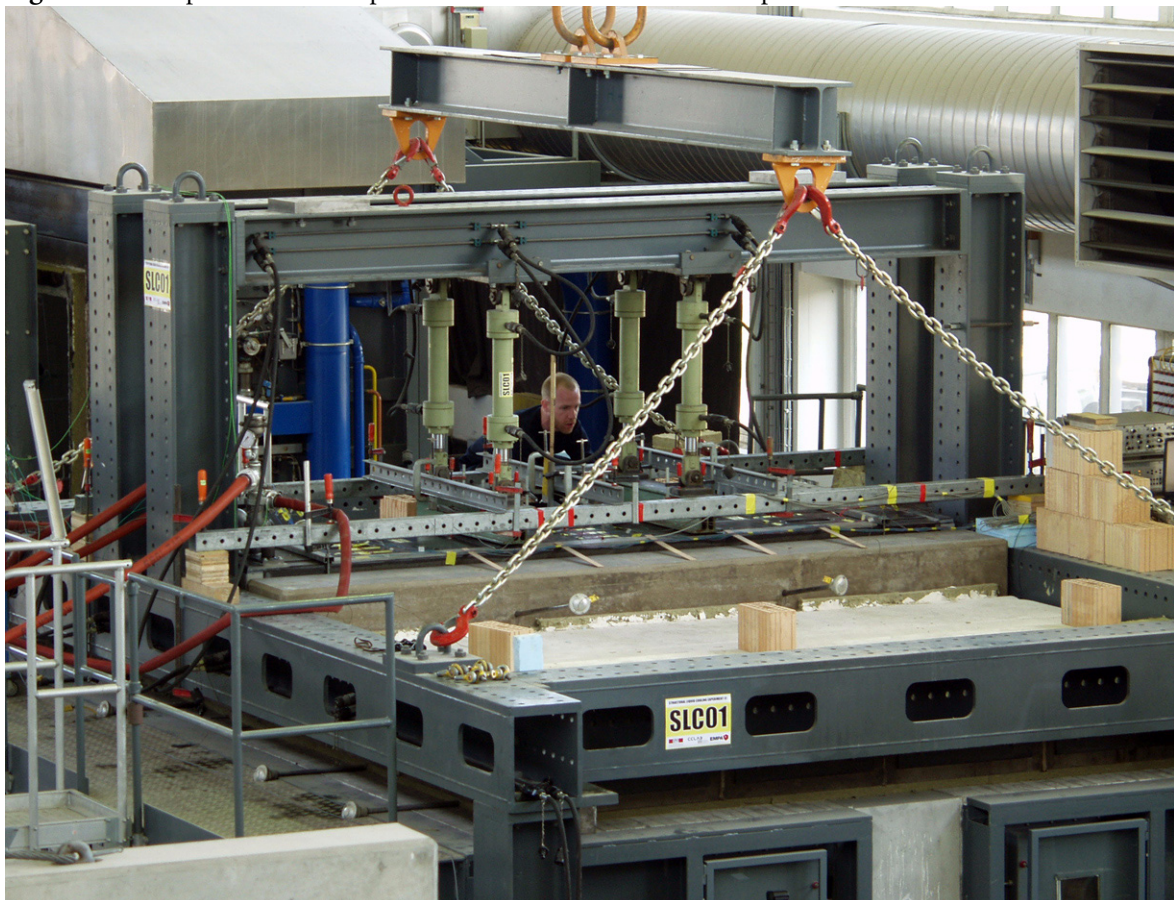
5. The three experiments are identified by the prefix SLC for *Structural Liquid Cooling*, plus a two digit number.

## 8.3 Experimental Set-up

### 8.3.1 Oven

The SLC Experiments were conducted on the EMPA's large horizontal oven (see Section 3.3 and Figure 5-25). A concrete frame was fabricated using high-temperature concrete to provide supports for the specimens at a span of 2.75 m and to protect the sides of the panels from fire. Steel rollers at both ends ensured simple-support conditions.

Figure 5-24. Experimental set-up for Structural Fire Endurance Experiments

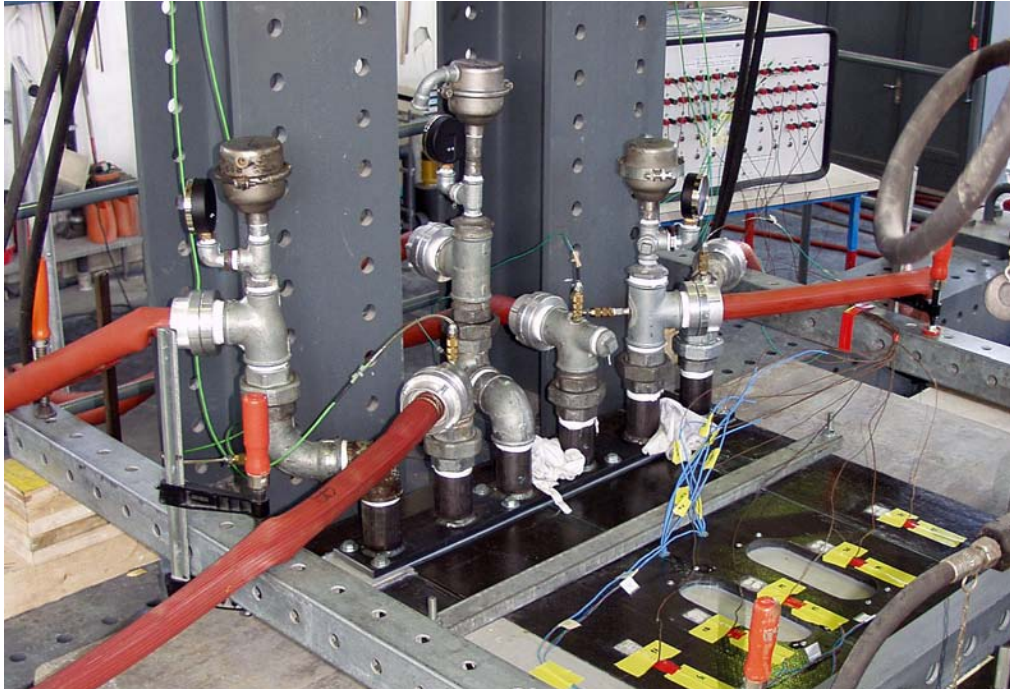


### 8.3.2 Liquid Cooling System

As in the LC Experiments, water connections were all made at one end of the panels (see Figure 5-25). Steel adapters were bonded and bolted to the upper face sheets of the specimens outside of the structurally loaded and fire-exposed section. Water was supplied by large-diameter flexible hoses. The flow-rate meters were placed along the input lines to precisely monitor and adjust the flow rate in each of the three plumbing circuits.

The first experiment (SLC01) was conducted at a conservative flow rate of  $2.00 \text{ m}^3/\text{hr}$ . The flow rate was reduced to  $1.00 \text{ m}^3/\text{hr}$  for the second experiment (SLC02). With two good data sets and satisfactory performances in the first two experiments, SLC03 was conducted without liquid cooling to serve as a basis for comparison.

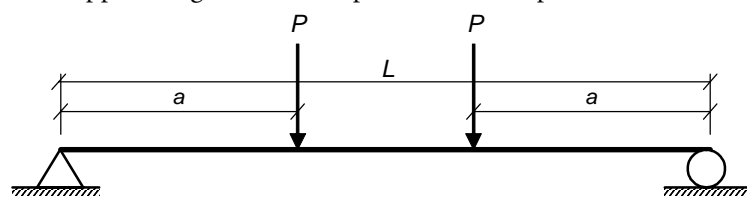
Figure 5-25. Water connections



### 8.3.3 Structural Loading

In order to best simulate an evenly distributed load using discrete hydraulic jacks, a four-point bending arrangement was selected (see Figure 5-26). Two jacks at roughly the third-points applied a force onto heavily-reinforced triple-web steel beams. A layer of rubber was used between the beams and the panels to help distribute the stress evenly across the three pultruded sections.

Figure 5-26. Load and support diagram of the experimental set-up



The load was calculated to impose a deflection that would normally limit the service load of such a panel in normal use. This deflection limit is equal to  $1/300$  of the clear span,<sup>6</sup>  $L$ . With a

clear span of 2,750 mm, a deflection of 9.2 mm should be imposed. Neglecting shear deformations, the deflection of a beam in four-point bending is calculated by Equation 5-7.

$$\delta = \frac{PL^3}{24EI} \left( \frac{3 \cdot a}{L} - \frac{4 \cdot a^3}{L^3} \right) \quad (5-7)$$

Rearranging this equation to solve for  $P$  and inputting  $a = 900$  mm (the distance from the supports to the loads),  $E = 26.96$  GPa,<sup>7</sup> and  $I = 2.732 \times 10^8$  mm<sup>4</sup>,  $P$  is found to be 92.9 kN. Because two jacks provided the load at each loading axis, the load applied by each jack was therefore one-half of the total load, or 46.5 kN.

### 8.3.4 Instrumentation

In order to measure the temperature profile through the lower face sheet, thermocouples were placed at various depths throughout the thickness. As in the LC Experiments, this was accomplished by cutting access hatches in the top face sheet and then machining slots into the lower face sheet. Slots of 4, 8, and 12 mm depths were routed into the lower face sheet below each of the four access hatches. Strain gages and thermocouples were also placed on the interior surface of the lower face sheet. Though it would have been most desirable to place these instrument clusters towards the mid-span, it was decided that the portions of the upper face sheet that would need to resist bending through compression resistance should not be weakened by the cutting of the access hatches. Thus, the instrument clusters were located 30 cm from the supports, or roughly at the outer 1/10 points. Upon the completion of the instrumentation, thin FRP plates were screwed and bonded to the interior of the upper face sheets to close the hatches.

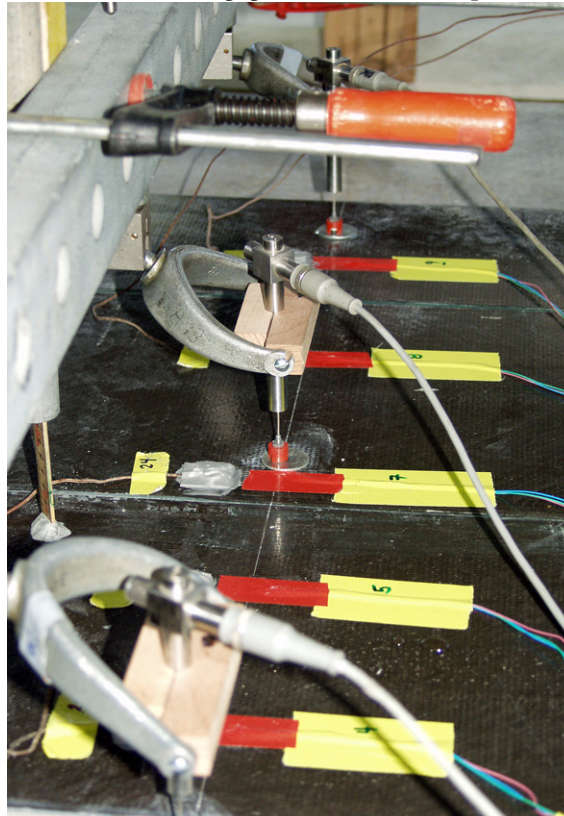
On the exterior surface of the upper face sheet, instrument clusters were placed at the same locations as the lower, as well as at the mid-span. In addition, displacement transducers were used to measure the vertical deflection at mid-span and at the loading axes (see Figure 5-27). Strains, deflections, and load were recorded at five second intervals while temperatures were recorded once each minute.

6. The Swiss building code (SIA-260:2003 Appendix A) dictates a deflection limit of 1/350 for adequate rigidity, comfort, and functionality of beams and decks. Relaxing this limit to 1/300 allows more severe loads, and thus, more conservative results.

7. This value was supplied by the deck manufacturer and was initially used. Subsequent studies have reported a reduced value of 21.24 GPa, as shown in Table 5-2. This reduced value is used throughout the remainder of this thesis.

For the control and measurement of the flowing water, calibrated and certified digital flow-rate meters were used for each of the three plumbing circuits. Water temperature was measured by special elbow joints fitted with thermocouples at the inlets and outlets of each cell.

Figure 5-27. Displacement transducers, strain gages, and thermocouples across mid-span of specimen



## 8.4 Procedure

As in all of the medium-scale experiments, the SLC Experiments were conducted according to the ISO 834 cellulosic time-temperature curve (see Section 4) [92].

When applicable, the experiments began with the circulation of water through the cells. This was continued for at least 30 minutes so that thermal equilibrium was reached on the side of the water supply and within the panels. Next, the structural load was slowly applied to the panels. Ten minutes were then given for the deflection to stabilize. Finally, the chronograph was started with the ignition of the oil burners.

Upon the occurrence of a failure criterion or after the planned 120 minutes of exposure, the burners were extinguished. As quickly as possible (roughly 5 minutes), the specimen and reaction frame were removed from the oven and placed outside of the laboratory to cool. After

sufficient time to allow the specimen to assume ambient temperature, structural loads were once again applied up to the capacity of the test equipment.

## 8.5 Results

Experiment SLC01 was stopped prematurely because of a small leakage of water at one of the bonded joints. Though the specimen was structurally sound, the leakage threatened to damage the lining of the oven and made it difficult to maintain the high temperatures prescribed by the ISO curve. No leakages were observed in SLC02 and thus the experiment was continued for the planned 120 minutes. Experiment SL03 was stopped after 57 minutes due to a structural failure.

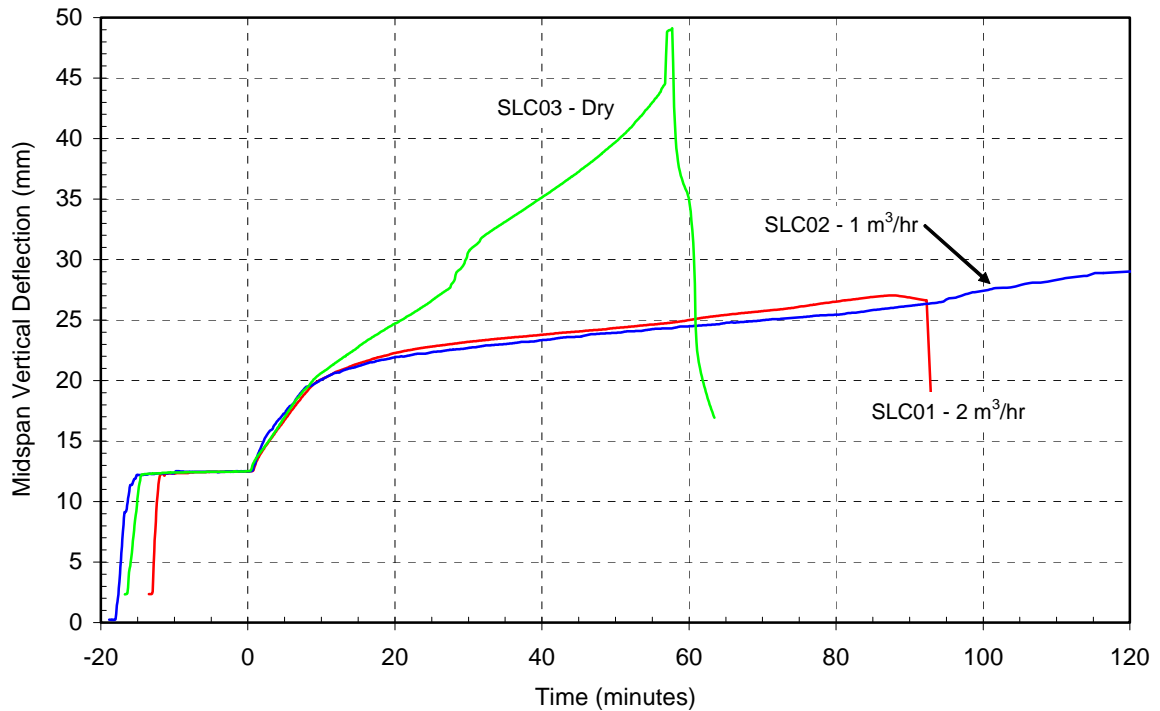
### 8.5.1 Deflections

The pre-fire mid-span deflections due to the structural load was roughly 12 mm for all specimens. After the ignition of the burners, the deflections and strains increased sharply in the first fifteen minutes for all experiments. While the liquid-cooled specimens stabilized thereafter,<sup>8</sup> the non-liquid cooled specimen (SLC03) continued to deflect at approximately the same rate for the remainder of the experiment (see Figure 5-28). Overall, the mid-span deflections in SLC02 were 2-3 mm less than in SLC01 despite the reduction of the water flow rate by 50%.

---

8. A gradual increase in deflections did occur, which was linked to temperature-induced creep and the loss of material at the hot face.

Figure 5-28. Average mid-span deflection (from three transducers across width) vs. time

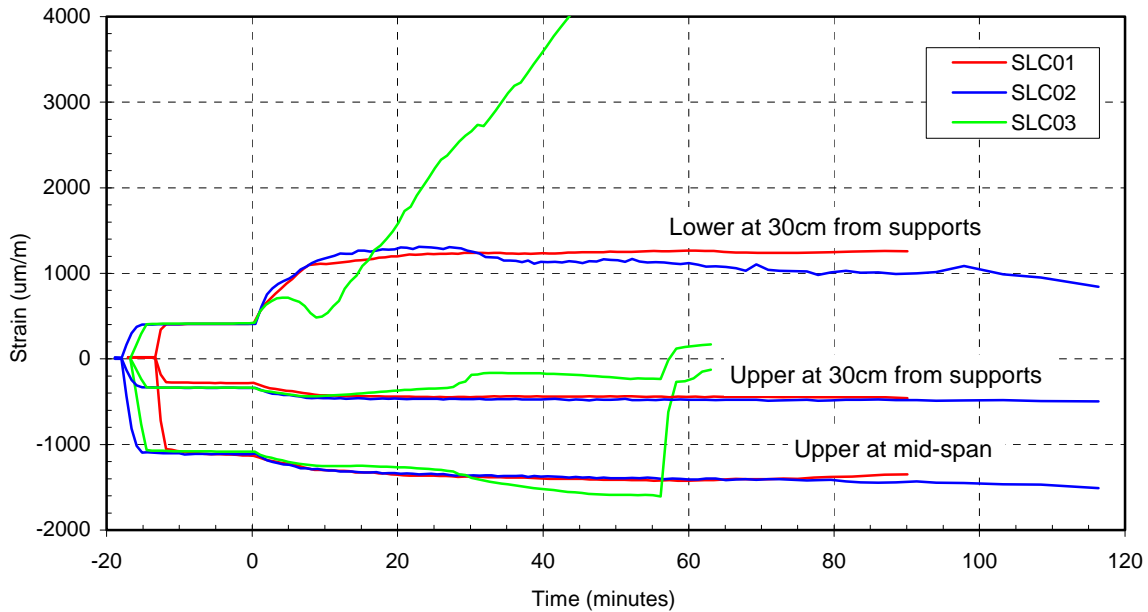


### 8.5.2 Strains

The axial strain versus time curves (Figure 5-29) show trends similar to the deflection vs. time curves shown in Figure 5-28. The axial strains at the time of burner ignition were the same in all specimens. The strains measured at the *outer* surface of the upper face sheets were approximately 15% higher than those measured on the *inner* surface of the lower face sheets because those on the outer surface were farther from the neutral axis.

After ignition of the burners, the strains in the liquid-cooled specimens rapidly increased for approximately 10-20 minutes, particularly in the lower face sheets, and then stabilized at an almost constant value for the remainder of the fire exposure. The strains in the compressed upper face sheet of the non-liquid cooled specimen were almost the same as in the liquid-cooled specimens. The strains on the tension-stressed lower face sheet, however, rapidly increased up to failure.

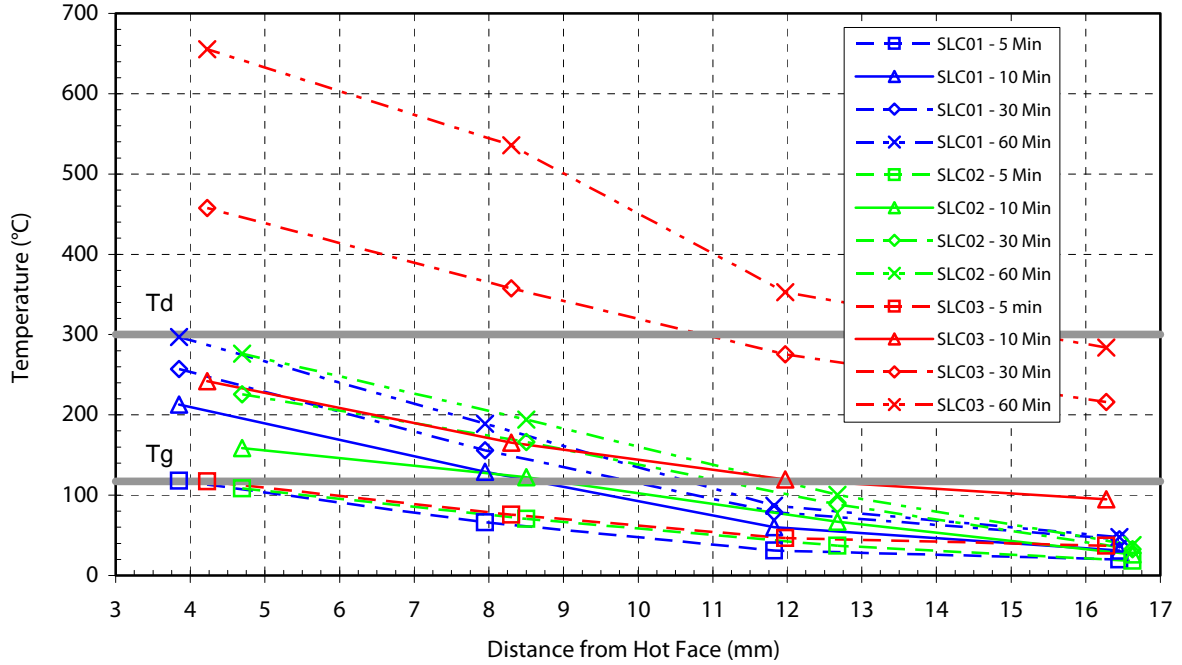
Figure 5-29. Strain at various locations versus fire exposure time



### 8.5.3 Specimen Temperatures

The temperature profiles through the thickness of the lower face sheet of the three specimens are shown in Figure 5-30. After 60 minutes of fire exposure, the cold face of the liquid-cooled specimens increased by roughly 30°C, while the cold face of the non-liquid cooled specimen increased by roughly 270°C. At the thermocouples closest to the hot face, the difference was less marked, with the liquid-cooled specimens increasing roughly 180°C and the non-liquid cooled specimen raising 550°C. Between the liquid-cooled specimens, the temperatures of the SLC02 specimen rose 10-30°C higher than in SLC01.

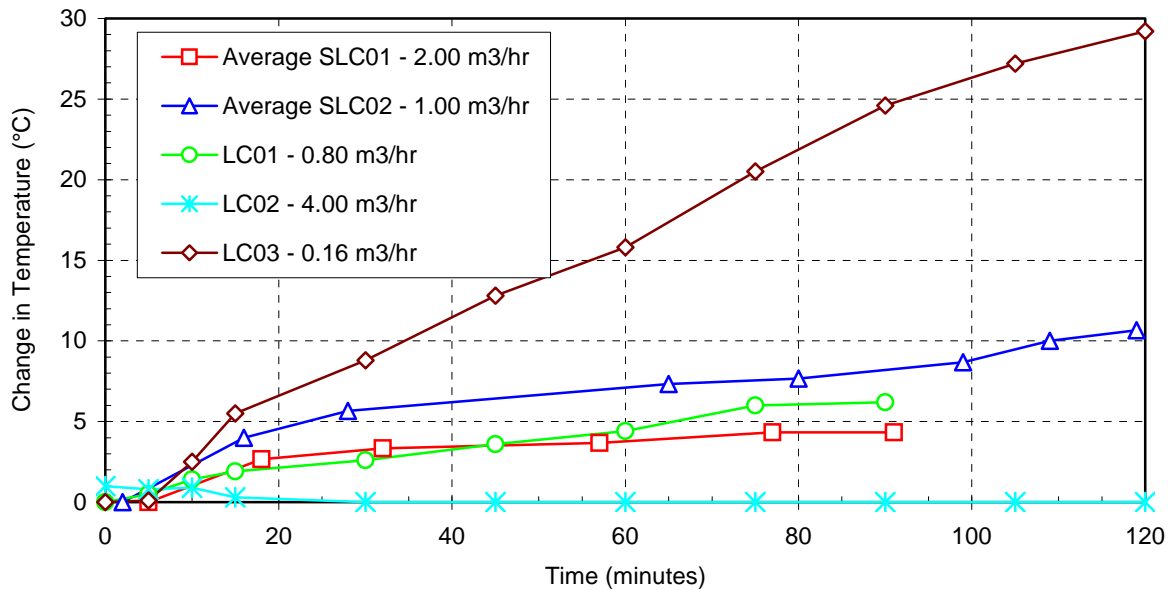
Figure 5-30. Average temperature through thickness versus time (from 4 thermocouples at same depth) (The first 3 mm of the x-axis is omitted because no thermocouples were positioned at that depth)



### 8.5.4 Water Temperatures

Figure 5-31 plots the change in water temperature from inlet to outlet versus time (the same values from the LC Experiments are included for comparison). After 60 minutes of fire exposure, the difference in the temperature of the water between the inlet and the outlet was 7°C for the slower flow rate of 2 m<sup>3</sup>/hr and 4°C for higher flow rate 1 m<sup>3</sup>/hr.

Figure 5-31. Average change in water temperature (inlet minus outlet) versus time

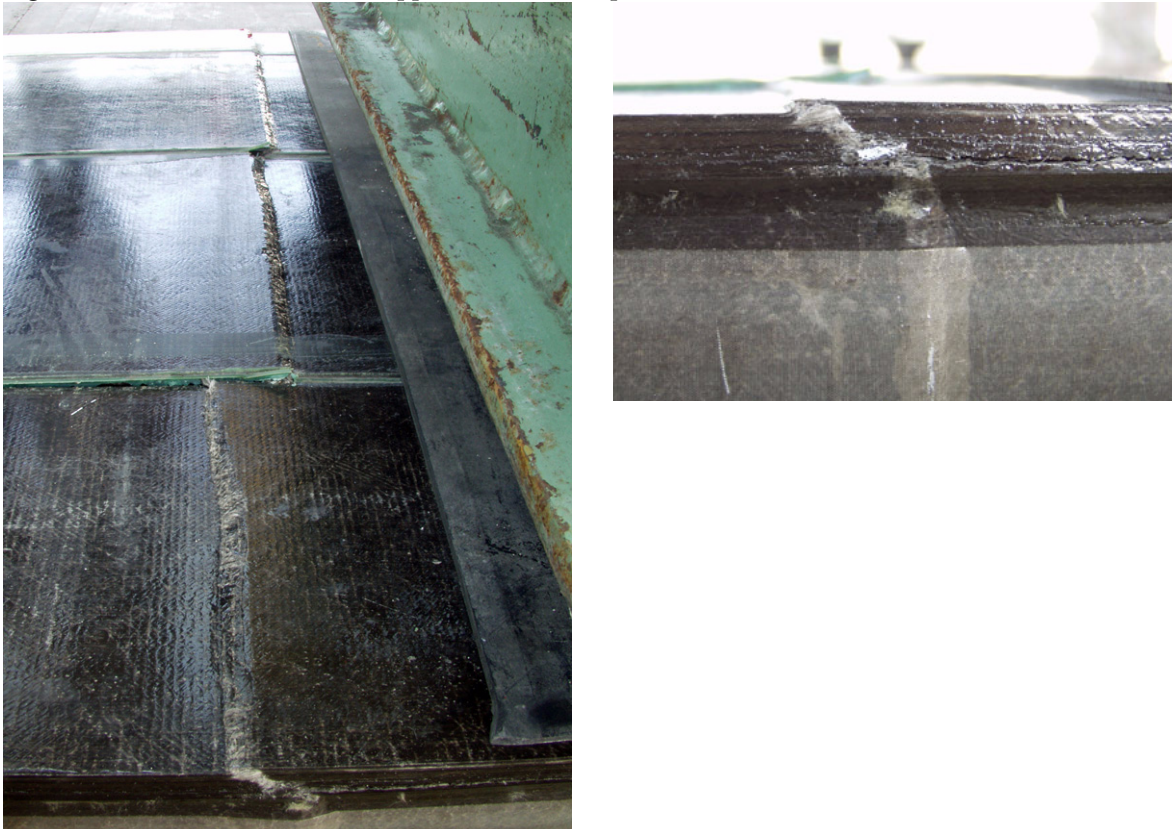


### 8.5.5 Structural Damage and Permanent Deformations

The mid-span deflection of SLC01 after unloading was roughly 16 mm. Though the specimen was no longer loaded structurally, it was still very hot on the lower face sheet. Numerical modeling has demonstrated that such deflections could easily be the result of uneven heating and thermal expansion rather than permanent structural deformations. As it was necessary to discontinue the deflection measurements to remove the specimen from the oven, the permanent deflections after cooling are unknown. In the post-fire loading of both SLC01 and SLC02, however, the roughly 60 mm of deflection (ratio 1/46) was completely recovered after unloading.

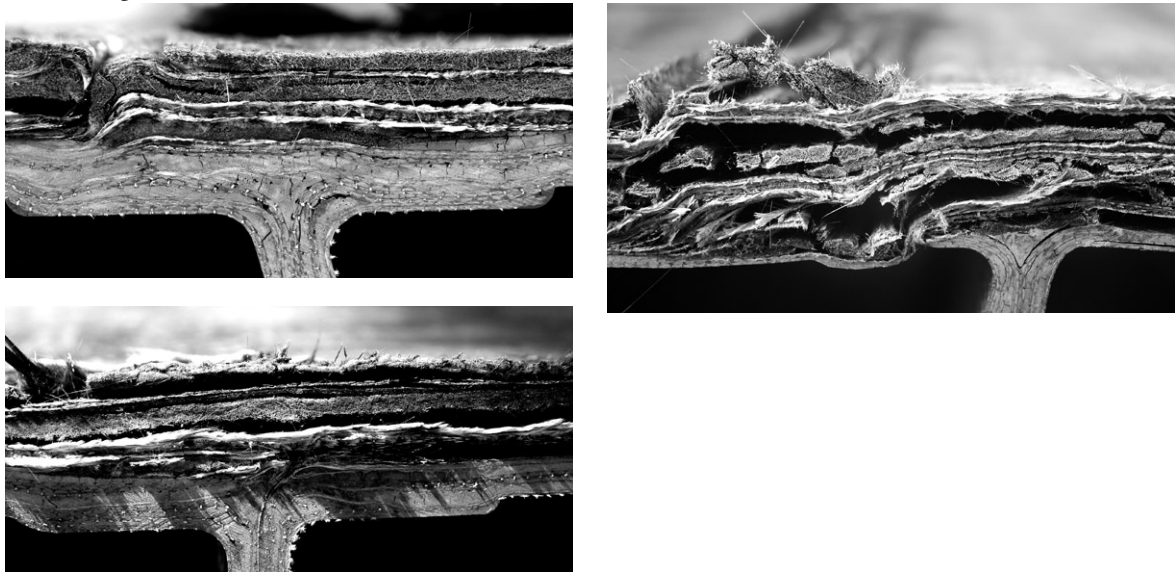
Post-fire deflections of the SLC03 specimen were not measured due to the structural failure. The upper face sheet, which was stressed in compression, suffered a local buckling failure after 57 minutes of fire exposure (see Figure 5-32). The buckling occurred along a nearly straight line running across all three of the pultruded elements between the two loading axes. One side vertically displaced 3 to 4 mm above the other (viewed from the side) following a roughly 45° angle through the upper face sheet. As such, post-fire structural testing was not possible.

Figure 5-32. Structural failure of upper face sheet of specimen SLC03



The specimens were cut into four sections in order to examine of their cross-sections (see Figure 5-33). The specimens from SLC01 and SLC02 showed similar fire damage at the lower face sheet. Two of the four roving layers became delaminated from the lower face sheet and had partially fallen away from the panel (visible in Figure 5-34). Damage was beginning to occur at the third roving layer for SLC02 and was slightly more advanced for SLC01.

**Figure 5-33.** Cross sections of specimens after cooling: SLC01 (top left), SLC02 (bottom left), and SLC03 (right)



**Figure 5-34.** Hot face of specimen SLC01 after 70 minutes of fire exposure



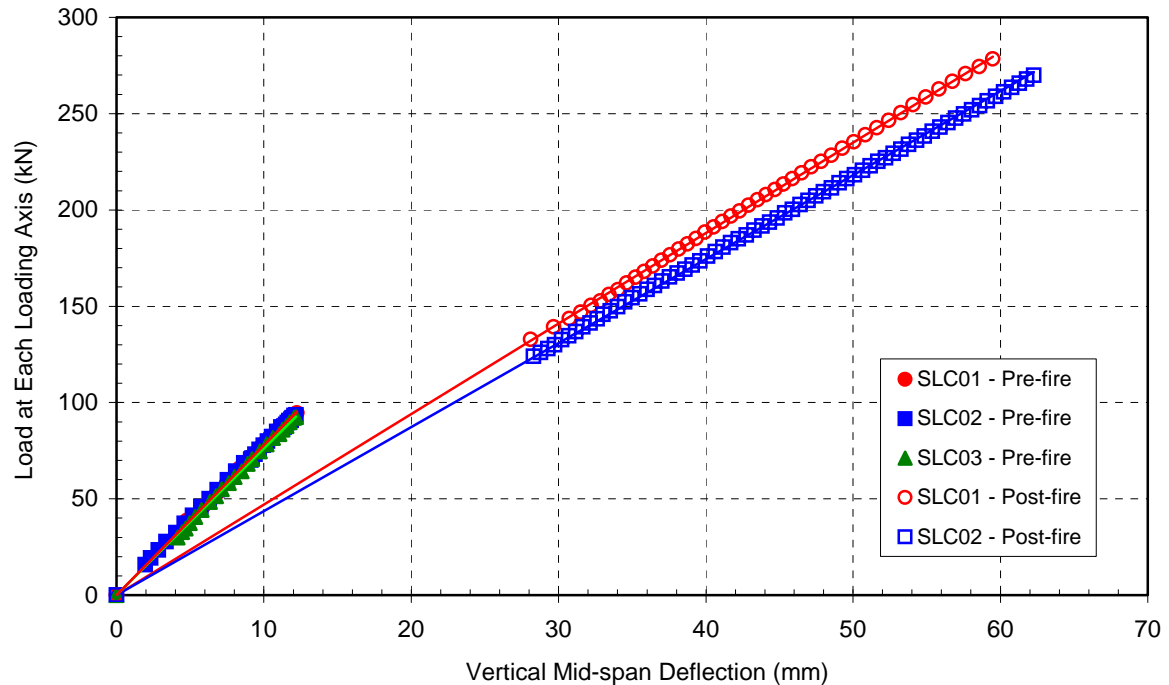
All fibers that drooped down into the oven were decomposed into a white foam-like char. Though quite flexible and string-like at high temperatures, this char became very brittle upon cooling. As was observed in the CE and LC Experiments, the damage from the hot face inwards in the following progression: whitish fiber char alone → brittle black fibers in black powdery resin char → slightly ductile black fibers in black resin char → very ductile fibers in partially degraded yellowed resin → undamaged fibers in undamaged resin.

The damage to the lower face sheet of the SLC03 specimen was more severe than in the previous two experiments (see Figure 5-33). All four roving layers were completely delaminated. As the face sheet warped and delaminated, the connection to the webs was broken in some areas. Overall, only a 1-2 mm thin layer containing the inner surface veil and stitched mat remained partially intact, which indicates that the webs eventually provided all of the tensile resistance in bending.

#### **8.5.6 Post-Fire Strength and Stiffness**

The specimens in Experiments SLC01 and SLC02 were loaded up to the capacity of the testing equipment (150 kN per jack) without any signs of structural failure. This load is equivalent to 306% of the service load. Such loading resulted in a mid-span deflection of 59 mm for SLC01 and 62 mm for SLC02 (see Figure 5-35). As previously described, the SLC03 specimen could not be subjected to post-fire loading because of the structural failure that occurred during the fire exposure.

Figure 5-35. Load versus mid-span vertical deflection (specimen SLC03 could not be tested post-fire because of a structural failure)



## 8.6 Discussion of Results

### 8.6.1 Strains

After ignition of the burners, the strains in the liquid-cooled specimens rapidly increased for approximately 10-20 minutes, particularly in the lower face sheets, and then stabilized at an almost constant value until the end of the experiments. In this phase of almost constant strains, the tensile strains were approximately 300% higher than the compressive strains. This was due to two factors: the reduction of lower face sheet thickness (which moved the neutral axis upward), and the thermal expansion of the reinforcement layers at the tensile face. This second phenomenon is the result of the elongation of the fibers due to thermal expansion being greater than the elongation caused by bending. The hottest reinforcement layers towards the lower face, which would normally be in tension at ambient temperatures, actually elongated so much more than the cooler, deeper reinforcement layers that they were forced into compression. The inner fibers, therefore, needed to resist the stress imposed by bending and by the expanding outer reinforcement layers, and thus exhibited much higher strains than the upper face sheets.

### 8.6.2 Stiffness Reduction

The relationship between the load and mid-span deflection of the experimental specimens is termed herein the *bending stiffness*,  $S$ .<sup>9</sup> This value can be calculated by measuring the slope of the curve created by plotting the experimental mid-span deflections,  $\delta$ , against load,  $P$  (see Figure 5-35). The derivation of the *rigidity*,  $EI$ , from  $S$  is described in Appendix C - Section 6.4. The values of  $S$  and  $EI$  are listed Table 5-4.

Table 5-4. Bending stiffness,  $S$ , resulting from measured mid-span deflections and rigidity,  $EI$  (kN·m<sup>2</sup>)

Property	SLC01		SLC02		SLC03
	Pre-Fire	Post-Fire	Pre-Fire	Post-Fire	Pre-Fire
$S$ (kN/mm)	7.59	4.71	7.49	4.37	7.67
$EI$ (kN·m <sup>2</sup> )	5,710	3,500	5,640	3,250	5,780

These calculations reveal that the bending stiffness and rigidity of specimen SLC01 was reduced by 38% as a result of the fire exposure. Specimen SLC02, which was exposed to fire for 30 minutes longer and had half the liquid cooling flow rate showed a similar reduction in bending stiffness and rigidity of 41%. These reductions are due to both the loss of cross-section and the reduction of the modulus of elasticity of the cross-section that remained in place.

### 8.6.3 Heat Transfer to Water

Using the recorded input and output temperatures of the flowing water, the amount of energy removed from the specimens by liquid cooling can be roughly calculated. The principles and mechanics of this procedure are described in Section 7.6.2. The results of the calculation for a 90 minute exposure duration with  $A_{xp}=0.745$  m<sup>2</sup> are tabulated in Table 5-5. The power drawn is plotted in function of fire exposure time in Figure 5-36 and in function of flow rate in Figure 5-37.

As shown in Figure 5-37, the power drawn by the flowing water increased with increased flow rates for the first 60 minutes of fire exposure. In the period between 60 and 90 minutes, however, an inconsistency began to emerge as the specimen with a flow rate of 0.80 m<sup>3</sup>/hr (LC01) drew more power than the specimen with 1.00 m<sup>3</sup>/hr (SLC02). This apparent discrepancy could be due to the effect of turbulence in the cells. In the shorter LC specimens, the effect of the inlet and outlet flow conditions was more pronounced, resulting in a more

9. The bending stiffness,  $S$ , differs from the rigidity,  $EI$ , in that the former is a characteristic of the entire structure, including its loading and support conditions, while the latter is simply a characteristic of the cross-section.

turbulent flow regime overall. With more turbulent flow, the convective heat transfer would be lower, allowing the lower face sheet to heat up quicker (as shown in Figure 5-39, the cold face of the LC specimens was indeed approximately 20°C higher than the liquid-cooled SLC specimens). As the surface of the lower face sheet became hotter, the thermal gradient between the water and the surface became greater, and thus the rate of heat transfer increased. As such, it is possible that the power drawn by the water in the LC specimens was initially less than in the SLC specimens, but then increased at a faster rate such that it exceeded the power drawn by the water in the SLC specimens after 60 minutes.

Table 5-5. Total energy absorbed by water over 90 minutes of fire exposure

Experiment	Flow Rate (m <sup>3</sup> /hr)	Coordinates of Bilinear Regression						$Q_{total}$ (MJ/m <sup>2</sup> )
		(s)	(kW)	(s)	(kW)	(s)	(kW)	
LC01	0.80	60	0	720	2.4	5400	8.6	26.5
LC02	4.00	-	-	-	-	-	-	- <sup>a</sup>
LC03	0.16	300	0	840	1.4	5400	6.5	18.4
SLC01	2.00	300	0	1140	4.7	5400	7.1	27.1
SLC02	1.00	120	0	1320	4.3	5400	6.5	24.6

a. the high flow rate resulted in a very small change in water temperature that could not be measured by the instruments used

Figure 5-36. Power drawn by flowing water per unit fire-exposed area versus time

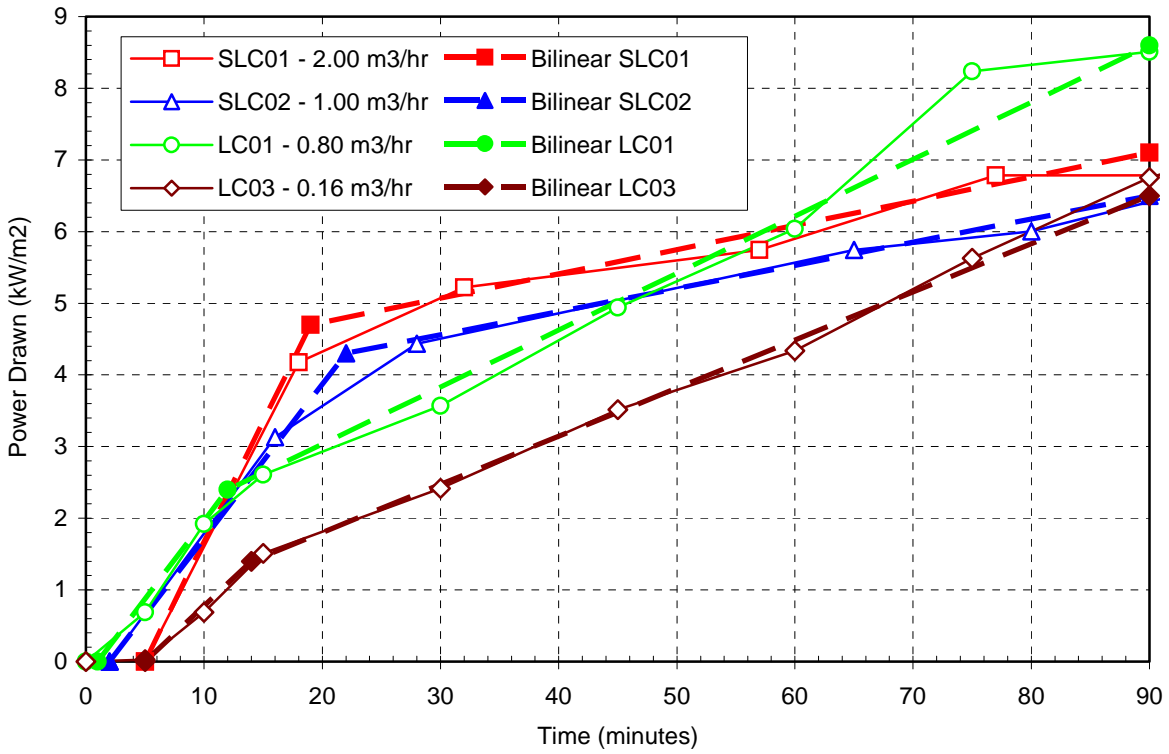
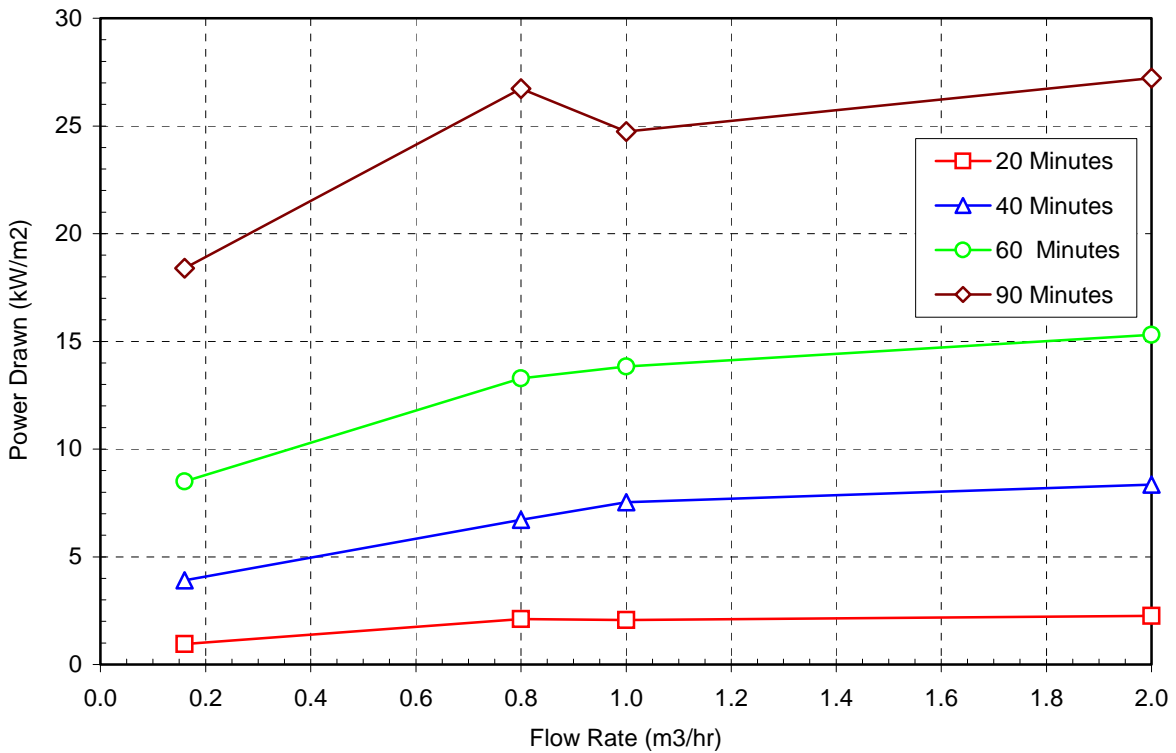


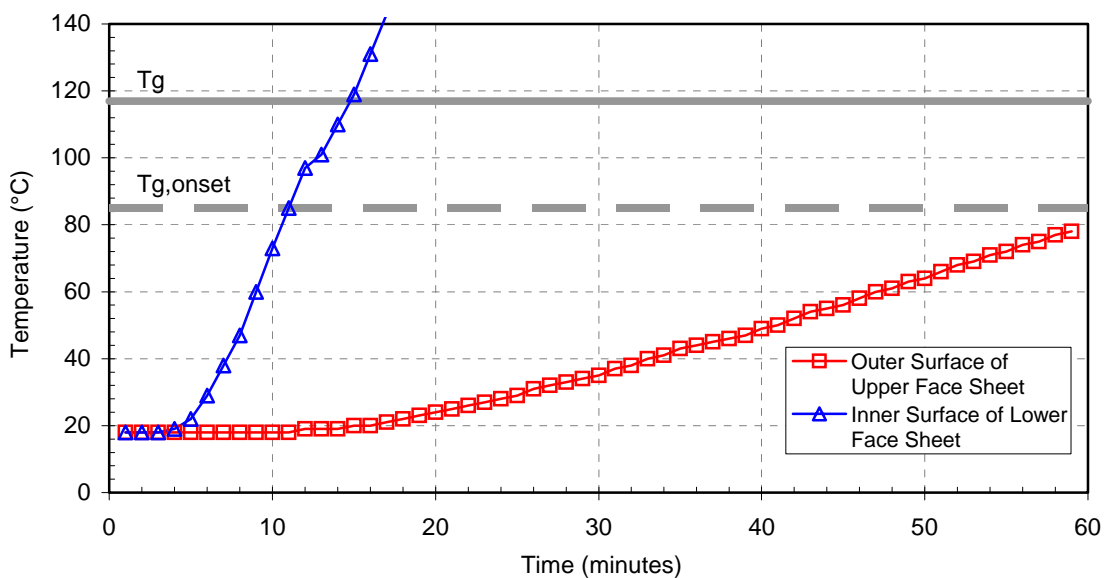
Figure 5-37. Power drawn by flowing water per fire-exposed area versus flow rate



### 8.6.4 Failure of SLC03

Without liquid cooling, significant amounts of heat were transferred from the lower to the upper face sheet through radiation and convection within the cells. Though no thermocouples were placed on the interior surface of the upper face sheet, the thermocouples on the outer surface were just approaching the onset glass transition temperature at the time of failure (see Figure 5-38). Because the outer surface was exposed to cool ambient temperatures and the inner surface was receiving radiation and convection from the lower face sheet, it is likely that the inner surface was far hotter than the outer surface, and thus above the glass transition temperature. As the upper face sheet was resisting compression and relied on the matrix to maintain alignment of the glass fibers, it was extremely vulnerable to the loss of stiffness of the matrix. The lower face sheet, however, was in nearly pure tension. Because the fibers remained anchored outside of the heated area, it remained able to resist its load even after all of the resin had decomposed. This explains why the relatively cooler upper face sheet failed before the lower face sheet.

Figure 5-38. Experiment SLC03 temperature vs. time

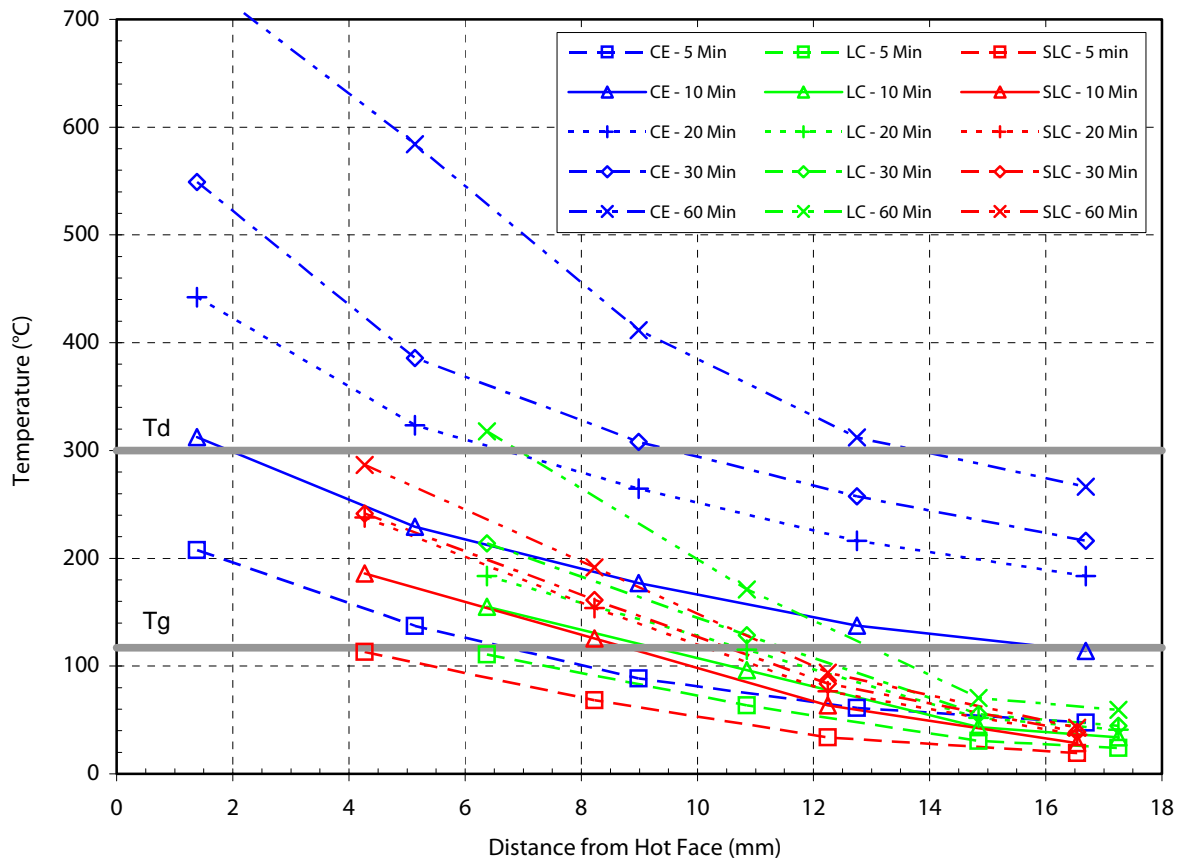


### 8.6.5 Liquid Cooling

The efficacy of liquid cooling has already been demonstrated by the LC Experiments (the temperature profiles from the CE, LC and SLC experiments are compared in Figure 5-39). Supporting this evidence through the addition of structural loading on full-sized specimens, the experiments provide a new and unexpected argument for liquid cooling. Prior to SLC03, it was assumed that damage to the lower flange would lead to the structural failure of the panels. Testing in the dry condition under structural load showed that heat transfer from the lower face

sheet can quickly bring the opposite face sheet above the glass transition temperature. This is equally important for panels in the vertical orientation, where design might require 50% of a column section to remain intact in order to support its load. Without liquid cooling, such columns would be subject to the same failure seen in SLC03.

**Figure 5-39.** Comparison of average temperature profiles of SLC, LC, and CE specimens (the non-liquid cooled SLC03 is not included in the average SLC profile)



## 8.7 Conclusions from the Structural Fire Endurance Experiments

The following conclusions can be made from the SLC Experiments:

- With the aid of liquid cooling, FRP panels supporting structural loads can resist the extreme temperatures presented by severe fire conditions for at least 120 minutes.
- Panels exposed to such conditions deflect significantly within the first 10 minutes. While the control panel (SLC03) continued the trend until failure, the deflection of the liquid-cooled panels (SLC01-02) approached a nearly steady-state condition, deflecting more in the first 10 minutes (8 mm) than in the following 80 minutes (6 mm).

- No significant difference in the performance of the two liquid-cooled specimens was noted.
- The post-fire bending stiffness of the liquid-cooled specimens was reduced by roughly 40%. This decrease is attributed to the reduction of the moment of inertia due to the loss of material from the lower face sheet and to a reduction in the Young's Modulus of regions that were heated above  $T_g$ .

## 9 Conclusions from Experimental Program

- Thermal and thermomechanical material properties were obtained for use in the mathematical models.
- No beneficial resin charring effect was observed. Charred glass fiber layers provided a barrier against radiation but not convection.
- Panels without liquid cooling reach  $T_g$  through their entire depth in under 10 minutes and  $T_d$  in roughly one hour. FRP components in stress states that require a mechanical contribution from the matrix would most likely fail after a very brief exposure to fire.
- The inner 20% of the thickness of the liquid cooled panels remained below  $T_g$  after 120 minutes of exposure at even the lowest flow rates.
- Despite some scale-effects, the amount of energy absorbed by the water increased with increasing flow rates. Benefits begin to diminish with flow velocities above 1.0 cm/s (flow rate 0.8 m<sup>3</sup>/hr).
- For the length of flow paths tested and flow velocities employed, the water never approached boiling. The slowest flow velocity of 0.2 cm/s resulted in an increase in temperature of 30°C, while the temperature increase at the highest flow velocity of 5 cm/s was too small to measure. It therefore appears possible to design longer flow paths in building applications without the risk of boiling.
- Water pressures were too small to measure at all flow velocities except the very highest. This suggests that high pressures related to head loss will not hinder the design of larger systems for buildings.
- The failure of specimen SLC03 showed that FRP elements in compression are far more vulnerable to temperature-induced failure than those in tension. The protection of such components is where liquid cooling can make the most valuable contribution.
- Code-required endurance times of 90 minutes and longer can be achieved for floor elements using the internal liquid cooling system. The liquid-cooled loaded panels quickly adjusted to nearly steady-state conditions after being exposed to fire conditions. Deflections increased more in the first 10 minutes than in the 80 minutes that followed.
- Post-fire structural loading showed a 40% reduction in the stiffness of the liquid-cooled panels. Calculations showed that this was not only due to the loss of cross-section, but also the degradation of Young's modulus in areas that exceeded  $T_g$ .

# 6

## **Mathematical Modeling**

*Analytical and Numerical Modeling with Experimental Validation*



## 1 Introduction

Mathematical models are used to simplify some chosen aspects of a real system down to set of components that behave and interact according to a list of rules. When validated by comparison to physical experiments, the model may be used to simulate the behavior of the system with the variation of one or several parameters, e.g., geometry, material properties, loads, boundary conditions, etc. Multiple analyses can be performed with little increase of time or expense, and may allow the observation of phenomena that cannot be easily measured or observed in practice.

Several models have been developed to study the proposed system described in Chapter 4 and have been validated through the physical experiments described in Chapter 5:

- Simple analytical models were formulated to predict the structural response of deck panels before and after fire exposure. These models treat only the mechanical behavior of the specimens and were used to select the experimental load and later to establish the range of allowable spans for the proposed flooring system.
- A two-dimensional thermochemical FEA model was devised to predict the transient behavior of the air-cooled and liquid-cooled deck panels. The simplification from three dimensions to two allowed much higher mesh refinement with quicker processing times. The results of this model were used as the boundary conditions for the more complex three-dimensional thermomechanical model.
- A three-dimensional thermomechanical FEA model was developed to simulate the transient structural response of liquid-cooled deck panels at elevated temperatures. Temperature distributions through the lower face sheet are calculated by the two-dimensional model and are used as boundary conditions in this model. This model can also predict the room-temperature structural behavior of the specimens.

Each of these models is described in greater detail in the following sections.

## 2 Analytical Mechanical Modeling

Simple mathematical expressions were used to approximate the static mechanical behavior of the specimens used in the physical experiments. Because the specimens in the physical experiments were loaded and supported continuously in the axis transverse to the span, they can be treated as beams rather than as panels. Timoshenko beam theory was found to provide deflection predictions that agree very well with experimental values, though simple Bernoulli beam theory works nearly as well.

### 2.1 Undamaged Section at Ambient Temperature

#### 2.1.1 Applied to Experimental Specimens

The load used in the large-scale experiments was selected based on the anticipated deflections. To determine this load, therefore, an expression relating load to deflection was required. This expression appears as follows:

$$\delta_{\text{TOTAL}} = \delta_{\text{SHEAR}} + \delta_{\text{BENDING}} \quad (6-1)$$

In the physical experiments conducted, the specimens were simply supported and subjected to four-point bending. Using the method of virtual forces to solve for these load and support conditions, each term is expanded as follows:

$$\delta_{\text{TOTAL}} = \frac{aP}{GA} \left( \frac{L-2a}{L} \right) + \frac{PL^3}{24EI} \left( \frac{3a}{L} - \frac{4a^3}{L^3} \right) \quad (6-2)$$

where  $a$  is the distance between the load,  $P$ , and support,  $A$  is the cross-sectional area of the webs,  $G$  is the shear modulus,  $E$  is the Young's Modulus, and  $I$  is the moment of inertia (see Figure 5-26). Because the Young's Modulus varies over the cross section, the *rigidity*,  $EI$ , must be calculated as the sum of the rigidities of the individual parts. For the specimens used in the experimental investigations, this calculation appears as follows:

$$\begin{aligned}
 EI &= E_w I_w + 2E_f I_f \quad (6-3) \\
 &= \left(17,380 \frac{\text{N}}{\text{mm}^2}\right) (4.66 \times 10^7 \text{ mm}^4) + 2 \left(21,240 \frac{\text{N}}{\text{mm}^2}\right) (1.21 \times 10^8 \text{ mm}^4) \\
 &= 5.98 \times 10^{12} \text{ N} \cdot \text{mm}^2
 \end{aligned}$$

where the subscripts  $w$  and  $f$  refer to the web and face sheets (material properties taken from Table 5-2). Having calculated the rigidity of the cross section, Equation 6-1 can be solved. The material properties (from Table 5-2) and dimensions of the loaded experiments (see Chapter 5 - Section 8) are then inserted.

$$\begin{aligned}
 \delta_{\text{TOTAL}} &= \frac{900 \text{ mm} \cdot 92,900 \text{ N}}{4,140 \frac{\text{N}}{\text{mm}^2} \cdot 11,206 \text{ mm}^2} \left( \frac{2,750 \text{ mm} - 2 \cdot 900 \text{ mm}}{2,750 \text{ mm}} \right) \\
 &+ \frac{92,900 \text{ N} (2,750 \text{ mm})^3}{24 (5.98 \times 10^{12} \text{ N} \cdot \text{mm}^2)} \left( \frac{3 \cdot 900 \text{ mm}}{2,750 \text{ mm}} - \frac{4 \cdot (900 \text{ mm})^3}{(2,750 \text{ mm})^3} \right) = 12.0 \text{ mm} \quad (6-4)
 \end{aligned}$$

The measured mid-span deflections from the three SLC experiments were 11.97 mm, 12.02 mm, and 12.34 (average 12.11 mm).<sup>1</sup> The discrepancy between the predicted deflection and the average measured deflection is therefore less than the variation of the measured deflection values themselves. Thus, the deflections of such structures may be quickly and accurately estimated through the correct expansion of Equation 6-1 for the particular loading and support conditions.

It is also useful to note that the shear deformations (represented by the first term on the right side of Equation 6-2) amount to 0.6 mm or only 5% of the overall predicted deflection of 12.0 mm. This indicates that fairly good predictions may be made even if shear deformations are neglected, i.e. employing Bernoulli beam theory rather than Timoshenko beam theory.

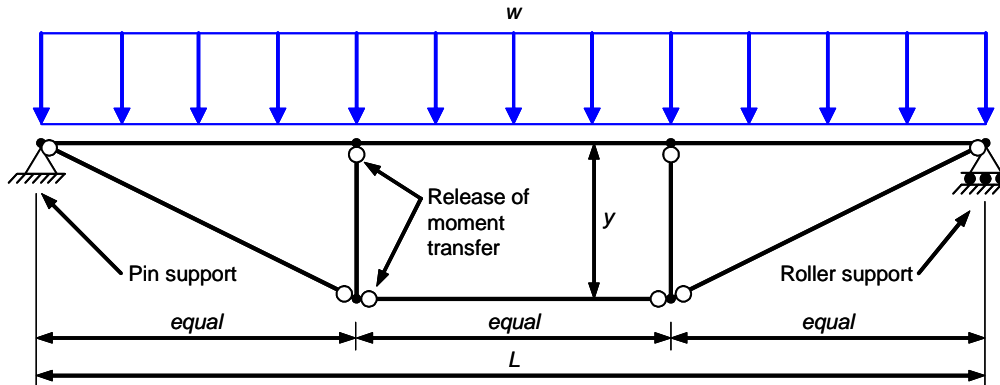
### 2.1.2 Applied to Proposed Flooring System

Having verified that simple beam theory provides fairly good predictions of the deflections of cellular FRP sections in bending, some design guidelines for the proposed system may be established. Because the system under consideration is internally statically indeterminate, software tools were employed to expedite the calculations. The commercial software *STAB2D*

1. The simpler version of this calculation shown in Equation 5-7 was used to select the loads imposed in the physical experiments. The predicted deflection of 9.2 mm differs from the value shown (12.0 mm) because the simpler version did not include shear deformations and employed an  $E$  value that has since been shown to be too high.

Version 5.67 was used to analyze various permutations of loads and dimensions of the proposed system (shown in Figure 6-1).

Figure 6-1. Load and support conditions used in undamaged model of proposed flooring system



Two conditions were studied: serviceability limit state (*s/s*), where performance is considered, and ultimate limit state (*u/s*), where safety is considered. In the *s/s*, the deflections resulting only from live loads are calculated to verify that they are not too large by accepted standards of span-to-deflection ratio.<sup>2</sup> In the *u/s*, the stresses are calculated to verify that they are acceptably lower than the resistance of the material under all dead and live loads.

A 1 m wide section of the proposed floor deck section with two carbon tendons, as shown in Figure 4-6, was considered for all calculations. Tables 6-1 to 6-4 list the system parameters and material properties also needed to study the proposed flooring system in the ambient temperature undamaged condition.

Table 6-1. Floor deck parameters

Parameter	Value	Notes
$A$	$3.90 \times 10^{-2} \text{ m}^2$	from Chapter 4 - Section 2.3.2
$I_{yy}$	$6.82 \times 10^{-5} \text{ m}^4$	from Chapter 4 - Section 2.3.2
$E_x$	21.24 GPa	from experimental material - see Table 5-2
$f_{c-x}$	-261 MPa	from experimental material - see Table 5-2
$f_{t-x}$	261 MPa	from experimental material - see Table 5-2
$d$	0.153 m	from Figure 4-3

2. Other *s/s* criteria such as vibrations are beyond the scope of this verification.

Table 6-2. Carbon tendon parameters

Parameter	Value	Notes
$A$	$7.70 \times 10^{-4} \text{ m}^2$	two tendons 55 mm wide x 7 mm thick, as drawn in Figure 4-6
$I_{yy}$	$3.14 \times 10^{-9} \text{ m}^4$	calculated
$E_x$	250 GPa	from Sika CarboDur® product literature
$f_t$	2.80 GPa	from Sika CarboDur® product literature
$d$	0.007 m	as drawn in Figure 4-6

Table 6-3. Carbon tendon deviation post parameters

Parameter	Value	Notes
$A$	$5.60 \times 10^{-3} \text{ m}^2$	tube steel sections 150 mm square with 10 mm wall thickness
$I_{yy}$	$1.84 \times 10^{-5} \text{ m}^4$	calculated
$E_x$	210 GPa	from [1]
$d$	0.150 m	tube steel sections 150 mm square

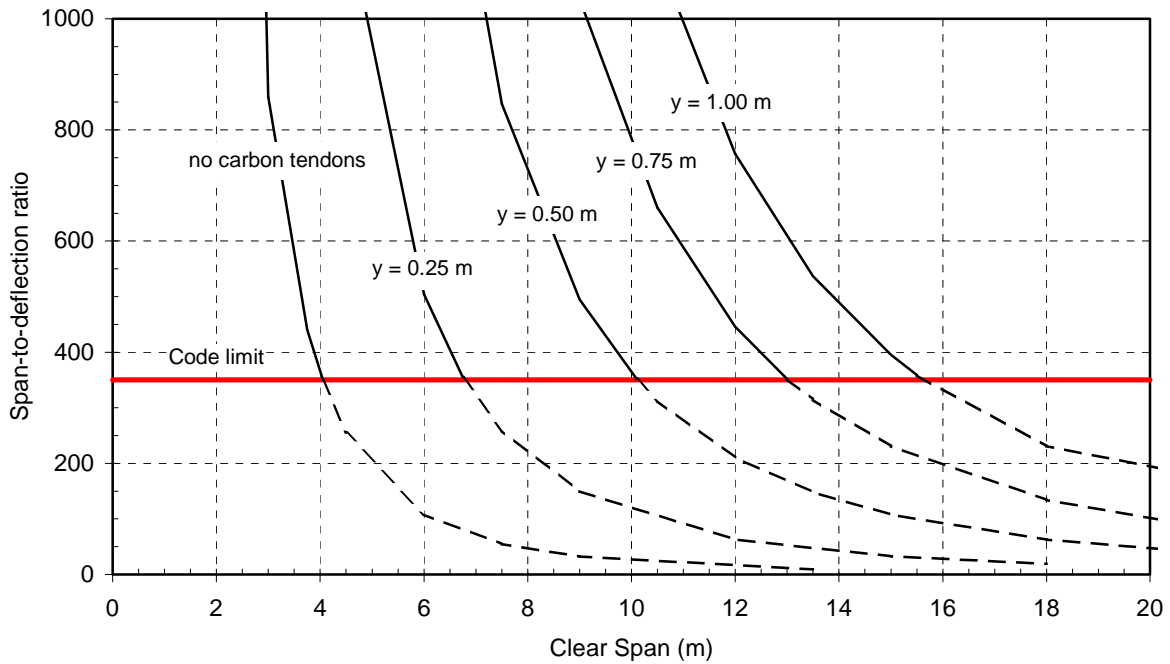
Table 6-4. Applied loads

Parameter	Value	Notes
$DL$	$2.28 \text{ kN/m}^2$	from Section 2.3.1
$LL$	$4.79 \text{ kN/m}^2$	from Section 2.3.1
$\gamma_{DL}$	1.2	from [1]
$\gamma_{LL}$	1.6	from [1]

### 2.1.2.1 Serviceability Limit State

For the simply-supported and symmetrically-loaded system shown in Figure 6-1, the maximum deflections occur at the mid-span. Applying the live load shown in Table 6-4, the vertical mid-span deflections were calculated for various deviation post heights,  $y$ . The ratio of these deflections to the span are graphed against the span in Figure 6-2 for post heights ranging from 0.25 to 1.00 m as well as without the carbon tendon system. Swiss building code (SIA 260) limits the deflections of floors to a span-to-deflection ratio of 350 under regularly occurring loads, thus only the values higher than this (indicating smaller deflections in comparison to the span) are allowable.

Figure 6-2. Ratio of span-to-deflection versus span for different post heights

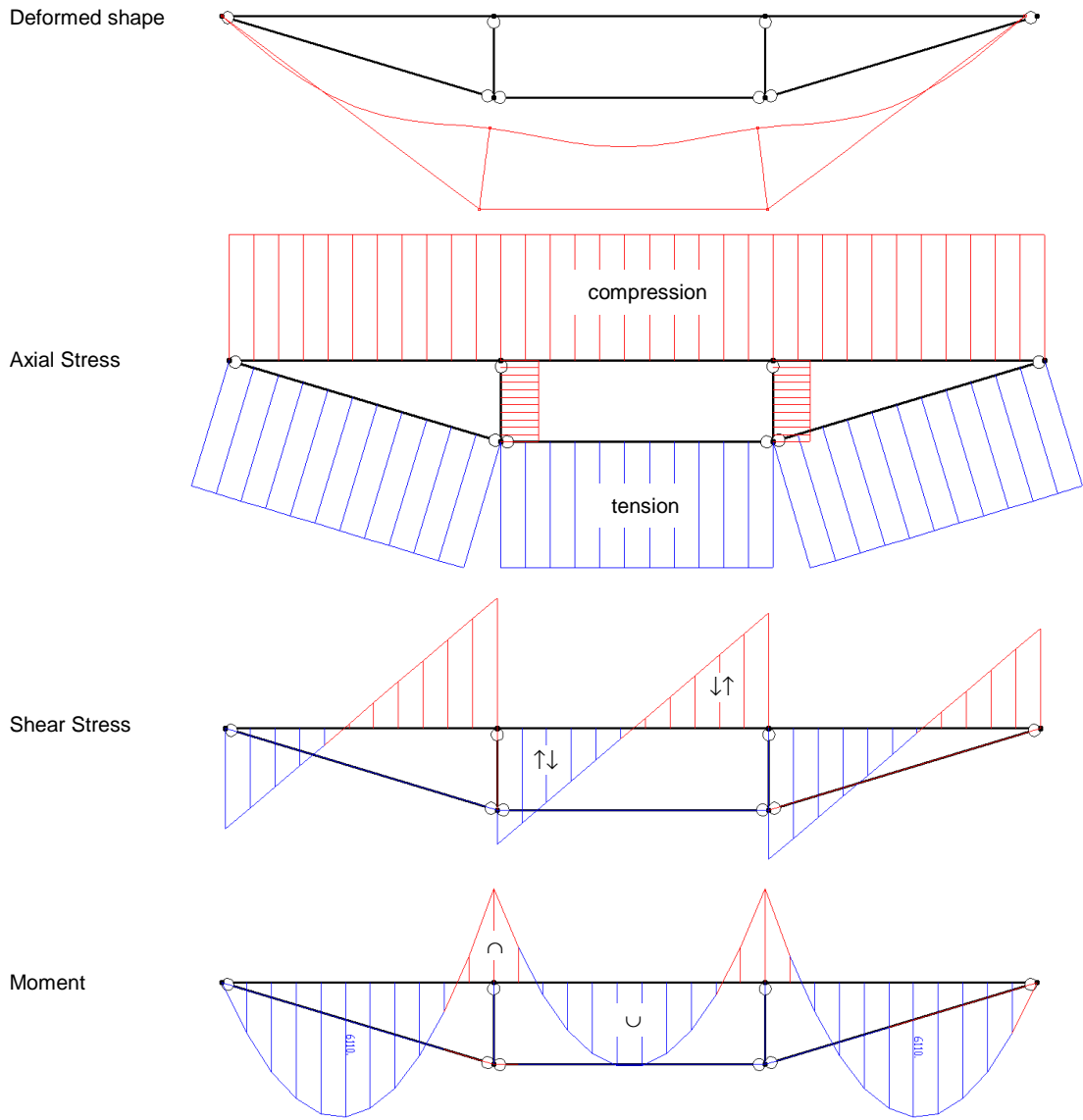


As shown in Figure 6-2, the carbon tendon system greatly increases the allowable span in serviceability limit state conditions. At the code limit (SIA 260) of span/deflection = 350, the tendon system increases the permissible span from 4 m to 10 m using 0.5 m tall deviation posts or 15.5 m using 1.0 m tall deviation posts.

#### 2.1.2.2 Ultimate Limit State

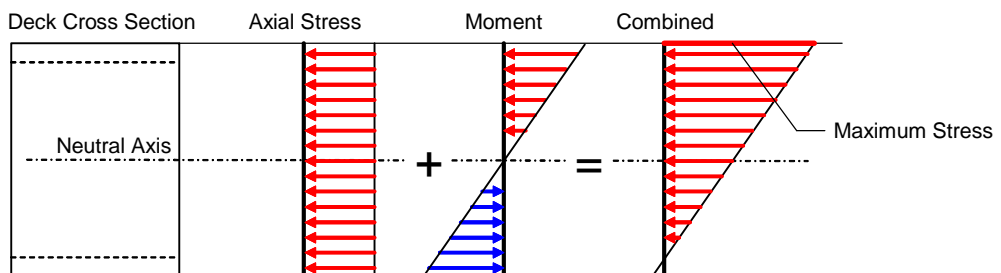
In the ultimate limit state, both the factored dead and live loads are applied to find the maximum stresses in the system. These stresses are then compared to the resistance to verify the safety of the system. Applying these loads to the system shown in Figure 6-1, the deformed shape, axial stress, shear, and moment are qualitatively shown in Figure 6-3.

Figure 6-3. Deformed shape, axial stress, shear stress, and moment distribution under a distributed load



As the axial force applied to the deck interacts with the moment to create higher compressive stresses, the two stresses must be combined to find the maximum stress, as shown in Figure 6-4.

Figure 6-4. Combination of axial stress and moment to find maximum stress in deck section

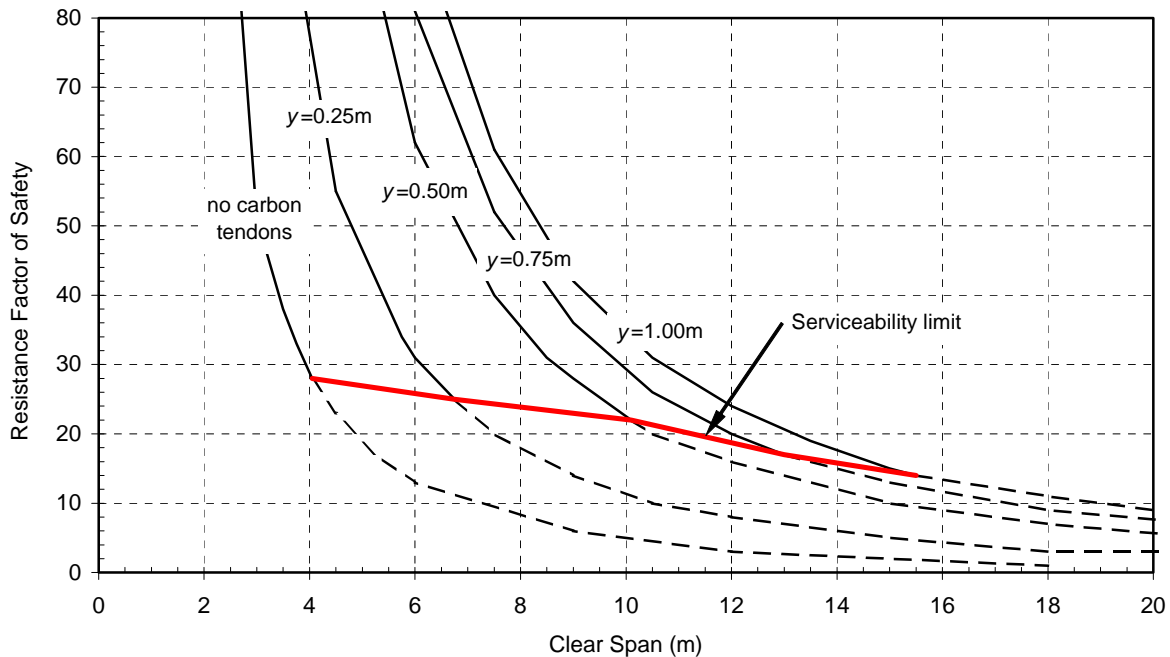


The resistance factor of safety,  $\gamma_R$ , is the factor by which the material resistance,  $R$ , is larger or smaller than the maximum stresses resulting from the factored dead and live loads. The relationship between loads, resistance, and their associated factors is expressed by Equation 6-5.

$$DL \cdot \gamma_{DL} + LL \cdot \gamma_{LL} = \frac{R}{\gamma_R} \quad (6-5)$$

At the *uls*, the stresses in the carbon tendons and deviation posts are far lower than their resistances, meaning that the deck is the governing member for the overall safety of the system.<sup>3</sup> Figure 6-5 shows  $\gamma_R$  versus span for the proposed deck element with various deviation post heights (neglecting buckling failure modes).

Figure 6-5. Resistance factor of safety ( $\gamma_R$ ) versus span for different post heights



As shown, the deck has adequate stiffness and strength without the carbon tendon system for spans shorter than 4 m. Figure 6-5 also shows that the resistance factor of safety varies between 14 and 28 for the systems that achieve the minimum serviceability requirements. Thus, even if the consideration of buckling failure modes reduces the  $\gamma_R$  factors by a factor of 10, the serviceability limit state would still be the governing condition and a sizeable margin of safety is ensured.

3. The connections are assumed to be designed with a larger margin of safety than the members.

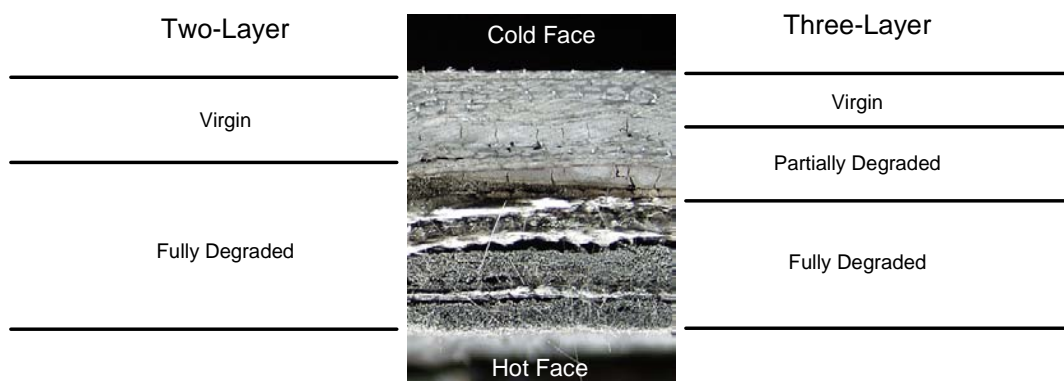
## 2.2 Fire-Damaged Section at Ambient Temperature

In the event of a building fire, it is useful to be able to estimate the remaining capacity of structural members that have been damaged. A significant percentage of the section's original strength and stiffness may be retained if the fire exposure is not too severe. For a multiple-story FRP building system, a small fire might cause some local damage before it is extinguished (or self-extinguishes) and before it leads to global failure. A reliable post-fire mechanical model would allow engineers and inspectors to evaluate the damage and to estimate the remaining capacity of the components. Informed decisions could then be made concerning repair and replacement.

The prediction of the mechanical behavior of fire-damaged structural elements requires some significant assumptions and simplifications because it is not only affected by the geometry of the section that remains intact, but also by the reduction in stiffness of the areas that were heated above  $T_g$ . Investigations Gardiner [57] and Seggewiß [165] have revealed that the post-fire modulus of elasticity of polymer composites can be reduced by as much as 70% by exposure to temperatures above  $T_g$  but below  $T_d$ . Accurate post-fire mechanical models of fire-damaged structural elements should therefore account for the temperature history of the seemingly unaffected regions in between the fully-degraded region at the hot face and the unaffected portion towards the cold face.

In a simple two-layer model [135], this *partially* degraded middle region is divided such that some falls within the “fire-degraded” region and some within the “unaffected” region. A more complex three-layer model treats this degraded region separately (see Figure 6-6). The most advanced model, of course, would have no discretized regions and material properties would be solved in function of temperature and time. These models are too complex to be solved analytically and thus require numerical methods. New two-layer and three-layer analytical mechanical models are presented in following sections.

Figure 6-6. Comparison of two-layer and three layer approximations



### 2.2.1 Two-Layer Model

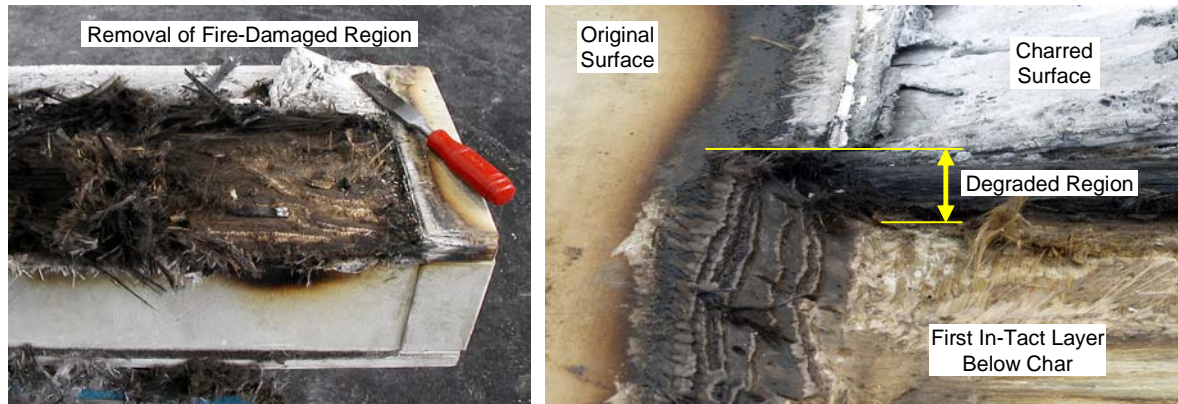
As described, the two-layer approximation divides the section into two discrete regions: a fully-degraded region and a region that retains its pre-fire mechanical properties (see Figures 6-8 and 6-8). Determination of the criterion used to dictate the location of this border is the only true difficulty. Several criteria are considered:

- by physical (visual) inspection of the specimen after cooling, the depth at which fibers are soundly bonded in firm resin (used initially by Mouritz *et al* in [132])
- by study of the through-thickness temperature profile of the specimen during the final minutes of the fire exposure, the greatest depth that reached some chosen temperature (currently used by Gardiner *et al* in [57] for zones in compression)
- by pulse-echo measurement, the depth at which some chosen percentage of the resin remains present (currently used by Gardiner *et al* in [57] for zones in tension)

In order to make the most accurate approximation using a two-layer system, the boundary should be drawn at the depth (defined herein as  $d_c$ , the distance from the hot face inwards) where the mechanical properties have degraded by one-half. In this way, the assignment of 0% remaining stiffness to a region that actually has 25% is counterbalanced by the assignment of 100% to a region that actually has only 75% remaining stiffness.

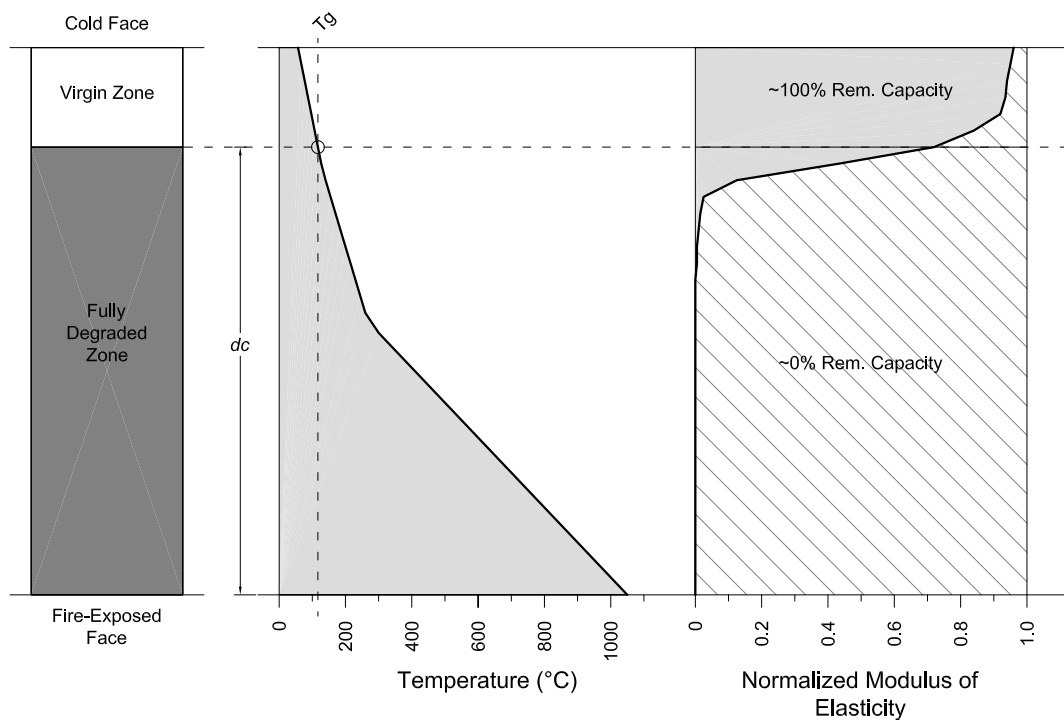
The first criterion (visual inspection) is the most simple and consistent (though not the most accurate) method because it requires no knowledge of the fire exposure and affords very few occasions to commit errors. The problem, however, is that the depth at which fibers begin to be anchored in sound resin does not directly correspond to the one-half degradation limit described above. The intensity of the exposure can change the relationship between the two depths, making calibration of the technique difficult. In the absence of all other options, however, the visual inspection criterion is better than nothing and can provide rough approximations. It is also useful as cross-check for the other criteria. Figure 6-7 illustrates the process for a pultruded FRP element that was exposed to 120 minutes of fire exposure. The depth  $d_c$  determined by this criterion for experimental specimens SLC01 and SLC02 is 7.0 mm, as shown in Table 6-5.

Figure 6-7. Determination of the depth of the degraded region by visual inspection



The second criterion (temperature) is obviously only useful if the section was instrumented during the fire exposure. In design, however, this information is determined through numerical analysis. Still, exact knowledge of the temperature history provides only an indication of the post-fire status, as degradation is both temperature and time-dependent. Nonetheless, the temperature criterion can yield more accurate results than the first criterion (visual inspection). Figure 6-8 shows the temperature profile through the thickness of a specimen exposed to fire for 120 minutes. For the two-layer model, the depth of the degraded region is defined as the depth that reached  $T_g$  and is found by the intersection of the temperature profile with a line corresponding to  $T_g$ .

Figure 6-8. Relationship of temperature profile to modulus of elasticity by the 2-layer approximation



The third criterion (percentage remaining resin) has an advantages over the second criterion in that it can be used for evaluation as well as design because no knowledge of the fire exposure is required. It does, however, require the use of a pulse-echo ultrasonic device. As the expense of this device was not anticipated in the planning of this project, the temperature criterion was adopted. This criterion places the boundary between the fully degraded and the virgin regions at the maximum depth that was heated to the glass transition temperature,  $T_g$ . Figure 5-30 from the previous chapter shows that the corresponding depth for experiment SLC01 was 11.7 mm at 90 minutes and 13.5 mm for experiment SLC02 at 120 minutes (see Table 6-5).

Once the two regions are defined, the bending analysis proceeds in the same manner as it would for any traditional composite section. The procedure is demonstrated in the following steps.

First, the neutral axis of the section is found by setting the sum of the moments of the areas equal to zero:

$$A_{ufs}d_{ufs}\eta_{ufs} + A_wd_w\eta_w + A_{lfs}d_{lfs}\eta_{lfs} = 0 \quad (6-6)$$

where  $A$  is the area of the individual part,  $d$  is the distance from the neutral axis to the centroid of the part,  $\eta$  is the ratio of the modulus of elasticity of the part to a reference modulus, and the subscripts  $ufs$ ,  $w$ , and  $lfs$  refer to the upper face sheet, web, and virgin region of lower face sheet, respectively. Each  $d$  term is expanded to be expressed in terms of the depth of the neutral axis so that there is only one unknown. For experiments SLC01 and SLC02, the neutral axis is found to be at 67.9 mm and 61.5 mm, respectively, from the top of the upper face sheet.

Next, the moment of inertia of the each area about the neutral axis calculated:

$$\begin{aligned} I_{ufs} &= \frac{1}{12}b_{ufs}y_{ufs}^3 + A_{ufs}y_{ufs}^2 \\ I_w &= \frac{1}{12}b_wy_w^3 + A_wd_w^2 \\ I_{lfs} &= \frac{1}{12}b_{lfs}y_{lfs}^3 + A_{lfs}d_{lfs}^2 \end{aligned} \quad (6-7)$$

where  $b$  is the width and  $y$  is the height of the individual parts. Finally, the rigidity,  $EI$ , of the composite section is computed as the sum of the rigidities of the individual parts.

$$EI = E_wI_w + E_f(I_{ufs} + I_{lfs}) \quad (6-8)$$

The results of this calculation as applied to experiments SLC01 and SLC02 are shown in Table 6-5 for both the visual inspection and temperature criteria, and are compared to the

rigidities derived from the measured bending stiffnesses,  $S$  (see Chapter 5 - Section 8.6.2 for a explanation of how  $S$  was derived from measured values). The geometrical values required to solve Equations 6-6 and 6-7, which are dependent on  $d_c$ , are provided in Table 6-6.

Table 6-5. Rigidity predictions by the 2-layer model

Experiment	Criterion	$d_c$ mm	$EI$ from 2-Layer Model N·mm <sup>2</sup>	$EI$ from Measured $S$ N·mm <sup>2</sup>	Disparity <sup>a</sup> %
SLC01	visual inspection	7.0	4.70x10 <sup>12</sup>	3.50x10 <sup>12</sup>	+34
SLC01	temperature	11.7	3.53x10 <sup>12</sup>	3.50x10 <sup>12</sup>	+1
SLC02	visual inspection	7.0	4.70x10 <sup>12</sup>	3.25x10 <sup>12</sup>	+45
SLC02	temperature	13.5	2.99x10 <sup>12</sup>	3.25x10 <sup>12</sup>	-8

a. Disparity = (calculated - measured) / measured

Thus, although the two layer model is fairly unsuccessful using the visual inspection criterion, the temperature criterion predicts the post-fire rigidity of the sections within roughly 10% of the measured values.

Table 6-6. Values entered into Equations 6-6 and 6-7 to solve for the  $EI$  values shown in Table 6-5

$d_c$ (mm)	$\eta_{uf_s}$	$\eta_w$	$\eta_{lf_s}$	$A_{uf_s}$ (mm <sup>2</sup> )	$A_w$ (mm <sup>2</sup> )	$A_{lf_s}$ (mm <sup>2</sup> )	$d_{uf_s}$ (mm)	$d_w$ (mm)	$d_{lf_s}$ (mm)	$b_{uf_s}$ (mm)	$b_w$ (mm)	$b_{lf_s}$ (mm)
7.0	1	0.82	1	15,350	11,480	8,950	73.4	15.5	104.4	913.6	71.3 <sup>a</sup>	913.6
11.7	1	0.82	1	15,350	11,480	4,660	59.5	29.4	118.3	913.6	71.3 <sup>a</sup>	913.6
13.5	1	0.82	1	15,350	11,480	3,015	53.1	35.8	124.7	913.6	71.3 <sup>a</sup>	913.6

a. Combined width of seven individual webs - see Figure 5-2

### 2.2.2 Three-Layer Model

Slightly more complex than the two-layer model, the three-layer model includes a region with degraded mechanical properties in addition to the fully-degraded and virgin zones (see Figure 6-8). For the same reasons cited in the discussion of the two-layer model, temperatures are used to define the depths of the zones. The border between the fully-degraded region and the partially degraded region is denoted  $d_{Td}$ , and is defined as the deepest layer to have been heated to the onset of decomposition,  $T_{d,onset}$ .<sup>4</sup> The border between the partially-degraded region and the virgin region is denoted  $d_{Tg}$ , and is defined as the deepest layer to have been heated to the onset of glass transition,  $T_{g,onset}$ . For the material used in the experimental investigations,  $T_{g,onset}$  is 32°C lower than the  $T_g$ , or 85°C, and  $T_{d,onset}$  is 50°C lower than  $T_d$  at

250°C. From Figure 5-30,  $d_{T_g}$  is at 13.8 mm and 15.1 mm deep, while  $d_{T_d}$  is 7.9 mm and 8.9 mm deep for experiments SLC01 and SLC02, respectively (see Figure 6-9 and Table 6-7).

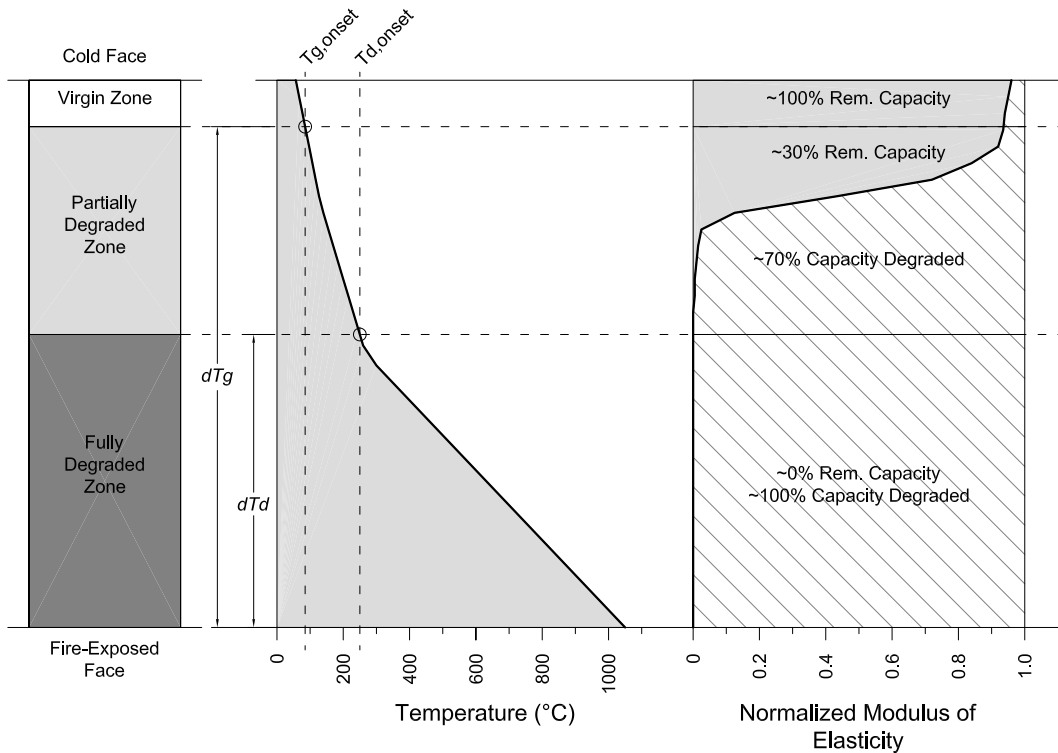
Because the stiffness of the partially-degraded layer,  $E_d$ , is unknown, the rigidity can only be found as a function of  $E_d$ . Using the rigidities derived from the experimentally measured bending stiffnesses, however, it is possible to solve for  $E_d$ . Because this analytical calculation employs experimental results, though, there is no comparison that can be made to judge the accuracy of the prediction. A more useful approach is to assume a percent reduction of  $E_d$  and then solve for the  $EI$ . This calculation is described in the following steps.

First,  $E_d$  is assumed to be 30% of the pre-fire  $E$ . This assumption is based on the fact that most of the degradation in the modulus of elasticity occurs in the immediate vicinity of  $T_{g,onset}$ ; very little reduction occurs in the temperatures approaching  $T_{d,onset}$  (see Figure 6-9). The 30% approximation was found by comparing the area below the  $E/E_0$  curve (representing the remaining stiffness - shown shaded grey) and above the  $E/E_0$  curve (representing stiffness lost - shown hatched). Figure 6-9 shows the temperature profile of a liquid-cooled specimen that was subjected to 120 minutes of fire exposure, though the ratio of the areas above and below the  $E/E_0$  curve is fairly consistent at all exposure times.

---

4. "Onset" values are defined here as the temperate at which a property begins to drop off sharply, while  $T_g$  and  $T_d$  values refer to the temperature where the property declines at the highest rate. With glass transition, for example,  $T_{g,onset}$  is defined as the temperature at which the  $E'$  (storage modulus) curve begins to sharply decline, while  $T_g$  is the peak of the  $\tan-\delta$  curve (see description of dynamic mechanical analysis [DMA] in Chapter 5 - Section 5.1)

Figure 6-9. Relationship of temperature profile to modulus of elasticity by the 3-layer approximation



Just as in the the two-layer model, the next step in the calculation is to find the depth of neutral axis. Once again, this is done by setting the sum of the moments of the areas about the neutral axis equal to zero.

$$A_{ufs}d_{ufs}\eta_{ufs} + A_wd_w\eta_w + A_{lfs}d_{lfs}\eta_{lfs} + A_{deg}d_{deg}\eta_{deg} = 0 \tag{6-9}$$

where  $A$  is the area of the individual part,  $d$  is the distance from the neutral axis to the centroid of the part,  $\eta$  is the ratio of the modulus of elasticity of the part to a reference modulus, and the subscripts  $ufs$ ,  $w$ ,  $lfs$ , and  $deg$  refer to the upper face sheet, web, virgin region of lower face sheet, and degraded region of lower face sheet, respectively. Each  $d$  term is expanded to be expressed in terms of the depth of the neutral axis so that there is only one unknown. For experiments SLC01 and SLC02, the neutral axis is found to be at 66.0 mm and 61.9 mm, respectively, from the top of the upper face sheet.

Next, the moment of inertia of the each area about the neutral axis calculated:

$$I_{ufs} = \frac{1}{12} b_{ufs} h_{ufs}^3 + A_{ufs} d_{ufs}^2 \quad (6-10)$$

$$I_w = \frac{1}{12} b_w h_w^3 + A_w d_w^2$$

$$I_{lfs} = \frac{1}{12} b_{lfs} h_{lfs}^3 + A_{lfs} d_{lfs}^2$$

$$I_{deg} = \frac{1}{12} b_{deg} h_{deg}^3 + A_{deg} d_{deg}^2$$

Finally, the rigidity is found by summing all of the rigidities of the individual components.

$$EI = E_w I_w + E_f I_{ufs} + E_f I_{lfs} + 0.3 E_f I_{deg} \quad (6-11)$$

The results of this calculation are shown in the following table (see Chapter 5 - Section 8.6.2 for a explanation of how  $S$  was derived from measured values). The values required to solve Equations 6-9 and 6-10, which are dependent on  $d_{Tg}$  and  $d_{Td}$ , are provided in Table 6-8.

Table 6-7. Rigidity predictions by the three-layer model

Experiment	$d_{Tg}$ mm	$d_{Td}$ mm	$EI$ from 3-Layer Model N·mm <sup>2</sup>	$EI$ from Measured $S$ N·mm <sup>2</sup>	Disparity <sup>a</sup> %
SLC01	13.8	7.9	$3.38 \times 10^{12}$	$3.50 \times 10^{12}$	-3
SLC02	15.1	8.9	$3.06 \times 10^{12}$	$3.25 \times 10^{12}$	-6

a. Disparity = (calculated - measured) / measured

Thus, the three-layer model with the temperature criterion and the assumption that  $E_d = 0.30E$  predicts the post-fire rigidity of the sections with nearly the same accuracy (within 10%) as the two-layer model when compared to the experimentally derived rigidities.

Table 6-8. Values entered into Equations 6-9 and 6-10 to solve for the  $EI$  values shown in Table 6-7

$d_{Tg}$ (mm)	$d_{Td}$ (mm)	$\eta_{ufs},$ $\eta_{lfs}$	$\eta_w$	$\eta_{deg}$	$A_{ufs}$ (mm <sup>2</sup> )	$A_w$ (mm <sup>2</sup> )	$A_{lfs}$ (mm <sup>2</sup> )	$A_{deg}$ (mm <sup>2</sup> )	$d_{ufs}$ (mm)	$d_w$ (mm)	$d_{lfs}$ (mm)	$d_{deg}$ (mm)	$b_{ufs},$ $b_{lfs},$ $b_{deg}$ (mm)	$b_w$ (mm)
13.8	7.9	1	0.82	0.30	15,350	11,480	2,740	5,390	56.6	31.3	113.3	117.7	913.6	71.3 <sup>a</sup>
15.1	8.9	1	0.82	0.30	15,350	11,480	1,553	5,660	53.5	35.4	116.7	120.7	913.6	71.3 <sup>a</sup>

a. Combined width of seven individual webs - see Figure 5-2

### 2.3 Post-Fire Safety of the Proposed System

In the case of fire, the load-bearing FRP portions of the wall and floor systems are well protected by the internal liquid-circulation system. Water flowing on the inside of the panels absorbs the heat produced by the fire and channels it away from the effected area. This maintains some portion of the cross section below the glass-transition temperature (the temperature at which the stiffness of the material greatly reduces). In the case where extreme exposure and physical ablation combine to cause a burn-through, a primitive sort of sprinkler system is created.

The physical experiments using the liquid cooling system on a similar FRP element have shown that the material on the interior surfaces remains essentially at the same temperature as the liquid, even when the outer faces exceed 1000°C (see Chapter 5 - Section 7). Even after two hours of severe fire exposure, the inner 20% of the thickness of the face sheets were found to be still structurally sound. To satisfy the code-required 90 minute structural fire endurance time [167] with a moderate margin of safety, therefore, the panels should be capable of supporting full design loads with only 20% of the thickness of the face sheet remaining on the fire-exposed side.

The carbon tendon system, on the other hand, is not protected by the liquid circulation system. Though the steel portions would be coated with standard spray fire-proofing and the carbon tendons themselves retain their tensile capacity fairly well in fire,<sup>5</sup> the worst-case scenario must be considered. In this scenario, it is assumed that there is no structural contribution from the carbon tendon system and that no resistance is provided by the outer 80% of the lower face sheet. In this section, the resistance factor of safety,  $\gamma_R$ , at the ultimate limit state, *uls*, is calculated for a typical set of support, span, and loading conditions common in commercial multi-story buildings using the properties of the experimental material.

Following the Load and Resistance Factor Design methodology (LRFD) [1], the estimation of the loads is followed by the calculation of the resistance. Prescribed “ $\gamma$ ” factors are then applied to magnify the loads and reduce the resistance. Once again, the resistance factor of safety,  $\gamma_R$ , is a factor by which the material resistance,  $R$ , is larger or smaller than stresses resulting from the factored dead and live loads, as shown in Equation 6-12.

$$DL \cdot \gamma_{DL} + LL \cdot \gamma_{LL} = \frac{R}{\gamma_R} \quad (6-12)$$

---

5. FRP members are far more sensitive to heat-induced weakening in matrix-critical stress states such as compression and shear than in pure tension. This phenomenon is discussed further in Section 3.2.8.1.

### 2.3.1 Loads

In the following verification, a unit width of the flooring system is considered. A free span of 7.62 m (25 feet) was chosen as it is a typical column spacing in commercial buildings.

#### *Dead Loads*

Dead loads are loads on a structure that do not change significantly after the completion of the building. The first step in the calculation of these loads is to determine the self-weight of the structure itself. The mass,  $m_{FRP}$ , of the FRP panels is thus:

$$m_{FRP} = \rho V = \left(1890 \frac{\text{kg}}{\text{m}^3}\right)(0.039 \text{ m}^2)(7.62 \text{ m}) = 562 \text{ kg} \quad (6-13)$$

where  $\rho$  is density (the density of the experimental material is used) and  $V$  is the volume of one panel 1 m wide and 7.62 m long (assuming no loss in cross-section). Next, the mass of the water filling the internal cells is added.

$$m_{WATER} = \rho V = \left(1000 \frac{\text{kg}}{\text{m}^3}\right)(0.114 \text{ m}^2)(7.62 \text{ m}) = 869 \text{ kg} \quad (6-14)$$

For a panel width of 1.00 m and length of 7.62 m, the total floor area of one panel is 7.62 m<sup>2</sup>. Thus, the total dead load per unit area,  $DL$ , is calculated as the sum of the mass of the water and FRP, plus a superimposed dead load,  $SDL$ , of 45 kg/m<sup>2</sup> (added to account for floor finishes, mechanical equipment, suspended ceilings, etc.). The masses are translated to forces by multiplying by the acceleration of gravity.

$$DL = \left[ \frac{(m_{WATER} + m_{FRP})}{A} + SDL \right] g = \left[ \frac{(869 \text{ kg} + 562 \text{ kg})}{7.62 \text{ m}^2} + 45 \frac{\text{kg}}{\text{m}^2} \right] \left( 9.81 \frac{\text{N}}{\text{kg}} \right) = 2.28 \frac{\text{kN}}{\text{m}^2} \quad (6-15)$$

Thus, the total dead load on the floor panels is estimated to be 2.28 kN/m<sup>2</sup>.

#### *Live Loads*

Live loads are loads that may change during the life of the structure, including loads that change quickly and often, such as people and wind, as well as loads that change infrequently, such as furniture and partitions. Since these loads cannot be calculated without an intimate knowledge of the loads that will be placed on the structure, building codes provide design values. In residential and commercial buildings, public meeting spaces incur the heaviest live loads (excluding special cases such as libraries). For such spaces, the ASCE recommends a distributed live load of 4.79 kN/m<sup>2</sup> [5].

### Total loads

The total factored linear load,  $\gamma_L w$ , acting on one floor panel is calculated as the sum of the factored live loads and dead loads divided by the width of the panel,  $b$ . Under the Load and Resistance Factor Design method [1], a load magnification factor,  $\gamma_L$ , is employed to allow for statistical aberrations and unexpected loading conditions. The factor is higher for live loads because there is greater uncertainty in their prediction.

$$\gamma_L w = (\gamma_{DL} DL + \gamma_{LL} LL) b = \left[ 1.2 \left( 2.28 \frac{\text{kN}}{\text{m}^2} \right) + 1.6 \left( 4.79 \frac{\text{kN}}{\text{m}^2} \right) \right] (1.00 \text{ m}) = 10.4 \frac{\text{kN}}{\text{m}} \quad (6-16)$$

With simple supports and the uniformly-distributed load calculated above, the maximum moment applied to the panel occurs at the mid-span and is equal to the following:

$$\gamma_L M_w = \frac{\gamma_L w L^2}{8} = \frac{\left( 10.4 \frac{\text{kN}}{\text{m}} \right) (7.62 \text{ m})^2}{8} = 75.5 \text{ kN-m} \quad (6-17)$$

### 2.3.2 Resistance

To calculate the bending resistance of the panel, three values are required: the moment of inertia of the fire-damaged cross-section,  $I_d$ , is the distance from the neutral axis to the outmost face of the fire-damaged section,  $c_d$ , and the ultimate strength of the material,  $f_u$ . The first two values are calculated from the geometry of the cross section assuming only the inner 20% of the lower face sheet remains. The third value is adopted from measurements on the experimental material [199]. Without the consideration of other failure modes such as buckling, punching, shear, etc., the capacity of the panel in pure bending,  $M_u$ , is estimated by Equation 6-18.

$$\sigma = \frac{M c}{I} \rightarrow M = \frac{\sigma I}{c} \rightarrow M_u = \frac{f_u I_d}{c_d} = \frac{(2.60 \times 10^8 \text{ Pa})(1.50 \times 10^{-4} \text{ m}^4)}{0.096 \text{ m}} = 406 \text{ kN-m} \quad (6-18)$$

### 2.3.3 Resistance Factor of Safety

The resistance factor of safety of the flooring system is the factored ultimate resistance divided by the factored load [1]. For the values derived above, the factor of safety is thus:

$$\gamma_R = \frac{M_u}{\gamma_L M_w} = \frac{406 \text{ kN-m}}{75.5 \text{ kN-m}} = 5.4 \quad (6-19)$$

meaning that even in the scenario where the entire surface of floor is loaded by the maximum imaginable load and that fire has destroyed the carbon tendon system and 80% of the lower face sheet (corresponding to roughly 2 hours of extreme fire exposure), the system's resistance is still 5.4 times greater than the load (for the loading, support, and span conditions considered).

### 3 Numerical Modeling

Closed-form analytical solutions are convenient for static problems with fixed material properties. A set of equations can be solved to produce an exact solution. As the level of complexity of the problem definition is increased, however, the level of the complexity of the analytical solution increases at a disproportionately high rate. The consideration of non-linear material properties in transient analyses, where both the boundary conditions and the response of the system are time-dependent, complicates matters so thoroughly that analytical solutions are rarely sought for such problems. In such cases, numerical modeling methods become economical and are the more suitable approach.

The ultimate goal of the modeling effort was to be able to accurately simulate the structural behavior of an element of the building system in ambient, fire, and post-fire conditions. This requires the consideration of several different interacting phenomena. A reliable and systematic approach to creating complex coupled models is to first create separate simpler models that treat each phenomenon separately. Without the interaction of phenomena, validation by physical experimentation is greatly simplified. When each of the simpler models is validated, they may then be merged into a more complex coupled model.

With respect to the proposed system, there was an additional motivation for the division of the model into separate simpler models: accuracy. Because the relevant thermal phenomena can be adequately represented by a two-dimensional model, the computational savings in geometrical complexity could be expended on greater mesh refinement and smaller time stepping. With sharply changing non-linear material properties, these refinements proved necessary to achieve solution convergence. Refinement of the 3-D model was not only impractical because of the already lengthy calculation times (spanning several days), but in fact, impossible because of the limited number of nodes allowed under the institute's educational software license.

Thus, separate models were developed for the mechanical and thermal behavior. The mechanical model simulates the response of an FRP element under static structural loading. The thermal model simulates the same material under thermal loading. Later, when the behavior of both models was validated by experimental data, the structural model was expanded to include many aspects of the thermal model.

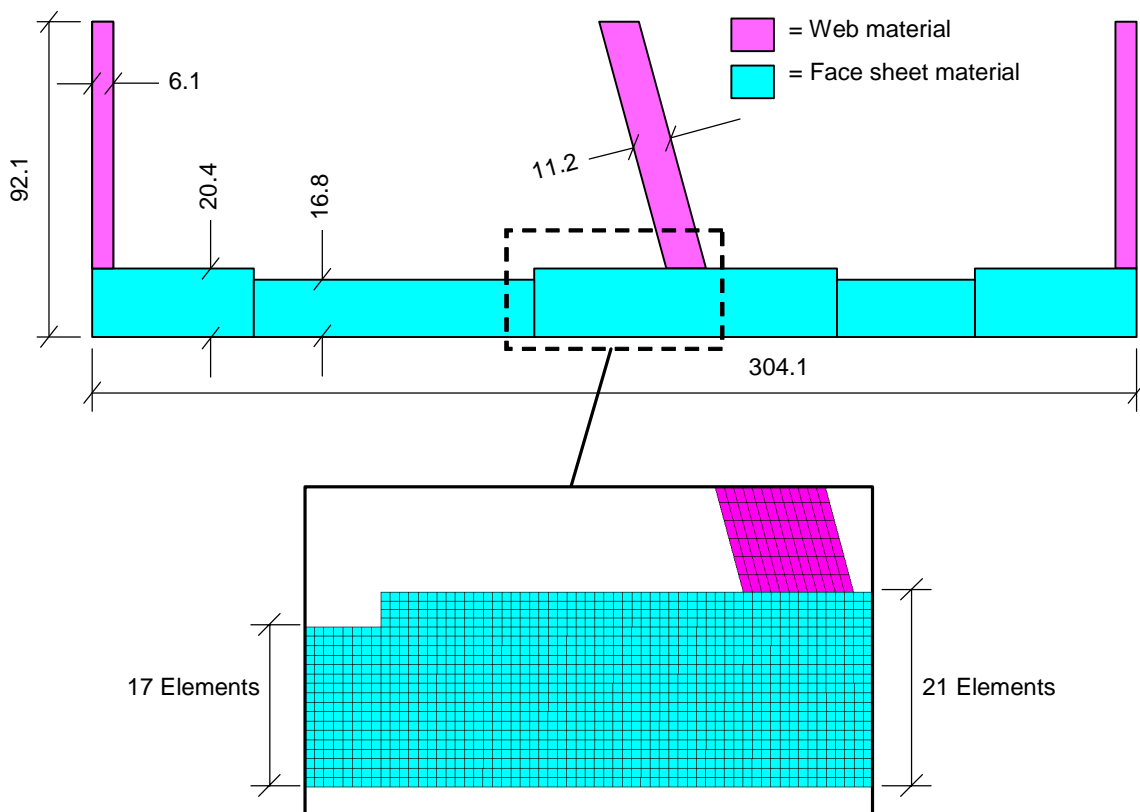
The source code for each of the two models is provided in Appendix D. A description of these models and a summary of their results is provided in the following sections.

### 3.1 Numerical Thermochemical Model

#### 3.1.1 General Description

The numerical thermochemical model simulates the flow of heat and the change in temperature of the FRP components used in the large-scale physical experiments. The component is heated from below and may be cooled on the interior surfaces by flowing water. The required input data includes temperature-dependent material properties (density, thermal conductivity, specific heat capacity), system parameters (geometrical dimensions), time and temperature dependent boundary conditions (convective heat transfer coefficients, emissivity/absorptance), and loading parameters (bulk gas temperature, time of exposure). The most important output data is the temperature distribution. The geometry, material distribution, and meshing are shown in Figure 3.1.3.

Figure 6-10. 2-D Thermochemical model geometry and meshing (dimensions in mm)

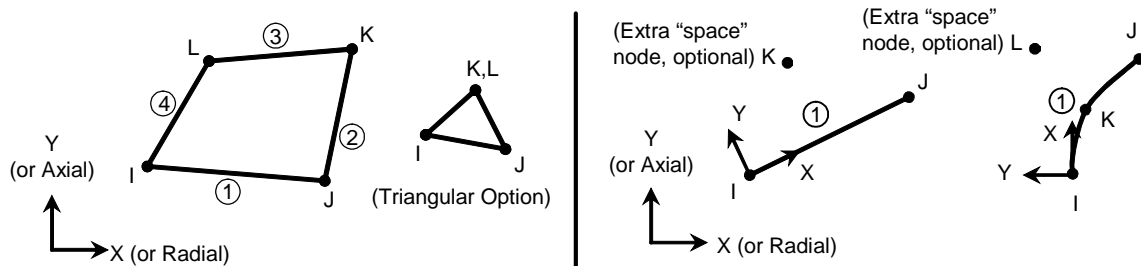


Though some variation of temperatures is seen with respect to the long axis of the element under consideration due to uneven oven heating and the warming of the liquid coolant along the 7.0 m flow path, the important thermal phenomena take place in only two dimensions. Heat flows from the fire side through the element and into the liquid coolant, dispersing

laterally as a result of geometrical irregularities (differences in face sheet thickness, webs, etc.). No heat flows in the third dimension because the conditions are nearly identical at all sections. Therefore, the thermal phenomena taking place in true conditions could be adequately represented by a two-dimensional cross-section [31].

As in all of the modeling efforts, the commercial software package *ANSYS Multiphysics* Version 7 was employed. The Plane-55 element was used to construct the model. The 2-D thermal element has either 3 or 4 nodes with only one degree of freedom (temperature) at each node, and is thus mathematically economical. In addition, the SURF-151 surface effects element was used to model the radiative heat transfer at the hot face (see Figure 6-11). The 1-D thermal element can be overlaid on any 2-D elements and has either 2 or 3 nodes. Once again, the nodes have only one degree of freedom: temperature. To model ambient radiation (radiation from a surface to the environment), the Surf-151 elements can be linked to an extra “space” node that represents the environment [201].

Figure 6-11. ANSYS element geometry: Plane-55 (left), Surf-151 (right) [201]

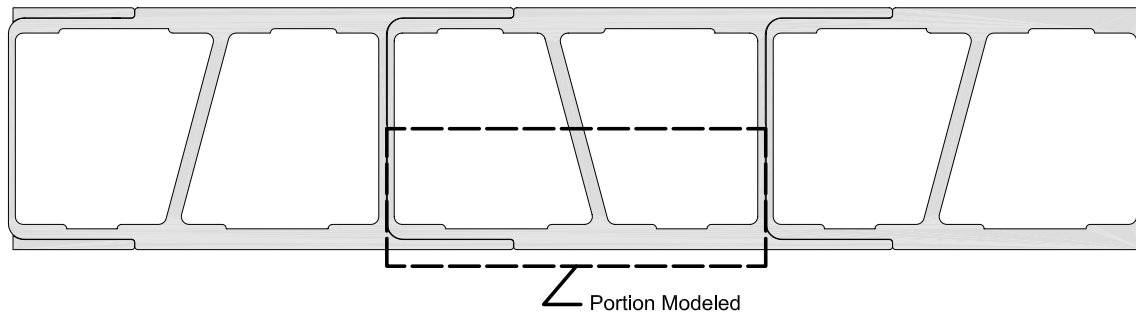


### 3.1.2 Geometrical Simplifications

As previously discussed, the most significant geometrical simplification was made by reducing the model from three to two dimensions. Further, the three pultruded sections bonded in the transverse direction were approximated by only one section (bonded joints were not considered). The single-section model incorporates all of the geometrical variety that exists transversely across the entire specimen and is thus a representation of an infinitely wide section. In addition, the filleted corners were squared off to enable the design of a high-quality mapped mesh. Finally, the lack of thermal activity in the upper portion of the section<sup>6</sup> permitted the consideration of only the lower half (see Figure 6-12).

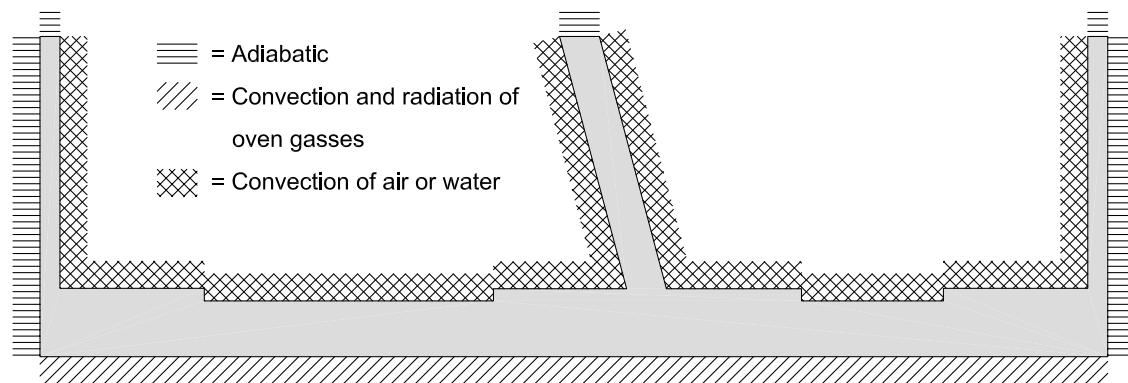
6. Measurements in the physical experiments confirmed that, in the case of liquid cooling, there was no measurable change in temperature at even one-quarter of the height of the webs connecting the lower face sheet to the upper face sheet (see Appendix B Figure B-15).

Figure 6-12. Portion of experimental specimen considered in 2-D thermochemical model



### 3.1.3 Boundary Conditions

Figure 6-13. 2-D Thermochemical model boundary conditions



#### 3.1.3.1 Internal Liquid Interface

Water flowing through the interior cells of the specimen were represented by a convective heat transfer boundary condition (see Figure 6-13). For forced flow through a rectangular tube, the convective heat transfer coefficient,  $h_c$ , is dependent on the Nusselt number,  $N_u$ :

$$h_c = \frac{N_u \lambda}{d_b} \quad (6-20)$$

where  $d_b$  is the hydraulic diameter and  $\lambda$  is the thermal conductivity of the fluid. For flow through a rectangular tube of width  $a$  and height  $b$ , the hydraulic diameter is defined as [146 pg. 194]:

$$d_b = \frac{2ab}{a+b} \quad (6-21)$$

Several empirical correlations have been proposed between the flow velocity and Nusselt number [69] [105] [150] [152]. To choose the most appropriate version, it is first necessary to

find the Reynolds number,  $\Re$ , that describes the turbulence of the fluid flow. For incompressible fluids, this is calculated according to the following equation [146 pg. 164]:

$$\Re = \frac{\rho V_{fl} d_b}{\eta} \quad (6-22)$$

where  $\rho$  is the density of the fluid,  $V_{fl}$  is the fluid flow velocity, and  $\eta$  is the dynamic viscosity. Flow conditions with Reynolds numbers up to 2,300 are generally considered to be laminar, between 2,300 and 4,000 transitional, and above 4,000 turbulent [146 pg. 238]. As shown in Table 6-9, the Reynolds numbers for the experiments performed indicate that flow was transitional in SLC01, turbulent in LC02, and laminar in all the rest. In reality, however, the path within the specimens was not long enough to develop consistent flow conditions. The turbulent flow at the inlets and outlets significantly effected the flow within the cells. Thus, a mixed turbulent/laminar empirical correlation (Gnielinski) was used to calculate the Nusselt number [69]:

$$N_u = \sqrt{N_{u,turb}^2 + N_{u,lam}^2} \quad (6-23)$$

where  $N_{u,turb}$  is calculated by the Petukhov correlation [150]:

$$N_{u,turb} = \frac{0.037 \cdot \Re^{0.8} \cdot P_r}{1 + 2.443 \cdot \Re^{-0.1} (P_r^{2/3} - 1)} \quad (6-24)$$

and the  $N_{u,lam}$  is calculated by the Pohlhausen correlation [152]:

$$N_{u,lam} = 0.664 \cdot P_r^{1/3} \cdot \Re^{1/2} \quad (6-25)$$

and  $P_r$  is the Prandtl number, which is defined by the following equation [47 pg. 51]:

$$P_r = \frac{C_p \eta}{\lambda} \quad (6-26)$$

where  $\eta$  is the dynamic viscosity of the fluid. The resulting convective heat transfer coefficients are shown as a function of flow velocity in Table 6-9. The values used to calculate the convective heat transfer coefficients shown in Table 6-9 that are not dependent on the flow velocity are provided in Table 6-10. The properties of the water were simplified as constant values because their variation within the range of temperatures encountered (20-50°C) is relatively insignificant.

Table 6-9. Values relating to convection of water in function of fluid flow velocity,  $V_{fl}$ 

Experiment	$V_{fl}$ (cm/s)	$\Re$ (unitless)	$N_{u,lam}$ (unitless)	$N_{u,turb}$ (unitless)	$N_u$ (unitless)	$h_c$ (W/m <sup>2</sup> ·K)
LC03	<b>0.2</b>	297	21.7	-	21.7	<b>90</b>
LC01	<b>1.0</b>	1,490	48.4	-	48.4	<b>200</b>
SLC02	<b>1.3</b>	1,930	55.2	-	55.2	<b>230</b>
SLC01	<b>2.5</b>	3,720	76.6	46.7	89.7	<b>370</b>
LC02	<b>5.0</b>	7,430	-	87.4	87.4	<b>360</b>

Table 6-10. Values relating to convection of water not dependent on flow velocity

$d_h$ (m)	$\rho$ (kg/m <sup>3</sup> )	$C_p$ (J/kg·K)	$\lambda$ (W/m·K)	$P_r$ (unitless)	$\eta$ (K/m·s)
0.146	997	4,179	0.604	6.78	9.80x10 <sup>4</sup>

### 3.1.3.2 Hot Face

The hot face of the specimen was represented by convective and radiative heat transfer boundary conditions.

#### *Convective Heat Transfer*

While radiation is the more dominant mode of heat transfer in fires, a significant contribution is made through convection as well [184 pg. 6.17]. The convective heat flux,  $q_c$ , is calculated through Newton's Law of Cooling [146 pg. 8]:

$$q_c = h_c (T_{sur} - T_{\infty}) \quad (6-27)$$

where  $h_c$  is the convective heat transfer coefficient,  $T_{sur}$  is the temperature of surface, and  $T_{\infty}$  is the bulk fluid temperature (temperature of the oven gasses). As all of the experiments were performed according to the ISO 834 cellulosic time-temperature curve,  $T_{\infty}$  was defined as a function of time according to Equation 5-1.

As described in the previous section,  $h_c$  is dependent on the Nusselt number,  $N_u$ :

$$h_c = \frac{N_u \lambda}{L_{pl}} \quad (6-28)$$

This equation is slightly different than Equation 6-20 because it refers to external flow over a flat plate rather internal flow within a tube. The hydraulic diameter term,  $d_h$ , is therefore

replaced by the length of the plate in the direction of the flow,  $L_{pl}$ . This replacement is also made in the calculation of the Reynolds number:

$$\Re = \frac{\rho V_{fl} L_{pl}}{\eta} \quad (6-29)$$

There are several uncertainties in the estimation of  $h_c$  at the hot face [189]. As  $h_c$  is dependent on  $N_u$  (Equation 6-28), and  $N_u$  is dependent on  $\Re$  (Equations 6-24 and 6-25), the calculation of  $h_c$  is strongly influenced by the estimation of the fluid flow velocity and the length of the plate. The fluid flow velocity was not experimentally measured and, from visual observation, appeared to vary widely with location and time. The estimation of the length of the plate is not easily estimated either. Because the gasses could flow in any direction,  $L_{pl}$  could refer to the long direction of the specimen (2.75 m), the short direction (0.91 m), or an even shorter direction in the corners (the specimens were placed in a recess approximately 40 cm deep - See Figure 6-14). It is further necessary to estimate the properties of the gasses. This requires the knowledge of which gasses are actually in the oven (a mixture of air and the combustion products from the oil burners and the specimen) and the pressure that they are under (the oven's ventilation system causes the internal pressure to be lower than atmospheric). The influence of these two factors ( $V_{fl}$  and  $L_{pl}$ ) is illustrated in Table 6-11.

**Table 6-11.** Convective heat transfer of air at 27°C on a flat plate in function of fluid flow velocity and plate length (using Petukhov correlation - see Equation 6-24), material properties from [105 pg. 714]

$V_{fl}$ (m/s)	$L_{pl}$ (m)	$\rho$ (kg/m <sup>3</sup> )	$\eta$ (K/m·s)	$C_p$ (J/kg·K)	$\lambda$ (W/m·K)	$\Re$ (unitless)	$P_r$ (unitless)	$N_u$ (unitless)	$h_c$ (W/m <sup>2</sup> ·K)
<b>0.10</b>	2.75	1.1774	1.846x10 <sup>-5</sup>	1006	0.0262	17,540	0.71	80.2	<b>0.78</b>
10	0.2	1.1774	1.846x10 <sup>-5</sup>	1006	0.0262	127,550	0.71	377	<b>49.4</b>

As shown in Table 6-11,  $h_c$  varies by more than a factor of 50 within the range of imaginable flow conditions. Thus, rather than guessing the values to use in the model at random, a parametric study was performed to determine the set of values that results in the best agreement between predicted and experimentally measured temperatures. The result is a convective heat transfer coefficient that increases linearly with the temperature of the oven gasses from  $h_c = 5 \text{ W/m}^2\cdot\text{K}$  at 20°C to  $h_c = 50 \text{ W/m}^2\cdot\text{K}$  at 1000°C. This result appears reasonable as the Eurocode 1 Part 1.2 recommends a simple constant value of  $25 \text{ W/m}^2\cdot\text{K}$  for real building fires [32].

Figure 6-14. View of recessed specimen from within oven (Exp. SLC01 - see Chapter 5 Section 8)



### *Radiative Heat Transfer*

Radiation was approximated as emitting from a black-body ambient cloud rather than from the interior surfaces of the oven [189]. Though air is essentially transparent to radiation, many combustion products including carbon dioxide, carbon monoxide, and soot have high emissivities [192]. With the quantity of burning hydrocarbons within the oven, this approximation is, at worst, slightly too severe. Moreover, it is a simplification that avoids the problematic estimation of the oven lining's temperature lag and emissivity.

The heat transferred through radiation is calculated using the Stefan-Boltzmann law, where the net radiative heat flux,  $q_r$ , is equal to [105 pg. 32]:

$$q_r = \epsilon_r \sigma_r (T_\infty^4 - T_{sur}^4) \quad (6-30)$$

where  $\epsilon_r$  is the emissivity of the solid surface and  $\sigma_r$  is the Stefan-Boltzmann constant (values listed in Table 6-12).

### *Combined Convection and Radiation*

The total heat flux,  $q$ , is the sum of the convection and radiation modes as written in the following equation.

$$q = q_c + q_r = h_c (T_{sur} - T_\infty) + \epsilon_r \sigma_r (T_\infty^4 - T_{sur}^4) \quad (6-31)$$

The thermal conditions are nearly symmetrical at the boundaries between adjacent pultruded profiles such that no thermal gradient exists. With no thermal gradient there can be no heat transfer, and thus these borders were assigned adiabatic boundary conditions ( $q=0$ ).

Table 6-12. Values relating to radiative and convective heat transfer at the hot face

$T_{\infty}$ (°C)	$h_c$ (W/m <sup>2</sup> ·K)	$\epsilon_r$ (unitless)	$\sigma_r$ (W/m <sup>2</sup> ·K <sup>4</sup> )
ISO 834 curve [92]	5-50 (linear from 20°C-1000°C)	0.75-0.95 (linear from 20°C-1200°C) [160]	$5.67 \times 10^{-8}$ [105 pg. 30]

### 3.1.4 Special Considerations

#### 3.1.4.1 Endothermic Decomposition

Though the burning of organic matrix composites is an exothermic process, the stage of chemical decomposition is quite endothermic. The energy that is used to decompose the polymer is no longer available as heat. Thus, a large portion of the energy transferred from the fire to the material is absorbed by the chemical decomposition of the resin and does not cause a change in temperature of the remaining materials. A strong analogy can be drawn to the latent heat required to cause phase changes in water. A simple example will be elaborated to illustrate the importance of this phenomenon.

The change in temperature of an object is related to the input energy according to the following equation:

$$\Delta Q = \int_{T_i}^{T_f} m C_p dT \quad (6-32)$$

Where  $Q$  is the input energy,  $m$  is the mass,  $C_p$  is the specific heat capacity, and  $T_i$  and  $T_f$  are the initial and final temperatures, respectively. To calculate the amount of energy required to bring a 1 kg mass of glass fiber-reinforced polyester composite with  $C_p = 1,170$  J/kg·K from 20°C to its decomposition temperature (300°C), the calculation follows (mass and specific heat capacity constant with temperature):

$$\Delta Q = (1 \text{ kg}) \left( 1170 \frac{\text{J}}{\text{kg} \cdot \text{K}} \right) (300^\circ\text{C} - 20^\circ\text{C}) = 328 \text{ kJ} \quad (6-33)$$

Thus, 328 kJ of energy is required to change the temperature of the mass by 280°C. The decomposition of the resin, on the other hand, is calculated by the equation:

$$\Delta Q = q_d m \quad (6-34)$$

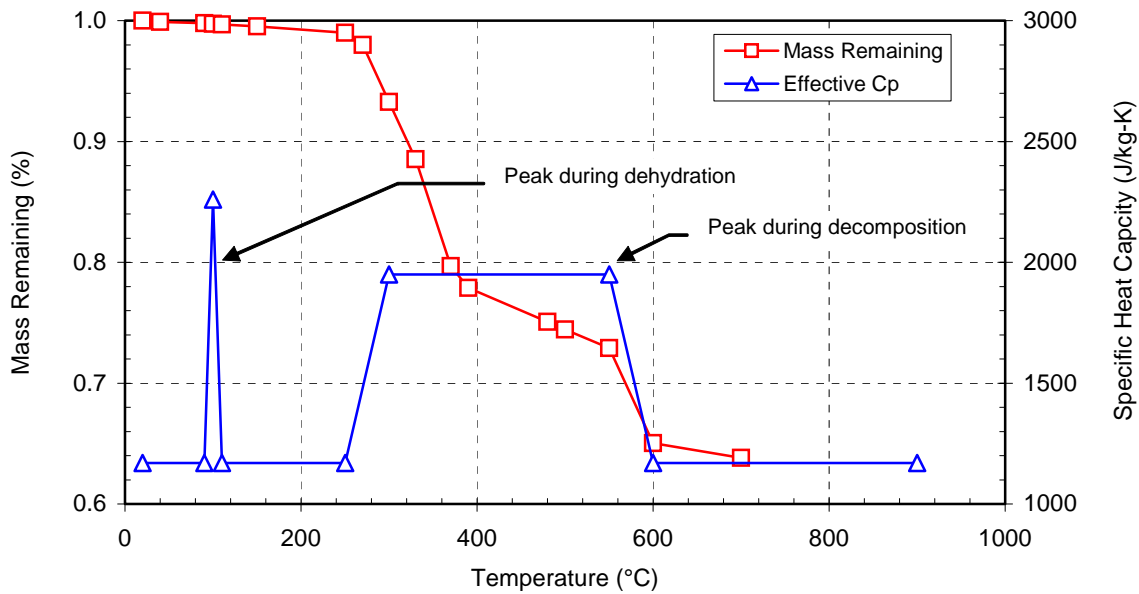
where  $q_d$  is the heat of decomposition by mass. To calculate the amount of energy required to decompose that same 1 kg mass with  $q_d = 234 \text{ kJ/kg}$  [81], the equation becomes:

$$\Delta Q = \left( 234 \frac{\text{kJ}}{\text{kg}} \right) (1 \text{ kg}) = 234 \text{ kJ} \quad (6-35)$$

Thus, the amount of energy required for the isothermal decomposition of the mass amounts to approximately 70% of the energy required to heat the mass from ambient to the decomposition temperature. In the absence of this energy-sinking effect, that same energy would raise the temperature of the mass and additional  $200^\circ\text{C}$ . Thus, the decomposition of the resin has an enormous influence on the change in temperature of the section.

To incorporate this effect into the numerical model, an “effective” specific heat capacity versus temperature curve was adopted (see Chapter 3 Section 3.1.4.2). Similar to Fanucci’s idealized curve (see Figure 3-36), this curve reflects a simple constant value for the specific heat of the material at all temperatures (the ambient temperature value) except in the range of temperatures in which decomposition occurs. In that range, a large hump is added to the curve such that the area between the constant value of  $C_p$  and effective  $C_p$  is equal to the heat of decomposition of the composite,  $q_d$ . An additional smaller hump in the region of  $100^\circ\text{C}$  reflects the evaporation of absorbed moisture (see Figure 6-15).

Figure 6-15. Comparison of remaining mass and proposed effective specific heat



As shown in Figure 6-15, steep reductions in mass occur between  $250\text{--}400^\circ\text{C}$  and  $500\text{--}600^\circ\text{C}$  (data from the TGA performed on the test material - see Chapter 5 - Section 5.2). These steep regions show where the decomposition reactions occur, and thus where to place the hump on

the effective specific heat curve. Thus the “width”, or temperature limits of the hump were decided by the TGA data. The “height”, or  $C_p$  limits of the hump were chosen so that the area between the effective and basic curves equals the heat of decomposition,  $q_d = 234$  kJ/kg. Finally, the sides of the hump were inclined to improve stability and solution convergence.

The area under the smaller hump at 100°C represents the evaporation of absorbed water. This area was calculated based on the assumption of 0.5% mass percentage of absorbed water [107]. The latent heat of vaporization of water is 2257 kJ/kg [105 pg. 710]. The area under the curve,  $q_w$ , should therefore equal the product of the mass fraction of water absorbed in the composite and latent heat of water:

$$q_w = \left( 0.005 \frac{\text{kg}_w}{\text{kg}_{\text{frp}}} \right) \left( 2257 \frac{\text{kJ}}{\text{kg}_w} \right) = 11.3 \frac{\text{kJ}}{\text{kg}_{\text{frp}}} \quad (6-36)$$

The shape of the hump that contains this 11.3 kJ/kg was chosen for stability and solution convergence. Although evaporation occurs within a few degrees of boiling (100°C), a triangular hump 2°C wide at the base would need to be 11,300 J/kg·K tall and would cause large instabilities. Spreading this 11.3 kJ/kg over the range from 90°C to 110°C, the peak of the triangular hump can be reduced to a more manageable 1,130 J/kg·K. The exact data points used to define the curve are provided in Table 6-13.

#### 3.1.4.2 Delamination and the Radiative Shielding Effect

A geometrical phenomenon was observed in the physical experiments that proved especially difficult to represent in the thermal model. This phenomenon involved the decomposition and delamination of reinforcement layers from the hot face. Over long exposures to fire, damage to composites proceeds in the following manner:

- The fire-exposed surface heats up. As the coefficient of thermal expansion of the resin is many times greater than that of the fibers, microcracking in the resin occurs [26]. When the composite reaches the decomposition temperature,  $T_d$ , the resin breaks down into various decomposition products. Most important of these decomposition products are the volatile gasses, which cause further microcracking and delamination as they force their way out of the resin. The non-volatile decomposition products and inorganic fillers remain as a fine powder among the fibrous reinforcement. The reinforcement is generally unharmed at these temperatures.
- As temperatures increase and the process advances deeper into the section, the original surface begins to resemble a mess of blackened reinforcement fibers rather than a solid material. Only the anchorage of the fibers outside of the effected area prevent the

reinforcement layers from falling away immediately after the decomposition of the resin. In this anchored position, the contact between the section and the fibers in the effected area is diminished.

- With diminished contact with the cooler section below, the fibers do not benefit from the section's heat sinking effect. Further, the flammable volatile decomposition products continue to pour from the deeper regions and contribute to combustion at the surface. This combustion further increases the temperature of the fibers.
- In time, the temperatures become hot enough to decompose the fibers themselves. As they reach their softening temperature,  $T_s$  at approximately 850°C, their stiffness reduces and they sag under their own weight. Depending strongly on the support conditions and fiber architecture of the specimen, these reinforcement layers will eventually break and fall away from the section.
- The loss of reinforcement layers is always followed by a period of vigorous flaming combustion at the new hot face. Without the shielding effect of the delaminated reinforcement layer below, the new hot face is fully exposed to the radiation of the fire and thus sees a sharp increase in the heat flux.
- The process continues through the section as the resin decomposes, fibers delaminate, sag, and fall away.

In light of the complexity of this mechanism, it is clear that a good deal of simplification and approximation is necessary to create a useful and manageable numerical model. Comparison of earlier models to the physical experiments demonstrated that failing to address this mechanism leads to significant over-prediction of the temperatures profile through the section. If the material that is directly heated by the radiation of the fire is in full contact with the rest of the section, heat is transferred to the deeper layers at an unrealistically high rate. The shielding effect of the delaminated reinforcement layer must be incorporated to achieve accurate results.

Thus, a simple technique was conceived to approximate the complex mechanism. This technique involves the modification of the thermal conductivity at high temperatures to assume *effective* values. Up to  $T_d$ , the thermal conductivity increases according to reported values. Beyond that temperature, however, the conductivity decreases to a very low effective thermal conductivity. The concept of an effective thermal conductivity is commonly employed in situations where, due to non-uniformity, the conductivity of the conglomerate differs significantly from that of its constituents (the effective thermal conductivity of expanded polystyrene, for example, is far lower than the true thermal conductivity of pure polystyrene resin). Fanucci proposed a similar concept for generic charring materials in [51].

### 3.1.5 Material Properties

As described in Section 3.1.1, several temperature-dependent material properties were required to create the thermochemical model ( $C_p$ ,  $\lambda$ ,  $\rho$ ,  $\epsilon_r$ ). These properties are described in the following sections.

#### 3.1.5.1 Specific Heat Capacity, $C_p$ :

The ambient-temperature value of the composite test material was determined through adiabatic calorimetry at the Swiss Federal Laboratories for Materials and Testing (EMPA) in Dübendorf. As discussed in Section 3.1.4.1, the  $C_p$  versus temperature curve was modified to include the heat-sinking effect of the decomposition of the resin and the evaporation of absorbed water. In light of the magnitude of the humps added to the curve, the minor variations in  $C_p$  with temperature become negligible. Thus,  $C_p$  was idealized as a constant value except in the range of water boiling (90-110°C) and resin decomposition (200-500°C). This curve is shown in Figure 6-15 while Table 6-13 provides the exact data points used within the numerical model.

#### 3.1.5.2 Thermal Conductivity, $\lambda$ :

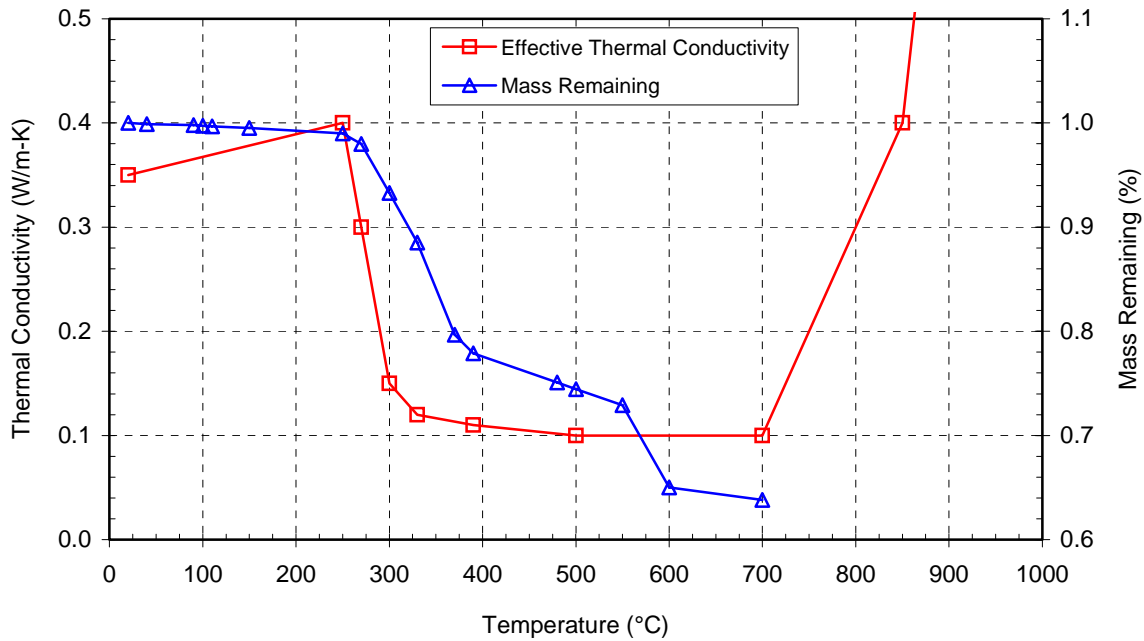
The conductivity versus temperature curve is composed of four segments:

- The ambient-temperature conductivity was determined through adiabatic calorimetry at the Swiss Federal Laboratories for Materials Testing and Research (EMPA) in Dübendorf.
- The curve of the thermal conductivity from ambient temperature to  $T_d$  was adopted from Samanta *et al* [160], who reported the conductivity of a similar material as a linear function of temperature. This trend was proportionally adjusted to match the experimentally measured ambient temperature value.
- Above  $T_d$ , the curve proposed by Fanucci [51] (see Figure 3-37) was adopted. This portion of the curve shows an artificially decreased thermal conductivity that serves to capture the conductivity-reducing effects of cracking and delamination. In effect, the system property of *thermal resistance*, which includes air gaps and reduced contact between surfaces, and cannot be modeled directly is applied instead as an effective material property. The motivation for this approximation is further described in Section 3.1.4.2.
- Approaching the softening temperature of the glass reinforcement,  $T_s$ , the conductivity was artificially increased to approximate the loss of the layer altogether. Although the charred layers temporarily provide insulation, they eventually fall away

from the material. Though the loss of such layers is dependent on several factors in addition to temperature (fiber architecture, support conditions, ablation, mechanical stress, etc.), only temperature dependence could be included in the numerical model.

Thus, the final thermal conductivity versus temperature curve is a combination of measured values, reported values, and “effective” approximations. Figure 6-16 shows this curve in comparison to the remaining mass while Figure 6-13 provides the exact data points used within the numerical model.

**Figure 6-16.** Effective thermal conductivity and density curves used in the thermochemical model



### 3.1.5.3 Density, $\rho$ :

The ambient temperature density was calculated through simple volume and weight measurements. The change in density with respect to temperature was approximated through the assumption that the volume remains constant. As such, the remaining mass curve obtained by thermogravimetric analysis (TGA) (see Chapter 5 Section 5.2) was equated to remaining density. The exact data points used in the numerical model are provided in Table 6-13.

### 3.1.5.4 Emissivity, $\varepsilon$ :

The temperature-dependent emissivity curve was adopted from a recent publication concerned with a very similar material [160]. The exact data points used in the numerical model are provided in Table 6-13.

Table 6-13. Temperature-dependent material properties used in the 2-D thermomechanical model

T (°C)	$\rho$ (kg/m <sup>3</sup> )	T (°C)	$C_p$ (J/kg·K)	T (°C)	$\lambda$ (W/m·K)	T (°C)	$\epsilon_r$ (unitless)
20	1890	20	1170	20	0.35	20	0.75
40	1888	90	1170	250	0.40	1000	0.95
90	1886	100	2300	300	0.15	-	-
150	1881	110	1170	330	0.12	-	-
250	1871	250	1170	500	0.10	-	-
270	1852	270	1482	700	0.10	-	-
330	1673	300	1950	850	0.40	-	-
370	1506	550	1950	900	0.80	-	-
390	1472	600	600	-	-	-	-
480	1419	-	-	-	-	-	-
550	1378	-	-	-	-	-	-
600	1229	-	-	-	-	-	-
850	1172	-	-	-	-	-	-
870	1096	-	-	-	-	-	-

### 3.1.6 Meshing

The irregular shape of the half-section was broken down into eight individual rectangular areas (see Figure 6-10). All segmented lines were concatenated so that only four lines comprised the perimeter of each area. This procedure permitted the use of mapped meshing, which produces the most accurate and efficient solutions. The edge length was limited to 1 mm for the lower face sheet to produce 17 elements across the thinnest portions. The webs were meshed with a slightly coarser 2 mm edge length because of their relatively minor participation in the thermal performance of the section. In all, only 7,575 elements incorporating 7,717 nodes were needed to mesh the solid-body model.

### 3.1.7 Governing Equations

At the fundamental level of heat transfer problems, the finite element software applies first law of thermodynamics, i.e. the law of the conservation of energy. Stated simply, the law stipulates that energy cannot be created or destroyed; it can be converted to another form but the total energy within a domain changes only by the quantity of energy entering or leaving the domain.

This law is expressed mathematically in the following expression that is known as the Heat Equation [105 pg. 56].

$$\nabla^2 T + \frac{q_{gen}}{\lambda} = \left( \frac{\rho C_p}{\lambda} \right) \frac{\partial T}{\partial t} \quad (6-37)$$

The first term represents the net amount of energy conducted out of the system and is derived from the Fourier equation [105 pg. 51]:

$$q = -\lambda \nabla T \quad (6-38)$$

which states that the heat flux,  $q$ , is the product of the vector derivative of the temperature profile,  $T$ , and thermal conductivity,  $\lambda$ . The product is negative to ensure that heat flows from hot to cold. The second term on the left side of Equation 6-37 represents the energy generated or dissipated within the system (such as the endothermic decomposition of the resin). Finally, the term on the right side of the Equation 6-37 represents the change in internal energy of the system.

To complete the formulation of the system, the change in sensible energy within the system, governed by Equation 6-37, is subject to the boundary conditions described in Section 3.1.3.

### 3.1.8 Results

To compare the predictions of the model to experimental results, temperature histories at depths matching the locations of thermocouples in physical experiments are plotted against measured values in Figure 6-17 and Figure 6-18. To compliment this comparison, temperature profiles through the thickness of the specimen are compared at discrete times in Figure 6-19 and Figure 6-20.

As shown in the figures, the agreement is very good between the experimentally measured and numerically predicted temperatures for both the liquid-cooled and dry condition. Average values by experiment are shown in the figures to improve readability. What is not shown is the large deviations that existed between similarly-placed thermocouples in the same experiments (sometimes as much as 200°C - see Figures C-31 to C-33). Overall, the predicted temperatures fall within 28°C of the average measured values.<sup>7</sup> Thus, the numerical predictions fall well within the range of measured values and are very close to the averages.

---

7. Average of difference between measured and predicted temperatures for all curves, calculated at 5 minute intervals for one hour in the dry condition and two hours in the liquid-cooled condition.

Figure 6-17. Comparison of temperature history of the liquid-cooled experiment SLC02 and 2-D thermochemical model (experimental values taken from thermocouple closest in depth to model node)

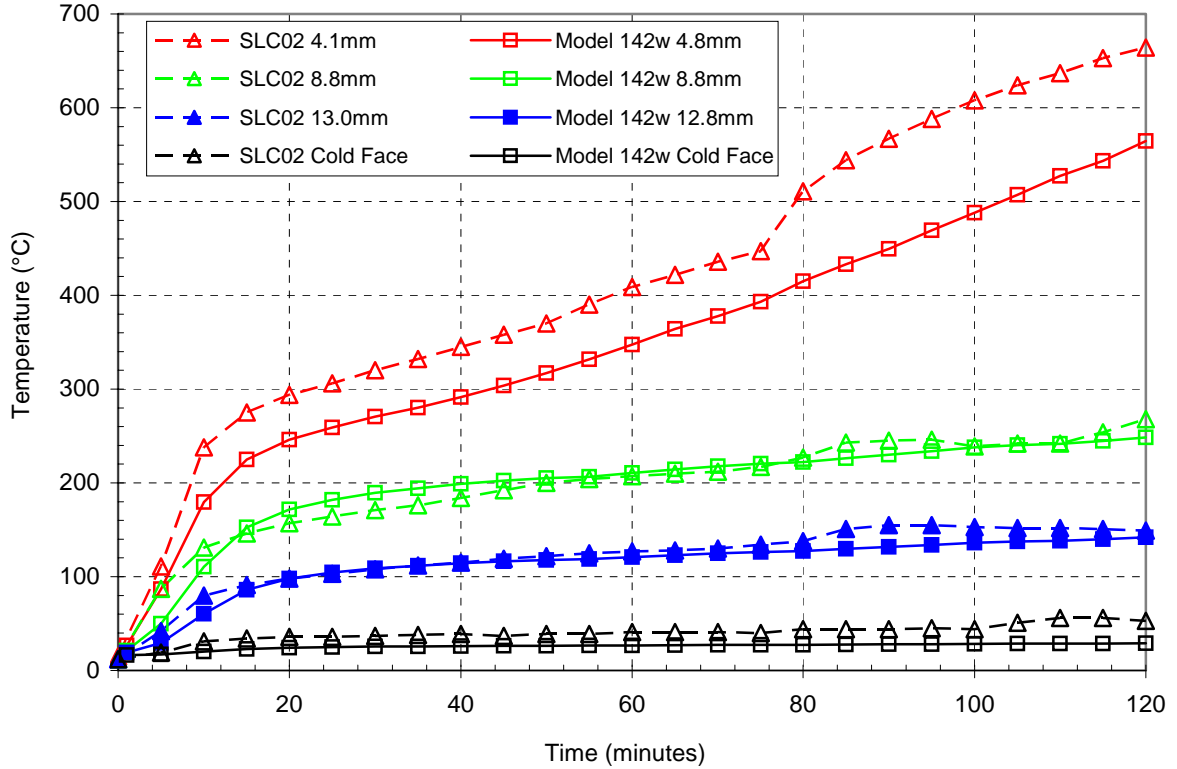


Figure 6-18. Comparison of temperature history of the non-liquid cooled experiment SLC03 and 2-D thermochemical model (experimental values taken from thermocouple closest in depth to model node)

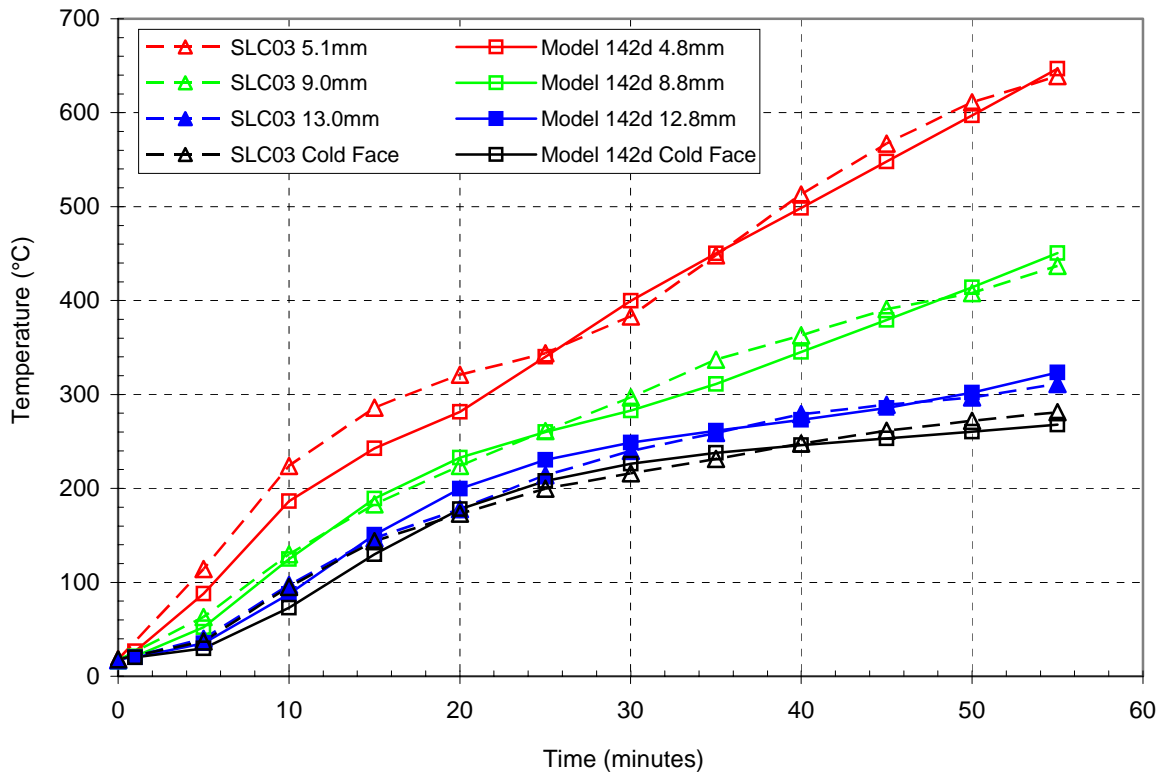


Figure 6-19. Comparison of temperature profiles of all experiments conducted without liquid cooling to the 2-D thermochemical model (average experimental values)

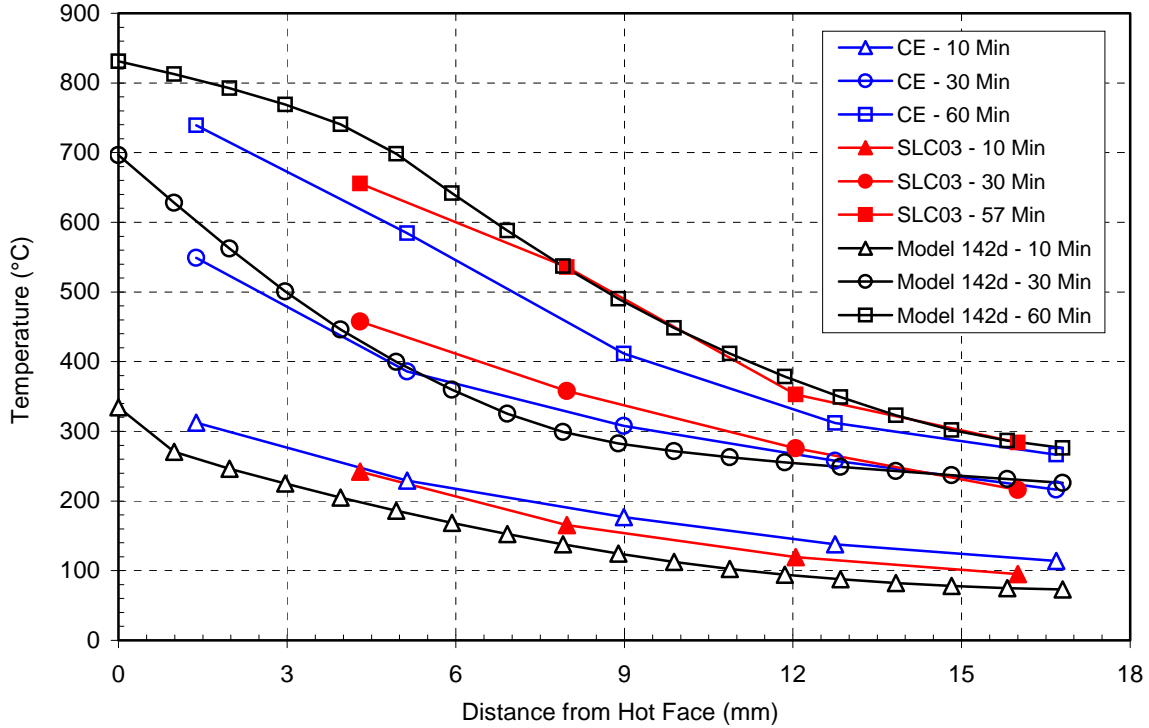
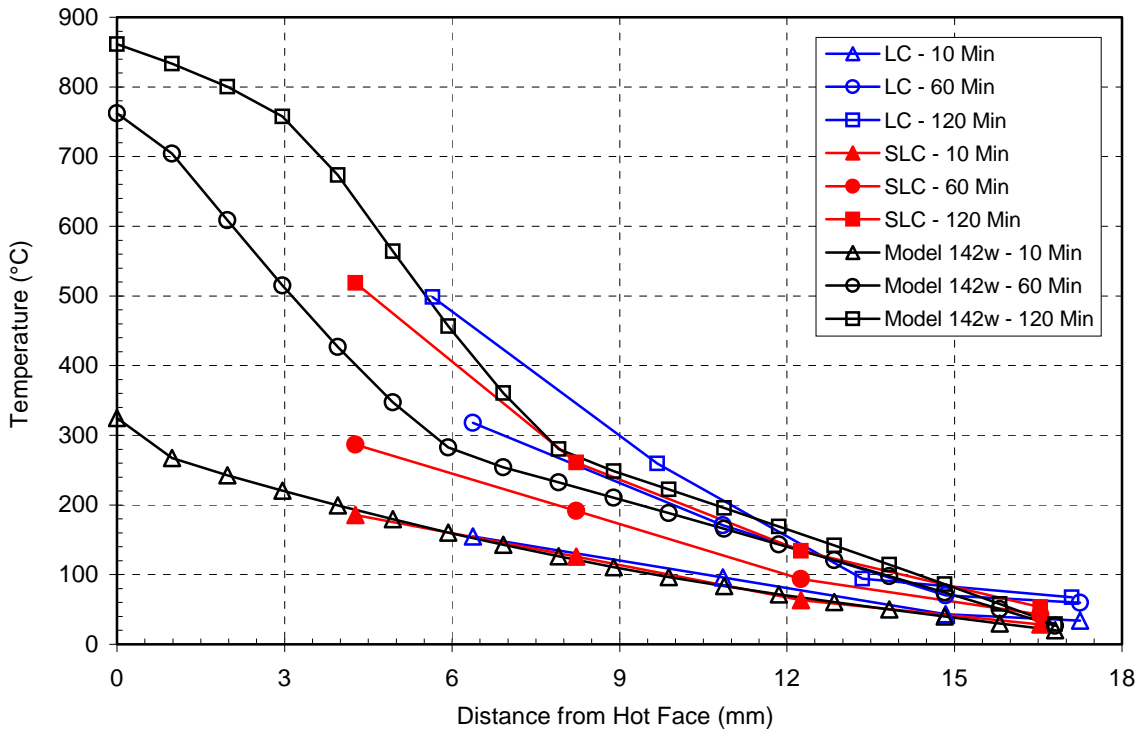


Figure 6-20. Comparison of temperature profiles of all liquid-cooled experiments to the 2-D thermochemical model (average experimental values)



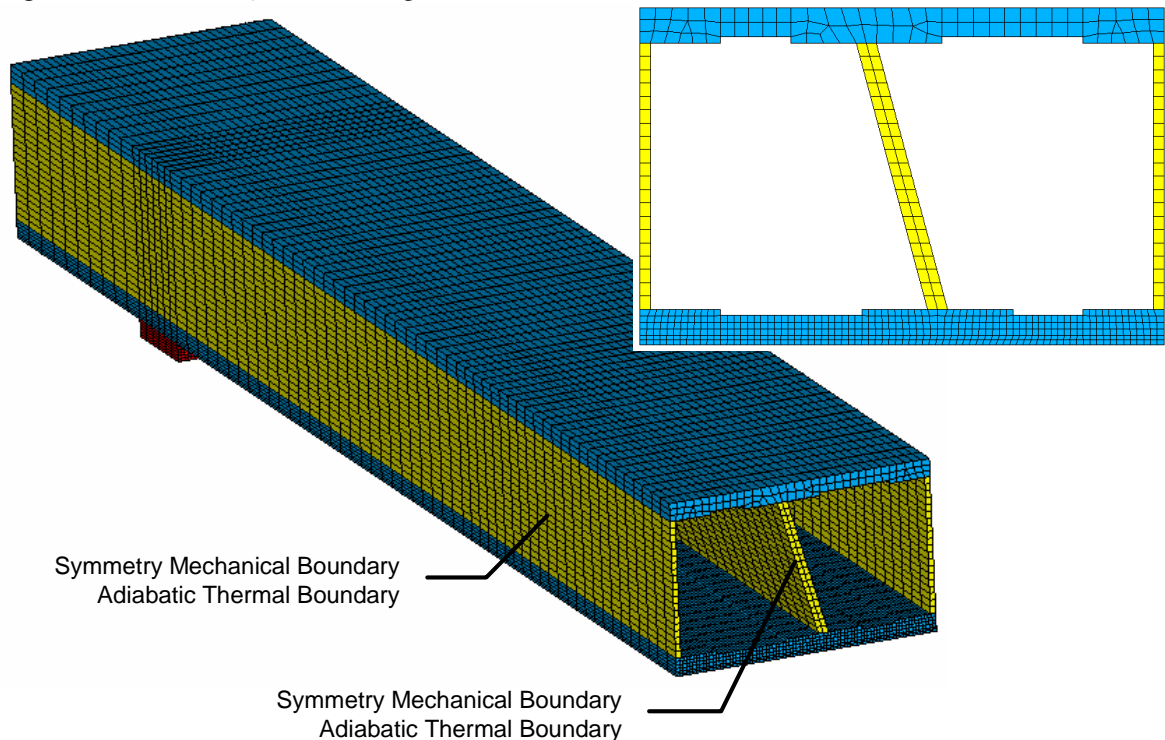
## 3.2 Numerical Thermomechanical Model

### 3.2.1 General Description

Coupling the effects of thermal and mechanically-induced stresses, the numerical thermomechanical model was created to provide the most realistic simulation of the behavior of loaded liquid-cooled FRP sections in fire. The section in the model is based on the dimensions and properties of the material employed in the experimental investigations (see Chapter 5 - Section 2). This section is statically loaded in four-point bending and exposed to fire conditions on the underside. Liquid cooling is simulated on the interior surfaces of the cells and natural air cooling is simulated on the outer surface of the upper face sheet.

The required input data includes material properties that are considered constant with temperature (coefficient of thermal expansion, Poisson ratio), temperature-dependent material properties (modulus of elasticity, shear modulus, density, thermal conductivity, specific heat capacity), system parameters (geometrical dimensions), time and temperature dependent boundary conditions (convective heat transfer coefficients), and loading parameters (mechanical pressures, bulk gas temperatures, time of exposure). The most important output data are the distribution of stresses, strains, and deformations.

Figure 6-21. Geometry and meshing of the 3-D thermomechanical model



Once again, the commercial software package ANSYS Multiphysics Version 7 was employed. The SOLID-5 multiphysical 8-node 3-D element was chosen for its ability to couple thermal and mechanical phenomena (see Figure 3.2.2). There are six degrees of freedom at each node: displacement in three dimensions, temperature, voltage, and magnetic potential. The element requires an iterative solution method, which is partially responsible for the calculation times of up to three days. In addition, the MESH-200 unsolved<sup>8</sup> element was used to create a high-quality and regular three-dimensional template mesh for the SOLID-5 elements (see Figure 3.2.2). Finally, BEAM-4 mechanical 2-node linear elements were used to create structural supports with no rotational fixity (see Figure 6-23).

Figure 6-22. ANSYS element geometry: Solid-5 (left), Mesh-200 (right) [201]

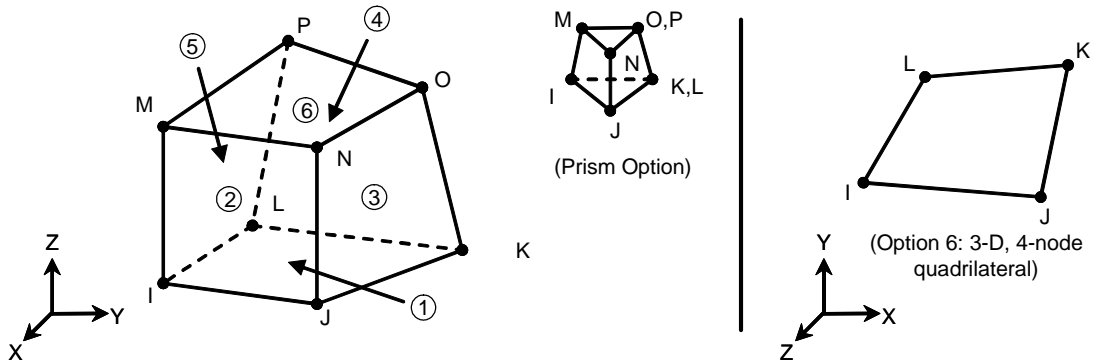
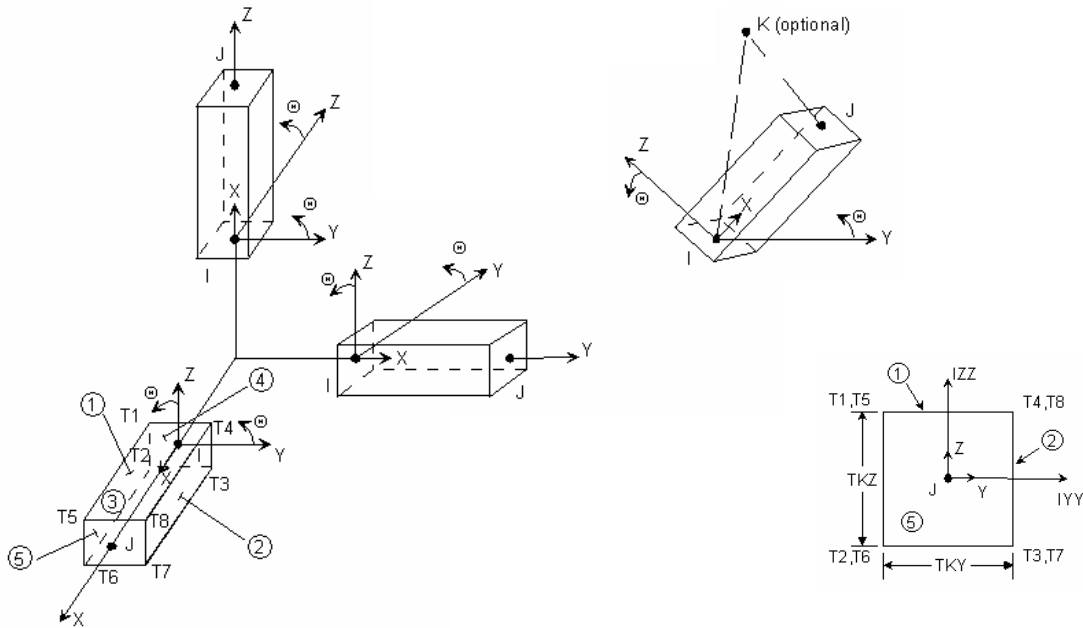


Figure 6-23. ANSYS element geometry: Beam-4 [201]



8. The elements are only a tool to create a better mesh using other elements; they have no mathematical significance in the model.

### 3.2.2 Justification for Thermal-Mechanical Coupling

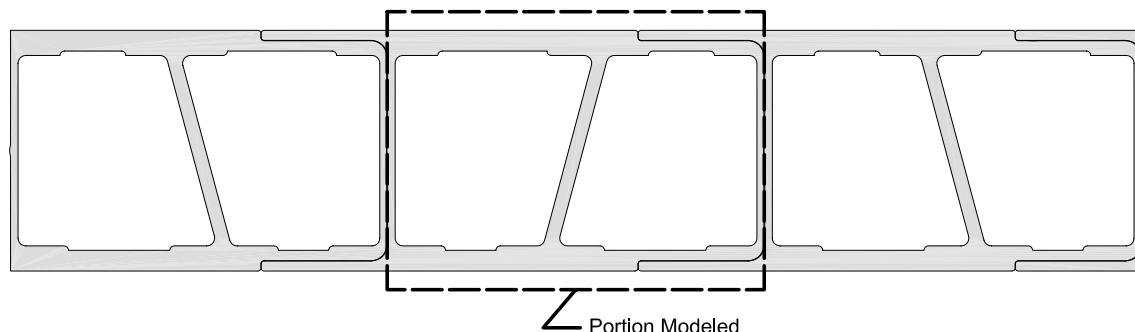
The question may be raised as to why a coupled model is necessary. It would seem that a simple approach to modeling the high-temperature mechanical behavior of the specimen would be to take the temperature distribution from a thermal model and correlate the temperatures at each region to the percentage of remaining modulus from an  $E$  versus  $T$  curve. As the temperatures increase, the modulus of the heated regions would decrease, and thus the effect of decaying mechanical properties in fire would be represented in a purely mechanical model.

The problem with this technique, however, is that the degradation of mechanical properties as a result of high temperatures is only one of two factors that effect the stresses, strains, and deformations. Thermal expansion has a large influence on these values for sections under uneven heating. Thus, a simple mechanical model with reduced moduli according to the temperature history is insufficient because it neglects thermally-induced stresses. A thermomechanical coupled model is necessary to capture both the effects of the reduction of mechanical properties and uneven thermal expansion.

### 3.2.3 Geometrical Simplifications

The specimens used in the experimental investigations had a constant cross-section along their lengths and were loaded and supported symmetrically. Thus, only one-half of the length of the specimen was included in the model. Further, the specimens consisted of three identical pultruded shapes bonded side-by-side, so it was possible to include only one-third of the cross-section in the transverse direction. The resulting model is therefore one-sixth the size of the true specimens, which permitted higher mesh refinement and faster calculation times.

Figure 6-24. Portion of experimental specimen considered in 3-D thermomechanical model



### 3.2.4 Mechanical Boundary Conditions

#### 3.2.4.1 Mid-span

As described in Section 3.2.3, the mid-span was treated as a symmetry boundary, meaning that translation was permitted in the vertical and transversal directions, but not in the longitudinal direction and no rotation was allowed about the transversal or z-axes (see Figure 6-25).

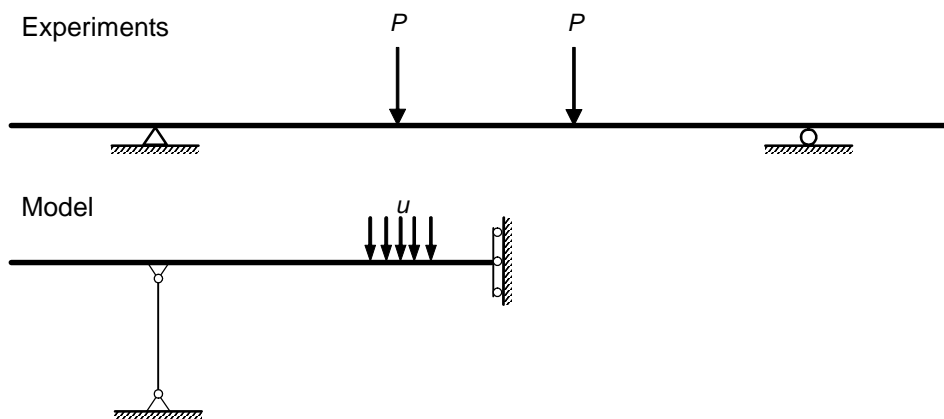
#### 3.2.4.2 End Supports

In the experimental investigations, the specimens were continuously supported by steel plates across their width. These steel plates sat upon cylindrical steel rollers such that translation was only permitted in the longitudinal direction. The standard method for modeling such roller supports is to apply fixity in the transversal and vertical directions but to allow translation in the longitudinal direction and rotation about the transversal axis.

Due to difficulties implementing this technique, however, an alternative method was used. The roller support was instead represented by tall rigid beams with pin joints at the tops and bottoms (see Figure 6-25). This allowed the steel plate to sway in the longitudinal direction of the beam and to rotate about the transversal axis, but vertical and transversal translation was only permitted as far as the change in length of the beams. By assigning very high moduli to the beams (cross-sectional area =  $10 \text{ m}^2$ ,  $I_{yy} = I_{zz} = 100 \text{ m}^4$ ,  $E = 210 \text{ GPa}$ ), these deformations were on the order of  $1 \text{ }\mu\text{m}$  and thus did not greatly affect the accuracy of the results.

Because the steel plate was supported at discrete points by the beam elements rather than by a continuous steel roller, some bending was noted in the transversal direction of the plate. To reduce this effect, the thickness of the plate was significantly increased.

Figure 6-25. Mechanical boundary conditions used to approximate experimental set-up<sup>9</sup>



9. Because the experimental specimens were continuously supported and loaded across their width, their boundary conditions and loads can be sufficiently represented in two-dimensions.

### 3.2.5 Thermal Boundary Conditions

#### 3.2.5.1 Cold Face

Because the 2-D thermal model did not include the upper half of the specimen (see Figure 6-12), it was necessary to solve for the temperatures at the outer surface of the upper face sheet. This surface, which faces away from the oven is exposed to air at ambient temperatures, is termed the cold face. At this boundary, heat is transferred to the surrounding environment by all three modes (conduction, convection, radiation), though convection is dominant. Several empirical correlations have been developed to estimate the convective heat transfer coefficient,  $h_c$ , for free (buoyant) convection. McAdams [122] provides the following correlation for laminar convection of air over a heated horizontal flat plate:

$$h_c = 0.14(G_r \cdot P_r)^{1/3} \frac{\lambda}{L_{cb}} \quad (6-39)$$

where  $L_{cb}$  is the characteristic length (the mean of the length and width of the plate), and  $P_r$  is the Prandtl number defined by Equation 6-26. The term  $G_r$  is the Grashof number, which is defined by the following equation [146 pg. 303]:

$$G_r \equiv \frac{g\beta L_{cb}^3}{\nu^2} (T_{sur} - T_{\infty}) \quad (6-40)$$

where  $g$  is the acceleration due to gravity,  $\beta$  is the volumetric coefficient of thermal expansion of air,  $\nu$  is kinematic viscosity of air,  $T_{sur}$  is the temperature of surface, and  $T_{\infty}$  is the ambient temperature, and  $P_r$  is the Prandtl number defined by Equation 6-26. Inserting the material and system values into Equation 6-39, the following values of  $h_c$  are found.

Table 6-14. Convective heat transfer coefficients for cold face according to temperature differential<sup>10</sup>

$T_{\infty}$ (°C)	$T_{sur}$ (°C)	$L_{cb}$ (m)	$C_p$ (J/kg·K)	$\eta$ (K/m·s)	$\lambda$ (W/m·K)	$\beta$ (K <sup>-1</sup> )	$\nu$ (m <sup>2</sup> /s)	$P_r$ (unitless)	$G_r$ (unitless)	$h_c$ (W/m <sup>2</sup> ·K)
20	20	1.83	1006	1.846x10 <sup>-5</sup>	0.0257	3.43x10 <sup>-3</sup>	1.57x10 <sup>-5</sup>	0.722	0.00	0.0
20	70	1.83	1006	1.846x10 <sup>-5</sup>	0.0257	3.43x10 <sup>-3</sup>	1.57x10 <sup>-5</sup>	0.722	4.20x10 <sup>8</sup>	6.1
20	120	1.83	1006	1.846x10 <sup>-5</sup>	0.0257	3.43x10 <sup>-3</sup>	1.57x10 <sup>-5</sup>	0.722	8.40x10 <sup>8</sup>	7.7
20	170	1.83	1006	1.846x10 <sup>-5</sup>	0.0257	3.43x10 <sup>-3</sup>	1.57x10 <sup>-5</sup>	0.722	12.60x10 <sup>8</sup>	8.8
20	220	1.83	1006	1.846x10 <sup>-5</sup>	0.0257	3.43x10 <sup>-3</sup>	1.57x10 <sup>-5</sup>	0.722	16.80x10 <sup>8</sup>	9.7
20	270	1.83	1006	1.846x10 <sup>-5</sup>	0.0257	3.43x10 <sup>-3</sup>	1.57x10 <sup>-5</sup>	0.722	21.01x10 <sup>8</sup>	10.5

In practice, liquid cooling maintains the temperature of the upper face sheet at room temperature or cooler, and therefore there is nearly no heat transfer between the upper face sheet and the surrounding environment.

#### 3.2.5.2 *Internal Surfaces - Liquid-Cooled Condition*

Once again, the upper surfaces of the liquid-FRP interface were not solved in the 2-D thermochemical model due to the geometrical simplifications (see Figure 6-12). Thus, forced convection of a fluid over a plate was simulated as described in Section 3.1.3.1.

The temperatures at the lower surface of the liquid-FRP interface, however, were solved by the 2-D thermochemical model and could be directly transferred to the thermomechanical model as temperature boundary conditions. Because the lower face sheet is composed of portions with differing thicknesses, the temperature history of a representative node at each thickness in the thermal model was applied to all of the nodes in the thermomechanical model at that same thickness.

#### 3.2.5.3 *Internal Surfaces - Dry Condition*

Without liquid cooling, some heat is transferred from the lower face sheet to the upper through convection and radiation within cells. In order to properly simulate this effect, a complex CFD treatment of the air within the cells would be required. Further, some key system parameters such as the orientation of the specimen (thermal chimney effect in vertical orientation) and whether the ends of the cells are open or sealed would have a large influence on the flow of air within the cells, which would require validation for each new set of conditions. Finally, modeling the air within the cells using even a coarse mesh would more than double the number of nodes, which would exceed the maximum number of nodes permitted under the educational software license and have a catastrophic effect on the already-lengthy calculation times.

Thus, the added level of complication created by CFD was judged to be unjustified. The internal surfaces in the dry condition were therefore treated as simple convection boundary conditions, as described in Section 3.2.5.1.

#### 3.2.5.4 *Hot Face*

The temperature history from the 2-D thermochemical model was transferred to the 3-D thermomechanical model to create temperature boundary conditions.

---

10. Eurocode 1 Part 1.2 (CEN 200a) simplifies the choice for fire protection engineering calculations by recommending a flat value of  $10 \text{ W/m}^2$ .

### 3.2.5.5 Other Boundaries

All boundaries not described in the previous sections were treated as adiabatic ( $q = 0$ ). This includes boundaries at the geometrical simplifications, i.e. at the cuts made between the adjacent pultruded shapes and at mid-span (see Figure 6-24).

### 3.2.6 Structural Load

In the experimental investigations, 96 kN loads were applied to stiffened steel beams at roughly the third points of the span. These steel beams spread the load from the discrete hydraulic jacks over a 18.7 cm wide patch and evenly between the three pultruded shapes through a soft rubber layer. To simulate this loading condition, a structural pressure of 561 kPa was applied over the area of the loading patch (see Equation 6-41).

$$\frac{96 \text{ kN}}{(0.187 \text{ m})(0.914 \text{ m})} = 561 \text{ kPa} \quad (6-41)$$

As only one-third of the width of the experimental specimen was modeled, the pressure summed over the whole area of the patch in the model is equivalent to one third of the total load applied by the jacks.

### 3.2.7 Thermal load

Temperature boundary conditions at the hot face were applied as provided by the 2-D thermal model.

### 3.2.8 Material Properties

#### 3.2.8.1 Young's Modulus, $E$ :

The ambient-temperature Young's Modulus was provided by the manufacturer with individual values for the face sheets and webs for loading in all three axes (see Table 5-2). These values have been confirmed by numerous structural experiments at the CCLab on the same material [98-100].

The dependence of  $E$  on temperature is difficult to represent by a single curve. While the behavior of the composite is moderately different in tension and compression at ambient temperatures, this difference is magnified at high temperatures. As the resin passes the glass transition temperature, the composite exhibits a large reduction in stiffness for loading conditions that rely on the contribution of the matrix, such as shear, compression, and torsion. In tension, however, the contribution of the matrix is minimal, and after some relaxation and

realignment of the fibers around  $T_g$ , the stiffness of the composite is quite similar to the behavior of the fibers themselves.

For the four-point bending condition used in the model and in the physical experiments, the bottom face sheet was exposed to fire conditions. By basic Euler-Bernoulli beam theory, it can be proven that region below the neutral axis of a beam in simple bending is stressed in tension. Thus, the divergence of the material's behavior in tension and compression at high temperatures should be of little influence because all of the material exposed to high temperatures should only be stressed in tension.

There is a second effect at play, however, which invalidates this assumption: thermal expansion. The elongation of the fibers at the hot face due to bending stresses is quickly relieved by thermal expansion. In the absence of all other loads, a temperature increase of 85°C would cause an elongation equal to the elongation caused by bending.<sup>11</sup> As the temperature of the oven increases by 85°C in less than 10 seconds after the ignition of the burners, there is a sudden relaxation of the bending stresses at the hot face (see Figure 5-28). This relaxation is accompanied by a sudden increase in deflections, which transfers the peak tensile stresses to the cool deeper layers. As the heated layers continue to expand, they are restrained by those same cool inner layers and are forced into compression. Thus, the inner layers must resist not only the tensile stresses created by bending, but also due to the thermal expansion of the layers towards the hot face.

This phenomenon becomes more influential as the temperatures increase, as long as the temperatures remain low enough that the composite retains some compressive stiffness. Above these temperatures, where the matrix has decayed enough that there is no shear transfer between the expanding hot layers and the resisting inner layers, the importance of the effect dwindles and the two layers act independently. As described in the previous chapter, this temperature range falls in between  $T_g$ , where there is sharp decline in  $E$ , and  $T_d$ , where material ceases to exist as a solid entity.

The ideal material model would therefore include different stiffnesses in tension and compression as a function of temperature. The tensile curve would show some slight reduction between  $T_g$  and  $T_d$ , but would maintain a relatively high stiffness all the way up to the softening temperature of the glass fiber (roughly 850°C). The compression curve would decline rapidly at  $T_g$  and approach null at  $T_d$ .

---

11. Using  $\epsilon = 1,080 \mu\text{m}/\text{m}$  from experimental measurements and  $\alpha_t = 12.6 \mu\text{m}/\text{m}\cdot^\circ\text{C}$  from a rule of mixtures approximation.

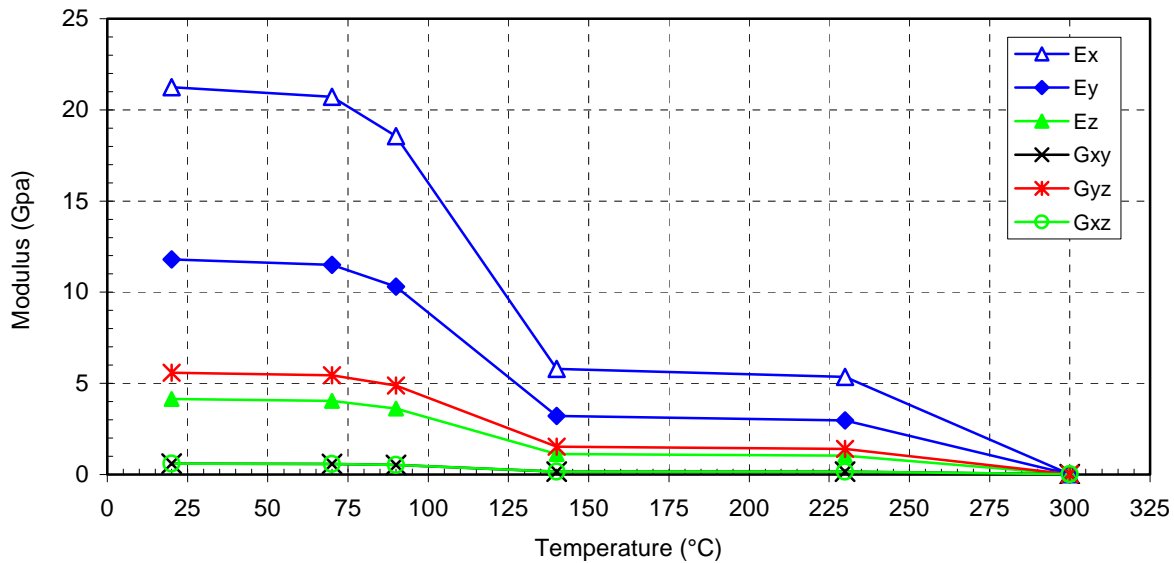
Unfortunately, the software package employed has only one material model that permits different moduli in tension and compression, and that model is not compatible with the coupled-field elements. Therefore, a compromise was made to assign a single  $E$  versus  $t$  curve for all stress states. This compromise falls in between the two extreme possibilities:

1. Use the tensile curve: the elements in tension would be correctly represented, but those exposed to high temperatures and loaded in compression would not. The layers at the hot face, which should have no residual compressive stiffness, would continue to exert a force on the cool inner layers even after the matrix has decomposed and there is no means of shear transfer between the layers.
2. Use the compressive curve: the elements in compression would be correctly represented, but those in tension would not. The cool inner layers, which provide the tensile resistance of the beam in bending would lose their stiffness at relatively low temperatures, causing the tensile forces to move further inward.

Hence, neither extreme is ideal, and any compromise between the two results in an mixture of the problems of each. What is important is that all variations of the  $E$  vs.  $t$  curve lead to some over-prediction of the deflections, though this over-prediction is less severe for curves approaching Option 2 than for Option 1. In design work, where a conservative but reasonable result is desirable, the model is a useful and informative tool. In pure scientific research, the model captures all of the critical mechanisms at play and provides insight into the interaction between thermal and mechanical effects within the FRP specimen. As such, the modeling effort was pursued despite the lack of an ideal  $E$  vs.  $t$  material model.

As described, an average  $E$  vs.  $t$  curve was used for all stress states. This curve was established by dynamic mechanical analysis (DMA) performed on the the material in the three-point bending arrangement (Chapter 5 Section 5.1). The resulting curve was proportionally adjusted to meet the ambient temperature values that were provided by the manufacturer and confirmed at the CCLab (see Figure 6-26).

Figure 6-26. Modulus versus temperature curves used in the thermomechanical model



### 3.2.8.2 Shear modulus, $G$ :

The shear modulus function was derived in the same manner as the Young's modulus described in Section 3.2.8.1 and is shown in Figure 6-26.

### 3.2.8.3 Poisson ratio, $\nu$ :

One again, the Poisson ratio was provided by the manufacturer [199]. As is customary in thermomechanical modeling of FRP materials, the ratio was simplified as being constant with respect to temperature [4] [78] [191].

### 3.2.8.4 Coefficient of Thermal Expansion, $\alpha_t$ :

The coefficient of thermal expansion was calculated based on a rule of mixtures formulation, or proportional combination of the coefficients of individual materials [162]. Because the material is non-isotropic, separate expressions are used for the longitudinal and transverse directions. For the longitudinal direction, the expression is given as follows:

$$\alpha_{i-1} = \frac{E_f \alpha_f V_f + E_m \alpha_m V_m}{E_c} \quad (6-42)$$

where  $V$  is the volume fraction and the subscripts  $f$ ,  $m$ , and  $c$  stand for *fiber*, *matrix*, and *composite*, respectively. In simple unidirectional composites, the expression for the coefficient of thermal expansion in the transverse direction, is given as follows:

$$\alpha_{t_{2-2}} = (1 + \nu_m) \alpha_m V_m + (1 + \nu_f) \alpha_f V_f - \alpha_{t_{1-1}} (\nu_f V_f + \nu_m V_m) \quad (6-43)$$

This expression does not account for the existence of transverse reinforcement. For the test material, a fiber volume fraction of approximately 10% was estimated to exist in the transverse direction. Thus, Equation 6-42 is used instead of Equation 6-43 using only the fiber volume fraction of the reinforcement oriented in the transverse direction.

Finally, no fibers are oriented in the through-thickness direction, so the coefficient is simply a volume-weighted average of the resin and *all* fiber reinforcement (i.e. not only volume fraction of the fibers oriented in the 3-3 direction, but of all fiber reinforcement present):

$$\alpha_{t_{3-3}} = \alpha_m V_m + \alpha_f V_f \quad (6-44)$$

Table 6-15. Values needed to calculate the coefficient of thermal expansion

Direction	$E_f$ (GPa)	$E_m$ (GPa)	$E_c$ (GPa)	$V_f$ (%)	$V_m$ (%)	$\alpha_f$ ( $\mu\text{m}/\text{m}\cdot\text{K}$ )	$\alpha_m$ ( $\mu\text{m}/\text{m}\cdot\text{K}$ )	$\alpha_c$ ( $\mu\text{m}/\text{m}\cdot\text{K}$ )
not applicable	72.4	3.38	-	-	-	4 [122]	75 [122]	-
1-1	-	-	21.24	42 <sup>a</sup>	58 <sup>a</sup>	-	-	12.6
2-2	-	-	11.79	10 <sup>a</sup>	90 <sup>a</sup>	-	-	21.8
3-3	-	-	4.14	52 <sup>b</sup>	48 <sup>b</sup>	-	-	37.0

a. Counting only fibers oriented in direction considered

b. Counting all fibers present

### 3.2.8.5 Specific Heat Capacity, $C_p$ :

The ambient-temperature specific heat capacity of the composite test material was determined through adiabatic calorimetry at the Swiss Federal Laboratories for Materials and Testing (EMPA) in Dübendorf (see Chapter 5 - Section 5.3 for a description of the method). Though an effective function was used in the 2-D thermochemical model to include the effects of endothermic decomposition, a simple constant value (1,170 J/kg·K) was used for the 3-D thermomechanical model for quicker solution convergence. With fixed temperatures at the hot face, the internal liquid interface, and midway between the faces, there is little opportunity for significant errors in the simulation of the thermal phenomena and the model is fairly insensitive to the thermal material properties.

### 3.2.8.6 Thermal Conductivity, $\lambda$ :

The ambient temperature value of the test material (0.35 W/m·K) was determined through adiabatic calorimetry at the Swiss Federal Laboratories for Materials Testing and Research (EMPA) in Dübendorf (see Chapter 5 Section 5.3). As with the specific heat capacity, the effective thermal conductivity function used in the 2-D thermochemical model was omitted from the 3-D thermomechanical model for quicker solution convergence. As previously stated, the use of temperature boundary conditions on the surfaces and within the lower face sheet makes the model fairly insensitive to thermal material properties.

### 3.2.8.7 Density, $\rho$ :

The temperature-dependent density function was retained from the 2-D thermal model (see Section 3.1.5.3).

## 3.2.9 Meshing

A two-dimensional cross-section of the model was first meshed using the MESH200 unsolved elements. The lower face sheet and webs were meshed using mapped quadrilaterals. In order to reduce the number of total elements used, the upper face sheet was meshed using coarse quadrilateral free meshing. A maximum edge length of 4 mm was permitted at the lower face sheet, which resulted in 5 elements through the thinnest portions, while 10 mm was permitted in the upper face sheet, which resulted in 2 elements through the thinnest portions.

Once the 2-D cross-section was completed, volume sweeping was used to transfer this pattern into the third dimension of the model. Edge lengths in the longitudinal direction varied from 6 mm under the loading patch to 20 mm at the portion beyond the support.

A total of 47,292 elements incorporating 61,045 nodes were needed to mesh the solid-body model, which is roughly seven times as many as were used in the 2-D thermal model.

## 3.2.10 Governing Equations

The equations described in Section 3.1.7 for the 2-D thermal model are also valid for the thermal aspects of the 3-D thermomechanical model. The fundamental governing equation for the mechanical aspects is a restatement of Hooke's Law:

$$\sigma = \varepsilon E \quad (6-45)$$

where  $\sigma$  is the stress,  $\varepsilon$  is the strain, and  $E$  is the stiffness. This equation is written for each of the hundreds or thousands of individual finite elements in the form of large matrices with the

consideration of forces, reactions, and displacements rather than stresses and strains in the generalized form:

$$\{\mathbf{R}\} = \{\mathbf{K}\}\{\mathbf{u}\} - \{\mathbf{F}\} \quad (6-46)$$

where  $\mathbf{R}$  is reaction matrix,  $\mathbf{K}$  is the stiffness matrix,  $\mathbf{u}$  is the displacement matrix, and  $\mathbf{F}$  is the load matrix.

Because the analysis involves two different types of phenomena (thermal and mechanical), the solver must couple the two associated systems of equations. In the case of thermomechanical coupling, the software employed uses weak, or *sequential* coupling, where solutions are iteratively converged between the two equation systems. In sequential coupling, a minimum of two iterations is required to achieve a coupled response, and additional iterations are required as a result of the non-linear materials functions [201]. The result is an extremely processor-intensive calculation that, for systems with many elements (many simultaneous equations) and using current hardware, may consume several hours to achieve convergence for each time step.

### 3.2.11 Results

#### *Ambient Temperature*

The numerical model predicts a mid-span deflection very close to the experimentally measured and analytically calculated values. These results are tabulated below.

Table 6-16. Comparison of predicted and experimentally measured pre-fire mid-span deflections

Source	Mid-span Deflection (mm)	Disparity from Experimental Results <sup>a</sup>
Avg. Experimental (Chapter 5 Section 8)	12.1	-
Analytical (Section 2.1)	12.0	-1%
Numerical (Section 3.2)	11.9	-2%

a. Disparity = (calculated - measured) / measured

As show in the table, both the numerical and analytical methods produce mid-span deflection predictions that differ from the experimentally results by less than 2%.

### *Liquid-Cooled Condition*

As shown in Figure 6-27, the numerical model slightly over-predicts the mid-span deflections (5% on average) in the liquid-cooled condition in comparison to the experimental results. This over-prediction was expected due to the assignment of a single modulus versus temperature curve, as discussed in Section 3.2.8.1. Nonetheless, the deflection versus time curve captures the important trends observed in the experimental investigations, including the sudden increase in deflections in the first 10 minutes and the stabilization after longer exposure times.

The predicted axial strains in the upper face sheet match well with the average experimentally measured values (see Figure 6-28). The predicted values for the lower face sheet also match well in the first 20 minutes, but then deviate from the average experimental results thereafter. This discrepancy is mostly due to problems with the measured values. As shown in Appendix C Figures C-26 and C-27, there was quite a large variation in the values recorded from the various strain gages due to several practical issues (temperature compensation, waterproofing measures, restricted access to placement area, etc.). As such the predicted strains match better with some of the measured strains than others.

The effect of thermal expansion on the total strains can be distinguished more easily in the liquid cooled condition because of the steep thermal gradient through the lower face sheet. As shown in Figure 6-29, the effects described in Chapter 5 Section 8.6.1 can be seen. While the structural load causes tensile strains on the hot face, the thermal expansion causes compressive strains that are roughly twice as high. The combination of both effects results in a strain distribution that is far different than what exists in a flexural members with no thermal gradient through their depth. The deflections caused by thermal expansion and mechanical loading are separated in Figure 6-30 to further illustrate this effect.

Figure 6-27. Comparison of the mid-span deflections of liquid-cooled specimens as predicted by the thermomechanical model and experimentally measured

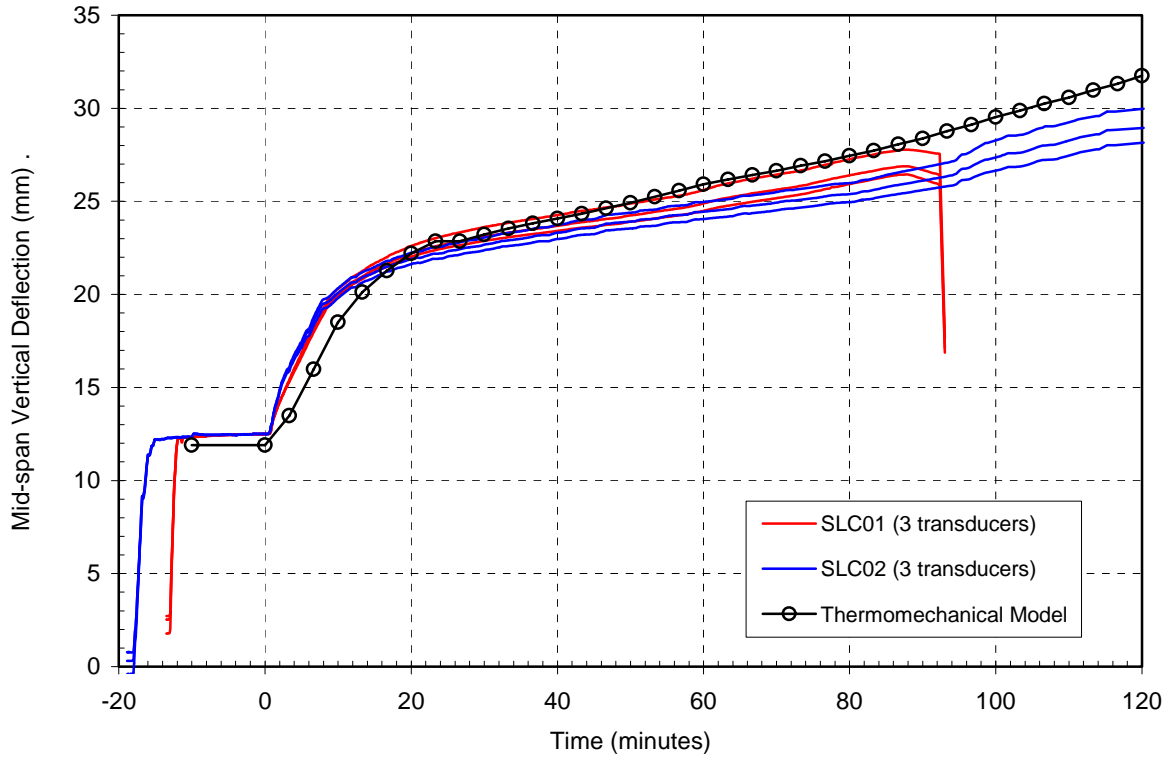


Figure 6-28. Comparison of axial strains of a liquid-cooled beam as predicted by the thermomechanical model and experimentally measured

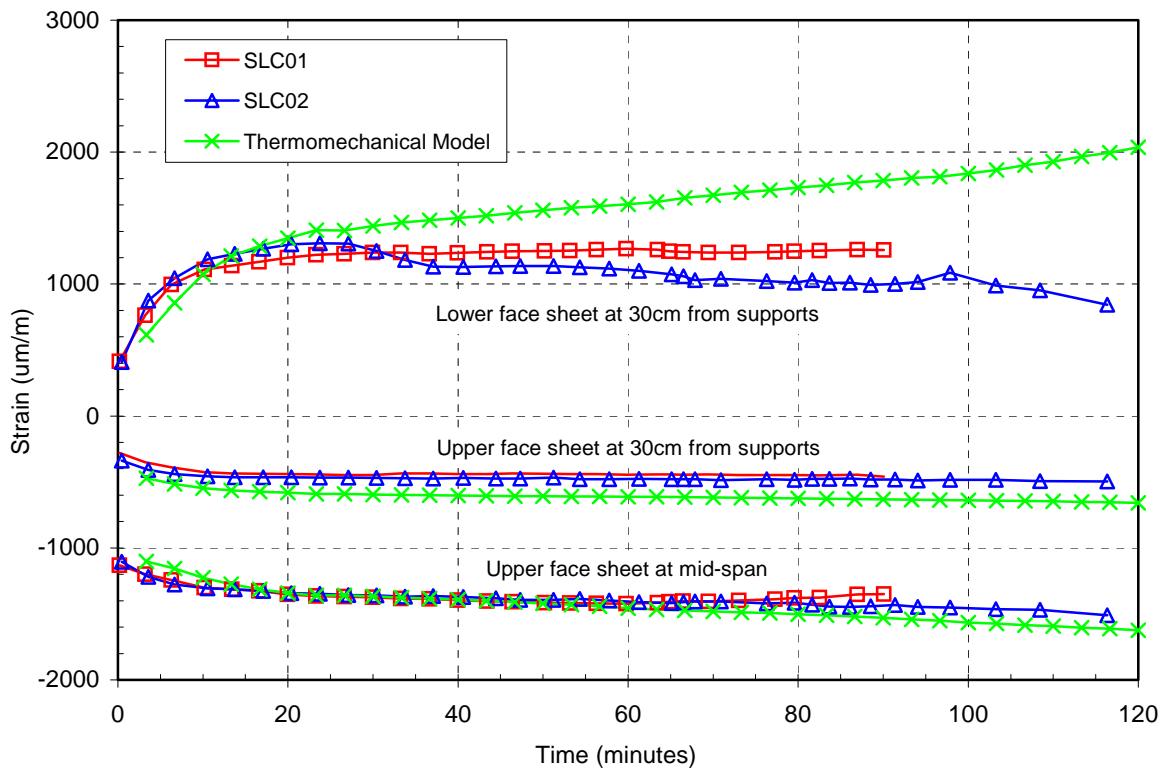


Figure 6-29. Comparison of mid-span axial strain distribution without thermal expansion and without structural load (liquid-cooled condition)

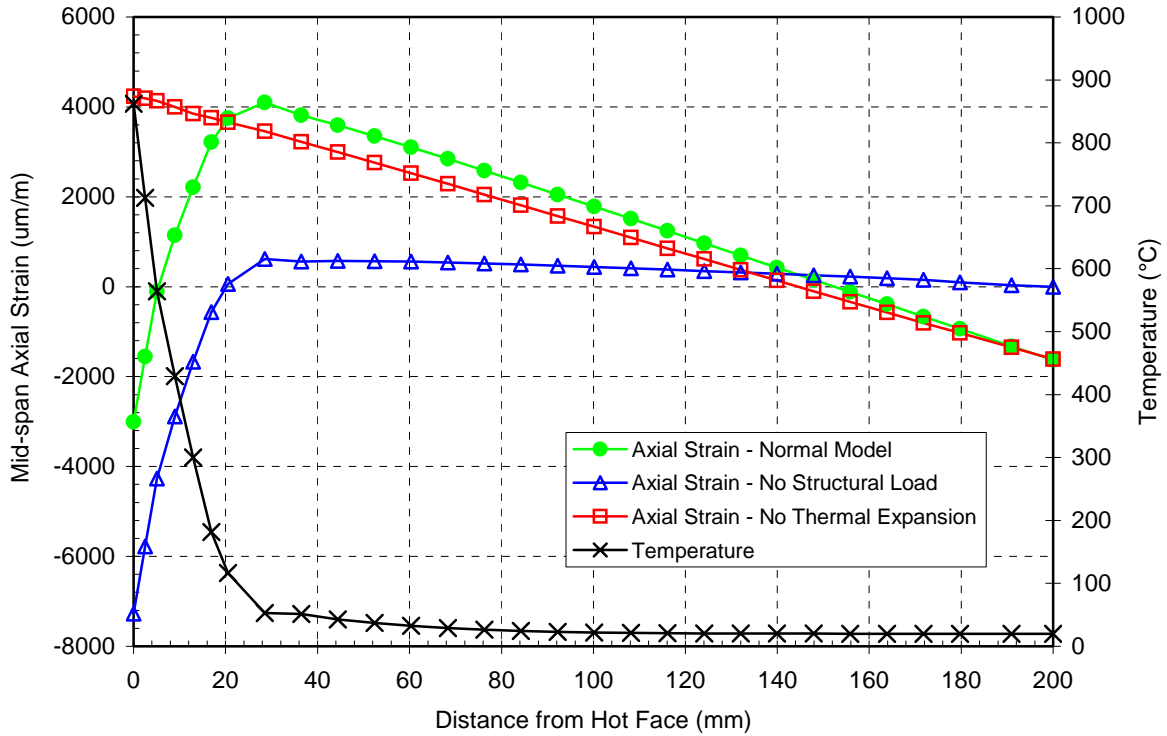
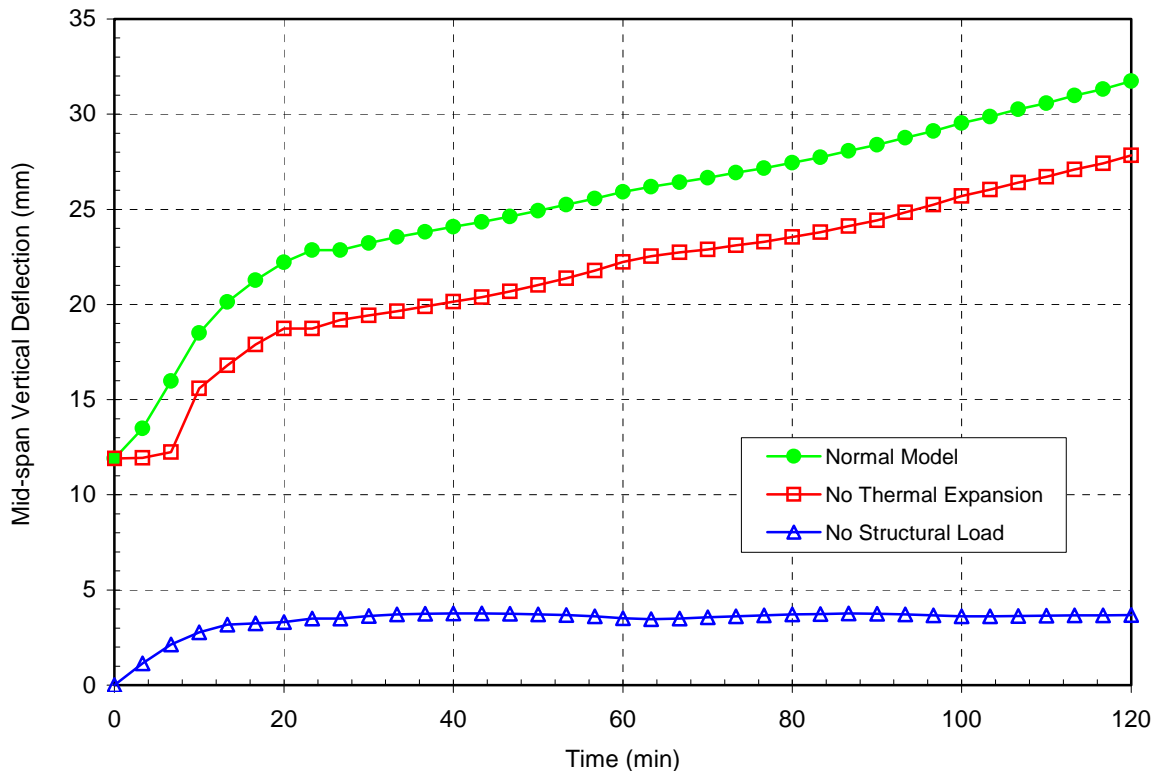


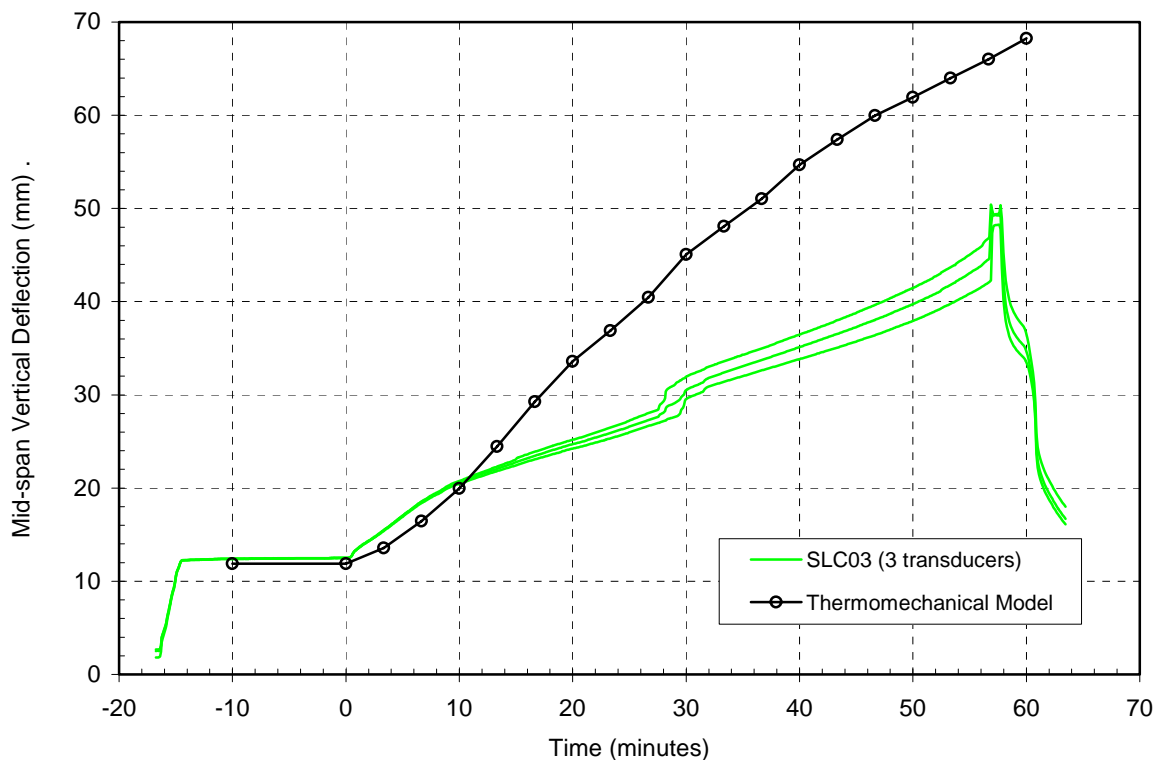
Figure 6-30. Comparison of the mid-span deflections without thermal expansion and without load (liquid-cooled condition)



### Dry Condition

The numerical model greatly over-predicts the mid-span deflections in the dry condition in comparison to the experimental results (see Figure 6-31). Once again, this was expected due to the assignment of a single  $E$  vs.  $t$  curve, as described in Section 3.2.8.1. The greatest factor that causes the over-prediction, however, is related to a different factor. Unlike the liquid-cooled condition, the high-temperature behavior of the upper face sheet played an important role in the overall mechanical behavior of the experimental specimen. Without the liquid-cooling system, the upper face sheet was also heated, which lead to a less severe thermal gradient across the section and thus smaller thermally-induced deflections. Because the convective and radiative heat transfer between the lower and upper face sheets was not modeled, however, the thermomechanical model does not accurately predict the temperatures in the upper face sheet in the dry condition. Thus, the thermal expansion of the upper face sheet is not captured and the deflections are therefore greatly over-predicted (see Figure 6-31).

**Figure 6-31.** Comparison of the mid-span deflections of a non-liquid cooled (dry) beam as predicted by the thermomechanical model and experimentally measured



## 4 Conclusions

The objective of the mathematical modeling effort was to develop and validate methods in which the behavior of load-bearing liquid-cooled FRP building elements exposed to fire conditions could be simulated. Analytical methods were presented for the prediction of mid-span deflections of such an element in 4-point bending for both the pre-fire and post-fire damaged conditions. These methods were compared very well with experimentally measured values, usually differing by less than 10%. These errors were mostly on the conservative side with respect to design.

For the more complex condition of combined thermal and mechanical loading, numerical methods were necessary. For efficiency and accuracy, two separate models were developed: a two-dimensional thermochemical model that calculates the temperature evolution through the cross-section of an FRP element, and a three-dimensional thermomechanical model that uses the temperatures calculated by the thermochemical model as boundary conditions, and calculates the mechanical response of an FRP beam element. To consider the separate cases of liquid-cooling or dry conditions, it is only necessary to change the convective heat transfer coefficient at the internal boundaries of the thermochemical model.

The thermochemical model incorporates *effective* material property curves with respect to temperature, as proposed in the literature. These curves account for highly influential phenomena that cannot be directly modeled without an enormous increase in complexity, such as the endothermic decomposition of the resin, delamination, and the loss of material from the hot face. Using these effective curves, the agreement between the predictions and experimentally measured values is very good in both the liquid-cooled and dry conditions.

The thermomechanical model also provides predictions of deflections that are in good agreement with the experimentally measured values for the liquid-cooled condition. A slight over-prediction results over time is due to the use of a single modulus vs. temperature curve for both tension and compression. The agreement between the predicted and experimentally measured deflections in the dry condition is less successful, as the model greatly over-predicts the deflections. This is related to the thermomechanical behavior of the upper face sheet, which was not adequately represented in the model. In order to properly simulate the thermal conditions in the upper face sheet, a computational fluid dynamics approach would have been necessary to solve for the transfer of heat through the air inside the cells. This level of complication was not only unjustified (the objective, once again, was simulate the liquid-cooled condition) but impossible due to software limitations on the number of nodes available.

Overall, the range of models are sufficient for the structural design of liquid-cooled FRP bending elements with consideration of the pre-fire, high-temperature, and damaged post-fire conditions. The agreement between mathematical predictions and experimental results is good in most respects, with models usually producing slightly conservative predictions.



7

## **Conclusion**



## 1 Overview

Modern buildings can benefit from better energy efficiency, lower maintenance, higher quality industrial manufacturing techniques, and quicker construction through the use of fiber-reinforced polymers. Thanks to their high specific strength, low thermal conductivity, good environmental resistance, and their ability to be formed into complex shapes, FRP materials are well-suited to fulfilling many building requirements. By integrating several layers into single *function-integrated* components and industrially fabricating those components, the amount of on-site labor can be greatly reduced. As such, FRP materials have a strong potential for fueling the next great advance in the conception of buildings.

These materials, however, are also relatively expensive, combustible, have low operating temperatures, and are generally less stiff than traditional building materials. In order to overcome these weaknesses in the development of optimized applications, their advantageous characteristics (high strength-to-weight ratio, good environmental resistance, low thermal conductivity, facilitate part-count reduction) must be fully exploited. This philosophy of *material-adapted* usage constituted the logical foundation of the project.

## 2 From Existing FRP Buildings to the Proposed System

The ultimate objective of the project was to develop concepts for a new multiple-story building system in which FRP materials are used in a material-adapted manner. Through a review of the significant building projects involving the use of FRP materials throughout history, it was found that although some single and two-story systems have been designed following a material-adapted approach, the challenges related to tall buildings have not been resolved.

The problem farthest away from a workable solution was found to be the poor fire safety. Thereby, a new building system was conceived with a strong focus on resolving that issue. Internal liquid cooling, a fire protection method already well-established in other applications, was incorporated and governed much of the design decisions. In this system, a fluid is circulated through cellular FRP components to draw heat away from load-bearing FRP components and thus prolong their endurance in fires.

In the spirit of material-adapted usage, the building system was also conceived with an interest in simplifying on-site assembly and maximizing industrial fabrication through the integration of building functions into single elements. The internal liquid-cooling fire protection system, therefore, was designed to serve as the room climate heating and cooling system as well. Further integrations and weakness-mitigating/strength-exploiting details were incorporated.

### 3 Experimental Investigations

Research into the high-temperature behavior of FRP composites has been conducted by a small group since the late 1970's. The focus has primarily been on the response of the materials to extreme heat fluxes for short durations, such as those related to the aerospace, military and petrochemical industries. Very little physical research has been conducted on the behavior of FRP materials in situations more likely to occur in buildings: lower heat fluxes and longer exposure durations. To date, no research has been conducted on the use of internal liquid cooling for the fire protection of FRP building components.

Thus, the experimental portion of the project was devoted to the study of the behavior of liquid-cooled FRP elements exposed to fire and protected by internal liquid cooling. The material and fire behavior properties of an available FRP material were first established through small-scale and bench-scale experiments. These experiments were followed by large-scale structural fire endurance experiments on both liquid-cooled and non-liquid cooled FRP panels. The most important results and conclusions from these investigations are:

- Cellular FRP panels are maintained at a lower temperature than non-cooled specimens when exposed to fire. While the entire thickness of non-liquid cooled specimens exceeded the temperature at which mechanical properties sharply decline ( $T_g$ ) in less than 10 minutes, 20% of the thickness of the liquid-cooled specimens remained below  $T_g$  after more than two hours of fire exposure with even the slowest flow rates.
- Code-required endurance times of 90 minutes and longer can be achieved for floor elements using the internal liquid cooling system. While the non-liquid cooled panel continued to deform until a failure occurred in less than one hour, the liquid cooled panels achieved a relatively stable condition through which they supported the structural loads for up to two hours.
- The panel without liquid cooling failed in compression in the relatively cooler upper face sheet. This failure demonstrates how FRP composites are far more vulnerable to heat-induced weakening in stress states that require the mechanical contribution of the matrix, such as compression or shear. The protection of components in such stress states is where internal liquid cooling can make the most valuable contribution.
- The amount of energy absorbed by the water increases with increasing flow rates. Benefits begin to diminish with flow velocities above 1.0 cm/s (flow rate 0.8 m<sup>3</sup>/hr) as the flow regime becomes less laminar and more turbulent.

- Within the range of flow circuit lengths and flow velocities employed, the water does not approach boiling. The slowest flow velocity of 0.2 cm/s resulted in an increase in temperature of 30°C, while the temperature increase at the highest flow velocity of 5 cm/s was too small to measure. It therefore appears possible to design longer flow paths in building applications without the risk of boiling.
- Water pressures were very low at all flow velocities except the very highest. This suggests that the design of larger systems for buildings will not be limited by pressures related to head loss.
- Post-fire structural loading showed a 40% reduction in the stiffness of the liquid-cooled panels. Calculations showed that this was not only due to the loss of cross-section, but also the degradation of Young's modulus in areas that exceeded  $T_g$ .

Overall, the internal liquid cooling concept was demonstrated to be a functional and effective method of postponing the thermally-induced structural failure of FRP members due to fire.

## 4 Mathematical Modeling

Experiments are indispensable in establishing the behavior and performance of unprecedented systems. Alone, however, their results are only useful for a particular assembly in a particular set of conditions. Further, there are many values and phenomena that are very difficult to physically measure. For these reasons, the proposed system was also studied through the use of mathematical models.

To model the stiffness reduction of liquid-cooled bending members after fire exposure, a new set of criteria were proposed for an existing “2-layer” analytical model. These criteria employ temperature profiles to determine the boundary between the idealized “fully degraded” and “virgin” layers of the burnt component. This model was compared to an all-new 3-layer approach in which a third “partially degraded” layer is included. This layer retains 30% of the pre-fire mechanical properties and employ a different set of temperature criteria. Both the revised 2-layer and new 3-layer models predict the rigidity of liquid-cooled bending members within 10% of experimentally measured values.

Numerical methods were necessary to model the high-temperature behavior of liquid-cooled FRP bending elements. Two separate models were developed to allow a greater degree of accuracy and stability: a finely-meshed 2-D thermochemical model with highly non-linear thermal properties, and a 3-D thermomechanical model with more stable thermal properties. The 2-D model produces the temperature distribution used in the 3-D model.

Numerous thermochemical models have been developed for FRP components since the early 1980's. None of these models are capable of simulating the gross changes in geometry that occur over extended fire exposures. Though the proposed 2-D thermochemical model is generally simpler than many of these existing models, it incorporates unique features that allow it to produce accurate temperature profiles through FRP elements for very long fire exposures. The first of these features is an "effective" specific heat capacity curve that represents the endothermic decomposition of the resin and dehydration of absorbed water. The second feature is an "effective" thermal conductivity curve that simulates the changes that occur due to cracking and delamination, as well as the radiative shielding effect of the burnt layers. Through these features, the model provides very accurate temperature predictions that differ by an average value of only 28°C from the average experimental values.

The second numerical model that was developed to study the thermomechanical behavior of liquid-cooled and non-liquid cooled FRP bending elements. This 3-D model utilizes the temperature profiles created by the 2-D thermochemical model and thus can incorporate simplified thermal material properties. A single temperature-dependent Young's modulus was defined for all stress states. This compromise detracts from the accuracy of the model in the non-liquid cooled condition but is less significant in the liquid-cooled condition. The non-liquid cooled condition also suffers from the lack of a computational fluid dynamics treatment convective heat transfer within hollow cells of the panels. The model in the liquid-cooled condition, however, predicts the mid-span deflection of a structurally loaded FRP panel within 5% (on average) of the average experimental values measured over a two-hour fire exposure. The strain predictions show very good agreement in the upper face sheet and fair agreement in the lower face sheet (though this is most likely related to inaccuracies in the experimentally measured values.)

## 5 Suggested Future Work

As this thesis represented the first step in the development of new building system, there are some aspects that have only been considered on basic level.

- The concept of using the internal liquid circulation system as the climate control system has not been deeply studied. Investigation of this aspect by both calculation and experimental validation are necessary to verify the feasibility of the proposed system.

- Only one wall element and one floor element have been described in the proposed system. In order to use materials in a more economical manner, more variants of these elements with different structural capacities should be elaborated.

With respect to the fire safety aspect of the proposed system, there are still some areas that merit further investigation.

- The experiments performed involved the exposure of bending elements to fire on their tensile-stressed lower face sheets. Because FRP materials are far less sensitive to heat-induced weakening when stressed in tension, the efficacy of the proposed system was only partially demonstrated. Physical experiments involving large-scale specimens exposed to fire and stressed in compression could reveal the true potential of internal liquid cooling for the fire protection of load-bearing FRP building components.
- The commercial software used to develop the thermomechanical model did not allow the definition of different temperature-dependent moduli for different stress states. This limitation noticeably detracted from the accuracy of the model. The possibility of making this differentiation in alternative software packages should be considered.
- Within the numerical models developed, delamination and loss of cross-section was only linked to temperature. Experimental investigations demonstrated that it is also dependent on fiber architecture, support conditions, mechanical stress, and ablation. Investigation of ways to incorporate these dependencies in the numerical models could lead to further improvements in their accuracy.



# Bibliography

- [1] AISC (1993). *AISC Load and Resistance Factor Design Specification for Structural Steel Buildings*. American Institute of Steel Construction, Chicago, USA.
- [2] Alaei, M., and Wenning, R. J. (2002). "The Significance of Brominated Flame Retardants in the Environment: Current Understanding, Issues and Challenges." *Chemosphere* (46), 579-82.
- [3] Allen, B. (2001). "Intumescent Coating Solutions in Fire Scenarios." *2<sup>nd</sup> Int. Conf. on Composites in Fire*, Newcastle upon Tyne, UK.
- [4] Anilturk, D., Chan, W. S. (2003). "Structural Stability of Composite Laminated Column Exposed to High Temperature or Fire." *J. of Composite Materials*, (37)8, 687-700.
- [5] ASCE (1998). *ASCE Minimum Design Loads for Buildings and Other Structures*. American Society of Civil Engineers.
- [6] ASTM (1981). *Terminology Relating to Fire Standards E-176-81a*. American Society for Testing and Materials, West Conshohocken, PA, USA.
- [7] ASTM (2003). *Standard Test for Fire Tests of Building Construction and Materials: ASTM E-119-00a*, American Society for Testing and Materials, West Conshohocken, PA, USA.
- [8] Audouin, J. (1969). "Plastiques et Architecture." Numéro hors série de la revue Plastiques Bâtiment, G. M. Perrin, ed., G. M. Perrin, Paris, FR 52-59, 77, 101.
- [9] Bamford, C.H., Crank, J., and Malan, D.H. (1946). "On the Combustion of Wood. Part I" *Proceedings of the Cambridge Philosophical Society* (42), 166-82.
- [10] Bausano, J., Boyd, S., Lesko, J., and Case, S. (2003). "Composite Life Under Sustained Compression and One-Sided Simulated Fire Exposure: Characterization and Prediction." *3<sup>rd</sup> Int. Conf. on Composites in Fire*, Newcastle upon Tyne, UK.
- [11] Bausano, J., Boyd, S., Lesko, J., and Case, S. (2004). "Composite Life Under Sustained Compression and One-Sided Simulated Fire Exposure: Characterization and Prediction." *Proceedings of the Int. SAMPE Symposium 2004*, Long Beach, CA, USA
- [12] Beratungsstelle für Stahlverwendung (1977). "Neue Wege des Brandschutzes im Stahl - und Verbundbau." (VHS video) Dusseldorf, DE.
- [13] Beyer, G. (2002). "Nanocomposites: A New Class of Flame Retardants for Polymers." *Plastics Additives & Compounding* (10), 22-8.
- [14] Bond, G. V. L. (1975). *Water Cooled Hollow Columns*.
- [15] Bouguerra, A., Ait-Mokhtar, A., Amiri, O., and Diop, M. (2001). "Measurement of Thermal Conductivity, Thermal Diffusivity and Heat Capacity of Highly Porous Building Materials Using the Transient Plane Source Technique." *Int. Comm. Heat and Mass Transfer*, 28(8), 1065-1078.
- [16] Briggs, P., and Hunter, J. (2004). "PYROMMS Final Report: Fire Tests on Composites." Warrington Fire Research Centre, Warrington, UK.
- [17] Briggs, P. (2003). "Fire Performance of Composites in European Construction Applications." *3<sup>rd</sup> Int. Conf. on Composites in Fire*, Newcastle upon Tyne, UK.
- [18] Brouwer, G. (2003). "Prototype of 'Carbon Tower' Developed." *Civil Engineering*, 73(4), 14-5.

- [19] Brown, J. (2003). "Yacht Design Inspires Fiber Composite Antarctic Building." *Civil Engineering*, 73(11), 24-7.
- [20] Brown, M. E. (1988). *Introduction to Thermal Analysis*, Chapman and Hall, London, UK.
- [21] BS (1990). *Fire Resistant Design - A Guide to Design of Structural Hollow Sections Using BS 5950 Part 8*. British Steel, Corby, Northlands, UK.
- [22] Buchanan, A. H. (2002). *Structural Design for Fire Safety*, John Wiley & Sons, Inc., New York, NY, USA.
- [23] Budiansky, B. and Fleck, N. A. (1993). "Compressive Failure of Fiber Composites." *J. of the Mechanics and Physics of Solids*, (41)1, 183-211.
- [24] Burdette, J. A. (2001). "Fire Response of Composite Structures - Experiments and Modeling," Masters Degree dissertation, Virginia Polytechnic Institute.
- [25] Cerny, R., Toman, J., Sestak, J. (1996). "Measuring the Effective Specific Heat of Building Materials." *Thermochimica Acta* (283), 239-50.
- [26] Chang, C. I. (1986). "Thermal Effects on Polymer Composite Structures." *Theoretical and Applied Fracture Mechanics*, (6)2, 113-20.
- [27] Chen, J.K., Sun, C.T., and Chang, C.I. (1985). "Failure Analysis of a Graphite/Epoxy Laminate Subjected to Combined Thermal and Mechanical Loading." *J. of Composite Materials*, (19)5, 216-35.
- [28] Chevin, D. (1989). "Plastic Homecoming." *Building*, (254)39, 78-9.
- [29] Chevin, D. (1990). "Plastic Showpiece." *Building*, (255)4, 74-5.
- [30] Clayssen, D. (1983). *Jean Prouvé - l'idée Constructive*. Dunod, Paris, FR.
- [31] Cooper, L. Y. and Franssen, J.-M. (1999). "A Basis for Using Fire Modeling with 1-D Thermal Analysis of Partitions to Simulate 2-D and 3-D Structural Performance in Real Fires." *Fire Safety Journal* (33), 115-28.
- [32] European Committee for Standardization (CEN). (1991). *Eurocode 1: Actions on Structures: Part 1.2: Actions on Structures Exposed to Fire*. Revised Edited Document, 2002.
- [33] Cote, A. E. (1997). *Fire Protection Handbook*. National Fire Protection Association, Quincy, MA, USA.
- [34] Cox, G. (1995). *Combustion Fundamentals of Fire*. Academic Press Limited, London, UK.
- [35] Crea, F., Porco, G., and Zinno, R. (1997). "Experimental Evaluation of Thermal Effects on the Tensile Mechanical Properties of Pultruded GFRP Rods." *Applied Composite Materials* 4), 133-43.
- [36] Cullen, C. G. (1958). "Fabricating the Structural Components of the All-Plastic 'House of the Future'." *Plastics Technology* (10), 921-7.
- [37] Dallaire, G. (1976). "Kansas City Bank Tower Features Water-Filled Columns, Exposed Spandrels." *Civil Engineering* (1), 58-62.
- [38] Dao, M. and Asaro, R. (1999). "A Study on the Failure Prediction and Design Criteria for Fiber Composites under Fire Degradation." *Composites: Part A*, (30)2, 123-31.

- [39] Davies, J. M. and Dewhurst, D. W. (1999). "The Fire Performance of GRE Pipes in Empty and Dry, Stagnant Water Filled, and Flowing Water Filled Conditions." *Proceedings of the 2<sup>nd</sup> Int. Conf. on Composites in Fire*, Newcastle upon Tyne, UK.
- [40] Davies, J. M., Dewhurst, D. W., Wang, H. B. (1998) The Performance of Wet and Dry GRE Pipes under Hydrocarbon Fire Conditions." *Proceedings of the 7<sup>th</sup> Int. Conf. on Fibre Reinforced Composites*, Newcastle-upon-Tyne, UK.
- [41] deWit, C. A. "An Overview of Brominated Flame Retardants in the Environment." *Chemosphere*, 46(5), 583-624.
- [42] Di Blasi, C. (1993). "Modelling and Simulation of Combustion Processes of Charring and Non-Charring Solid Fuels." *Progress in Energy and Combustion Science* (19), 71-104.
- [43] Dimitrienko, Y. I. (1997). "Thermomechanical Behaviour of Composite Materials and Structures Under High Temperatures: 1. Materials." *Composites: Part A*, (28)5, 453-61.
- [44] Dodds, N., Gibson, A. G., Dewhurst, D., and Davies, J. M. (2000). "Fire Behaviour of Composite Laminates." *Composites: Part A*, (31)7, 689-702.
- [45] Doernach, R., Burkhardt, B., Delekat, W., Dorn, H., Hübner, P., and Lehmann, K. (1974). "Bausysteme mit Kunststoffen." *architektur; forschung und entwicklung*, K. W. Schmitt, ed., Deutsche Vergals-Anstalt GmbH, Stuttgart, 24, 48.
- [46] Dooley, S. (2004). *The Development of Material-Adapted Structural Form*, Ph.D Thesis, École Polytechnique Fédéral de Lausanne, Lausanne.
- [47] Drysdale, D. (1998). *An Introduction to Fire Dynamics*. John Wiley & Sons, Inc., New York, NY, USA.
- [48] Duthinh, D., and Bajpai, K. (2001). "Strength of an Interlocking FRP Connection." National Institute of Standards Report NISTIR 6829, Gaithersburg, MD, USA.
- [49] Dutta, P. K., Hui, D. (2000). "Creep Rupture of a GFRP Composite at Elevated Temperatures." *Computers and Structures*, (76)1, 153-61.
- [50] Ehrenkrantz, E. D. (1989). *Architectural Systems*. McGraw-Hill Publishing Co., New York.
- [51] Fanucci, J. P. (1987). "Thermal Response of Radiantly Heated Kevlar and Graphite/Epoxy Composites." *J. of Composite Materials*, (21)2, 129-139.
- [52] Fargent, M. (2002). *ASSET Supafloor: The Integrated, Prefabricated, Modular Flooring System for Buildings*. Fiberline Composites, Kolding, DK.
- [53] Feierbach, W. (2003). *Fiberglass House 1970, Development, Design und Prototype*. Altenstadt-Hessen.
- [54] Fire, F. L. (1991). *Combustibility of Plastics*. Van Nostrand Reinhold, New York, NY, USA.
- [55] Fredlund, B. (1993). "Modelling of Heat and Mass Transfer in Wood Structures During Fire." *Fire Safety Journal*, (20)1, 36-69.
- [56] Gardiner, C. P., Mathys, Z., and Mouritz, A. P. (2002). "Tensile and Compressive Properties of FRP Composites with Localized Fire Damage." *Applied Composite Materials* (9), 353-67.
- [57] Gardiner, C. P., Mathys, Z., and Mouritz, A. P. (2004). "Post-Fire Structural Properties of Burnt GRP Plates." *Marine Structures*, (17)1, 53-73.

- [58] Gardiner, C. P., and Mouritz, A. P. "Post-Fire Flexural Response of GRP Composite Ship Panels." *The 11<sup>th</sup> International Offshore and Polar Engineering Conference*, Stavanger, NW, 160-7.
- [59] Garner, P. (1996). *Sixties Design*. Taschen GmbH, Köln.
- [60] Ghazi Wakili, K., Binder, B., and Vonbank, R. (2003). "A Simple Method to Determine the Specific Heat Capacity of Thermal Insulations Used in Building Construction." *Energy and Buildings* (35), 413-415.
- [61] Gibson, A. G., Mouritz, A. P., Wu, Y.-S., Gardiner, C. P., and Mathys, Z. (2003). "Validation of the Gibson Model for the Fire Reaction Properties of Fibre-Polymer Composites." *3<sup>rd</sup> Int. Conf. on Composites in Fire*, Newcastle upon Tyne, UK.
- [62] Gibson, A. G., Wright, P. N. H., Wu, Y.-S., Evans, J. T. (2004). "Laminate Theory Analysis of Composites under Load in Fire." *Proceedings of the Int. SAMPE Symposium 2004*, Long Beach, CA, USA.
- [63] Gibson, A. G., Wright, P. N. H., Wu, Y.-S., Mouritz, A. P., Mathys, Z., and Gardiner, C. P. (2004). "Fire Integrity of Polymer Composites Using the Two Layer Model." *Proceedings of the Int. SAMPE Symposium 2004*, Long Beach, CA, USA.
- [64] Gibson, A. G. (2003). "Basic Mechanisms of Fire Damage in Organic Matrix Composites." *3<sup>rd</sup> Int. Conf. on Composites in Fire*, Newcastle upon Tyne, UK.
- [65] Gibson, A. G., Wright, P. N. H., Wu, Y. S., Mouritz, A. P., Mathys, Z., and Gardiner, C. P. (2003). "The Integrity of Polymer Composites During and After Fire." *3<sup>rd</sup> Int. Conf. on Composites in Fire*, Newcastle upon Tyne, UK.
- [66] Gibson, A. G., Wright, P. N. H., Wu, Y. Z., Mouritz, A. P., Mathys, Z., and Gardiner, C. P. (2003). "Modelling Residual Mechanical Properties of Polymer Composites After Fire." *Plastics, Rubber and Composites*, 32(2), 81-90.
- [67] Gibson, A. G., Wu, Y.-S., and Dodds, N. (2001) "Measurement and Modelling of the Integrity of Composite Structures in Fire." *2<sup>nd</sup> Int. Conf. on Composites in Fire*, Newcastle upon Tyne, UK, 207-15.
- [68] Gibson, A. G., Wu, Y. S., Chandler, H. W., and Wilcox, J. A. D. (1995). "A Model for the Thermal Performance of Thick Composites Laminates in Hydrocarbon Fires." *Revue de L'Institute du Pétrol*, 50(1), 69-74.
- [69] Gnielinski, V. (1975). "Berechnung mittlerer Wärme- und Stoffübergangskoeffizienten an laminar und turbulent überströmten Einzelkörpern mit Hilfe einer einheitlichen Gleichung." *Forschung im Ingenieurwesen* (41), 145-153.
- [70] Grand, A. F., and Wilkie, C. A. (2000). *Fire Retardancy of Polymeric Materials*. Marcel Dekker, Inc., Basel.
- [71] Griffis, C. A., Masumra, R. A., Chang, C. I. (1981). "Thermal Response of Graphite Epoxy Composite Subjected to Rapid Heating." *J. of Composite Materials* (15), 427-42.
- [72] Griffis, C. A., Nemes, J. A., Stonesfiser, F. R., and Chang, C. I. (1986). "Degradation in Strength of Laminated Composites Subjected to Intense Heating and Mechanical Loading." *J. of Composite Materials*, (20)3, 216-235.
- [73] Guiton, J. L. (1997). "Sandwich Structure." US Patent # 6,202,376, Shell Research Ltd., USA

- [74] Gulvanessian, H. and Menzies, J. B. (2000). "The Eurocode for Structural Loading: Eurocode I." *Progress in Structural Engineering Materials* (2), 472-82.
- [75] Haddow, R. (1996). "House of the Future or House of the Past: Populist Visions from the USA." *AI Architecture and Ideas*, 68-79.
- [76] Hagentoft, C.-E. (2001). *Introduction to Building Physics*. Studentlitteratur, SWE.
- [77] Halverson, H., Bausano, J., Case, S. W., Lesko, J. J. (2004). "Simulation of Response of Composite Structures Under Fire Exposure." *Proceedings of the Int. SAMPE Symposium 2004*, Long Beach, CA, USA.
- [78] Halverson, H., Bausano, J., Case, S. W., Lesko, J. J. (2004). "Simulation of Response of Composite Structures Under Fire Exposure." *Proceedings of the Conference on Advanced Composite Materials in Bridges and Structures*, Calgary, Alberta, CA.
- [79] Harris, C. M. (1994). *Noise Control in Buildings*. McGraw-Hill, Inc., New York, NY, USA.
- [80] Hawthorne, C. (2003). "Carbon Fiber Future." *Metropolis Magazine*, Aug. 25.
- [81] Henderson, J. B., Wiebelt, J. A., and Tant, M. R. (1985). "A Model for the Thermal Response of Polymer Composite Materials with Experimental Verification." *J. of Composite Materials*, (19)6, 579-595.
- [82] Henderson, J.B. and Wiecek, T. E. (1987). "A Mathematical Model to Predict the Thermal Response of Decomposing, Expanding Polymer Composites." *J. of Composite Materials*, (21)4, 373-93.
- [83] Henderson, J.B. and Emmerich, W.-D. (1991). "Measurement of Specific Heat and Energetic Characterization of Materials up to High Temperatures." *J. of Thermal Analysis* (37), 1979-85.
- [84] Henry, S. D. (2001). *ASM Handbook. Volume 21 - Composites*. ASM International, Materials Park, OH, USA, 4.
- [85] Hess, A. (1986). "Monsanto House of the Future." *Fine Homebuilding*, 70-75.
- [86] Hilado, C. J. (1990). *Flammability Handbook for Plastics*. Technomic Publishing Co., Inc., Lancaster, PA, USA.
- [87] Home, M., and Taanila, M. (2003). "From Snowy Slopes to the Foot of Minarets." *Futuro. Tomorrow's House from Yesterday*, Desura, Helsinki, FI.
- [88] Horrocks, A. R., and Price, D. (2001). *Fire Retardant Materials*. Woodhead Publishing Ltd., Cambridge, UK.
- [89] Huber, B., and Steinegger, C. (1971). *Jean Prouvé: Une Architecte par l'Industrie*. Zurich Artemis, Zurich.
- [90] ICC Evaluation Service (2004). "Legacy Report on the 1997 Uniform Building Code ER-5174." Whittier, CA, USA.
- [91] ICC (1999). *International Fire Code*. International Code Council, Inc., 2000 edition, Falls Church, VA, USA.
- [92] ISO (1975). "Fire Resistance Tests-Elements of Building Construction." *International Standard ISO 834*, Geneva.
- [93] Janssens, M. L. (2004). "Modeling the Thermal Degradation of Structural Wood Members Exposed to Fire." *Fire and Materials* (28), 199-207.

- [94] Johanson, B. E. (2003). *The Dirty Dozen: Toxic Chemicals and the Earth's Future*. Praeger, Westport, CT, USA.
- [95] Kansa, E. J., Perlee, H. E., Chaiken, R. F. (1977). "Mathematical Model of Wood Pyrolysis Including Forced Convection." *Combustion and Flame* (29), 311-24.
- [96] Keller, T. (1999). "Towards Structural Forms for Composite Fiber Materials." *Structural Engineering International* (4), 297-300.
- [97] Keller, T. (2002). "Fiber Reinforced Polymers in Building Construction." *Symposium Towards a Better Built Environment*, Melbourne, AU.
- [98] Keller, T., and Gürtler, H. (2003). "Composite Action and Adhesive Bond Between FRP Bridge Decks and Main Girders." *J. of Composites for Construction* (accepted for publication).
- [99] Keller, T., and Gürtler, H. (2003). "In-Plane Compression and Shear Behavior of FRP Bridge Decks." *J. of Composites for Construction* (approved for publication).
- [100] Keller, T., and Schollmayer, M. (2004). "Plate Bending Behavior of a Pultruded GFRP Bridge Deck System." *Composite Structures* (64), 285-95.
- [101] Kung, H.-C. (1972). "A Mathematical Model of Wood Pyrolysis." *Combustion and Flame* (18), 185-95.
- [102] Landrock, A. H. (1983). *Handbook of Plastics Flammability and Combustion Toxicology*. Noyes Publications, Park Ridge, NJ, USA.
- [103] Lattimer, B., and Ouellette, J. "Thermal Properties of Composites for Heat Transfer Modeling During Fires." *Proceedings of the Int. SAMPE Symposium 2004*, Long Beach, CA, USA.
- [104] Lee, J., Hollaway, L., and Head, P. (1995). "The Structural Characteristics of a Polymer Composite Cellular Box Beam in Bending." *Construction and Building Materials*, (9)6, 333-40.
- [105] Lienhard, J. I., and Lienhard, J. V. (2002). *A Heat Transfer Textbook*. Phlogiston Press, Cambridge, MA, USA.
- [106] Ljung, L. (1999). *System Identification - Theory for User*, 2<sup>nd</sup> ed., Prentice Hall, Engelwood Cliffs, NJ, USA.
- [107] Loos, A. and Springer, G. (1980). "Moisture Absorption of Polyester-E Glass Composites." *J. of Composite Materials* (14), 142-54.
- [108] Looyeh, M. R. E., and Bettess, P. (1996). "An Axi-Symmetric Finite Element Model for the Fire Performance of GRP Pipes used for Natural Gas Transmission." *Proceeding of the 2<sup>nd</sup> Int. Mechanical Engineering Conference*, Shiraz, Iran.
- [109] Looyeh, M. R. E., Bettess, P., Gibson, A.G. (1997). "A One-Dimensional Finite Element Simulation for the Fire Performance of GRP panels for Offshore Structures." *Int. J. of Numerical Methods for Heat & Fluid Flow*, (7)6, 609-25.
- [110] Looyeh, M. R. E., and Bettess, P. (1998). "A Finite Element Model for the Fire-Performance of GRP Panels Including Variable Thermal Properties." *Finite Elements in Analysis and Design*, (30)4, 313-24.
- [111] Looyeh, M. R. E., Rados, K., and Bettess, P. (2001). "Thermomechanical Responses of Sandwich Panels to Fire." *Finite Elements in Analysis and Design* (37), 913-27.

- [112] Lua, J., and O'Brien, J. "Fire Simulation of Woven Fabric Composites with Temperatures and Mass Dependent Thermal-Mechanical Properties." *3<sup>rd</sup> Int. Conf. on Composites in Fire*, Newcastle upon Tyne, UK.
- [113] Ludwig, M. (1998). "Wohnhaus aus Kunststoff." *Deutsche Bauzeitung*, 76-80.
- [114] Maekawa, Z., and Lord, P. (1994). *Environmental and Architectural Acoustics*, E & FN Spon, an imprint of Chapman & Hall, London, UK.
- [115] Mapleston, P. (2000). "EU Legislation Turns the Heat on Brominated Flame Retardants." *Modern Plastics*, 77(9), 56.
- [116] Makowski, Z. S. (1964), "The Structural Applications of Plastics." *Proceedings of the Conference on Plastics in Building Construction*, University of Surrey, Surrey, UK.
- [117] Marks, P. R. (1987). "The Fire Endurance of Glass-Reinforced Epoxy Pipes." *Proceedings from the 2<sup>nd</sup> Int. Conf. on Polymers in a Marine Environment*, London, UK.
- [118] Maroni, M., Seifert, B., and Lindvall, T. (1995). *Indoor Air Quality - A Comprehensive Reference Book*. Elsevier, Amsterdam, ND.
- [119] Marsh, G. (2002). "Fire Safe Composites for Mass-Transit Vehicles." *Reinforced Plastics*, 46(9), 26-30.
- [120] Martínez, S. (2000). "Housing Turmoil: Experimental Homes Fail Urban Test." *Sacramento Bee*, Sacramento, CA.
- [121] Mathys, Z., Gardiner, C. P., Townsend, C. R., Russo, S., and Mouritz, A. P. "Modeling the Mechanical Properties of Fire-Damaged Composite Materials." *2<sup>nd</sup> Int. Conf. on Composites in Fire*, Newcastle upon Tyne, UK, 190-206.
- [122] Matweb (2004). "Material Property Data." [www.matweb.com](http://www.matweb.com)
- [123] McAdams, W. H. (1954). *Heat Transmission*. 3<sup>rd</sup> Ed., McGraw-Hill, New York, NY, USA.
- [124] McManus, L. N. and Springer, G. S. (1992). "High Temperature Thermomechanical Behavior of Carbon-Phenolic and Carbon-Carbon Composites, I. Analysis." *J. of Composite Materials*, (26)2, 206-29.
- [125] McManus, L. N. and Springer, G. S. (1992). "High Temperature Thermomechanical Behavior of Carbon-Phenolic and Carbon-Carbon Composites, II. Results." *J. of Composite Materials*, (26)2, 230-51.
- [126] McManus, L. N. and Coyne, D.C. (1982). "TRAP4 - A Digital Computer Program for Calculating the Response of Mechanically and Thermally Loaded Aircraft Structures to the Thermal Radiation of a Nuclear Explosion or High Energy Laser." TM-141, Kaman Avidyne Technical Memorandum.
- [127] Meikle, J. L. (1995). *American Plastic: A Cultural History*, Rutgers University Press, New Brunswick, NJ, USA.
- [128] Milke, J. A. and Vizzini, A. J. (1990). "Modeling and Evaluation of the Thermal Response of Fire Exposed Composites." *Proceedings from the Conference on Heat and Mass Transfer in Fires*, Seattle, WA, USA, 15-21.
- [129] Milke, J. A. and Vizzini, A. J. (1991). "Thermal Response of Fire Exposed Composites." *J. of Composites Technology and Research*, (13)3, 145-51.

- [130] Miller, J. R., and Weaver, P. M. (2003). "Temperature Profiles in Composite Plates Subject to Time-Dependent Complex Boundary Conditions." *Composite Structures*, (59)2, 267-78.
- [131] Minguzzi, G. (1998). *Fiber Reinforced Plastics*. Firenze, IT.
- [132] Mouritz, A. P. (2000). "Mechanical Properties of Fire Damaged Glass-Reinforced Phenolic Composites." *Fire and Materials* (24), 67-75.
- [133] Mouritz, A. P. (2002). "Post-Fire Properties of Fibre-Reinforced Polyester, Epoxy and Phenolic Composites." *J. of Materials Science* (37), 1377-86.
- [134] Mouritz, A. P. (2003). "Fire Resistance of Aircraft Composite Laminates." *J. of Materials Science Letters* (22), 1507-9.
- [135] Mouritz, A. P. (2003). "Simple Models for Determining the Mechanical Properties of Burnt FRP Composites." *Materials Science and Engineering*, (359)1-2, 237-46.
- [136] Mouritz, A. P., and Gardiner, C. P. (2002). "Compression Properties of Fire-Damaged Polymer Sandwich Composites." *Composites: Part A* (33), 609-20.
- [137] Mouritz, A. P., and Mathys, Z. (1999). "Post-Fire Mechanical Properties of Marine Polymer Composites." *Composite Structures* (47), 643-53.
- [138] Mouritz, A. P., and Mathys, Z. (2001). "Post-Fire Mechanical Properties of Glass-Reinforced Polyester Composites." *Composites Science and Technology* (61), 475-90.
- [139] Mouritz, A. P., Mathys, Z., and Gardiner, C. P. (2004). "Thermomechanical Modelling the Fire Properties of Fibre-Polymer Composites." *Composites: Part B*, (35)6-8, 467-74.
- [140] Mouritz, A. P., and Mathys, Z. (2004). "Heat Release of Polymer Composites in Fire." *Proceedings of the Int. SAMPE Symposium 2004*, Long Beach, CA, USA.
- [141] Nelson, G. L. ed. (1995). *Fire and Polymers II: Materials and Tests for Hazard Prevention*, American Chemical Society, Washington, DC.
- [142] Nelson, G. L., and Wilkie, C. A. (2001). *Fire and Polymers II: Materials and Solutions for Hazard Prevention*, American Chemical Society, Washington, D.C., USA.
- [143] Newburg, A. S. (1973). *Design and Development of Housing Systems for Operation Breakthrough, Phase I*, U.S. Department of Housing and Urban Development, Washington, D.C., 215, 220-1.
- [144] NFPA (2004). "Fire Loss Statistics." National Fire Protection Agency, [www.nfpa.org](http://www.nfpa.org).
- [145] Ohelmiller, T. J., and Shields, J. R. "The Effect of Surface Coatings on Fire Growth Over Composite Materials." BFRL - National Institute of Standards and Technology, Gaithersburg, MD, USA.
- [146] Özisik, M. N. (1977). *Basic Heat Transfer*. Robert E. Krieger Publishing Company, Malabar, FL, USA.
- [147] Panaskevopoulos, S. C. A. (1966). *Structural Potential of Foam Plastics for Housing in Underdeveloped Areas*. University of Michigan, Ann Arbor, MI.
- [148] Panpuch, M. (2004). "Marcin Panpuch Design and Architecture." [www.marcinpanpuch.com](http://www.marcinpanpuch.com).
- [149] Pering, G. A. Farrell, P. V. and Springer, G. S. (1980). "Degradation of Tensile and Shear Properties of Composites Exposed to Fire or High Temperatures." *J. of Composite Materials* (14), 54-68.

- [150] Petukhov, B. S. (1970). "Heat transfer and Friction in Turbulent Pipe Flow with Variable Physical Properties." *Advanced Heat Transfer* (6), 503-65.
- [151] Pilger, C. W. (1997). "TVOCs from Extruded PVC Building Components." ALARA Industrial Hygiene Services, Toronto, Ontario, CA.
- [152] Pohlhausen, E. (1921). "Der Wärmeaustausch zwischen festen Körpern und Flüssigkeiten mit kleiner Reibung und kleiner Wärmeleitung." *Z. Angew. Math. Mech.* (1), 115-121.
- [153] Polyzois, D., McLeod, L., and Philopulos, D. (2004). "An Alternative Housing System Using Advanced Composite Materials for the Communities of Northern Canada." *Proceedings of the Conference on Advanced Composite Materials in Bridges and Structures*, Calgary, CA.
- [154] Porter, D., Metcalfe, E., and Thomas, J.K. (2000). "Nanocomposite Fire Retardants - A Review." *Fire and Materials* (24), 45-52.
- [155] Quarmby, A. (1974). *The Plastics Architect*. Pall Mall Press, London, UK.
- [156] Roßbach, S. (1999). "Wassergefüllte Stahlstützen - ein alternatives Brandschutzkonzept." Technical report, Technical University of Darmstadt, DE.
- [157] Royal Building Systems (2001). *Wall Patching Procedures*, Construction Bulletin (7)1, May, 2001.
- [158] Roulet, C.-A. (2000). *Thermique du Bâtiment*. École Polytechnique Fédéral de Lausanne, Section de Génie Civil, 6-8.
- [159] Sagelsdorff, R. (1995) "Kurzzeit-Prüfverfahren zur Bestimmung der Wärmeleit-Fähigkeit und der Spezifischen Wärmekapazität von Nichtmetallischen Baustoffen." Federal Institute for Materials Research and Testing (BAM), Berlin, DE.
- [160] Samanta, A., Looyeh, M. R. E., Jihan, S., and McConnachie, J. (2004). "Thermo-mechanical Assessment of Polymer Composites Subjected to Fire." Engineering and Physical Science Research Council & The Robert Gordon University, Aberdeen, UK.
- [161] Sas (1992). "Plastic Fantastic." *Baumeister*, (89)5, 58-9.
- [162] Schapery, R. (1968). "Thermal Expansion Coefficients of Composite Materials Based on Energy Principles." *J. of Composite Materials*, 2(3), 380-404.
- [163] Schein, L. (1971). "Maisons en Matières Plastiques." *Techniques et Architecture*, 34-7.
- [164] Schwabe, A., and Saechtling, H. J. (1971). *Plasticconstruction*, Carl Hanser Verlag, Munich, DE, 261-5, 310.
- [165] Seggewiß, P. G. B. "Properties of Fire-Damaged Polymer Matrix Composites." *3<sup>rd</sup> Int. Conf. on Composites in Fire*, Newcastle upon Tyne, UK.
- [166] Seggewiß, P. G. B. "Methods to Evaluate the Fire Resistance of Carbon Fiber Reinforced Plastics." *Proceedings of the Int. SAMPE Symposium 2004*, Long Beach, CA, USA.
- [167] SIA (2003). *SN 520 261 - Actions sur les Structures Porteuses*. SIA 261:2003, Swiss Society of Engineers and Architects, Zurich.
- [168] SIA (1997). *SN 520 183 - La Protection Contre l'Incendie dans le Construction*. SIA 183, Swiss Society of Engineers and Architects, Zurich.
- [169] Skeist, I. (1966). *Plastics in Building*. Reinhold Publishing Corporation, New York, NY, USA, 419.

- [170] Sorathia, U., Beck, C., and Dapp, T. (1993). "Residual Strength of Composites During and After Fire Exposure." *J. of Fire Sciences*, (11)3, 255-69.
- [171] Sorathia, U., Telegadas, H., and Bergen, M. (1994). "Mechanical and Flammability Characteristics of Phenolic Composites for Naval Applications." *Proceedings of the 39<sup>th</sup> Int. SAMPE Symposium*, Corvina, CA, USA.
- [172] Springer, G. S. (1984). "Model for Predicting the Mechanical Properties of Composites at Elevated Temperatures." *J. of Reinforced Plastics and Composites*, (3)1, 85-95.
- [173] Stewart, A. (1992). "Plastic Finnish." *Building*, (257)9, 44-5.
- [174] Strakhov, V. L., Kaledin, VI. O., Kaledin, Val. O., and Sukhaniv, A. V. (2004). "Fire Resistance and Fire Protection Calculations for Polymer Composite Structural Bridge Elements." *Proceedings from the Conference on Advanced Composite Materials in Bridges in Structures*, Calgary, Alberta, CA.
- [175] Sullivan, R. M. and Salamon, N. J. (1992). "A Finite Element Method for the Thermochemical Decomposition of Polymeric Materials - I. Theory." *Int. J. of Engineering Science*, (30)4, 431-41.
- [176] Sullivan, R. M. and Salamon, N. J. (1992). "A Finite Element Method for the Thermochemical Decomposition of Polymeric Materials - II. Carbon Phenolic Laminates." *Int. J. of Engineering Science*, (30)7, 939-51.
- [177] Tangle, L. and Drohmann, D. (2004). "Environmental Issues Related to End-of Life Options of Plastics Containing Brominated Fire Retardants." *Fire and Materials* (28), 403-10.
- [178] Tant, M. R. (1994). "High Temperature Properties and Applications of Polymeric Materials." *Proceedings of the ACS Symposium Series 603*, San Diego, CA, USA.
- [179] Teti, C. G. R. (1989). *Sandwich Structures Handbook II*. Prato, Padua, IT.
- [180] Tomblin, J., Salah, L., and Ng., Y. (2001). "Determination of Temperature/Moisture Sensitive Composite Properties." *DOT-FAA Report DOT/FAA/AR-01/40*, Washington D.C., USA.
- [181] Troitzsch, J. (2004). *International Plastics Flammability Handbook*, 3<sup>rd</sup> ed., Hanser Publishers, Munich, DE.
- [182] Tsai, S. W. and Hahn, H. T. (1980). *Introduction to Composite Materials*. Technomic Publishing.
- [183] VFK/AEAI (1993). *Norme de Protection Incendie*. Association des Établissements Cantonaux d'Assurance Incendie, Berne.
- [184] Wang, Y. C. (2002). *Steel and Composite Structures*. Spon Press, London, UK.
- [185] Watanabe, I., Sakai, S. (2003) "Environmental Release and Behavior of Brominated Flame Retardants." *Environment International*, 29(6), 665-82.
- [186] Wasserman, N. (2002). "Plastic Didn't Feel Like Home: Predictions from the Past that Haven't Come True, Yet." *Future Newsday*, New York, NY, USA.
- [187] Weijger, J. C. A. (1997). "Fire Behaviour of Various Construction Materials." *Proceedings of the conference on Fire Hazards, Testing, Materials, and Products*, Shawbury, UK.
- [188] Wichman, I. S. (1989) "A Continuum-Mechanical Derivation of the Conservation Equations for the Pyrolysis and Combustion of Wood." *Tutkimukia Forskinigsrapporter Research Reports 591*, Technical Research Centre of Finland.

- [189] Wickström, U. (2004). "Heat Transfer by Radiation and Convection in Fire Testing." *Fire and Materials*, (28)5, 411-15.
- [190] Wilson, F. (1990). "Plastic for the People: An Electricity Pioneer Builds a Lab that Functions Like a Home." *Architecture: the AIA Journal*, (79)3, 165-8.
- [191] Wong, P. M. H., Davies, J. M., and Wang, Y. C. (2004). "An Experimental and Numerical Study of the Behaviour of Glass Fibre Reinforced Plastics (GRP) Short Columns at Elevated Temperatures." *Composite Structures* (63), 33-43.
- [192] Woodward, M. (2003). "Achieving Very Low Smoke & Toxicity - without Compromising Structural Performance." *3<sup>rd</sup> Int. Conf. on Composites in Fire*, Newcastle upon Tyne, UK.
- [193] Woolley, W. D., and Fardell, P. J. (1977). "The Prediction of Combustion Products." *Fire Research* (1), 11-21.
- [194] Yamada, S. "Streamlining: Norman Bel Geddes and the Rhetoric of Modernism." Inventing the "Jet Age" in America, [www2.sjsu.edu/depts/commstudies/woz/woz3/](http://www2.sjsu.edu/depts/commstudies/woz/woz3/).
- [195] Young, A. (2004). "New Living Quarters for Davis Station." *Australian Antarctic Magazine* (6), 55-6.
- [196] (1970). "Suisse, Système Rondo." *Techniques et Architecture*, (32)3, 96-7.
- [197] "Plastics in Building and Construction: Realities and Challenges." Pittsburgh, PA, USA.
- [198] (1993). "Plastic All the Way." *World Architecture* (22), 84-5.
- [199] (2000). "Final Technical Report: Phase II, Task 16 - Modular Composite Bridge." Defense Advanced Research Projects Agency (DARPA).
- [200] (2003). "Art Contemporain / Mobilier d'Architectes", Jousse Entreprise, Paris, FR.
- [201] (2003). *ANSYS Inc. Theory Reference*. SAS IP Inc., Urbana, IL, USA



# List of Symbols

(Some terms are also described in Chapter 1 Section 5.)

## GENERAL SUBSCRIPTS

$c$	Compression, Convective, Composite
$f$	Fiber, Final
$i$	Initial
$L$	Load
$lfs$	Lower face sheet
$m$	Matrix
$r$	Radiative
$R$	Resistance
$s$	Shear
$t$	Tension
$u$	Ultimate
$ufs$	Upper face sheet
$w$	Web
$x$	Longitudinal direction
$y$	Transverse direction
$z$	Through-thickness direction

## CAPITAL LETTERS

$A$	Area
$A_{deg}$	Area of partially-degraded region
$C_p$	Specific heat capacity
$DL$	Dead load
$E$	Young's modulus
$E_d$	Young's modulus of degraded region
$E'$	Storage modulus
$E''$	Loss modulus
$EI$	Rigidity
$G$	Shear modulus
$G_r$	Grashof number
$H$	Enthalpy
$I$	Moment of inertia
$I$	Moment of inertia of burnt section

$L$	Length of component
$L_{ch}$	Characteristic length
$L_{pl}$	Length of component in direction of fluid flow
$LL$	Live load
$M$	Mass fraction
$M_u$	Ultimate moment capacity
$M_w$	Maximum applied moment
$N_u$	Nusselt number
$P$	Point load
$P_r$	Prandtl number
$Q$	Total heat
$Q_{dot}$	Heat flow rate
$R$	Thermal resistance
$R_{SI}$	Thermal resistance at interior surface
$R_{SE}$	Thermal resistance at exterior surface
$S$	Bending stiffness
$SDL$	Superimposed dead load
$T$	Temperature
$T_g$	Glass transition temperature
$T_{g,onset}$	Onset glass transition temperature
$T_d$	Decomposition temperature
$T_{d,onset}$	Onset decomposition temperature
$T_s$	Softening temperature
$T_{SI}$	Temperature of interior surface
$T_{SE}$	Temperature of exterior surface
$T_{sur}$	Surface temperature
$T_\infty$	Bulk fluid temperature
$U$	Thermal transmittance, Sensible energy
$V$	Volume, Volume fraction
$V_{fl}$	Fluid flow velocity
$W$	Mechanical work

## LOWERCASE LETTERS

$a$	distance from support to load axis
$b$	Thermal effusivity, Width of component
$c_d$	Distance from neutral axis to outermost face
$d$	Thickness of component
$d_c$	Distance from hot face of boundary between virgin and fully-degraded regions
$d_h$	Hydraulic diameter
$d_{vg}$	Distance from hot face to boundary between virgin and partially-degraded regions
$d_{vg}$	Distance from hot face to boundary between partially-degraded and fully-degraded regions
$f$	Ultimate strength
$g$	Acceleration of gravity
$h$	Total heat transfer coefficient
$h_r$	Radiative heat transfer coefficient
$h_c$	Convective heat transfer coefficient
$m$	Mass
$\bar{m}$	Mass flow rate
$q$	Heat flux
$q_d$	Heat of decomposition by mass
$q_{gen}$	Energy generated within the system
$q_w$	Latent heat of vaporization of water
$s/s$	Seviceability limit state
$t$	Time
$\tan-\delta$	Damping factor
$uls$	Ultimate limit state
$w$	Linear distributed load
$y$	Height of component

## GREEK LETTERS

$\alpha_t$	Coefficient of thermal expansion
$\alpha_d$	Thermal diffusivity
$\alpha_r$	Radiative absorptance
$\beta$	Volumetric coefficient of thermal expansion
$\delta$	Deflection
$\epsilon$	Strain
$\epsilon_r$	Radiative emissivity
$\gamma_{LL}$	Load magnification factor
$\gamma_R$	Strength reduction factor
$\eta$	Ratio of modulus of part to reference modulus (Chapter 6 Section 1), Dynamic viscosity (Chapter 6 Sections 2-3)
$\lambda$	Thermal conductivity
$\nu$	Poisson's ratio
$\rho$	Density
$\rho_r$	Radiative reflectance
$\sigma$	Stress
$\sigma_r$	Stefan Boltzmann constant
$\tau$	Shear stress

## OTHER SYMBOLS

$\Re$	Reynolds number
-------	-----------------

# List of Figures

## 1. Introduction

Figure 1-1. FRP vs. composite materials.....	8
Figure 1-2. Global and local coordinate systems.....	10

## 2. FRP Buildings & Building Systems

Figure 2-1. Monsanto House of the Future (left), Exploded diagram (right).....	25
Figure 2-2. HVAC distribution diagram.....	28
Figure 2-3. Fiber-Shell housing complex .....	29
Figure 2-4. Laminate (left), Arrangement of modules in Sacramento housing complex (right) .....	30
Figure 2-5. HVAC distribution between levels (left), Routing diagram (right).....	31
Figure 2-6. Assembly of flat panel system (left), Transport of pre-assembled house (right).....	32
Figure 2-7. Other mandrels that could be used to produce different modules.....	34

## 3. The State of the Art

Figure 3-1. GE Living Environment House.....	43
Figure 3-2. Molded baseboard raceway (left), Utilities embedded in waffle slab (middle), Integrated shelf connection system in foundation wall form work (right).....	44
Figure 3-3. Nestehaus (left), Floor plan (middle), Tri-column section (right) .....	45
Figure 3-4. The main ACCS components (left), Assembled corner section (right).....	46
Figure 3-5. Box-beam assembly (left), Aberfeldy footbridge (middle and right) .....	46
Figure 3-6. Severn Visitor's Center (left), Automated car wash enclosure (right).....	47
Figure 3-7. Building applications of the ACCS proposed by Minguzzi .....	48
Figure 3-8. The BEET Building System: Two-story schematic (left), Keyed connections (right).....	49
Figure 3-9. Sandwich panel compressive failure modes.....	50
Figure 3-10. The Royal Building System: Insulated wall panel (left), Various wall elements (right) ....	52
Figure 3-11. The ASC System .....	53
Figure 3-12. The Eyecatcher: Frame schematic (left), Built-up members (middle), Frame (right) .....	55
Figure 3-13. The Eyecatcher: Under construction (left), Completed (middle), Translucency (right) ...	55
Figure 3-14. First PDG Domus unit built (left), Assembly of modules (right).....	56
Figure 3-15. Connection between wall elements (left) and between wall and roof elements (right).....	59
Figure 3-16. Davis Station building: Initial design rendering (left), Final design rendering (right).....	60
Figure 3-17. Davis Station building: Rendering of complex (left), Completed bridge structure (middle), Rendering of building interior (right).....	60
Figure 3-18. British Antarctic Survey facility - 1963 .....	62
Figure 3-19. Cluster at Delft Technical University (left), Construction at Utrecht University (right) ..	62
Figure 3-20. Mechanical connections and steel supports .....	63
Figure 3-21. Dock Tower: Elevation renderings (left and middle), Selected floor plan (right).....	64

Figure 3-22. Woven Building elevation (left), Section (middle), Detail (right).....	66
Figure 3-23. Four adjacent ASSET bridge deck sections (left), The Supafloor section (right).....	67
Figure 3-24. Cross section of the flooring system with mechanical systems.....	68
Figure 3-25. Cross section of the flooring system with mechanical systems.....	68
Figure 3-26. Sphere house concept .....	69
Figure 3-27. Hanselmann's Sphere - ca.1970 (left) [163], Panpuch's Sphere concept- 2004 (right) .....	70
Figure 3-28. Futuro Hotel concept - 1968 (left), Rondo System concept - 1969 (middle), Sphere concept - 2004 (right) .....	71
Figure 3-29. The fire tetrahedron .....	79
Figure 3-30. Temperature dependence of selected properties of glass-reinforced epoxy composite.....	81
Figure 3-31. Effective or specific heat capacity of phenolic resin as measured by Henderson.....	81
Figure 3-32. Schematic of pore pressure, temperature, and remaining mass through the thickness of a fire-exposed FRP plate.....	83
Figure 3-33. Methods of achieving fire safety objectives.....	84
Figure 3-34. Time for cold face to reach 160°C versus thickness.....	93
Figure 3-35. Sketches from Guiton's patent of a unique sandwich system .....	99
Figure 3-36. Fanucci's idealized effective specific heat capacity curve for epoxy resins .....	108
Figure 3-37. Idealized effective thermal conductivity curve for generic charring materials.....	109

## 4. The Proposed System

Figure 4-1. Basic wall element (dimensions in millimeters).....	122
Figure 4-2. Usage of cells in floor and wall panels.....	122
Figure 4-3. Basic floor element (dimensions in mm).....	123
Figure 4-4. Global building stability issues .....	125
Figure 4-5. Global resistance mechanisms.....	125
Figure 4-6. Schematic of carbon tendon system (dimensions vary by application) .....	126
Figure 4-7. Carbon tendon tensioning and anchorage system (blue), floor shelf angle (red).....	127
Figure 4-8. Inter-story wall connector elements (blue).....	129
Figure 4-9. Inter-story wall connector tabs (red).....	129
Figure 4-10. Cutaway view of circulation path through a typical floor panel .....	137
Figure 4-11. Cutaway view of the wall circulation path .....	138
Figure 4-12. Cutaway detail of the wall circulation path .....	139
Figure 4-13. Plumbing connections at the inlet/outlet end of a floor panel.....	140

## 5. Experimental Investigations

Figure 5-1. DuraSpan 766 Bridge Deck System.....	152
Figure 5-2. Derivation of experimental specimens (dimensions in mm).....	153
Figure 5-3. Diagram of the pultrusion process .....	153

Figure 5-4. Face sheet fiber architecture as seen after a resin burn-off analysis.....	154
Figure 5-5. EMPA small horizontal oven with purpose-built concrete exposure frame.....	158
Figure 5-6. EMPA large horizontal oven and structural reaction frame.....	159
Figure 5-7. ISO 834 cellulosic time-temperature curve and typical oven gas temperatures measured by oven piloting thermocouples .....	160
Figure 5-8. Storage modulus ( $E'$ ), Loss modulus ( $E''$ ), and damping factor ( $\tan\delta$ ) vs. time.....	163
Figure 5-9. TGA remaining and derivative weight versus temperature (20°C/min. heating rate).....	164
Figure 5-10. TGA remaining mass versus temperature .....	165
Figure 5-11. Application of foil tape (left), Completed assembly (right) .....	167
Figure 5-12. Electrical heating element (left), Liquid cooling element (right) .....	167
Figure 5-13. Typical specimen for Fire Reaction Experiments .....	170
Figure 5-14. Hot face of specimen after 50 minutes of fire exposure.....	171
Figure 5-15. Hot faces of specimens (clockwise from top left: 15, 30, 60, and 45 minutes).....	172
Figure 5-16. Temperature through thickness vs. time .....	173
Figure 5-17. Specimen situated on small horizontal oven .....	177
Figure 5-18. Temperature through thickness of LC specimens over time .....	178
Figure 5-19. Comparison of average temperature profiles of LC and CE specimens .....	179
Figure 5-20. Change in water temperature (inlet minus outlet) vs. time .....	179
Figure 5-21. Hot face of the LC02 specimen after 120 minutes of fire exposure.....	180
Figure 5-22. Drooping reinforcement on hot face of specimen LC01 after 45 minutes (left) and 90 minutes (right) of fire exposure .....	181
Figure 5-23. Power drawn by flowing water per fire-exposed square meter vs. time .....	183
Figure 5-24. Experimental set-up for Structural Fire Endurance Experiments .....	186
Figure 5-25. Water connections.....	187
Figure 5-26. Load and support diagram of the experimental set-up.....	187
Figure 5-27. Displacement transducers, strain gages, and thermocouples across mid-span.....	189
Figure 5-28. Average mid-span deflection (from three transducers across width) vs. time .....	191
Figure 5-29. Strain at various locations versus fire exposure time.....	192
Figure 5-30. Average temperature through thickness versus time .....	193
Figure 5-31. Average change in water temperature (inlet minus outlet) versus time .....	193
Figure 5-32. Structural failure of upper face sheet of specimen SLC03 .....	194
Figure 5-33. Cross sections of specimens after cooling: SLC01 (top left), SLC02 (bottom left), and SLC03 (right) .....	195
Figure 5-34. Hot face of specimen SLC01 after 70 minutes of fire exposure.....	195
Figure 5-35. Load versus mid-span vertical deflection .....	197
Figure 5-36. Power drawn by flowing water per unit fire-exposed area versus time .....	200
Figure 5-37. Power drawn by flowing water per fire-exposed area versus flow rate .....	200
Figure 5-38. Experiment SLC03 temperature vs. time.....	201
Figure 5-39. Comparison of average temperature profiles of SLC, LC, and CE specimens .....	202

## 6. Mathematical Modeling

Figure 6-1.	Load and support conditions used in undamaged model of proposed flooring system ..	210
Figure 6-2.	Ratio of span-to-deflection versus span for different post heights.....	212
Figure 6-3.	Deformed shape, axial stress, shear stress, and moment distribution .....	213
Figure 6-4.	Combination of axial stress and moment to find maximum stress in deck section .....	213
Figure 6-5.	Resistance factor of safety ( $\gamma_R$ ) versus span for different post heights .....	214
Figure 6-6.	Comparison of two-layer and three layer approximations .....	215
Figure 6-7.	Determination of the depth of the degraded region by visual inspection.....	217
Figure 6-8.	Relationship of temperature profile to modulus of elasticity by the 2-layer .....	217
Figure 6-9.	Relationship of temperature profile to modulus of elasticity by the 3-layer .....	221
Figure 6-10.	2-D Thermochemical model geometry and meshing .....	228
Figure 6-11.	ANSYS element geometry: Plane-55 (left), Surf-151 (right) .....	229
Figure 6-12.	Portion of experimental specimen considered in 2-D thermochemical model.....	230
Figure 6-13.	2-D Thermochemical model boundary conditions .....	230
Figure 6-14.	View of recessed specimen from within oven .....	234
Figure 6-15.	Comparison of remaining mass and proposed effective specific heat .....	236
Figure 6-16.	Effective thermal conductivity and density curves used in the thermochemical model ..	240
Figure 6-17.	Comparison of temperature history of the liquid-cooled experiment SLC02 and 2-D thermochemical model .....	243
Figure 6-18.	Comparison of temperature history of the non-liquid cooled experiment SLC03 and 2-D thermochemical model .....	243
Figure 6-19.	Comparison of temperature profiles of all experiments conducted without liquid cooling to the 2-D thermochemical model .....	244
Figure 6-20.	Comparison of temperature profiles of all liquid-cooled experiments to the 2-D thermochemical model (average experimental values) .....	244
Figure 6-21.	Geometry and meshing of the 3-D thermomechanical model.....	245
Figure 6-22.	ANSYS element geometry: Solid-5 (left), Mesh-200 (right) .....	246
Figure 6-23.	ANSYS element geometry: Beam-4 .....	246
Figure 6-24.	Portion of experimental specimen considered in 3-D thermomechanical model .....	247
Figure 6-25.	Mechanical boundary conditions used to approximate experimental set-up.....	248
Figure 6-26.	Modulus versus temperature curves used in the thermomechanical model.....	254
Figure 6-27.	Comparison of the mid-span deflections of liquid-cooled specimens as predicted by the thermomechanical model and experimentally measured .....	259
Figure 6-28.	Comparison of axial strains of a liquid-cooled beam as predicted by the thermomechanical model and experimentally measured.....	259
Figure 6-29.	Comparison of mid-span axial strain distribution without thermal expansion and without structural load (liquid-cooled condition) .....	260
Figure 6-30.	Comparison of the mid-span deflections without thermal expansion and without load (liquid-cooled condition).....	260
Figure 6-31.	Comparison of the mid-span deflections of a non-liquid cooled (dry) beam as predicted by	

the thermomechanical model and experimentally measured ..... 261

## 7. Conclusion

# Appendix

## A. Fire Reaction Experiments - Technical Report

Figure A-1. Martin Marietta Composites' DuraSpan® 766 deck system.....	316
Figure A-2. Origin of specimens .....	316
Figure A-3. Typical specimen after machining of thermocouple slots .....	317
Figure A-4. DuraSpan 766 reinforcement layers (numbers correspond to Table A-5 - Schedule B) .	317
Figure A-5. CNC routing of slots for placement of thermocouples throughout depth.....	318
Figure A-6. Close-up photo of thermocouple slots.....	318
Figure A-7. Layout of thermocouples (all dimensions in millimeters) .....	319
Figure A-8. CE02 - EMPA small horizontal oven with custom-built concrete cap .....	320
Figure A-9. CE02 - Ceramic wool insulation used to prevent the escape and spread of flames .....	321
Figure A-10. CE02 - Specimen hot face showing dark spots with no flaming combustion .....	321
Figure A-11. CE02 - 12 Minutes - Flaming combustion engulfing hot face of specimen .....	322
Figure A-12. CE02 - 34 Minutes - Black char from resin mostly cleared out from hot face, white glass fiber char from random mat clearly visible .....	322
Figure A-13. CE03 - 52 Minutes - Surface veil/random mat cleared of resin char, fibers whitened, some fiber tips hanging down and glowing red.....	323
Figure A-14. CE02 - 59 Minutes - White char from surface veil/random mat fibers beginning to crack (flames still present, though not visible due to long exposure time of photograph) .....	323
Figure A-15. CE02 - Epoxy used to fill in slots over thermocouples 1, 4, 5, and 8 of specimen 02D softening and flow out of slots.....	324
Figure A-16. CE03 - Styrene slowly bubbling up through cold face of specimen 03D .....	324
Figure A-17. CE02 - Removal of specimen 02D from oven exposure window after 30 minutes.....	325
Figure A-18. CE03 - Removal of specimen 03C from oven exposure window after 45 minutes .....	325
Figure A-19. CE03 - Cold faces of specimens after conclusion of experiment	326
Figure A-20. CE03 - Hot faces of specimens after conclusion of experiment.....	326
Figure A-21. CE02 - Temperature vs. time .....	327
Figure A-22. CE03 - Temperature vs. time .....	327
Figure A-23. Comparison of thermocouple readings from CE02 and CE03 .....	328

## B. Liquid Cooling Experiments - Technical Report

Figure B-1. Construction of specimens .....	341
Figure B-2. Layout of thermocouples .....	342
Figure B-3. LC01 Specimen prepared for installation of thermocouples .....	344
Figure B-4. Installation of thermocouples on Specimen LC03 .....	344
Figure B-5. Detail of specimen LC02 showing end-closure channels and water connections .....	345
Figure B-6. Experimental set-up for LC03 with inlet hose on left and outlet hose on right .....	345
Figure B-7. Progression of damage across hot face of LC03 demonstrates the uneven heat flux applied by the oven.....	346
Figure B-8. Progression of damage across hot face of LC02.....	346
Figure B-9. Random mat whitened and bubbling into foam-like char in LC02.....	346
Figure B-10. Reinforcing fibers drooping down and oxidizing during LC03 .....	347
Figure B-11. Drooping reinforcement layers turning to foam-like char during LC03 .....	347
Figure B-12. High pressure in LC02 causes water to leak up through pinholes in the thin plates used to cover the access holes.....	348
Figure B-13. Post-experiment hot face of LC03 .....	348
Figure B-14. Water temperature versus time - All LC Experiments .....	349
Figure B-15. Temperatures recorded during LC01 .....	350
Figure B-16. Temperatures recorded during LC02 .....	351
Figure B-17. Temperatures recorded during LC03 .....	352
Figure B-18. Comparison of temperatures recorded during Charring and Liquid Cooling Experiments (temperatures are averages from all four instrument clusters) .....	353

## C. Structural Fire Endurance Experiments - Technical Report

Figure C-1. Martin Marietta DuraSpan® 766 bridge deck.....	381
Figure C-2. Removal and placement of specimen tails for constant face sheet thickness.....	381
Figure C-3. End view of large horizontal oven and experimental set-up (not to scale).....	382
Figure C-4. Side view of large horizontal oven and experimental set-up (not to scale) .....	382
Figure C-5. Instrumentation of upper face sheet of specimens.....	383
Figure C-6. Instrumentation and as-built dimensions of lower face sheet (Cells II-III) .....	384
Figure C-7. Instrumentation and as-built dimensions of lower face sheet (Cells IV-V) .....	385
Figure C-8. SLC01 - Experimental set-up .....	386
Figure C-9. SLC02 - Experimental set-up .....	386
Figure C-10. SLC02 - After approx. 30 minutes of thermal loading (uneven heating evident).....	387
Figure C-11. SLC01 - After approx. 70 minutes of thermal loading (broken rovings visible).....	387
Figure C-12. SLC01 - Removal of specimen and reaction frame at conclusion of experiment .....	388
Figure C-13. SCL01 - Hot face of specimen directly after conclusion of experiment .....	388
Figure C-14. SLC03 - Smoke and steam escaping through steel adapter pipes.....	389
Figure C-15. SLC03 - Location of failure in upper face sheet .....	389

Figure C-16. SLC03 - Failure of upper face sheet.....	390
Figure C-17. SLC03 - Close-up view of failure in upper face sheet .....	390
Figure C-18. Depth of fire damage .....	391
Figure C-19. Specimens post-experiment, quartered to allow layer-wise inspection.....	391
Figure C-20. SLC01 remaining lower face sheet thickness .....	392
Figure C-21. SLC02 remaining lower face sheet thickness .....	392
Figure C-22. SLC03 remaining lower face sheet thickness .....	392
Figure C-23. SLC01 delamination.....	393
Figure C-24. SLC02 delamination.....	393
Figure C-25. SLC03 delamination.....	393
Figure C-26. SLC01 - Strain vs. time.....	394
Figure C-27. SLC02 - Strain vs. time.....	394
Figure C-28. SLC03 - Strain vs. time.....	395
Figure C-29. All SLC Experiments - Average adjusted mid-span deflection vs. time.....	395
Figure C-30. All SLC Experiments - Change in water temperature vs. time ( $T_{outlet} - T_{inlet}$ ).....	396
Figure C-31. SLC01 - Temperature vs. time .....	397
Figure C-32. SLC02 - Temperature vs. time .....	398
Figure C-33. SLC03 - Temperature vs. time .....	399
Figure C-34. Average temperature profiles through lower face sheet at selected times.....	400
Figure C-35. SLC01 - Illustration of corrections made to “As-recorded” deflections .....	401
Figure C-36. SLC01 - Deflection vs. time (adjusted values - see text) .....	402
Figure C-37. SLC02 - Deflection vs. time (adjusted values - see text) .....	403
Figure C-38. SLC03 - Deflection vs. time (adjusted values - see text) .....	404
Figure C-39. All SLC Experiments - Strain distributions at 30 cm from supports (units: $\mu\text{m}/\text{m}$ ).....	405

## D. Numerical Model Source Code



# List of Tables

## 1. Introduction

Figure 2-1. Monsanto House of the Future (left), Exploded diagram (right).....	25
--------------------------------------------------------------------------------	----

## 2. FRP Buildings & Building Systems

## 3. The State of the Art

Table 3-1. Summary of fire safety measures .....	101
--------------------------------------------------	-----

## 4. The Proposed System

Table 4-1. Approximate thermal properties of common materials .....	145
---------------------------------------------------------------------	-----

## 5. Experimental Investigations

Table 5-1. Properties of DuraSpan deck constituent materials.....	155
Table 5-2. DuraSpan coupon properties .....	156
Table 5-3. Total energy absorbed by water over 90 minutes of fire exposure .....	183
Table 5-4. Bending stiffness, $S$ , resulting from measured mid-span deflections and rigidity, $EI$ .....	198
Table 5-5. Total energy absorbed by water over 90 minutes of fire exposure .....	199

## 6. Mathematical Modeling

Table 6-1. Floor deck parameters .....	210
Table 6-2. Carbon tendon parameters.....	211
Table 6-3. Carbon tendon deviation post parameters .....	211
Table 6-4. Applied loads .....	211
Table 6-5. Rigidity predictions by the 2-layer model.....	219
Table 6-6. Values entered into Equations 6-6 and 6-7 to solve for the $EI$ values in Table 6-5 .....	219
Table 6-7. Rigidity predictions by the three-layer model.....	222
Table 6-8. Values entered into Equations 6-9 and 6-10 to solve for the $EI$ values in Table 6-7 .....	222
Table 6-9. Values relating to convection of water in function of fluid flow velocity, $V_f$ .....	232
Table 6-10. Values relating to convection of water not dependent on flow velocity.....	232
Table 6-11. Convective heat transfer of air at 27°C on a flat plate.....	233
Table 6-12. Values relating to radiative and convective heat transfer at the hot face .....	235
Table 6-13. Temperature-dependent material properties used in the thermomechanical model .....	241
Table 6-14. Convective heat transfer coefficients for cold face.....	249

Table 6-15. Values needed to calculate the coefficient of thermal expansion.....	255
Table 6-16. Comparison of predicted and experimentally measured pre-fire mid-span deflections ..	257

## 7. Conclusion

# Appendix

## A. Fire Reaction Experiments - Technical Report

Table A-1. CE02 - Measurement of as-built thermocouple slot depths from cold face and calculation of material thickness below slots .....	308
Table A-2. CE03 - Measurement of as-built thermocouple slot depths from cold face and calculation of material thickness below slots .....	309
Table A-3. Notes taken during CE02.....	310
Table A-4. Notes taken during CE03.....	311
Table A-5. Glass fiber architecture schedule resulting from dissection of experimental specimens (02A through 02D) and from independent resin burn-off tests .....	312
Table A-6. Dissection of reinforcement layers from hot face towards cold face.....	313
Table A-7. Dissection of reinforcement layers from hot face towards cold face.....	314
Table A-8. Dissection of reinforcement layers from hot face towards cold face.....	315

## B. Liquid Cooling Experiments - Technical Report

Table B-1. Notes taken during LC01 - December 18, 2003 .....	339
Table B-2. Notes taken during LC03 - January 15, 2004.....	339
Table B-3. Notes taken during LC02 - January 16, 2004.....	340
Table B-4. Measurement of as-built thermocouple slot depth and flange thickness .....	343

## C. Structural Fire Endurance Experiments - Technical Report

Table C-1. Bending stiffness, $S$ (kN/mm), resulting from measured mid-span deflections.....	373
Table C-2. Rigidity, $EI$ (N·mm <sup>2</sup> ), resulting the experimental bending stiffness, $S$ .....	374
Table C-3. Rigidity predictions by the 2-layer model .....	375
Table C-4. Stiffness of the partially degraded region according to the 3-layer model .....	376
Table C-5. Post-experimental layer-wise status of specimens .....	380

## D. Numerical Model Source Code





# Curriculum Vitæ

## EDUCATION

**Swiss Federal Institute of Technology**, Lausanne, Switzerland

Doctor ès Sciences, May 2005

Subject Area: Development of a novel fiber-reinforced polymer multiple-story building system with integrated climate-control and structural fire endurance systems

**Lehigh University**, Bethlehem, Pennsylvania

Bachelor of Science in Civil Engineering, May 1998

Cumulative GPA: 3.0

Honors: Stabler Scholarship recipient

## RELATED EXPERIENCE

**Senior Project Engineer**, *DeSimone Consulting Engineers, PLLC*, New York, NY (July 1998 - July 2001)

- Structural designer for the 1.3 million ft<sup>2</sup> Ritz-Carlton Hotel in Washington DC
  - Designed concrete columns, beams, slabs, shear walls, and foundation walls
  - Worked on-site as consultant and inspector for duration of construction
- Structural designer for renovation and reconstruction of 70 year-old 35-Story St. Moritz Hotel in New York City
  - Designed new steel columns, beams, composite deck, and lateral bracing
  - Analyzed existing structure for adequacy under new loads, including its 7 transfer levels, terra-cotta façade lateral system, and semi-rigid wind connections
  - Designed reinforcement strategies for columns, beams, and slabs with excessive corrosion, new loading conditions, or large HVAC penetrations
  - Represented structural interest in meetings with architects, managers, and owners

**Engineering Intern**, *Miller/Thompson Constructors, Inc.*, San Francisco, CA (Summer 1997)

- On-site support for San Francisco International Airport Expansion Project
  - Drafted shop drawings for RFI's, as-builts, and traffic plans
  - Surveyed for grading, cuts & fills, and elevation contours

**Carpenter**, *A. Ramaglia, General Contractor*, Montclair, NJ (Summer 1995)

- Demolished, framed, and remodeled residential structures

## SELECTED PUBLICATIONS

"A Study on the Fire Behavior of Multifunctional and Fire Resistant FRP Building Components." *2<sup>nd</sup> Int. Conf. on FRP Composites in Civil Engineering*, December 8-10, 2004, Adelaide, Australia.

"Experimental Study on the Concept of Liquid Cooling for Improving Fire Resistance of FRP Structures for Construction." *Composites: Part A*. (accepted for publication)

"Fire Endurance of Loaded and Liquid Cooled GFRP Slabs for Construction." *Composites: Part A*. (accepted for publication)

## COMPUTER SKILLS

ANSYS, AutoCAD, RISA 3D, SAP2000, Mathematica, SODA, ADOSS, RAM Steel, MS Office, FrameMaker, Illustrator, Indesign

## ACTIVITIES

**Swiss Federal Institute of Technology Rowing Club** (2001-Present)

- Silver medal, *Swiss National Collegiate Championships* (2003)
- Silver medal, *Championship of Swiss-Romandie* (2004)

**Lehigh University Crew Club**

- Team Captain (1995-1998)

## LANGUAGES

French

